Chapter 2 Meteorology and Oceanography

1 Meteorology and Oceanography Items to be Considered for Performance Verification

1.1 General

The following meteorology and oceanography items and effects on the facilities subject to the Technical Standards shall be considered with regard to the performance verification of the facilities.

① Atmospheric pressure and its distribution are dominant factors that generate winds and storm surge.

② Winds which generate waves and storm surge induce the pressure on the facilities subject to the Technical Standards and moored vessels, and can hamper cargo handling and other port operations. See **2 Winds** for further details.

③ The tidal level affects the earth pressure and water pressure, which act on facilities subject to the Technical Standards, and can interfere with cargo handling and other port operations. Furthermore, it affects wave transformation in areas of shallow water. See **Part II, Chapter 2, 3 Tidal Level** for further details.

④ Waves exert force on the facilities subject to the Technical Standards and become an important factor which affects the function of the facilities depending on their scales and frequencies. They also cause moored vessels to move and interfere with cargo handling and other port operations. They can also cause the rise of the mean water level, which has effects similar to the tidal level, as mentioned above. See **Part II, Chapter 2, 4 Waves** for further details.

⑤ Tsunamis exert forces as waves and fluid on the facilities subject to the Technical Standards and become a factor in the interference with the facilities concerned. It also causes moored ships to move. See **Part II, Chapter 2, 5 Tsunamis** for further details.

⑥ Wave forces appear due to the actions of the waves, storm surge, and tsunamis on the facilities subject to the Technical Standards and their scales and properties depend on location, shape, structural type, and other factors of facilities. See **Part II, Chapter 2, 6 Wave Force** for further details.

⑦ Water currents affect the sedimentation of the sea bottom sediments and become a factor which interferes the function of facilities subject to the Technical Standards. See **Part II, Chapter 2, 7 Water Currents** for further details.

2 Winds

[Public Notice] (Winds)

Article 6

The characteristics of winds shall be set by the methods provided in the subsequent items corresponding to the single action or combination of two or more actions to be considered in the performance criteria and performance verification:

(1) The ocean surface winds to be used in the estimation of waves and storm surge shall be appropriately defined in terms of wind velocity, wind direction, etc., on the basis of long-term measured values or estimated values of weather.

(2) The winds to be used in the calculation of wind pressures shall be appropriately defined in terms of wind velocity and direction corresponding to the return period on the basis of the statistical analysis of the long-term measured values or estimated values of winds or other methods.

(3) The winds to be used in the calculation of wind energy shall be appropriately defined in terms of the joint frequency distribution of wind velocity and direction for a certain duration of time on the basis of the long-term measured values or estimated values of winds.

[Interpretation]

7. Setting of Natural Conditions and Others

(1) Requirements for Winds (Article 6 of the Ministerial Ordinance and the interpretation related to Article 6 of the Public Notice)

The single action or combination of two or more actions indicates a design state. The conditions for winds shall be properly set by the subsequent provisions in accordance with the performance criteria and the design state considered in the performance verification.

① **Winds for the estimation of waves and storm surge:**

Winds for the estimation of waves and storm surge shall be observed or hindcasted values for 30 years or more as a standard.

② **Winds for the calculation of wind pressure:**

Winds for the calculation of wind pressure shall be observed or hindcasted values for 30 years or more as a standard.

③ **Winds for the calculation of wind energy**

Winds for n the calculation of wind energy shall be observed or hindcasted values for on the order of three years or more as a standard. A certain period shall be one year as a standard.

2.1 General

(1) Wind is one of the most distinctive meteorological phenomena, namely, the phenomenon that the air moves owing to atmospheric pressure differences and heat. The states of the wind blows over the ocean are usually very different from those over land. Wind velocities over the ocean are higher than those over land near the shore.[1)] For the performance verification of facilities subject to the Technical Standards, the effects of winds must be appropriately evaluated. At the same time, it is also important to perform verifications from the viewpoint of the effective utilization of wind energy considering that wind is an energy resource that creates clean energy and does not exhaust carbon dioxide.[2)]

(2) Gradient Winds

① The velocity of the gradient wind can be expressed as a function of air pressure gradient, radius of curvature of barometric isolines, latitude, and air density, as in **equation (2.1.1)**.

$$V_g = r\omega\sin\phi\left(-1+\sqrt{1+\frac{\frac{\partial p}{\partial r}}{\rho_a r\omega^2\sin^2\phi}}\right) \quad \textbf{(2.1.1)}$$

where

V_g : velocity of gradient wind (m/s)
In the case of an anticyclone, **equation (2.1.1)** provides a negative value; therefore, the absolute value should be taken.

$\partial p/\partial r$: pressure gradient (positive for a cyclone, and negative for an anticyclone) ($kg/m^2/s^2$)

r : radius of curvature of barometric isolines (m)

ω : angular velocity of Earth's rotation (1/s) $\omega = 7.27 \times 10^{-5}$/s

ϕ : latitude (°)

ρ_a : density of air (kg/m^3)

Before performing the calculation, practical units should first be converted into the MKS units listed above. Note that an air pressure of 1.0 hPa is 100 $kg/m/s^2$.

② A gradient wind for which the barometric isolines are straight lines (i.e., their radius of curvature in **equation (2.1.1)** is infinite) is called the geostrophic wind. In this case, the wind velocity is expressed as **equation (2.1.2)**.

$$V = \frac{\frac{\partial p}{\partial r}}{2\rho_a\omega\sin\phi} \quad \textbf{(2.1.2)}$$

③ The nomograph in **Fig. 2.1.1** is helpful in calculating the velocity of the gradient wind. This assumes that $1\rho_a$ = 1.1 kg/m^3. As a usage example, if the interval (pressure gradient) between contours per 2 hPa at latitude 40° is equivalent to 0.6° in latitude and if the cyclonic curvature radius of contours is equivalent to 6°, the velocity of the gradient wind can be calculated to be approximately 21.5 m/s by connecting points A and B with a straight line, by determining point C where the curvature radius crosses the curve with the curvature radius of 6°, and by reading the scale of the vertical line.

④ The actual sea surface wind velocity is generally lower than the value obtained from the gradient wind equation. Moreover, although the direction of a gradient wind is parallel to the barometric isolines in theory, the sea surface wind blows at a certain angle α to the barometric isolines in reality (**Fig. 2.1.2**). In the northern hemisphere, the winds around a cyclone blow in a counterclockwise direction and inwards, whereas the winds around an anticyclone blow in a clockwise direction and outwards. It is known that the relationship between the velocity of gradient winds and that of the actual sea surface wind varies with the latitude. **Table 2.1.1** summarizes this relationship under the average conditions,[3)] where V_s is the wind velocity at 10 m above the sea surface and V_g is the wind velocity of gradient wind. However, this is just a rough standard. When estimating the sea surface wind, it is necessary to refer to the actually measured values on the shore, and the values reported from ships on the sea, which are written on the meteorological chart, and to properly correct these values if necessary.

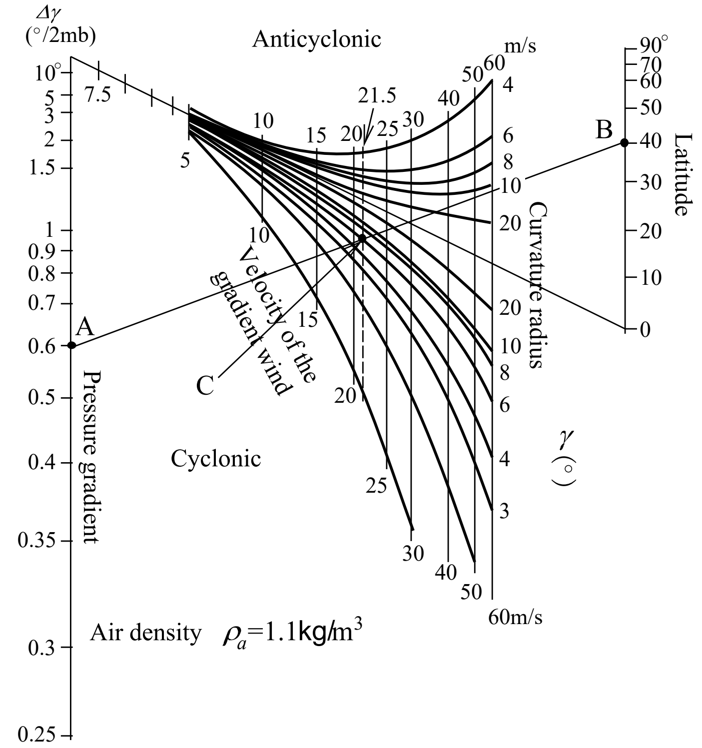

Fig. 2.1.1 Nomograph to Calculate the Gradient Wind

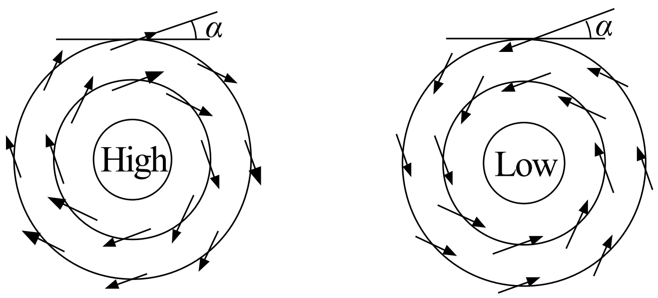

(a) Anticyclone (b) Cyclone

Fig. 2.1.2 Wind Direction for an Anticyclone (High) and a Cyclone (Low)

Table 2.1.1 Relationship between Sea Surface Wind Speed and Gradient Wind Speed

Latitude (°)	10	20	30	40	50
Angle α (°)	24	20	18	17	15
Velocity ratio V_s/V_g	0.51	0.60	0.64	0.67	0.70

(3) Typhoon Winds

In calculations concerning the generation of storm surge or waves due to a typhoon, it is common to assume that the air pressure distribution follows either Fujita's equation (**equation (2.1.3)**)[4] or Myers' equation (**equation (2.1.4)**)[5]; the constants in the chosen equation are determined on the basis of actual air pressures measured in the region of the typhoons.

Fujita's equation

$$p = p_\infty - \frac{\Delta p}{\sqrt{1+\left(\frac{r}{r_0}\right)^2}} \qquad \textbf{(2.1.3)}$$

Myers' equation

$$p = p_c + \Delta p \cdot \exp\left(-\frac{r_0}{r}\right) \quad \textbf{(2.1.4)}$$

where

p : air pressure at a distance r from the center of typhoon (hPa)

r : distance from the center of typhoon (km)

p_c : air pressure at the center of typhoon (hPa)

r_0 : estimated distance from the center of typhoon to the point where the wind velocity is maximum (km)

Δp : air pressure drop at the center of typhoon (hPa) $\Delta p = p_\infty - p_c$

p_∞ : air pressure at $r = \infty$ (hPa); $p_\infty = p_c + \Delta p$

The size of a typhoon varies with time; thus, r_0 and Δp must be determined as functions of time

(4) Meteorological GPV and Mesoscale Meteorological Model

Organizations such as the Japan Meteorological Agency, the European Center for Medium-Range Weather Forecasts, and America's National Center for Environmental Protection, calculate the values of items such as air pressure, wind velocity, wind direction, and water vapor flux on the basis of 3D grid calculation models for meteorological values, and the calculated values at the grid points (GPV: grid point values) are saved. These GPVs may be used instead of wind hindcasting on the basis of **equations (2.1.1)** to **(2.1.4)**. However, when a grid with large spacing is used for meteorological calculations, the atmospheric pressure and winds may not be satisfactorily reproduced at places where meteorological conditions change drastically with position, such as near the centers of typhoons. Therefore, when GPVs are used, it is preferable to verify the precision by using observational values. Moreover, the meteorological fields may be hindcasted by a numerical model (mesoscale meteorological model; MM5,[6] WRF,[7] or others) that sets these meteorological GPV as initial and boundary values. The mesoscale meteorological model enables the hindcasting (downscaling) of the meteorological field with more minute time and spatial resolutions by considering the influence of land (elevation of land and land utilization) in the vicinity of the sea area concerned on the meteorological field. In this case, it is also desirable to verify the precision of the meteorological fields obtained from a local weather model by comparing it with the observed values. Therefore, by using a meteorological field hindcasted from a mesoscale meteorological model, it is expected that the precision of hindcasted waves and storm surge will be improved, particularly in the inner bay area,.[8), 9)]

(5) Wind Energy

If winds are considered the movement of air, then the wind energy that crosses a unit cross-sectional area in unit time is given by **equation (2.1.5).**[1)]

Winds for estimating the wind energy shall be appropriately specified with joint statistic distributions for velocity and direction for a fixed time (usually one year) on the basis of observed or hindcasted data for three years or more.

$$P = \frac{1}{2}\rho_a V^3 \quad \textbf{(2.1.5)}$$

where

P : wind energy per unit cross-sectional area (W/m^2)

ρ_a : air density (kg/m^3)

V : wind velocity (m/s)

In other words, the wind force energy is proportional to the cube of the wind velocity; therefore, a small difference in wind velocity can mean a big difference in energy (power generation). Therefore, during the performance verification of facilities that use wind force energy, it is important to accurately understand how the conditions change with regard to time and space.

In the coastal zone, the wind conditions vary drastically between land and sea. Furthermore, wind velocity shows significant variations owing to land altitude. Over the sea, the changes in wind velocity with altitude are gradual; therefore, it is possible to obtain highly stabilized winds that are appropriate for power generation at relatively low altitudes. For example, the results of measurements in the vicinity of the Kansai International Airport show that the wind energy over the course of a year at a measurement tower (MT station) placed at a height of 15 m over the ocean were roughly same as those at a land station (C station) with an altitude of 100 m; as the results the wind energy at MT station is approximately five times greater than that at a land station with an altitude of 10 m.[10)]

Fig. 2.1.3 shows a comparison of wind conditions at each observation point by showing the annual mean wind velocity at coastal wind observation points all over Japan collected and processed by the Nationwide Ocean Wave information network for Ports and HArbourS (NOWPHAS) on the vertical axis and the mean coefficient of variation during the 10-minute observation period on the horizontal axis.[2)] Here, the mean coefficient of variation is the mean value of the coefficient defined as the value of the standard variation of wind velocity fluctuation divided by the mean wind velocity. The difference between sea and land observation points appears more distinctly than the area difference. It shows that the mean wind velocity at the sea is faster and the variance at the sea in a short period is smaller, comparing corresponding those at the land.

When designing facilities that utilize wind energy, it is important to properly estimate and simulate the production of electric power by considering the temporal and spatial variations of winds and by referring to the design examples of coastal wind power illumination system.[10)–12)] See Ref.[13)] for the installation of wind power generation facilities utilizing wind energy.

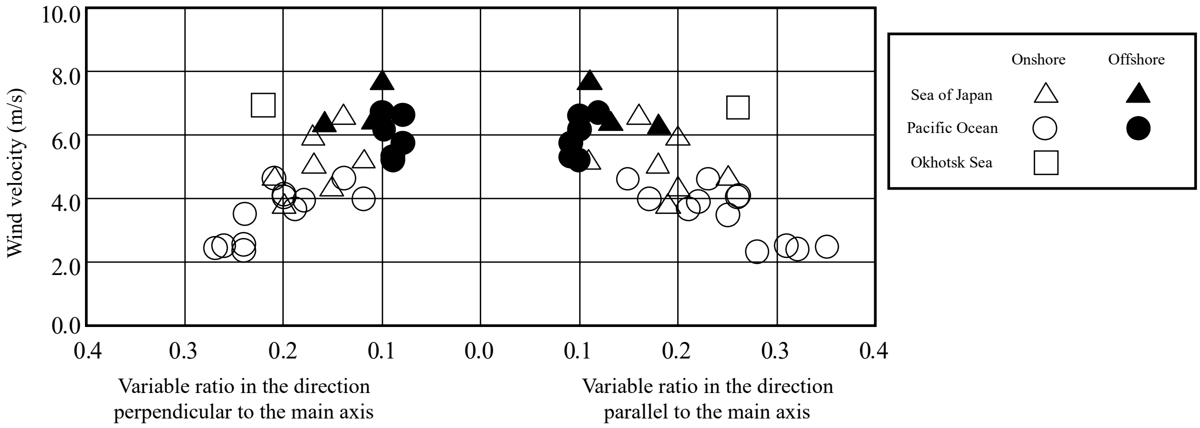

Fig. 2.1.3 Distribution of Mean Wind Velocity and Variable Ratio at Each NOWPHAS Observation Point[2)]

2.2 Characteristic Values of Wind Velocity

(1) Determination of Characteristic Value of Winds

The elements of winds are direction and velocity. The wind direction and velocity are expressed as one of 16 directions, and the mean velocity over 10 minutes, respectively. The velocity of winds that acts directly on facilities subject to the Technical Standards and moored ships is specified in general as a velocity corresponding to a certain period of re-occurrence on the basis of the occurrence probability distribution of wind velocity derived measured or hindcasted long-term values over 30 years. By using the annual maximum 10-minute mean wind velocities over approximately 35 years based on Measurement Technical Data Sheet #34 of the Japan Meteorological Agency[14)] and by assuming a double exponential distribution, the expected wind velocities over 5, 10, 20, 50, 100, and 200 years have been calculated at 141 meteorological stations. For the performance verification of facilities, these data can be used as reference values; however, if the location of interest has topographical conditions different from those at the close meteorological stations, it is preferable to take measurements at least for 1 year to determine the effect of the topography.[15)]

(2) The wind velocities obtained at the meteorological stations are approximately 10 m above the ground. Therefore, if the height of the target facility is different from the height mentioned above at the estimation of the wind over the sea from the observed values, height correction shall be performed for the wind velocity. The vertical distribution of wind velocity is usually shown on a logarithmic scale; however, for simplicity, an exponential scale is often used for the performance verification of various types of facilities.

$$U_h = U_0 \left(h / h_0 \right)^n \qquad \textbf{(2.2.1)}$$

where

U_h : wind velocity at height h (m/s)

U_0 : wind velocity at height h_0 (m/s)

n : index according to the situation, such as roughness degree near the earth's surface

(3) The exponent n in **equation (2.2.1)** varies with the roughness of the nearby terrain and the stability of the air. In general, it is possible to use a value of n = 1/10 to 1/4 for performance verification when specifying the wind velocity for purposes such as calculating wind pressure, and a value of $n \leq 1/7$ is often used over the ocean. Statistical data for wind velocity is usually the mean wind velocity over 10 minutes; however, depending on the facility, the mean wind velocity over a shorter time period may be required, or the maximum instantaneous wind velocity may be required. In such cases, one should understand the gust factor (the ratio of the maximum instantaneous wind speed to the 10-minute mean wind velocity) and the characteristics of the region, such as the relationship between the main wind velocity and maximum wind velocity.

2.3 Wind Pressure

(1) Wind pressure shall be appropriately specified by considering items such as structure and location of the facility.

(2) Wind pressure that acts on sheds, warehouses, and cargo handling equipment shall be specified as follows.

① Wind pressure acting on sheds and warehouses shall conform to the **Order for Enforcement of the Building Standards Act** (Cabinet Order No. 246 of 2005) Article 87.

② Wind pressure acting on cargo handling equipment shall conform to the **Structural Standard for Cranes** (Health, Labour and Welfare Ministry Public Notice No. 399 of 2003), the **Structural Standard for Mobile Cranes** (Health, Labour and Welfare Ministry Public Notice No. 400 of 2003), or the **Structural Standard for Derrick Cranes** (Ministry of Labour Public Notice No. 120 of 2000). Refer to **Comment of Each Structural Standard for Cranes and Others**.[16)] However, cargo handling equipment that is not covered by the same codes is excluded.

(a) Structural Standard for Crane

In Article 9, **Structural Standard for Crane**, it is specified that the wind load shall be calculated as follows:

1) The value of the wind load is calculated by using **equation (2.3.1)**:

$$W = qCA \tag{2.3.1}$$

where

W : wind load(N)

q : velocity pressure (N/m^2)

C : wind pressure coefficient

A : pressure-receiving area (m^2)

2) The value of the velocity pressure in **equation (2.3.1)** can be calculated from either **equation (2.3.2)** or **equation (2.3.3)** depending on the condition of the crane. **Equations (2.3.2)** and **(2.3.3)** correspond to wind velocity values of 16 and 55 m/s, respectively.

Crane in operation: $$q = 83\sqrt[4]{h} \tag{2.3.2}$$

Crane stopped: $$q = 980\sqrt[4]{h} \tag{2.3.3}$$

where

h : height (m) *above* the ground of the crane surface that receives the winds

Use 16 m as the value of h if height < 16 m.

3) For the value of the wind pressure coefficient it is possible to use the value found in the wind tunnel tests on the surface of the crane that receives the winds or the value given in **Table 2.3.1** for the category of the surface of the crane that receives the winds. A "surface composed of flat surfaces" in **Table 2.3.1** is the surface of a structure with a box-like shape such as a box girder, operator's cab,

machine chamber, or electrical chamber. A "cylindrical surface" includes the surface of a wire rope. The "face area" is the shaded portion in **Fig. 2.3.1**.

Table 2.3.1 Wind Pressure Coefficients for the Wind Load on a Crane

Classification of crane surfaces that receive winds		Value
Surfaces composed with horizontal trusses (Other than horizontal trusses made with steel pipe)	$W_1 < 0.1$	2.0
	$0.1 \leq W_1 < 0.3$	1.8
	$0.3 \leq W_1 < 0.9$	1.6
	$0.9 \leq W_1$	2.0
Surfaces composed of flat surfaces	$W_2 < 5$	1.2
	$5 \leq W_2 < 10$	1.3
	$10 \leq W_2 < 15$	1.4
	$15 \leq W_2 < 25$	1.6
	$25 \leq W_2 < 50$	1.7
	$50 \leq W_2 < 100$	1.8
	$100 \leq W_2$	1.9
Surfaces composed of cylindrical surfaces or horizontal trusses made with steel pipe	$W_3 < 3$	1.2
	$3 \leq W_3$	0.7

Note: In this table, W_1, W_2, and W_3 represent the following values:

W_1: area occupying ratio (the value obtained by dividing the projected area of the surface of the crane that receives the winds by the area of the surface that receives that same winds)

W_2: the value obtained by dividing the length in the longitudinal direction of the surface of the crane that receives the winds by the width of the surface that receives that same winds

W_3: the value obtained by multiplying the projected width of the cylinder or steel pipe (unit: m) by the square root of the value shown in 2) for the velocity pressure (unit: N/m^2) when the crane stops.

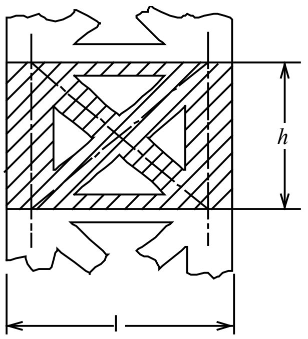

Projected Area A_r : Area of the shaded portion

Area Occupying Ratio $W_l = \dfrac{A_r}{l\,h}$

Fig. 2.3.1 Projected Area

4) The pressure-receiving area in **equation (2.3.1)** shall be the area of the surface of the crane that receives the winds projected onto a surface perpendicular to the direction of the winds (hereinafter "projected area"). When there are two or more surfaces of the crane that receive the winds, the area subject to wind pressure calculation is determined by summarizing the following;

   i) The projected area of the first surface in the direction of the winds

   ii) The areas obtained by multiplying the portions of the surface areas of the second and later surfaces in the direction of the winds (hereinafter "second and later surfaces" in this paragraph) that overlap the first surface in the direction of the winds by the reduction factors shown in **Fig. 2.3.2**

   iii) The projected areas of the portions of the surface areas of the second and later surfaces that do not overlap the first surface in the direction of the winds

   In **Fig. 2.3.2**, b, h, ϕ, and η represent the following values:

   b : distance between the beams of the crane that receive the winds (see **Fig. 2.3.3**)

   h : height of the first beam in the direction of the winds among the beams that receive the winds (see **Fig. 2.3.3**)

ϕ : the area occupying ratio of the first beam in the direction of the winds among the beams for the surfaces of the crane that receive the winds (For surfaces that are formed of horizontal trusses, ϕ is the value W_1 specified in the note of the table of the previous section; for surfaces formed of flat surfaces or cylindrical surfaces, it is one.)

η : reduction factor

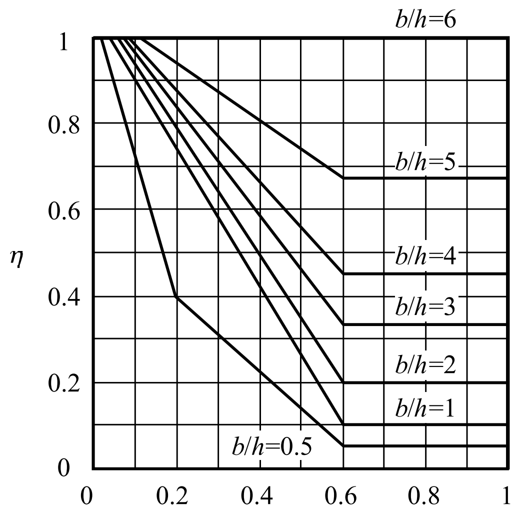

Fig. 2.3.2 Reduction Factors for Projected Areas

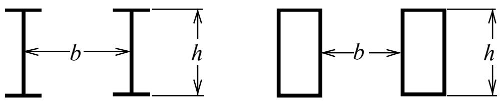

(a) Beams of Steel Structure (b) Beams of Box Type Structure

Fig. 2.3.3 Measurement of *b* and *h*

(b) Structural Standards for Mobile Crane

Article 9 of **Structural Standard for Mobile Crane**, specifies that the wind load shall be calculated as follows:

1) The value of the wind load can be calculated from **equation (2.3.1)**.

2) The velocity pressure can be calculated from **equation (2.3.2)**.

3) For the value of the wind pressure coefficient, it is possible to use the value found in the wind tunnel tests of the mobile crane that receives the winds or the value given in **Table 2.3.1** of **Section a) Structural Standard for Crane**. For the value of velocity pressure in W_3 calculation, the value from **equation (2.3.3)** shall be used.

4) The pressure-receiving area can be calculated by the method of **4)** in **Section a) Structural Standard for Crane**.

(c) Structural Standard for Derrick Crane

Article 11, **Structural Standard for Derrick Crane**, specifies that the wind load shall be calculated as follows:

1) The value of the wind load can be calculated from **equation (2.3.4)**. In this case the wind velocity is taken to be 50 m/s at the time of storms and 16 m/s at all other times.

$$W = qCA \tag{2.3.4}$$

where

W : wind load(N)

q : velocity pressure (N/m^2)

C : wind pressure coefficient

A : pressure-receiving area (m^2)

2) The wind velocity pressure can be calculated from **equation (2.3.5)**:

$$q = \frac{U^2}{30}\sqrt[4]{h} \tag{2.3.5}$$

where

q : velocity pressure (N/m^2)

U : wind velocity (m/s)

h : height (m) of the surface of the crane above the ground
(Use h = 15 m if the height is less than 15 m.)

3) For the value of the wind pressure coefficient, it is possible to use the value found in wind tunnel tests or the value given in **Table 2.3.2** for the type of surface and the area occupying ratio of the surface that receives the winds.

Table 2.3.2 Wind Pressure Coefficients for the Wind Load of a Derrick

Classification of the surface that receives the winds	Area occupying ratio	Wind pressure coefficient
Surfaces composed of horizontal lattices or horizontal trusses	$W_1 < 0.1$	2.0
	$0.1 \leq W_1 < 0.3$	1.8
	$0.3 \leq W_1 < 0.9$	1.6
	$0.9 \leq W_1$	2.0
Surfaces of structures composed of flat surfaces	-	1.2
Wire rope surfaces	-	1.2

Note: The value of the area occupying ratio is the value obtained by dividing the projected area of the surface of the crane by the area of the surface that receives the same winds.

4) The pressure-receiving area is the wind area projected onto a surface perpendicular to the direction of the winds. When there are two or more surfaces that overlap in the direction of the winds, it shall be calculated as follows;

The area subject to wind pressure calculation is determined by summarizing the following;

i. In case there are two overlapping surfaces that receive the winds

i) The projected area of the first surface in the direction of the winds

ii) The 60% areas of the portions of the second surface in the direction of the winds that overlap the first surface

iii) The projected areas of the portions of the second surface in the direction of the winds that don’t overlap the first surface.

ii. In case there are three or more surfaces that receive the winds

i) The area where three or more surfaces overlap receiving the winds

ii) 50% of the projected areas of the portions of the third and later surfaces in the direction of the winds that overlap the front surfaces

iii) The projected areas of the portions of the third and later surfaces in the direction of the winds that do not overlap the front surfaces

(3) The wind pressure that acts upon structures such as highway bridges and elevated highways shall be set as follows:

① The wind pressure that acts upon structures such as highway bridges and elevated highways can be specified according to the **Highway Bridge Specifications and Commentary**.[17)]

② In the **Highway Bridge Specifications and Commentary**, the wind load that acts upon a bridge is specified by appropriately considering the location, topography, and ground conditions at the bridge construction, the structural characteristics, and the cross-sectional shape of the bridge.

(a) Steel beams

Table 2.3.3 shows the wind pressure force on a steel beam per 1m long in the bridge axial direction for one span.

Table 2.3.3 Wind Load for Steel Beams (Units: kN/m)

Cross-sectional shape	Wind pressure force
$1 B/D < 8$	$\{4.0 - 0.2\,(B/D)\}D 6.0$
$8 B/D$	$2.4 D 6.0$

where

B = total width of the bridge (m) (see **Fig. 2.3.4**)

D = total height of the bridge (m) (see **Table 2.3.4**)

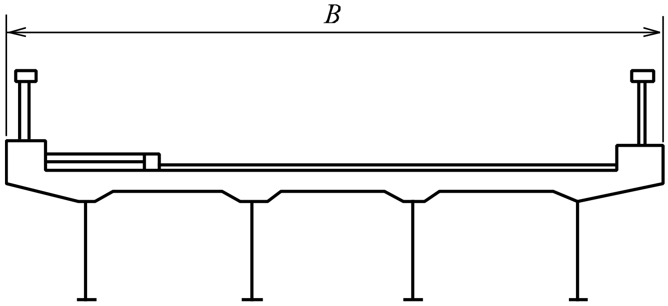

Fig. 2.3.4 Measurement of *B*

Table 2.3.4 Measurement of *D*

Bridge guard fence	Wall type rigid guard fence	Other than a wall type rigid guard fence
Measurement of *D*	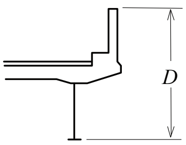	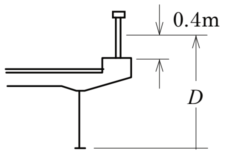

(b) Dual main truss

Table 2.3.5 shows the wind load on a dual main truss per 1 m^2 of the effective perpendicular projected area on the windward side. For a standard dual **main** truss, it is also possible to use the wind load shown in **Table 2.3.6** per 1 m of length of the arch material on the windward side in the bridge axial direction.

Table 2.3.5 Wind load on a Dual Main Truss (Unit: kN/m^2)

Truss	a live load	$1.25/\sqrt{\phi}$
	no live load	$2.5/\sqrt{\phi}$
Bridge foundation	a live load	1.5
	no live load	3.0
$0.1 \leq \phi \leq 0.6$ where ϕ = area occupying ratio of the truss (the ratio of the truss projected area to the truss enveloped area)		

Table 2.3.6 Wind load on a Standard Dual Main Truss (Units: kN/m)

Arch material		Wind load
Loaded arch	a live load	$1.5 + 1.5D + 1.25\sqrt{\lambda h} \geq 6.0$
	no live load	$3.0D + 2.5\sqrt{\lambda h} \geq 6.0$
Not loaded arch	a live load	$1.25\sqrt{\lambda h} \geq 3.0$
	no live load	$2.5\sqrt{\lambda h} \geq 3.0$

$7 \leq \lambda/h \leq 40$

where

D: total height of the bridge floor (m) (not including the height of the portion that overlaps the arch portion, as seen from the horizontal direction perpendicular to the bridge axis) (see **Fig. 2.3.5**)

h : height of the arch portion (m)

λ : main truss height (m) from the center of the lower arch portion to the center of the upper arch portion

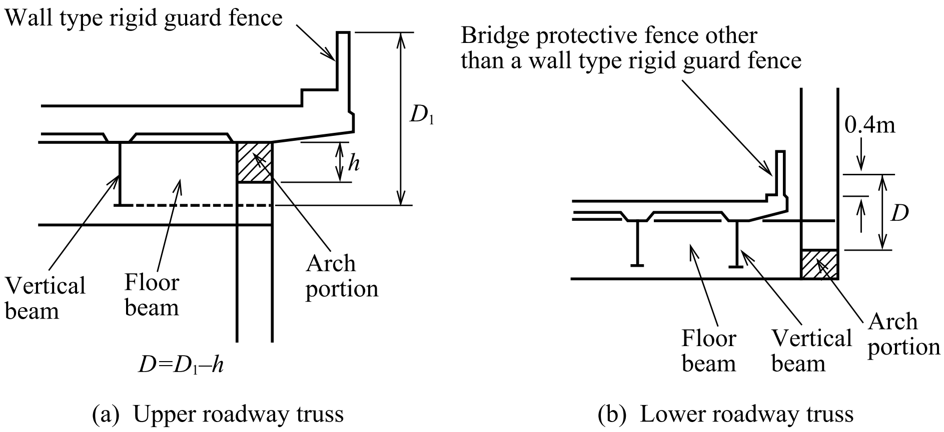

Fig. 2.3.5 Measurement of *D* for a Dual Main Truss

(c) Other types of bridges

Depending on the beam shape, either (a) or (b) shall be applied to obtain the wind load on other types of bridge beams. The wind load on members not described under (a) or (b) is given by the value in **Table 2.3.7** depending on the cross-sectional shape. When there is a live load, the wind load is taken to be 1.5 kN/m for the live load at a position 1.5 m from the bridge's upper surface.

Table 2.3.7 Wind Pressure Force Acting on Bridge Members Other than Steel Beams and Dual Main Trusses (Unit: kN/m^2)

Cross-sectional shape of members		Wind load	
		Members on the leeward side	Members on the windward side
Circular shape	a live load	0.75	0.75
	no live load	1.5	1.5
Polygonal shape	a live load	1.5	0.75
	no live load	3.0	1.5

(d) Parallel bridges

When the steel beams are parallel, appropriately correct the wind pressure force in **Table 2.3.3** by considering the effect of the parallel beams.

(e) The wind load that acts directly on the lower portion of the structure is taken to be a horizontal load that is either perpendicular or parallel to the axial direction of the bridge. It is assumed that it does not act simultaneously in both directions. The magnitude of the wind load shall be the value shown in **Table 2.3.8** for the effective vertical projected area in the wind direction.

Table 2.3.8 Wind load Acting on the Lower Portion of the Structure (Unit: kN/m^2)

Cross-sectional shape of the body		Wind load
Circular or elliptical shape	a live load	0.75
	no live load	1.5
Polygonal shape	a live load	1.5
	no live load	3.0

2.4 Meteorological Observations and Investigations

(1) Overview

Facilities subject to the Technical Standards must be designed to have the required performance with regard to natural phenomena, such as strong winds. Therefore, in the performance verification of the facilities, it is necessary to examine items relevant to that purpose by observing meteorological elements or conducting numerical simulations.

A meteorological investigation includes various methods such as statistical analysis of past data, analysis through numerical simulations, and on-site meteorological observations. Furthermore, it is necessary to formulate a plan by generally considering the following items of ① to ⑥ to determine which methods are desirable: See **Reference (Part II), 2.2 Meteorological Observation and Examination** for details.

① Determination of the required meteorological elements

② Necessity for real-time on-site meteorological data

③ Possibility to obtain meteorological observation data from the past

④ Possibility to use observational data from the closest meteorological stations or the AMeDAS observation stations

⑤ Necessity for numerical simulations

⑥ Necessity for on-site meteorological observations

Based on these investigation results, determine which of the following methods to use in order to specify the natural conditions:

① Statistical analysis of past data

② Analysis by numerical simulations

③ On-site meteorological observations

(2) Meteorological Observations

Meteorological observations aim to measure the atmospheric conditions in physical ways and clarify the structure and mechanism of atmospheric phenomena. It is important as a means to clarify the meteorological conditions of the points concerned. If the situation at the site permits, it is desirable to do fundamental on-site meteorological observation rather than relying on the numerical simulation. Proper meteorological observation equipment shall be selected by setting meteorological items to be considered in the design and performance verification of the facilities subject to the Technical Standards.

Meteorological observation points and points to note for facilities are indicated below:

① It is desirable that the observation points are the locations where the observation results obtained there represent the area. Therefore, it is necessary to select a flat and open place for installing instruments and to avoid tall building or topographic valleys, which may affect the observation results.

② The names, latitude, longitude, land elevation, altitude above the ground where instruments are installed, and other items of the observation points need to be clarified.

③ When observing the precipitation, temperature, and humidity, it is desirable to have the observation field. The observation field shall be flat and open, and turf grass shall be planted on horizontal ground not shaded by buildings and surrounded by airy fence.

The Guides for Meteorological Observation[18)] and the Commentary on Statistics of Meteorological Observation [19)] published by the Japan Meteorological Agency may be used as a reference for meteorological observation methods, type and structure of instruments, handling method of instruments, processing and statistical methods of observation data, etc.

(3) Meteorological Simulation

As described in **Part II, Chapter 2, 2.1 General (4)**, the meteorological simulation using a numerical model (mesoscale meteorological model) may be conducted to hindcast a meteorological field required for the hindcasting of waves and storm surge, particularly in the inner bay area. On the contrary, the eddies of wind around high buildings in urban areas where many high-rise buildings appear may become a social problem as a smaller-scale meteorological phenomenon. The generating mechanism of these eddies of wind around high buildings is the obstruction of the fast flow in the upper air by the building, and a positive pressure area and negative pressure area appear around the building; therefore, strong wind flows from the positive pressure area to the negative pressure area.[20)]

The same influence may be considered when building facilities subject to the Technical Standards. Therefore, it is desirable to understand the influence that the facilities exert to the meteorological environment beforehand with the meteorological numerical simulation when planning large facilities. k-ε model or large eddy simulation model is available as a simulation model that can consider up to turbulence around the building in such a small scale as eddies of wind around high buildings and is often used for the examination of influence of strong wind around facilities.[21)–23)]

As described above, it is necessary to use a simulation model that corresponds to the meteorological phenomenon concerned in the meteorological simulation. It is desirable to apply these simulation models to individual verification cases after validating accuracy and reliability with actual observation values.

(4) Obtaining of Weather Prediction and Weather Information

It is desirable to obtain locally predicted information such as wind (strong wind), precipitation, fog (visual range), in addition to generally available weather information to improve construction efficiency and avoid disaster in large-scale port and harbor construction. This type of information[24)] is instantly available on the Internet and other media.

[References]

1) Nagai, T., K. Sugahara, K. Sato and K. Kawaguchi: Characteristic of Japanese Coastal Wind Power based on Long Term Observation, Technical Note of PHRI, No.999, p.59, 2001 (in Japanese)

2) Nagai, T: Observed Offshore Wind Characteristics from a View of Energy Utilization, Technical Note of PHRI, No.1034, p.34, 2002 (in Japanese)

3) Takahashi, K: Study on quantitative weather forecasting based on extrapolation (Part 1), Study Bulletin No. 13, 1947 (in Japanese)

4) Fujita,T: Rep. Met. Lab., Kyushu Inst. Tech., Vol.2, No.1-2, 1952.

5) Myers,V.A. and Malkin, W.: Some properites of hurricane wind fields as deduced from tralectores, U.S. Weather Bureau, National Hurricane Research Project, Report 49, 1961.

6) Mesoscale and Microscale Meteorology Division National Center for Atmospheric Research: PSU/NCAR Mesoscale Modeling System Tutorial Class Notes and User’s Guide MM5:Modeling System Version 3, 2015.

7) The National Center for Atmospheric Research: WRF-ARW V3:User's Guide, 2017.

8) Kawaguchi, K. and H. Kawai: Estimation of wind and wave during typhoon based on mesoscale model, Technical Note of PARI, No.1169, 19p, 2007 (in Japanese)

9) Kawai, H and K. Kawaguchi: Applicability of typhoon bougus and mesoscale model to simulation of storm surge in bays, Report of PARI, Vol.46, No.3, pp.43-86, 2007 (in Japanese)

10) Nagai, T., H. Ogawa, A, Nakamura, K. Suzuki and T. Nukada: Characteristics of occurrence of offshore wind energy based on observation data, JSCE Proceedings of Coastal Eng,. ,pp.1306-1310, 2003 (in Japanese)

11) Nagai, T, I. Ushiyama, Y. Nemoto, K. Kawanishi, T. Nukada, K. Suzuki and T. Otozu: Examination of field application of lighting system utilizing coastal wind force, Journal of the Japan Society for Marine Survey and Technology Vol. 17 No. 1, JSMST, 2005 (in Japanese)

12) Shiraishi, S., K. Shimosako, H. Yoneyama, I. Ushijima, Y. Nishizawa, M. Hosomi, R. Ogawa and T. Nagai: Wind power utilization at port facilities and future view of smart energy system in ports, Journal of Japan Society of Civil Engineers, Ser. B3 (Ocean Engineering), Vol.70, No2, pp.I_121-I_126, 2014 (in Japanese)

13) Ministry of Land, Infrastructure, Transport and Tourism Port Authority and Ministry of the Environment Global Environment Bureau: Wind power generation at ports -Manual for symbiosis with port management and operation-, 104p, 2012 (in Japanese)

14) Japan Meteorological Agency, Catalogue of annual maximum wind speed (1929-1966) at various places in Japan and the probability of occurrence, Meteorological Agency observation Technical Note No. 34, 1971 (in Japanese)

15) JSCE, Civil Engineering Handbook, Giho-do Publications, 1974, pp. 541-544 (in Japanese)

16) Industrial Health Division, Industrial Safety and Health Dept., Labour Standards Bureau, Ministry of Health, Labour and Welfare: Commentary of structural standards of various types of cranes (Revision 3), Japan Crane Association, 2015 (in Japanese)

17) Japan Road Association: Specifications and commentary of highway bridges, Part I General and Part II Steel Bridge, 2012 (in Japanese)

18) Japanese Meteorological Agency: Guides for Meteorological Observation, http://www.jma.go.jp/jma/kishou/know/kansoku_guide/tebiki.pdf, 81p, 2007 (in Japanese)

19) Japanese Meteorological Agency: Commentary on Statistics of Meteorological Observation, http://www.data.jma.go.jp/obd/stats/data/kaisetu/,2016 (in Japanese)

20) Kiyohide Takeuchi: Wind meteorology, University of Tokyo Press, p.172, 1997 (in Japanese)

21) Nagai T., H. Ogawa, A. Nakamura, Y. Suzuki and K. Nukada: Appearance characteristics of coastal wind energy based on observation data, JSCE Proceedings of Coastal Engineering, Vol.50, pp.1306-1310, 2003 (in Japanese)

22) Nagai, T, I. Ushiyama, Y. Nemoto, K. Kawanishi, T. Nukada, K. Suzuki and T. Otozu: Examination of field application of lighting system utilizing coastal wind force, Journal of the Japan Society for Marine Survey and Technology Vol. 17 No. 1, JSMST, pp.1-12, 2005 (in Japanese)

23) Architectural Institute of Japan: Evaluation and planning of urban wind environment, Maruzen Publishing, p.208, 1993 (in Japanese)

24) Eguchi, I., K. Okada, T. Nakata, Y. Uchida, K. Kubota and Y. Utsunomiya : Improvement of the coastal oceanographic and meteorological information system, Journal of Japan Society of Civil Engineers, Ser. B3 (Ocean Engineering), Vol.70, No2, pp.I_61-I_66, 2014 (in Japanese)

3 Tide Level

[Public Notice] (Tidal Level)

Article 7

The tidal level shall be appropriately specified as the water level relative to a datum level for port and harbor management through the statistical analysis of measured values or estimated values and/or others by taking into account the astronomical tides, meteorological tides, wave setup (rise of water level by waves near the shore), and abnormal tidal levels due to tsunamis and others.

[Interpretation]

7. Setting the Environmental Conditions and Other Conditions

(2) Requirements for Tidal Level (Article 6 of the Ministerial Ordinance and the interpretation related to Article 7 of the Public Notice)

① **Tide level**

When specifying the tide level for the performance verification of the facilities subject to technical standards, appropriately consider how the tide level affects the action of waves and water pressure. Furthermore, when specifying the combination of tide level and waves in the performance verification of the facilities, take as a standard the tide level that would be the most dangerous among the tide levels that have a high likelihood of occurring simultaneously with waves from the viewpoint of the performance verification of such facilities.

② **Astronomical tides**

With regard to astronomical tides that are considered in the specification of the tide level, take as a standard the specification of chart datum level (C.D.L.), mean sea level (M.S.L.), mean monthly highest water level (H.W.L.), and mean monthly lowest water level (L.W.L.) on the basis of measured values for one year or more.

③ **Storm surge**

With regard to storm surges that are considered in the specification of the tide level, take as a standard the observation values for 30 years or more, hindcasted values of storm surges caused by the past largest or more typhoons or cyclones, past disaster records, etc. In storm surge hindcasting, wave step-up due to wave breaking near the shore shall be appropriately considered as necessary.

3.1 Astronomical Tides

(1) Definitions[1) 2) 3)]

Astronomical tides are tides produced by the gravity of the moon and sun and can be viewed as a super-imposition of components known as tidal constituents. The definitions for the representative types of water level are as follows:

① **M.S.L.**

The average height of the sea level over a certain period is referred to as the M.S.L. for that period. For practical purposes, the M.S.L. is taken to be the average of the water level over one year.

② **C.D.L.**

The standard water level obtained by subtracting the sum of the amplitudes of the four principal tidal constituents (M_2, S_2, K_1, and O_1) from the M.S.L.. This is used as the standard for water depth in nautical charts.

③ **Mean monthly H.W.L.**

The average of the monthly H.W.L., where the monthly H.W.L. for a particular month, is defined as the H.W.L. occurring in the period from 2 days before to 4 days after the day of the lunar syzygy (new moon and full moon).

④ **Mean monthly L.W.L.**

The average of the monthly L.W.L., where the monthly L.W.L. for a particular month, is defined as the L.W.L. occurring in the period from 2 days before to 4 days after the day of the lunar syzygy.

⑤ **Mean high water level (M.H.W.L.)**

This is the mean value of all H.W.L.s, including the spring tide and neap tide.

⑥ **Mean low water level (M.L.W.L.)**

This is the mean value of all of low water levels, including the spring tide and the neap tide.

⑦ **Near highest high water level (N.H.H.W.L.)**

The water level obtained by adding the sum of the amplitudes of the four principal tidal constituents (M_2, S_2, K_1, and O_1) to the MSL.

⑧ **High water of ordinary spring tides (H.W.O.S.T.s)**

This is the water level obtained by adding the sum of an amplitude of the tidal constituents M_2 and S_2 to the M.S.L.. The height of the H.W.O.S.T. as measured from the chart datum is known as the spring rise.

⑨ **Low water of ordinary spring tides (L.W.O.S.T.s)**

This is the water level obtained by subtracting the sum of an amplitude of the tidal components M_2 and S_2 from the M.S.L..

⑩ **M.S.L. of Tokyo Bay (T.P.)**

The M.S.L. for Tokyo Bay was determined during the Meiji period from tidal level observations. Since then, T.P. has become the standard for measuring altitude in Japan. The bench mark is located in Nagata-cho, Chiyodaku, Tokyo. Incidentally, T.P. does not correspond to the present day M.S.L. of Tokyo Bay.

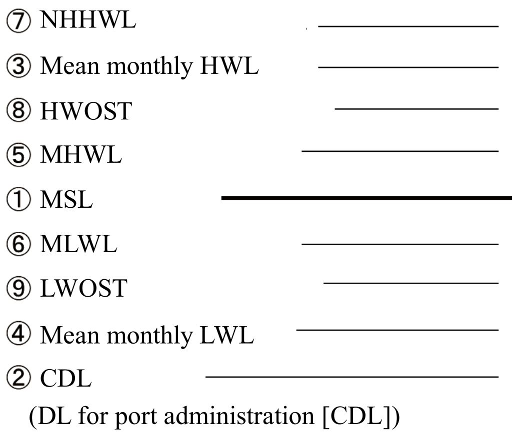

Fig. 3.1.1 Datum Level (DL) of Tidal Levels

There are four principal tidal constituents, namely, the M_2 tide (the principal lunar semidiurnal component of tides, period = 12.421 hours), the S_2 tide (the principal solar semidiurnal component of tides, period = 12.00 hours), the K_1 tide (the luni-solar diurnal component of tides, period = 23.934 hours), and the O_1 tide (the principal lunar diurnal component of tides, period = 25.819 hours). Moreover, Z_0 is defined as the plane with a lower sum of amplitudes of four principal tidal constituents, namely, M_2, S_2, K_1, and O_1, than the MSL.

Fig. 3.1.2[2)] shows the relation between tide levels ①, ③, ④, and ⑩ and other regularly used various tide levels at the Tokyo (Harumi) tide observatory as an example. Given that similar D.L. names are used for the D.L.s of tide levels, such as tide level table D.L., observation D.L. (O.D.L.; D.L. may be used as an abbreviation of datum line), C.D.L., DL for port administration (nautical C.D.L.), it is necessary to confirm to the corresponding D.L. of the tide level. The D.L. for port administration shall be the same value as the C.D.L. so that the nautical chart matches the port facilities, but they do not necessarily coincide with the observed value. When a significant difference becomes apparent, it shall be amended through discussions with the Japan Coast Guard. See **Reference (Part II), 2.3 Observation and Examination of Tidal Levels** for details.

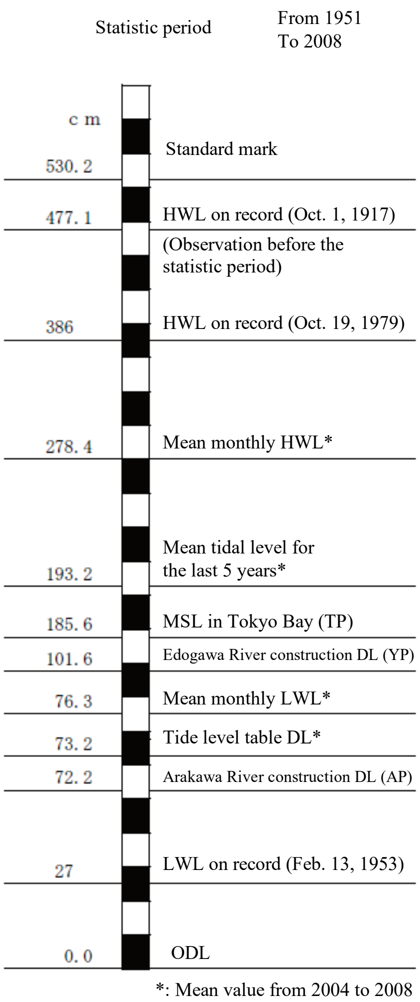

Note: YP (Edogawa River construction DL) is -0.84 m from TP (Tokyo MSL) as a reference, AP (Arakawa River construction DL) is -1.134 m.

Fig. 3.1.2 Actual Status Values of Tide Level in the Tokyo (Harumi) Tide Observatory[2)]

(2) Seasonal and Annual Changes in Mean Water Level[3)]

The mean water level for each month varies over the year owing to factors such as the ocean water temperature and atmospheric pressure distribution near the Japanese islands. In many places, the mean water level can vary by ±5 to 20 cm over the years. Along the Japanese coast, it is typically higher in the summer and lower in the winter.

The annual mean water level is also affected by factors such as the ocean water temperature and atmospheric pressure distribution for that year, and there may be variations of ±10 cm depending on the ocean region.

(3) Occurrence Probability Distribution of Astronomical Tidal Levels[4)]

Astronomical tidal levels have repeated high tides and low tides approximately twice per day and repeated highest tides and lowest tides approximately twice per month. The shape of the occurrence probability distribution of these astronomical tidal levels varies with location, and the tide levels that have the highest probability of occurrence are the tidal levels that are close to the M.S.L.. By contrast, the occurrence probability of high tide levels (e.g., the mean monthly H.W.L.) or low tide levels (e.g., the mean monthly L.W.L.) are small.

3.2 Storm Surge

(1) Definitions

In addition to the astronomical tides caused by the gravity of the moon and sun, the height of the ocean surface can change because of factors such as changes in atmospheric pressure and winds accompanying the passage of low atmospheric pressure systems (including typhoons, hurricanes, and cyclones) and high atmospheric pressure systems. These meteorological changes of the sea surface are called meteorological tides, and the difference between the measured tidal level and the forecasted astronomic tidal level is called the tidal level anomaly. In particular, among meteorological tides, the rise of tidal level due to the passage of a typhoon or low atmospheric pressure system is called a storm surge.

(2) Causes of Storm Surge

If the atmospheric pressure at the sea surface is lowered by 1 hPa for a sufficiently long time so that the sea surface is in equilibrium with the atmospheric pressure at the sea surface, the ocean surface rises by approximately 1 cm higher than the normal level. If the winds blow at a constant velocity for a long time from the mouth of an internal bay toward the innermost of the bay so that the sea surface rises toward the innermost of the bay and reaches equilibrium, the amount of sea level rise at the furthest point inside the bay is roughly proportional to the square of the wind velocity; furthermore, the amount is also larger when the bay is longer or shallower. During an actual typhoon, the atmospheric pressure, wind velocity, and wind direction on the sea surface changes in a complicated manner at different locations and times.

(3) Past Storm Surges

Table 3.2.1 shows the typical storm surges observed in tide observatories along Japan's shores. Tidal levels of 2 m or more have been observed on the Pacific and East China Sea coasts. The highest tidal level was 3.5 m, which occurred in the Port of Nagoya during the Ise Bay Typhoon in 1959. Furthermore, although it is not included in this table, significant tidal levels were recorded in the Yatsushiro Sea and Kagoshima Bay.[3), 5)] Moreover, tidal levels in storm surge due to extratropical cyclones, which were higher than those due to typhoons, have been observed in Hokkaido, Tohoku District, and Hokuriku District since 2003.[6)] Therefore, storm surges due to extratropical cyclones shall also be properly considered in these areas.

Even in the same sea area, the tidal level differs place by place and depends on the location of a tide observatory that does not necessarily show the highest tidal level in that sea area. For example, an on-site observation reveals that some shores in the northern Yatsushiro Sea experienced a 3.9 m tidal level by Typhoon #9918 (the 18th typhoon in 1999).[7)] Furthermore, where the coast line significantly changed from the past owing to reclamation and the like, another typhoon with a condition that is identical with a past typhoon provides different tidal levels from the past.

Table 3.2.1 Major Storm Surges with 2 m or Higher Instantaneous Highest Deviation Observed in 1900–2016 (Japan Meteorological Agency,[3)] revised)

Month/Day/Year	Location	Highest deviation (m)	Cause
10/1/1917	Tokyo Bay	2.1Ext	Typhoon
7/18/1930	Ariake Sea	2.5Ext	Typhoon
9/21/1934	Osaka Bay	3.1 Ext	Muroto Typhoon
9/1/1938	Tokyo Bay	2.2 Ext	Typhoon
9/3/1950	Osaka Bay	2.4	Jane Typhoon
8/17/1956	Ariake Sea	2.4 Ext	Typhoon #5609
9/26/1959	Ise Bay	3.5	Ise Bay Typhoon
9/21/1961	Osaka Bay	2.5	Daini Muroto Typhoon
9/25/1964	Osaka Bay	2.1 Ext	Typhoon #6420
9/10/1965	Eastern Setonaikai Sea	2.2	Typhoon #6523
8/21/1970	Tosa Bay	2.4 Est	Typhoon #7010

Month/Day/Year	Location	Highest deviation (m)	Cause
9/16/1972	Ise Bay	2.0	Typhoon #7220
9/27/1991	Ariake Sea	2.7	Typhoon #9119
9/17/1995	Hachijo Is.	3.4	Typhoon #9512
9/22/1996	Hachijo Is.	2.9	Typhoon #9617
9/24/1999	Suonada Sea	2.1 Ext	Typhoon #9918
7/8/2000	Hachijo Is.	2.5	Typhoon #0003
10/1/2002	Hachijo Is.	2.4	Typhoon #0221
9/7/2004	Ariake Sea	2.1	Typhoon #0418
9/7/2004	Western Setonaikai Sea	2.1	Typhoon #0418
10/20/2004.	Tosa Bay	2.5	Typhoon #0423

No marks: from a document of the tide observatory operated by the Japan Meteorological Agency; Est: Estimated value; Ext: from a document of the tide observatory not controlled by the Japan Meteorological Agency

(4) Empirical Formula to Predict Storm Surge

The tide anomaly due to a typhoon can be roughly estimated from an empirical formula, such as **equation (3.2.1)**.[3)]

$$\zeta = a(p_0 - p) + bW^2 \cos\theta + c \tag{3.2.1}$$

where

ξ : tide anomaly (cm)

p_0 : reference atmospheric pressure (1010 hPa)

p : lowest atmospheric pressure at the target location (hPa)

W : maximum value of the mean 10-minute wind velocity at the target location (m/s)

θ : angle between the main wind direction for the bay and that of the maximum wind velocity W

a, b, c : constants determined from past observational results at the target location

(5) Numerical Calculation of Storm Surge

A numerical calculation is conducted to analyze the phenomenon of storm surge in more detail. In this numerical calculation, items such as the atmospheric pressure that acts on the sea surface, the frictional stress on the sea surface due to winds, the frictional stress that acts on the currents at the sea bottom, and the eddy viscosity of the sea water are taken into consideration, and the changes in tidal level and flux at the grid points are calculated at each time step from the time the typhoon approaches until it passes.[8)] The topography is approximated using a grid with a spacing of several hundred meters or finer than that and the water depth is given at each grid point. The distributions of the atmospheric pressure and the wind velocity of the typhoon are calculated from the central (atmospheric) pressure, the radius of the maximum wind velocity, and the forwarding speed of the typhoon. The MASCON model that considers influence of the onshore topography on the wind fields, or the local meteorological model that can reproduce complicated pressure and the wind fields may be applied in the calculations.[9)] Furthermore, numerical models that consider density layers and water discharge from rivers have been developed, as well as models that do not consider storm surge, astronomical tides, and waves as independent phenomena but rather consider them together with their interactions.[10), 11), 12), 13)] (**Fig. 3.2.1**) There are various models for the numerical calculation of storm surge; therefore, an appropriate calculation method that sufficiently reproduces storm surges in the target sea region shall be employed.

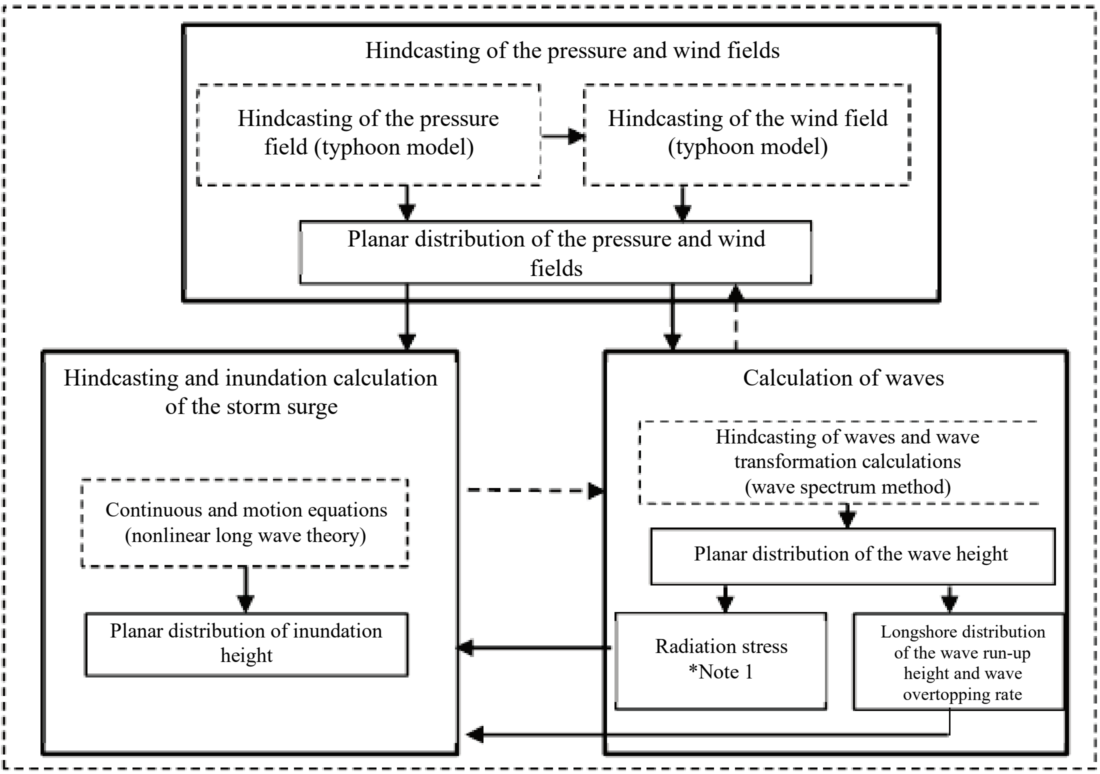

*Note 1: Radiation stress: required when calculating the tide level and considering the wave setup.

*Note 2: Dotted arrows are limited to cases wherein interactions can be considered such as integrated models.

Fig. 3.2.1 Flow of the Numerical Calculation of Strom Surge Due to a Typhoon[6)]

(6) Storm Surge and Astronomical Tides

A storm surge is caused by meteorological disturbances, such as typhoons, whereas astronomical tides are caused mainly by the gravity of the moon and sun. Considering that storm surges and astronomical tides are phenomena with independent causes each other, the time of maximum tide anomaly due to storm surges might overlap either the astronomical high tide or the low tide. In particular, the astronomical tide range is large at internal bays in the Seto Inland Sea and along the coast of the East China Sea; therefore, even if a remarkable tide anomaly occurs, severe damage is unlikely to occur at astronomical low tide. When specifying the design tidal level so that one does not overlook such a superimposition of storm surge and astronomical tide, one should not only consider the tidal level obtained by combining the storm surge with the astronomical tide, but also one should consider the characteristics of the occurrence of tide anomalies due to the storm surge.

(7) Coincidence of Storm Surges and High Waves

A storm surge in an internal bay mainly occurs owing to the suction effect of depression and wind setup effect. The suction effect usually predominates at the bay mouth, and the tide anomaly reaches the maximum value when a typhoon is closest and when the atmospheric pressure has decreased the most. The wind setup effect often predominates at the bay innermost; therefore, the tidal level anomaly is the greatest when the typhoon winds are blowing from the bay mouth toward its innermost. On the contrary, waves are not directly related to the suction effect but develop owing to winds; furthermore, their propagation is affected by the bathymetry in shallow sea areas. Waves are also affected by the surrounding bathymetry and can easily be sheltered by capes or islands. Considering that a storm surge differs from waves, the peak of the tide anomaly and the peak of the waves may not occur simultaneously depending on the track and location of the typhoon within the bay.[14]

(8) Rise of Mean Water Level due to Waves Breaking

In the surf zone, regardless of whether the sea level is being drawn up by depression or wind setup effect, the mean water level increases due to wave breaking, and there is a long period of oscillation. As part of this process, the increase in the mean water level is called the wave setup. The amount of increase depends on factors such as the slope of the sea bottom and the steepness of the incident waves. It tends to be larger near the shoreline and may be 10% or more of the significant wave height offshore (see **Part II, Chapter 2, 4.4.8 Rise of Mean Water Level Due to Waves and Surf Beats**). Therefore, at the shore that is directly hit by waves, the absolute increase amount of mean water level is large; this is also an important factor of tide anomaly.

For example, a study of several typhoons revealed that the tidal level observed in the Minami-izu tide observatory cannot be explained by the storm surge numerically calculated by considering only the depression and wind setup; the rise of water level due to wave breaking need to be considered.[15), 16] Moreover, it is considered that approximately half of the tidal level in Tosa Bay caused by Typhoon #7010 listed on **Table 3.2.1** was attributable to the rise of mean water level due to wave breaking.[17]

For the performance verification of facilities in the surf zone, it is necessary to consider the rise of the mean water level due to wave breaking and oscillation; however, the calculation formulas and diagrams for factors such as wave height in surf zone, wave force, and wave overtopping rate usually include the effect of rise of the mean water level. Therefore, it is not necessary to separately add the amount of rise of mean water level into the design tidal level. However, in areas where reefs form a large increase in water level of 1 meter or more, it is preferable to include the rise of mean water level in the tidal level for the purpose of performance verification in such locations.

3.3 Harbor Resonance

(1) Definition

Harbor resonance is a phenomenon of resonance on the sea surface in a closed or semi-closed water area, bay, or strait. The period of resonance is up to several tens of minutes and differs according to the topography of the water area (depth and size). Generally, the sea level change occurs due to ocean disturbance owing to meteorological disturbance such as typhoons, cyclones, and others or tsunamis resonates with the natural frequency in the bay and becomes harbor resonance.

Harbor resonance is divided into two main types: One occurs within a bay owing to the suction effect of the depression and wind setup effect due to a typhoon. This phenomenon is called seiche, which is characterized by free waves propagating independently in the meteorological field. **Fig. 3.3.1** shows the observed records of tidal level in Tokyo Bay during Typhoon #0115, when remarkable seiche occurred (shown by the triangles [▽]).

The other is the type of oscillation forced in a bay or harbor owing to waves from the outer ocean and their accompanying long-term water level variations and currents. This type of oscillation can cause a large resonance with an oscillation period that is unique for the shape and size of the bay or harbor. In particular, remarkable harbor resonance often occurs in places wherein the shape is long and narrow, such as an artificially excavated port, and wherein the water area is surrounded by facilities with a high reflection coefficient, such as quaywalls,

The period for harbor resonance is usually from several minutes to several tens of minutes, and the amplitude may reach several tens of centimeters. Nagasaki Bay has shown amplitudes of approximately 2 meters. Even though the vertical variational amplitude due to harbor resonance may only be several tens of centimeters, the current velocity in the horizontal direction is large; therefore, this can be a significant problem for ship mooring and cargo handling operations. Component waves with a period of 30 to 300 seconds in the frequency spectrum analyzed from continuously observed records for 20 minutes or more, are defined as long-period waves (for long-period waves, see **Part II, Chapter 2, 4.5, Long-Period Waves**).

Therefore, it is necessary to know the natural frequency period of a port for the performance verification of port facilities. Unoki[18] studied the characteristics of harbor resonance in the major ports of Japan. It is also possible to numerically estimate the amplification factor in a harbor resonance to the incident waves with the period of several minutes to an hour.[19]

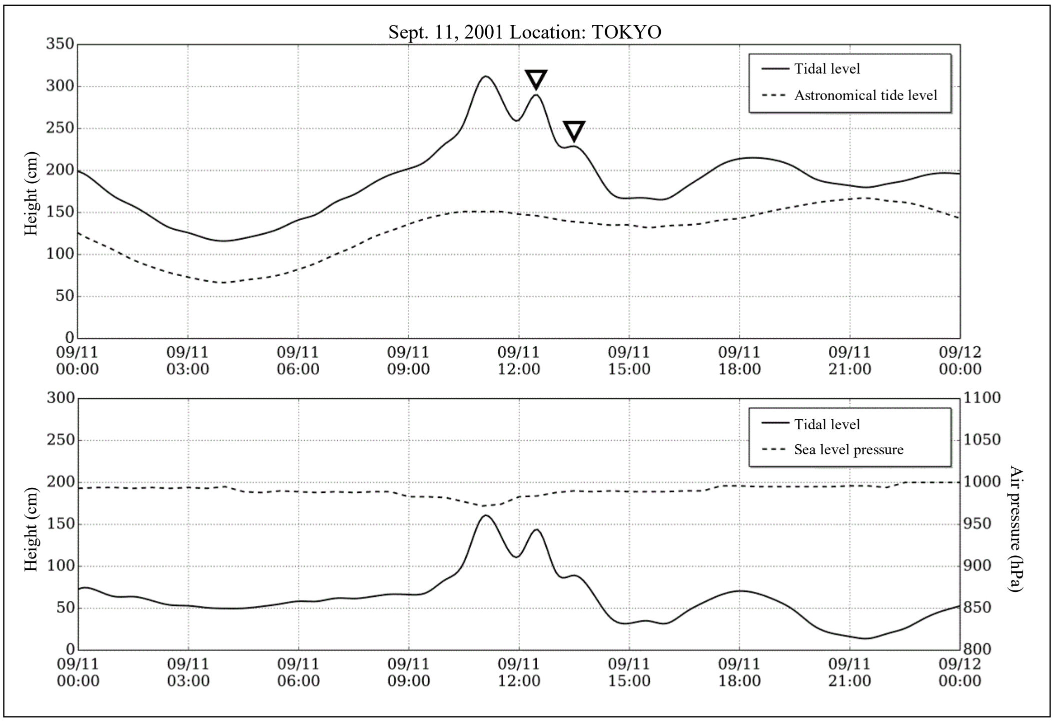

Fig. 3.3.1 Tidal Level Observational Recordings during Typhoon #0115

(2) Harbor Resonance Periods

For harbors that can be modeled in a simple shape, their natural frequency period and amplitude amplification ratio can be found by theoretical calculations. However, the shapes and boundary conditions of actual harbors are extremely complicated; therefore, it is preferable for their natural frequency periods and amplitude amplification ratios to be found by on-site observations or numerical calculations.[19] For reference, formulas for the natural frequency periods in the simplest cases are given as follows:

① Rectangular harbor of constant depth (surroundings are closed and no water enters or leaves; **Fig. 3.3.2(a)**):

$$T = \frac{2l}{m\sqrt{gh}} \tag{3.3.1}$$

where

T : natural frequency period (s)

l : length of the water surface (the longitudinal direction) (m)

m : mode of the oscillation (1, 2, 3, ...)

g : gravitational acceleration (9.8 m/s^2)

h : water depth (m)

② Rectangular harbor of constant depth (water can freely enter and leave in one place, and the harbor is narrow and long; **Fig. 3.3.2(b)**):

$$T = \frac{4}{2m+1}\frac{l}{\sqrt{gh}} \tag{3.3.2}$$

The amplitude amplification ratio often takes its maximum when m is zero or one; therefore, in practice, it is acceptable to investigate just this case. In reality, the sea waters within the harbor and in the outer ocean near the harbor entrance oscillate to some extent; therefore, the natural period becomes somewhat longer than that given by **equation (3.3.2)** and becomes closer to the value given by **equation (3.3.3)**[20]:

$$T = \alpha\frac{4l}{\sqrt{gh}} \tag{3.3.3}$$

where

l : longitudinal length of a harbor (m)

α : harbor entrance modification coefficient (**equation (3.3.4)**):

$$\alpha = \left\{1 + \frac{2b}{\pi l}\left(\frac{3}{2} - \gamma - \ln\frac{\pi b}{4l}\right)\right\}^{1/2} \tag{3.3.4}$$

where

π : ratio of the circular constant

b : width of a harbor (m)

γ : Euler–Mascheroni constant (= 0.5772)

Table 3.3.1 shows the values of the harbor entrance modification coefficient α for the representative values of b/l, as calculated from **equation (3.3.4)**.

Table 3.3.1 Harbor Entrance Modification Coefficients

b/l	1	1 / 2	1 / 3	1 / 4	1 / 5	1 / 10	1 / 20
α	1.320	1.261	1.217	1.186	1.163	1.105	1.064

③ Rectangular harbor of constant depth (water can freely enter and leave in one place, and the harbor entrance is narrow; **Fig. 3.3.2 [c]**):

$$T = \frac{2}{\sqrt{gh\left\{\left(\frac{m}{l}\right)^2 + \left(\frac{n}{b}\right)^2\right\}}} \tag{3.3.5}$$

where

b : width of a harbor (m)

l : length of a harbor (m)

n : number of nodes in the width direction of a harbor (n = 0, 1, 2, ...)

In actual cases, the natural period has a somewhat smaller value than that calculated from **equation (3.3.5)** because of the effect of the harbor entrance.

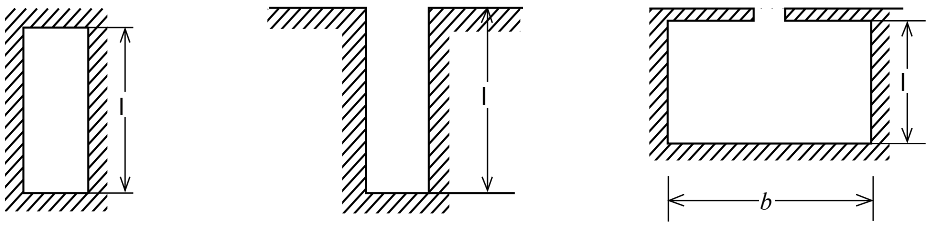

Fig. 3.3.2 Models of Harbor Shapes

(3) Amplitude

The amplitude of harbor resonance is determined by the amplification ratio to the incident long wave. As the period of the incident wave is closer to the natural period of the harbor, the phenomena of harbor resonance become clearer and more severe; therefore, the amplification ratio takes a high value. The large amplification of the resonance causes very strong currents around the narrow harbor entrance. The strong current induces the sea bottom friction, disturbed waves and eddies at the harbor entrance. Consequently, these friction, waves and eddies cause some amount loss of energy. As a result, the amplitude of the harbor resonance does not increase without any limitations. A harbor resonance with small amplitude still forms even if the period of the action is different from the natural period of the harbor.

If the width of the harbor entrance is narrowed to increase the calmness inside the harbor, it may instead make harbor resonance more likely to occur. This phenomenon is called the harbor paradox. When the shape of the harbor is changed, such as by extending the breakwaters, one must be careful not to cause a remarkable harbor resonance.

If the energy loss at the harbor entrance is neglected, the amplitude amplification ratio R at the inside corners of a rectangular harbor can be calculated from the ratio of the length of the harbor to the wavelength by using **Figs. 3.3.3**[21)] and **3.3.4**.[21)] These figures show that resonance occurs at relatively shorter harbor lengths in a wide port than narrow one. In **Fig. 3.3.4**, the resonance points are roughly the same as the resonance points for a completely closed rectangular shaped lake, as approximated by **equation (3.3.6)**:

$$\frac{l}{L} = \sqrt{m^2 + \frac{n^2}{\left(\frac{2b}{l}\right)^2}} \qquad m, n=0, 1, 2, \cdots \tag{3.3.6}$$

where

L : wave length (m)

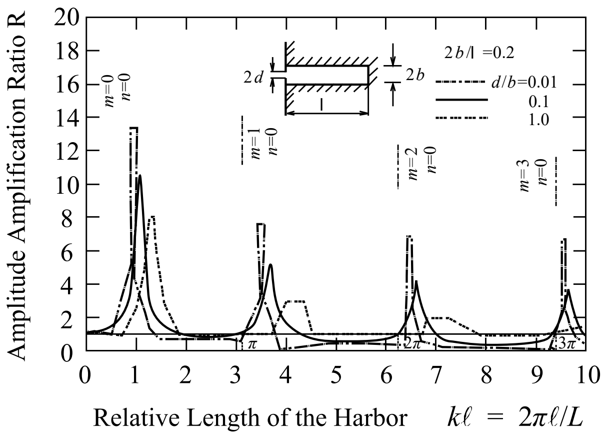

Fig. 3.3.3 Resonance Spectrum for a Long and Narrow Rectangular Harbor[21)]

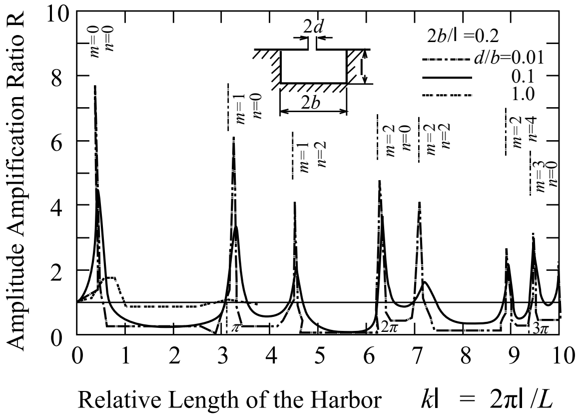

Fig. 3.3.4 Resonance Spectrum for a Wide Rectangular Harbor[21)]

(4) Countermeasures against Harbor Resonance

Harbor resonance is the phenomenon whereby long-period waves penetrate into a harbor from the entrance, repeat perfect reflection inside the harbor, and increase their amplitude. To hold down the amplitude of harbor resonance, it is necessary to minimize the reflectance around the inner perimeter of the harbor or alter the shape of the harbor to reduce resonance generation or to increase the energy loss within the harbor. Therefore, it is not advisable to build upright quaywalls around the whole perimeter of a harbor. If a permeable rubble-mound breakwater with a gentle slope is built, wave reflection can be reduced. Furthermore, one can expect a certain energy loss on a sloping breakwater. By installing an inner breakwater close to the position of a node of the harbor resonance, the amplitude of the harbor resonance can be reduced. Regarding the shape of the harbor, it is considered that an irregular shape is better than a geometrically regular shape.

3.4 Abnormal tidal levels

(1) Causes of Abnormal Tidal Levels

In addition to the storm surge caused by typhoons and tsunamis, various other reasons can be given for abnormal tide generation, such as current variations of the Kuroshio current, rise of the ocean water temperature due to the influx of warm water, and the long-term continuation of westward wind-driven currents.[22)] Abnormal tidal levels may continue from several days to several months, and in cases such as when the monthly highest tides overlap with a storm surge, water flooding damage can occur.

The analysis of abnormal tidal levels reveals not only abnormally high tidal levels but also abnormally low tidal levels. It is important to clarify their causes for each ocean region.

(2) Effects of Abnormal Tidal Levels

In the performance verification of facilities, an abnormally high tidal level can increase the buoyancy of breakwaters and decrease their stability.[23)] Yoshioka et al.[24)] evaluated the probability distribution of abnormal tide levels at 97 places throughout Japan on the basis of tide observational data (as much as 29 years) and performed a reliability analysis to study the effect on the sliding and overturning stability of breakwaters. Within the scope of their results, the decrease in the safety index due to abnormal tidal levels is small enough to be neglected.

3.5 Long-Term Variation in the Mean Sea Level

(1) Variations in the Mean Sea Level

Both in Japan and abroad the studies on the long-term rise of the mean sea level (M.S.L.) have been conducted separately from the studies on astronomical tidal levels and storm surge in the specification of design tidal levels.

According to the Fifth Assessment Report of the Intergovernmental Panel on Climate Change, it is very likely that the mean yearly rate of global averaged sea level rise was 1.7 mm/year between 1901 and 2010, 2.0 mm/year between 1971 and 2010, and 3.2 mm/year between 1993 and 2010.[25)]

On the contrary, **Fig. 3.5.1** shows the variations in the M.S.L. on Japanese coasts examined by the Japan Meteorological Agency.[26] It shows no clear rising trend but the two-decadal variations with a local maximum around 1950 until 1990s. Decadal variations have been observed since the 1990s with a rising trend.

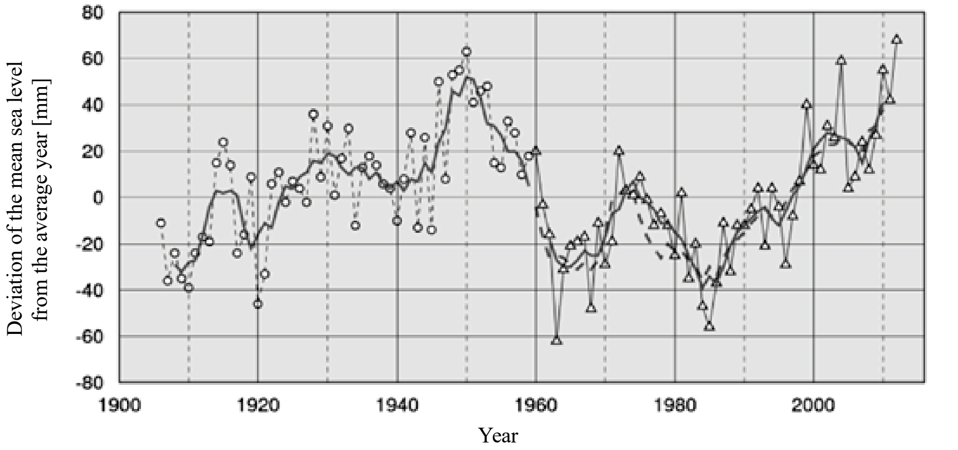

Fig. 3.5.1 Variations in the Mean Sea Level on Japan's Coasts[26]

Furthermore, interannual variability in the M.S.L. can be examined from the long-term tide records in ports. As shown in **Fig. 3.5.2**, it is estimated that the M.S.L. rose 3.0 mm/year in Kurihama Bay in 53 years, whereas the M.S.L. rose 4.4 mm/year in Karatsu Port in 31 years.[27] This variability in the M.S.L. seems to differ on the location of the tide station or the period. In organizing long-term tide records, it is necessary to properly consider the displacement of the ground on which the tide station is built. For example, the ground subsidence at a tide station seems the same as the rise of the M.S.L. Furthermore, the ground height may change before and after an earthquake. See **Part II, Chapter 5, 2 Change in the Crust Caused by Earthquake**. The ground displacement at GNSS-based Continuously Operating Reference Station (CORS) survey may be utilized for the correction of ground displacement at tide station.[27]

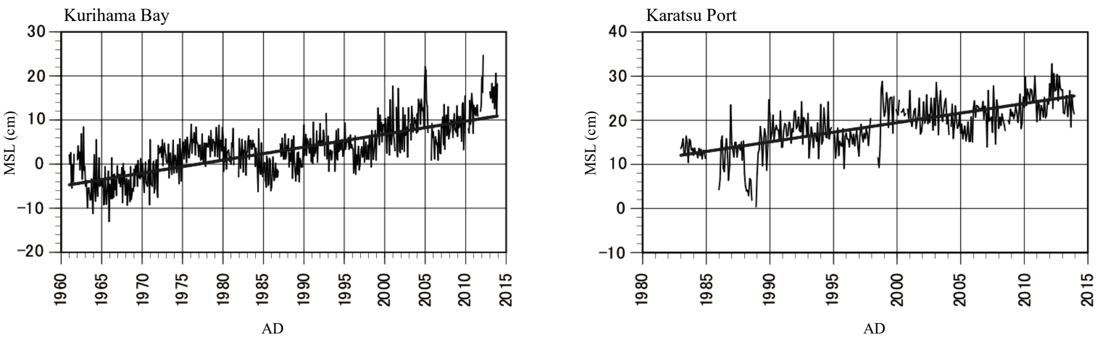

Fig. 3.5.2 Example of Interannual Variability in the MSL in Ports[27]

(2) Impact of the M.S.L. Rise and Countermeasures

If the M.S.L. rises, the stability of facilities will be lost, and the usage will be restricted owing to inundation or reduced clearance. Furthermore, there will be an impact on the logistics infrastructure.

The countermeasures against the M.S.L. rise include the development and improvement of facilities, modification of land use, and strengthening of disaster prevention systems. It is also necessary to clearly understand the advantages and disadvantages of such countermeasures by taking into account factors such as the social characteristics and natural conditions of the target areas and to combine all countermeasures into adaptable plans.[28] In the construction of new facilities or the improvement of existing facilities such as quaywalls, seawalls, roads, and bridges in port areas, it is necessary to consider countermeasures against impacts of climate change in the construction or renewal stages of facilities so that stepwise adaptation to gradual increases in the impacts can be performed without significant additional costs. It is also necessary to judge the timing of countermeasures on the basis of the result of M.S.L. monitoring and to consider construction plan, design working life, cost-effectiveness, effect on the surrounding environment of these facilities.

3.6 Conditions for Design Tidal Level

(1) Fundamental Concept of Design Tidal Level

A different design tidal level may be used depending on the aim of performance verification even for the facilities used for the same purpose. For example, the design tidal level in protection facilities against storm surge is determined as the tide level wherein wave overtopping becomes highest because the crown height is determined by the amount of wave overtopping. However, a much lower tidal level may become dangerous for the stability of the facilities, and the design tidal level must be determined as such a tidal level. In the performance verification of a breakwater, the tidal levels that make the facility unstable are employed. The highest of these tidal levels is called the planned tidal level.

(2) Design Tidal Level of Protection Facilities against Storm Surge

The design highest tidal level for protection facilities against storm surge shall be determined by using one of the following four methods by considering the occurrence of storm surges.

① Use the past highest tidal level or the tidal level by adding some allowance to it.

② Use the tide level by adding the past maximum storm surge or the tidal level hindcasted from the model storm surge to the mean monthly highest water level.

③ Use the tidal level obtained by determining the occurrence probability curve of the past abnormally high tidal levels and by selecting a tide level that has one or less time of higher tidal levels occurring in a certain return period.

④ Economically determine the tidal level by considering the occurrence probability of abnormally high tidal levels, the amount of damage in the hinterland per each tidal level and the construction cost of protection facilities against storm surge.

Each of these methods has the following merits and demerits. Method ① is simplest but requires long-term data. Furthermore, there is no occurrence guarantee of an abnormally high storm surge which exceeds the past highest storm surge level. Method ② is excellent in focusing on the tide level, which is a principal characteristic of a storm surge, but is the same as method ① in that there is no occurrence guarantee for the future. Method ③ is based on the probabilistic concept and clearly shows much occurrence probability exists in the design tidal level. However, reliability and other parameters are doubtful if long-term estimation is made from data covering only a short period of time. Method ④ is reasonable and is the most useful in the context of national economy but requires high technology and labor costs in the estimation of the amount of damage and others.

Methods ① and ② are the most widely adopted. In method ②, the mean monthly highest water level in the typhoon season (July to October) may be adopted instead of the mean monthly highest water level. Normally, the mean monthly highest water level in the typhoon season is higher than the mean monthly highest water level with a difference of 10 cm or more on the Pacific Coast.

Selection among these methods shall be made by comparing each value and considering the observation period, frequency of occurrence, demand and economy of facilities, etc. If the mean monthly highest water level plus the past maximum storm surge is too high to fit the actual plan, the design high water level may be corrected by thoroughly examining the past documents and by considering the frequency of simultaneous occurrence of both events.

In the performance verification of protection facilities against storm surge, it is common to determine the crown height by setting the design high water level as the mean monthly highest water level overlapped by the peak value of storm surge and by considering the worst condition where this design high water level is overlapped by the peak wave height. If the design high water level becomes extremely high under this condition, it is a good idea to examine the design high water level from the frequency of simultaneous occurrence of high tide, peak of storm surge, and peak of wave height.

(3) Tide Level to Set to Accidental Waves

In a shallow water area, the wave height, wave direction, and others are also varied by the tide level. When setting the tide level combined with accidental waves, typhoons or cyclones with adequate strength, size, and route should be assumed under the base on the development limit of typhoons indicated on the records of meteorological disturbance not only in the area concerned but also in the whole of Japan and meteorology irrespective of the past highest high water level or the past maximum tidal level due to storm surges. On the basis of this scenario, hindcast the temporal change in tide level and waves, including storm surges, and examine the condition of tide level and waves that causes the most extensive damage on the port and harbor concerned.[29) 30) 31) 32)] It is desirable to confirm that the return period of the set tidal level or accidental wave is long enough by the extremal statistics of observation values,[33)] the probabilistic typhoon simulation,[34)] etc.

(4) Simultaneous Occurrence of Storm Surges, Tsunamis, and Harbor Resonance

Both storm surges and tsunamis are rare phenomena and are not generally considered to occur simultaneously. See **Part II, Chapter 2, 5 Tsunamis**.

Harbor resonance is often induced by storm surges or tsunamis. However, harbor resonance is not generally considered to occur simultaneously with storm surges and tsunamis, because the long-period fluctuation of water surface (harbor resonance in the narrow sense) developed, except in storm surges and tsunamis.

(5) Performance Verification of Protective Facilities against Storm Surges, Tsunamis, and Others

Storm surges and tsunamis exceeding the protection objective of the protective facilities against storm surges, tsunamis, and others may occur. To conduct comprehensive disaster prevention countermeasures, including evacuation, if a possible disaster exceeds the design condition on the basis of the generating mechanism of storm surges or tsunamis, it is necessary to set it as the worst case scenario in disaster prevention and to evaluate its protection performance in that case. If damage due to flooding or others is supposed to occur, disaster prevention countermeasures that combine evacuation support countermeasures such as a hazard map also need to be considered. When setting conditions for disaster prevention, it is desirable to calculate the return period (in years) of the disaster.

3.7 Observations and Investigation of Tidal Level

(1) Overview

Tidal levels are continuously observed as the ocean surface variation, excluding relatively short frequency variations such as waves. Tidal level observations have various purposes, as listed below; therefore, it is preferable for the observations to be done appropriately on the basis of the purpose. The equipment to be installed in tide level observatories (e.g., the tide observation well and tidal level measuring equipment [float type or radio type]), shall be properly selected according to the objective, continuity, and other parameters of the observation. See **Reference (Part II), Chapter 1, 2.3 Observation and Examination of Tide Levels** for details.

① **Standard water level**

Various datum levels are used for different purposes, such as observation, maintenance, and management of port construction and nautical charts. When observing the tidal level, it is necessary to understand to which datum level the water level should be observed.

② **Mean sea level monitoring**

Recently, the rise in sea level due to global warming has become a major concern. However, there are great variations in the predictions of the amount of sea level rise; therefore, mean sea level monitoring based on long-term tide level observation is necessary.

③ **Understanding tsunamis, storm surge, and long-period waves**

When structures along the shore suffer a disaster, the understanding of marine conditions, including tide level records, is the first step in the process of understanding the cause of the disaster and planning recovery measures.

④ **Others**

The setting of the datum level is also important in the supervision of construction work or environmental monitoring.

(2) Confirmation of Observation Benchmarks

Given that the benchmark (standard mark) of the tide observatory and the benchmark installed near the tide observation booth are subjected to the influence of ground subsidence and others, it is important to properly evaluate the amount of ground subsidence. Therefore, it is desirable to adjust the level to the first-order benchmark of the Geospatial Information Authority of Japan every few years.

The Geospatial Information Authority of Japan periodically surveys the elevation of its first-order benchmarks. If it judges that the ground has risen or subsided excessively, the elevation of the first-order benchmarks is reviewed as survey mean results. The Geospatial Information Authority of Japan makes public the review history of the mean results and the annual survey results of its first-order benchmarks so that everybody can view them.[35]

(3) Obtaining Documents Related to the Tidal Level Observation

The tidal level is observed by various institutions, such as the national government, which administers ports and harbors, fishery harbors, coasts, and local governments. Among these institutions, the Hydrographic and Oceanographic Department of the Japan Coast Guard and the Japan Meteorological Agency publish the Tidal Table[36] and Tide Table,[37] respectively, and provide anticipated information on the tidal level calculated by the harmonic analysis at major ports and harbors. Moreover, the Japan Meteorological Agency publicizes the tide level observation records, namely, the "Diagnosis Table and Data on Tide and Sea Level," on its website.[38] Furthermore, the Coastal Movements Data Center of the Geospatial Information Authority of Japan publicizes the monthly and yearly mean tide levels in its registered tidal level observatories on its website; these levels were organized from the data presented by the Ports and Harbours Bureau of the Ministry of Land, Infrastructure, Transport and Tourism, Hokkaido Regional Development Bureau, Okinawa General Bureau, Hydrographic and Oceanographic Department of the Japan Coast Guard, Japan Meteorological Agency, Geospatial Information Authority of Japan, local governments, and others.[39]

[References]

1) Japan Coast Guard: Tide Table, Vol. 1, 1996 (in Japanese)

2) Japan Meteorological Agency: Tide Table 2011, 2010 (in Japanese)

3) Japan Meteorological Agency: Tide Table 2004, 2003 (in Japanese)

4) Study Group of Analysis and utilization of coastal wave observation data,: measurement of tide, Coastal Development Institute of Technology, Coastal development Technical Library. No.13,2002. (in Japanese)

5) Takahashi, H. A. Takeda, K. Tanimono Y. Tsuji and I. Isozaki: Prediction and preventive measure of coastal disaster- How to prepare for tsunamis and storm surges, Hakua Publishing, 408p. 1988 (in Japanese)

6) Ministry of Agriculture, Forestry and Fisheries and Ministry of Land, Infrastructure, Transport and Tourism: Guide to creating a storm surge flooded area map, p.60, 2015 (in Japanese)

7) HIRAISHI, T. K. HIRAYAMA and H. KAWAI: A Study on Wave-0vertopping by Typhoon No. 9918, Technical Note of PHRI, No.972, 2000.12, 19p (in Japanese)

8) Shibaki, H., T. Ando, T. Mikami and C. Goto: Development of integrated numerical research system for prevention and estimation of coastal disaster, Jour. JSCE No586/11-42, pp.77-92,1998 (in Japanese)

9) Kawai, H and K. Kawaguchi: Applicability of typhoon bougus and mesoscale model to simulation of storm surge in bays, Report of PARI, Vol.46, No.3, pp.43-86, 2007 (in Japanese)

10) Yamashita, T., Y. Nakagawa: Simulation of a storm surge in Yatsushiro Sea due to Typhoon No. 9918 by wave-storm surge coupled model considering shear stress of white cap breakers, Proceeding of Coastal Eng. No. 48, pp.291-295, 2001 (in Japanese)

11) Takigawa, K.. and M. Tabuchi: Preparation of hazard maps of storm surges and high waves under the most probable occurrence based on tide-wave interaction analysis, probable assumption, Proceeding of Coastal Eng. No. 48, pp. 1366-1370, 2001 (in Japanese)

12) Shibaki, H. and A. Watanabe: Study on Multi-level simulation model fore storm surge considering density stratification and wave setup, Journal of the JSCE, No. 719/II pp. 47-61, 2002 (in Japanese)

13) Kawai, Y., K. Kawaguxhi and N. Hashimoto: Modeling of wave-storm surge two-way joint hindcasting and case study for Typhoon 9918 hindcasting,, Proceeding of Coastal Eng. No. 50, pp. 296-300, 2003 (in Japanese)

14) Kawai, Y., S. Takemura and N. Hara: Characteristics of storm surge-high wave joint occurrence and duration in Tokyo Bay, Proceeding of Coastal Eng. No.49, pp. 241-245, 2002 (in Japanese)

15) Konishi, T.: Situations of damages of storm surges and status of the study for forecasting, Oceanographic Society of Japan, Coastal Oceanography Research Vol. 35 No. 2, 1998 (in Japanese)

16) Tatsuo KONISHI: A Cause of Storm Surges Generated at the Ports Facing Open Oceans- Effect of Wave Setup-, Sea and sky Vol. 74, No. 2, 1997 (in Japanese)

17) Shibaki, H., F. Kato and K. Yamada: Hindcasting of abnormal storm surge in Tosa Bay considering density stratification and wave setup, Proceeding of Coastal Eng. No. 48, pp. 286-290, 2001 (in Japanese)

18) Unoki, S: On seiche and long period waves in harbours, Proceeding of 6th conference on coastal Engineering, pp. 1-11,1959 (in Japanese)

19) TAKAYAMA, T. and T. HIRAISHI: Amplification Mechanism of Harbor Oscillation Derived From Field Observation And Numerical Simulation, Technical Note of PHRI No.636, pp.70, 1988 (in Japanese)

20) Honda, K,, Terada, T., Yoshida, Y. and lshitani, D.: Secondary undulation of oceanic tides, Jour. Collage of Science, Univ. of Tokyo, Vol.26, 1943

21) Goda, Y: Secondary undulation of tide in rectangular and fan-shaped harbour, JSCE 10th conference on Coastal Eng., pp. 53-58, 1963 (in Japanese)

22) Shimono T., K. Nakai, H. Nagai, H. Matsumoto, K. Watanabe and M. Isobe: Regional characteristics of abnormal tide levels in coastal areas of Japan, JSCE Proceedings of Coastal Engineering, Vol.51, pp.1221-1225, 2004 (in Japanese)

23) Coastal Development Institute of Technology (CDIT): Survey report on Extra-high tide level Fiscal 2002, pp. 86, 2003 (in Japanese)

24) Yoshioka, K., T. Nagao, E. Kibe, T. Shimono and H. Matsumoto: Effect of extra-high tide on the external stability of caisson type breakwaters, Technical Note of National Institute for Land and Infrastructure Management, No.241, 2005 (in Japanese)

25) IPCC WG1: Fifth Assessment Report Climate Change 2013 (AR5) Summary for Policy-Makers, 2013

26) Japanese Meteorological Agency: Marine health checkup table, comprehensive diagnosis table 2nd edition, No2, Monitoring sea level on the coast of Japan 2013, http://www.data.jma.go.jp/kaiyou/shindan/sougou/html_vol2/1_2_vol2.html (in Japanese)

27) Naito, R., T. Asai, K. Kawaguchi, T. Inomata, D, Tasumi and K. Narita: Estimation of sea level rise using the tide gauge records in port areas and their characteristics, Technical Note of National Institute for Land and Infrastructure Management, No.855, pp.1-36, 2015 (in Japanese)

28) Assemblymen in charge of Environment, Synthetic Science and Technology Conference and, Cabinet Office Director-general for Politics on Science and Technology Condition: Study Report on Climate Change, Synthetic Science and Technology Conference, Global Warming Study Initiative, Frontier of Climate Change Studies, Knowledge and Technology in the Century of Environment, 2002, p. 92, 2003 (in Japanese)

29) Takahashi, S., T. Tomita and H. Kawai: Performance design concept applied for storm surge defense, Technical Note of PARI, No.1042, 27p, 2003 (in Japanese)

30) Takahashi, S., H. Kawai, T. Hiraishi, K. Oda and T. Takayama: Characteristics of storm surge disaster and worst case scenario in Hurricane Katrina, JSCE Proceedings of Coastal Engineering, Vol.53, pp.411-415, 2006 (in Japanese)

31) Ministry of Agriculture, Forestry and Fisheries and Ministry of Land, Infrastructure, Transport and Tourism: Guide to creating a storm surge flooded area map, Ver.1.00, 60p, 2015 (in Japanese)

32) Utsunomiya, Y., M. Miyata, T. Takayama, H. Kawai, K. Hirayama, Y. Suzuki, M. Kimizuka and Y. Fukinaga: Estimation and application of the largest class storm surge predicted by scenario typhoons, Journal of Japan Society of Civil Engineers, Ser. B2 (Coastal Engineering), Vol.73, No2, pp.I_247-I_252, 2017 (in Japanese)

33) Kawai, H., Y. Goda, N. Kudaka and K. NAKAI: Extreme statistics of storm surge heights around Japan through regional frequency analysis, Journal of Japan Society of Civil Engineers, Ser. B2 (Coastal Engineering), Vol.66, No1, pp.121-125, 2010 (in Japanese)

34) Kawai H., N. Hashimoto and K. Matsuura: Estimation of extreme value and duration of storm surge in bays by using stochastic typhoon model, JSCE Proceedings of Coastal Engineering, Vol.54, pp.301-305, 2007 (in Japanese)

35) Geospatial Information Authority of Japan: Site for browsing benchmark point results, http://sokuseikagis1.gsi.go.jp/. (in Japanese)

36) Japan coast guard: 2017 tide table Vol.1 Japan and nearby, Japan hydrographic association, 2016 (in Japanese)

37) Japanese Meteorological Agency: Tide table, http://www.data.jma.go.jp/gmd/kaiyou/db/tide/suisan/index.php (in Japanese)

38) Japanese Meteorological Agency: Diagnostic table and data on tide and sea level, http://www.data.jma.go.jp/gmd/kaiyou/shindan/index_tide.html (in Japanese)

39) Castal movements data center of Geospatial Information Authority of Japan: http://cais.gsi.go.jp/cmdc/centerindex.html. (in Japanese)

4 Waves

[Public Notice] (Waves)

Article 8

Characteristics of waves shall be set by the methods provided in the subsequent items corresponding to the single action or combination of two or more actions to be considered in the performance criteria and the performance verification:

(1) Waves to be employed in the verification of the structural stability of the facilities, the failure of the section of a structural member (excluding failure due to fatigue), and others shall be appropriately defined in terms of the wave height, period, and direction corresponding to the return period through the statistical analysis of the long-term measured values or estimated values or other methods.

(2) Waves to be employed in the verification of the assurance of the functions of a structural member and the failure of its section due to fatigue shall be appropriately defined in terms of the wave height, period, direction and others of waves having a high frequency of occurrence during the design service life through the statistical analysis of the long-term measured values or estimated values.

(3) Waves to be employed in the verification of the harbor calmness shall be appropriately defined in terms of the joint frequency distributions of the wave height, period, and direction for a certain duration of time based on the long-term measured values or estimated values.

[Interpretation]

7. Setting of the Natural Conditions

(3) Items related to waves (Article 6 of the Ministerial Ordinance and the interpretation related to Articles 8 and 9 of the Public Notice)

Combined conditions of actions in item (1) or actions in items (2) later indicate a design state. Combined conditions for waves shall be properly set pursuant to the subsequent provisions in accordance with the performance criteria and the design state considered in the performance verification.

① **Waves employed to verify the stability of facilities and to verify the failure of the section of a structural member.**

a) Return period of variable waves

When setting the waves to be considered in the verification of serviceability for a variable state where dominating action is variable waves, the purpose of the facilities and the performance requirements must be satisfied, and in addition, the return period of the waves is set appropriately by considering suitably the design service life and degree of importance of objective facilities, as well as the natural condition of objective location.

b) Return period of accidental waves

When setting the waves to be considered in the verification of serviceability for an accidental situation where dominating action is accidental waves, the waves that become most disadvantageous among the waves that can occur in objective marine waters are set appropriately.

c) Period of observed values or estimated values

A period of 30 years or longer is used as the standard for the long-term observed values or estimated values.

② **Waves employed to verify the assurance of the functions and the failure of sections due to fatigue of the facilities relating to structural members.**

a) The verification of the assurance of the functions of the facilities relating to structural members refers to the verification of the limit state in which function-related trouble occurs in structural members due to frequently-occurring actions, and in addition, the verification of failure of sections due to fatigue refers to the verification of the limit state in which destruction of a section occurs in a structural member due to repeated action.

b) The waves to be considered in the verification of the assurance of the functions of the facilities relating to structural members employ as the standard waves for which the number of times which the waves with a wave height greater than that strike in the design service life is about 10,000 times.

c) When setting the waves to be considered in the verification of destruction of a section due to fatigue, various conditions such as the natural condition of objective facilities are considered, and the number of times of appearance relating to the wave height and period of the waves that occur during the design service life shall be appropriately set. The standard period of the observed values and estimated values is about 5 years or longer.

③ **Waves employed to verify harbor calmness**

A period of 5 years or longer is used as the standard period for the long-term observation or estimation. In addition, when setting the waves to be considered in the verification of harbor calmness, long period wave shall be considered appropriately as necessary.

4.1 Setting Wave Conditions

4.1.1 Setting of the Wave Conditions for the Verification of Stability of Facilities and the Safety (Section Failure) of Structural Members

(1) Setting of the variable wave conditions

① **General**

For the performance verification of port facilities, the wave conditions such as the wave height, period, and direction shall be set appropriately. These wave conditions are preferably set by statistical analysis based on long-term observational data, but in cases where the observation data are inadequate, it is common to supplement the data by wave hindcasting. [1) 2) 3)]

The waves for the stability verification of the facilities and the safety (section failure) of structural members are generally the probabilistic waves whose return period is 50 years, for facilities whose design service life is 50 years. This is the return period of waves that is generally taken into consideration in conventional design, and conventional design is followed in order to provide continuity of the philosophy of conventional design methods and to avoid confusion in practical design work. However, when the return period is set equal to the design service life, it should be noted that the probability to encounter waves exceeding the design external force [4)] reaches about 63%.

Moreover, the return period needs to be set to three times or more of the design service life in order to suppress the encounter probability on the order of 30%. Owing to this, the return period may be established appropriately by taking into consideration the design service life and degree of importance of objective facilities, as well as the natural conditions of objective location.

The return period of waves should be also set to the swell in order to properly accommodate the swell having longer periods than waves generally considered in the previous design. The swell in this case can be defined as waves having the significant wave period of about more than 8 seconds and the wave steepness less than about 0.025. [5) 6)]

On the other hand, the design tidal level generally uses the astronomical tidal level that causes the severest actions to the stability of facilities concerned and the ultimate limit state of structural members. However, recent disaster examples show that many such facilities that set the high tidal level as the design tidal level for wave pressure calculation suffer from storm surges. [7)] Therefore, the design tidal level for the calculation of wave pressure may be set to the severest tidal level like the tidal level which adds proper storm surge height to the high tidal level for facilities considering the simultaneous occurrence with waves, as well as the performance verification for wave overtopping.

② **Extreme Waves**

As far as the abnormal wave characteristics that are employed for the examination of the stability of facilities are concerned, it is preferable to carry out statistical treatment for the peak waves and to express this as the probabilistic wave height. **Reference 8)** is a document concerning design waves based on probabilistic wave height.

③ **Statistical Treatment of Extreme Waves**

The wave height at abnormal weather that is the object of the design is generally expressed as the probabilistic wave height in respect to the return period for peak waves, from the long-term data i.e., a period of at least 30 years as the standard. Since the number of locations for which it is possible to utilize observational data over the long term is still small, wave hindcasting results are generally used instead.

Peak waves, which are the hindcasting data for probabilistic wave height, refer to waves, in general, significant waves, when the wave height reaches the maximum in the process where the waves develop and attenuate under one certain meteorological disturbance, and it is assumed that the peak waves sampled are statistically independent from each other. To estimate the probabilistic wave height, there are two cases: One is to use the wave data whose peak heights exceed a certain designated value in the subject duration and the other is to use the annual maximum wave data among the peak wave heights observed or hindcasted each year. The ratio of the number of actually used data N against the total number of data N_T is called the data adoption rate $\nu = N / N_T$. As the parent distribution function of the extreme wave heights is unknown in general in either case, the Gumbel distribution, the Weibull distribution, or some other distribution functions is applied. The distribution form most suited to the data distribution is found, and the probabilistic wave height corresponding to the required return period, for example, 50 years or 100 years, is estimated by using the most suited distribution function. The Gumbel distribution is also called the double-exponential distribution, extreme value type I distribution, or type FT-I distribution.

However, if it is clear that a distribution function enough reliable cannot be estimated due to an extremely small number of swell peak wave data, the estimation of the probabilistic wave height for swell can be omitted.

Such estimated values are not absolute, but there are certain confidence intervals. Moreover, the accuracy of such estimated values is dependent more on the reliability of the data than the method of statistical treatment. Therefore, when using actually observed waves observed for 20 min every 2 h, for example, keep in mind that there is a possibility that waves higher than the observed waves may have attacked. On the other hand, in the event that the data for the peak waves is prepared by wave hindcasting, care should be taken of appropriate selection of the hindcasting method and verification of the hindcasted results based on the observed values. The hindcasted value shall be corrected if necessary.

Moreover, the period corresponding to the probabilistic wave height is appropriately estimated through the correlative relation between the wave heights and periods plotted for observed or hindcasted wave data. Furthermore, the following equation [9] based on Wilson's wave hindcasting equation can be used for wind waves. The equation estimates the periods of waves with the steepness around 0.04 for small waves and less than 0.03 for large waves. On the coasts of the Sea of Japan and the East China Sea where wind waves are dominant, the wave steepness seems to be on the order of 0.035 to 0.04. [10]

$$T_{1/3} \approx 3.3\left(H_{1/3}\right)^{0.63} \qquad \textbf{(4.1.1)}$$

④ **Process in the Statistical Treatment of Extreme Waves**

In the statistical treatment, the wave data is sorted in the order of height, and the non-exceedance probability for each wave height value is calculated.

Assuming that the number of data is N, and the number mth wave height from the larger side is $x_{m,N}$, the probability F_m that the wave height does not exceed $x_{m,N}$ is calculated using the following equation:

$$F_m = 1 - \frac{m-\alpha}{N+\beta} \qquad \textbf{(4.1.2)}$$

The values for each probability distribution function shown on **Table 4.1.1** are employed for α and β in the above equation. Since Gringorten has calculated the values for the Gumbel distribution[11], it has been set so that the effects of the statistical variance of the data are minimized with the non-exceedance probability F corresponding to the anticipated value of the order statistics x_m. Petruaskas and Aagaard have calculated the values for the Weibull distribution based on the same viewpoint [12] . Moreover, as N is the number of data for data adoption rate $\nu = 1$ (whole extreme data), the total number of extreme data N_T instead of N should be used for $\nu < 1$ (partial extreme data) to estimate the shape of parent distribution function as precisely as possible.

However, as the accumulated data of the maximum wave height for a long time is still not enough, it is not clearly known what distribution function fits at each longshore location.

Table 4.1.1 Parameters for Non-exceedance Probability Calculation of Extreme Waves

Distribution function	α	β
Gumbel distribution	0.44	0.12
Weibull distribution (k = 0.75)	0.54	0.64
Same as above (k = 0.85)	0.51	0.59
Same as above (k = 1.0)	0.48	0.53
Same as above (k = 1.1)	0.46	0.50
Same as above (k = 1.25)	0.44	0.47
Same as above (k = 1.5)	0.42	0.42
Same as above (k = 2.0)	0.39	0.37

⑤ **Proposed Example of Fitted Distribution Functions**

(a) Following Petruaskas and Aagaard, in **Reference 13)**, Goda has proposed a method that the function that accords the most data among following eight kinds of functions is selected with the correlation coefficient: the Gumbel distribution in **equation (4.1.3)** and the Weibull distribution in **equation (4.1.4)** wherein k = 0.75, 0.85, 1.0. 1.1, 1.25, 1.5, and 2.0 are applied.

$$F(x) = \exp\left[-\exp\left\{-\left(\frac{x-B}{A}\right)\right\}\right] \tag{4.1.3}$$

$$F(x) = 1 - \exp\left\{-\left(\frac{x-B}{A}\right)^k\right\} \tag{4.1.4}$$

Here, the non-exceedance probability F_m is calculated using **equation (4.1.2)**. The values shown in **Table 4.1.1** are adopted for the values of α and β.

Next, from the non-exceedance probability F_m, the standard amount of change y_m is calculated by using **equation (4.1.5)** in the case of the Gumbel distribution and **equation (4.1.6)** in the case of the Weibull distribution, respectively.

$$y_m = -\ln\{-\ln(F_m)\} \tag{4.1.5}$$

$$y_m = \{-\ln(1-F_m)\}^{1/k} \tag{4.1.6}$$

If the data completely accord with **equation (4.1.3)** or **equation (4.1.4)**, a linear relationship exists between x_m and y_m. Therefore, the estimation equation for the probabilistic wave height is calculated by assuming a linear relationship for **equation (4.1.7)** and establishing its coefficients (A ,B) by the least squares method.

$$x_m = \hat{A}y_m + \hat{B} \tag{4.1.7}$$

Here, Aˆ , Bˆ are the estimated values for the coefficients A and B in **equation (4.1.3)** or **equation (4.1.4)**.

(b) Moreover, in **Reference 14)**, Goda has proposed the following method, which revises the abovementioned procedure.

1) Modification of the fitted distribution function (introduction of extreme value type II)

The extreme value distribution of the type II is given by the following equation. The type II distribution is also called the FT-II distribution or Frechet distribution.

$$F(x) = \exp\left[-\{1 + (x-B)/kA\}^{-k}\right] \tag{4.1.8}$$

Here, the examination has been done in a total of nine ways, one way with the Gumbel distribution in **equation (4.1.3)**, four ways with the Weibull distribution in **equation (4.1.4)** (k = 0.75, 1.0, 1.4, and 2.0), and four ways with the type II distribution in **equation (4.1.8)** (k = 2.5, 3.33, 5.0, and 10.0), as the fitted distribution functions.

In addition, formulation of the following equation is carried out instead of **Table 4.1.1**, for α and β in **equation (4.1.2)**.

In other words, it is set as follows:

In the Gumbel distribution:

$$\alpha = 0.44, \quad \beta = 0.12 \qquad \textbf{(4.1.9)}$$

In the Weibull distribution:

$$\begin{aligned} \alpha &= 0.20 + 0.27\big/\sqrt{k} \\ \beta &= 0.20 + 0.23\big/\sqrt{k} \end{aligned} \qquad \textbf{(4.1.10)}$$

In the type II:

$$\begin{aligned} \alpha &= 0.44 + 0.52\big/k \\ \beta &= 0.12 - 0.11\big/k \end{aligned} \qquad \textbf{(4.1.11)}$$

Moreover, the standard amount of change is calculated by using **equation (4.1.5)** in the case of the Gumbel distribution, **equation (4.1.6)** in the case of the Weibull distribution without any modification, and the following equation in the case of the type II distribution.

$$y_m = k\left\{\left(-\ln F_m\right)^{-1/k} - 1\right\} \qquad \textbf{(4.1.12)}$$

2) Modification of the procedure for selecting the optimal fitted distribution function by introduction of rejection criteria

The estimated probabilistic wave height for a certain return period varies according to adopted fitted distribution function. There are two kinds of criteria of the REC criterion and the DOL criterion to reject unsuitable functions. In practical work the following procedure is adopted in the analysis of extreme values by the least square method: after an unsuitable function has been rejected under either of these criteria, the optimal fitted function is selected according not to the value of the simple correlation, but rather the MIR criterion.

In DOL criterion, the maximum value x_1 in the data is made dimensionless with the overall mean value x and standard deviation s as shown in the following equation, and if this value ξ is below the 5% value or above the 95% value in the fitted distribution function, that function is rejected as unsuited.

$$\xi = \left(x_1 - \bar{x}\right)\big/s \qquad \textbf{(4.1.13)}$$

The 5% and 95% non-exceedance probability values of fitted distribution function are calculated using the following equation using coefficients a, b, and c set as in **Table 4.1.2** as a function of the data adoption rate v by the distribution function.

$$\xi_P = a + b\ln N + c(\ln N)^2 \qquad : P\text{=5\% and 95\%} \qquad \textbf{(4.1.14)}$$

Table 4.1.2 Coefficients of Non-exceedance Probability Values of the Maximum Deviation in Used Data

(a) 5% Non-exceedance Probability Values $\xi_{5\%}$

Distribution function	Coefficient a	Coefficient b	Coefficient c
Extreme type I distribution	$0.257 + 0.133\nu^2$	$0.452 - 0.118\nu^2$	0.032
Weibull distribution (k = 0.75)	$0.534 - 0.162\nu$	$0.277 + 0.095\nu$	0.065
Sane as above (k = 1.0)	0.308	0.423	0.037
Sane as above (k = 1.4)	$0.192 + 0.126\nu^{3/2}$	$0.501 - 0.081\nu^{3/2}$	0.018
Sane as above (k = 2.0)	$0.050 + 0.182\nu^{3/2}$	$0.592 - 0.139\nu^{3/2}$	0
Extreme type II distribution (k = 2.5)	$1.481 - 0.126\nu^{1/4}$	$-0.331 - 0.031\nu^2$	0.192
Sane as above (k = 3.33)	1.025	$-0.077 - 0.050\nu^2$	0.143
Sane as above (k = 5.0)	$0.700 + 0.060\nu^2$	$0.139 - 0.076\nu^2$	0.100
Sane as above (k = 10.0)	$0.424 + 0.088\nu^2$	$0.329 - 0.094\nu^2$	0.061

(b) 95% Non-exceedance Probability Values $\xi_{95\%}$

Distribution function	Coefficient a	Coefficient b	Coefficient c
Extreme type I distribution	$-0.579 + 0.468\nu$	$1.496 - 0.227\nu^2$	-0.038
Weibull distribution (k = 0.75)	$-0.256 - 0.632\nu^2$	$1.269 + 0.254\nu^2$	0.037
Sane as above (k = 1.0)	-0.682	1.600	-0.045
Sane as above (k = 1.4)	$-0.548 + 0.452\nu^{1/2}$	$1.521 - 0.184\nu$	-0.065
Sane as above (k = 2.0)	$-0.322 + 0.641\nu^{1/2}$	$1.414 - 0.326\nu$	-0.069
Extreme type II distribution (k =2.5)	$4.653 - 1.076\nu^{1/2}$	$-2.047 + 0.307\nu^{1/2}$	0.635
Sane as above (k = 3.33)	$3.217 - 1.216\nu^{1/4}$	$-0.903 + 0.294\nu^{1/4}$	0.427
Sane as above (k = 5.0)	$0.599 - 0.038\nu^2$	$0.518 - 0.045\nu^2$	0.210
Sane as above (k = 10.0)	$-0.371 + 0.171\nu^2$	$1.283 - 0.133\nu^2$	0.045

The residual Δr from 1 is calculated using the following equation using the correlation coefficient r between the order statistics x_m and standard amount of change y_m. The REC criterion is used to reject the fitted distribution function as unsuited if Δr exceeds the 95% non-exceedance probability value of the residual of the correlation coefficient in the fitted distribution function.

$$\Delta r = 1 - r \tag{4.1.15}$$

The 95% non-exceedance probability value of the residual of the correlation coefficient of the fitted distribution function is calculated by the following equation for coefficients a, b, and c set on **Table 4.1.3** as a function of the data adoption rate ν by the distribution function.

$$\Delta r_{95\%} = \exp\left[a + b\ln N + c(\ln N)^2\right] \tag{4.1.16}$$

Table 4.1.3 Coefficients of the 95% Non-exceedance Probability Values $\Delta r_{95\%}$ of the Residual of Correlation Coefficients

Distribution function	Coefficient *a*	Coefficient *b*	Coefficient *c*
Extreme type I distribution	-1.444	$-0.2733 - 0.0414\nu^{5/2}$	-0.045
Weibull distribution (k = 0.75)	$-1.473 - 0.049\nu^{2}$	$-0.2181 + 0.0505\nu^{2}$	-0.041
Sane as above (k = 1.0)	-1.433	-0.2679	-0.044
Sane as above (k = 1.4)	-1.312	$-0.3356 - 0.0449\nu$	-0.045
Sane as above (k = 2.0)	$-1.188 + 0.073\nu^{1/2}$	$-0.4401 - 0.0846\nu^{3/2}$	-0.039
Extreme type II distribution (k = 2.5)	$-1.122 - 0.037\nu$	$-0.3298 + 0.0105\nu^{1/4}$	0.016
Sane as above (k = 3.33)	$-1.306 - 0.105\nu^{3/2}$	$-0.3001 + 0.0404\nu^{1/2}$	0
Sane as above (k = 5.0)	$-1.463 - 0.107\nu^{3/2}$	$-0.2716 + 0.0517\nu^{1/4}$	-0.018
Sane as above (k = 10.0)	$-1.490 - 0.073\nu$	$-0.2299 - 0.0099\nu^{5/2}$	-0.034

The MIR criterion judges the most suitable distribution function which has the minimum ratio of Δr (residual from 1 of the correlation coefficient r between the order statistics x_m and the standard amount of change y_m) to the mean value Δr_{mean} of residual of the correlation coefficient in the fitted distribution function. The mean value of residual of the correlation coefficient in the fitted distribution function is calculated by the following equation for coefficients a, b, and c on **Table 4.1.4** as a function of the data adoption rate v by the distribution function.

$$\Delta r_{mean} = \exp\left[a + b\ln N + c(\ln N)^2\right] \tag{4.1.17}$$

Table 4.1.4 Coefficient of Residual Mean Values Δr_{mean} of Correlation Coefficients

Distribution function	Coefficient *a*	Coefficient *b*	Coefficient *c*
Extreme type I distribution	$-2.364 + 0.054\nu^{5/2}$	$-0.2665 - 0.0457\nu^{5/2}$	-0.044
Weibull distribution (k = 0.75)	$-2.435 - 0.168\nu^{1/2}$	$-0.2083 + 0.1074\nu^{1/2}$	-0.047
Sane as above (k = 1.0)	-2.355	-0.2612	-0.043
Sane as above (k = 1.4)	$-2.277 - 0.056\nu^{1/2}$	$-0.3169 - 0.0499\nu$	-0.044
Sane as above (k = 2.0)	$-2.160 + 0.113\nu$	$-0.3788 - 0.0979\nu$	-0.041
Extreme type II distribution (k = 2.5)	$-2.470 + 0.015\nu^{3/2}$	$-0.1530 - 0.0052\nu^{5/2}$	0
Sane as above (k = 3.33)	$-2.462 - 0.009\nu^{2}$	$-0.1933 - 0.0037\nu^{5/2}$	-0.007
Sane as above (k = 5.0)	-2.463	$-0.2110 - 0.0131\nu^{5/2}$	-0.019
Sane as above (k = 10.0)	$-2.437 + 0.028\nu^{5/2}$	$-0.2280 - 0.0300\nu^{5/2}$	-0.033

⑥ **Probabilistic Wave Heights Corresponding to Return Periods**

Suppose that the most suitable extreme distribution has been selected by analyzing extreme statistics for N peak waves among abnormal waves in K years. The used peak wave heights occur every K / N (= $1 / (\nu\lambda)$ (λ: mean occurrence rate) years on average. The non-exceedance probability of the wave height x is given by $F(x)$ as the most suitable extreme distribution. One wave height exceeding the height x exists on average among m (= $1 / (1 - F(x))$) wave heights randomly extracted from this distribution form. It takes $R = m$ (K / N) years on average for m peak waves to occur. Therefore, the non-exceedance probability of wave heights with the return period of R years is given by the equation $F(x) = 1 - (K / N) / R$. For example, if the most suitable extreme distribution is set by 40 peak waves for 30 years, the wave height of the return period of 50-years corresponds to the wave height, of which the non-exceedance probability is $F(x) = 1 - (30 / 40) / 50 = 0.985$. Moreover, the peak wave height at this time is calculated as $x = F^{-1}(1 - (K / N) / R)$, where F^{-1} is an inverse function of the most suitable fitted distribution function F.

⑦ **Challenges in Statistic Processing of Extreme Waves for the Future**

Goda et al. further developed the studies described above, published **Reference 15)**, and indicated the direction of extreme statistical analysis in the future. That is to say, although the most suitable fitted distribution function has been verified until now by the area of each port and port business, it is not reasonable that the distribution functions discontinuously differ per neighboring points concerned. They think that it is more physically reasonable to select specially designated distribution functions based on the properties of oceanographical phenomena in wider sea area in nature.

Table 4.1.5 showing the verification results on the northeast coast of the Pacific indicates that the Weibull distribution at k = 1.0 indicated by G in the table is most likely selected commonly at each observation point.

In order to verify most suitably by the sea area, vast cases at high waves must be verified in future. Although more wave observation data have been accumulated than before, some data are still missing during high waves. On the other hand, the wave observation results and the hindcasting results currently do not necessarily indicate good coincidence, as the precision and reliability of the wave hindcasting results largely depend on the estimated precision of offshore wind and pressure fields. Therefore, how to properly estimate high wave extreme specifications by meteorological disturbance based on wave observation data, including partial missing data, is a big challenge in the future, and the verification is progressing now.

Table 4.1.5 Statistical Analysis Results on All High Wave Extreme Data

Location	N	λ	Conformance/rejection test		H_{100} (m)	
			ABCDE	FGHI	Optimal	Type G
Tomakomai	293	21.47	■■▼◇▲	■○◎▲	6.39	7.48 ± 0.43
Mutsuogawara	358	16.85	▲◇◇◎▲	▲○■■	10.58	10.05 ± 0.53
Hachinohe	431	20.57	◇◇○◇▲	▲◎▲▲	9.45	9.45 ± 0.44
Miyako	117	11.44	◇◇◇○◇	◇◎◇■	6.50	6.50 ± 0.61
Kamaishi	375	24.11	■■■▲▲	■◎▲▲	8.30	8.30 ± 0.47
Sendai Shinko	406	27.40	■■▼○▲	■◎▲■	7.15	7.15 ± 0.37
Souma	224	18.59	■◇◇○▲	◇◎▲■	7.23	7.23 ± 0.47
Onahama	352	27.48	■▼○◇▲	▼◎▲■	9.67	9.67 ± 0.55
Hitachinaka	426	29.12	■■○◇▲	■◎▲■	8.78	8.78 ± 0.44
Kashima	188	22.60	■■▼◇◇	■▼○▲	9.71	9.71 ± 0.70
Habu	409	22.67	■▼○◇▲	◇◎▲■	9.68	9.68 ± 0.44

Note: 1) In Kashima, the type G distribution is at the rejection limit by the DOL criteria but is judged as most suitable by the MIR criteria.
2) The value after ± in type G distribution among the 100-year probabilistic wave height (H_{100}) indicates a standard deviation for an estimated value.

Code	Distribution function	Sign	Conformance/rejection judgment
A	Type FT-II (k = 2.50)	◎	The most suitable distribution by the MIR criterion
B	Type FT-II (k = 3.33)	○	The next most suitable distribution by the MIR criterion
C	Type FT-II (k = 5.00)	◇	Distribution not corresponding to the rejection criterion
D	Type FT-II (k = 10.00)	▲	Distribution rejected by the REC criterion
E	Type FT-I distribution	▼	Distribution rejected by the DOL criterion
F	Weibull distribution (k = 0.75)	■	Distribution rejected by both criteria
G	Weibull distribution (k = 1.00)		
H	Weibull distribution (k = 1.40)		
I	Weibull distribution (k = 2.00)		

⑧ **Design Waves of Temporary Structures**

In the performance verification of temporary structures as well, the design waves are basically set based on the above-described principles. However, since the installation period is limited in the case of temporary structures, it is possible to set the objective return period of the action shorter. If it is a temporary structure whose period is about 2 to 3 years, it is common for the verification to be carried out for action with a return period of about 10 years.

(2) Setting of the Accidental Wave Conditions

Waves as an accidental action are basically set by considering simultaneous occurrence with storm surges (see **Part II, Chapter 2, 3.2 Storm Surges**) as necessary and hindcasting waves (see **Part II, Chapter 2, 4.3 Occurrence, Propagation, and Damping of Waves**) based on assumed disturbance due to typhoons, rapidly developing cyclones and others. [16] In setting the strength, size and route of the assumed disturbance, also consider the extensiveness to social influence due to disaster by storm surges.

(3) Response to Waves Exceeding the Design

Depending on the design service life and degree of importance of target facilities and natural conditions of the point concerned, it is desirable to ensure restorability or safety even for actions exceeding the variable waves used for stability verifications as necessary. For the time being, it is assumed that the performance verification method for toughness is applied. These wave specifications can be set by selecting either variable waves that have relatively longer return period than those used for serviceability verification or waves due to disturbance conforming to the maximum class that sets accidental waves.

4.1.2 Setting of Wave Conditions for the Verification of Serviceability of the Structural Members

(1) The waves for the verification of the serviceability of the structural members are set appropriately as waves acting during the design service life. For the setting of such waves, a joint frequency distribution table of the wave height and period by wave direction is preferably calculated from wave observation data broken down by month, by season, and annually. In the event that the design service life is 50 years, this may be calculated using the following method.

① **Wave data**

It is possible to employ the NOWPHAS (Nationwide Ocean Wave Information Network for Ports and Harbors) wave observation data, which are obtained by continuous wave observations in ports throughout Japan. The occurrence frequency statistics by wave height class of the significant waves every 2 hr. or every 20 min. are summarized in the annual Wave Observation Annual Report [17] or Long-Term Statistical Report [18] issued by NOWPHAS. Estimation of the circumstances of occurrence of individual waves within an observation time of 2 hr. or 20 min. is carried out based on the significant wave height values provided once in these 2 hr. or 20 min.

② **Estimation of the occurrence circumstances of individual waves**

Since the abovementioned wave observation materials concern the occurrence frequency of significant waves, the **occurrence circumstances of** individual waves during the observation period are estimated based on the following hypothesis.

(a) The occurrence distribution of individual wave height follows a Rayleigh distribution. Assuming that the significant wave height during 2 hr. or 20 min. is constant, it is possible to assume that the distribution of several individual wave heights occurring during the 2 hr. or 20 min. follows a Rayleigh distribution where the significant wave height is equal.

(b) The number of individual waves during the time differs depending on (their wave period of) each observation; however, since it is extremely difficult to set the number of respective individual waves for each observation for 2 hr. or 20 min., it can be hypothesized that the value obtained by dividing 2 hr. (7,200 seconds) or 20 min. (1200 seconds) by the long-term mean period of objective wave observation point is the number of waves during 2 hr, or 20 min.

③ **Frequency distribution of individual waves in the design service life**

The number of wave occurrence in the design service life is calculated with the mean period of individual waves during the observation period. The wave for the verification of the serviceability for facilities whose design service life is 50 years can be set as the wave for which the number of waves with a wave height that or above strike is the order of 10^4 in the total number of the waves in the design service life, counted by the abovementioned method. In the **Design Manual for Prestressed Concrete Structure for Ports and Harbors Facilities**, these waves are the waves for the verification of the serviceability limit state, [19)] based on the provisions of the International PC Association, and this is applied here as well.

4.1.3 Setting of Wave Conditions for the Verification of Harbor Calmness

The ordinary wave properties that are employed for the verification of harbor calmness are generally expressed as a joint frequency distribution table of the wave height and period by wave direction for data broken down by month, by season, and annually from the wave data. In a detailed examination of events in which the effects of the period appear strongly, for example, the operating rate, it is preferable to arrange an occurrence distribution for the equivalent wave height and wave direction for each period band. Conducting an examination of the wave conditions by using observed data serves as the criterion. If the wave observation data are not available, the wave hindcasting results can be utilized. However, in the utilization of the wave hindcasting results, it is preferable to undertake the verification by observed data. It is possible to refer to the manual in **Reference 20)** as regards the setting of the ordinary wave conditions for the verification of harbor calmness.

4.2 Handling of Waves for Design

4.2.1 Setting Method of Waves

(1) Setting procedure of waves

Sea waves are one of the principal actions acting on port facilities. In the performance verification, the offshore waves composing variable action or accidental action shall first be determined in accordance with the function of the facilities. The conditions of the set waves can be expressed by the significant wave height, significant wave period, wave direction, directional spreading of the wave energy, and so on (see **Part II, Chapter 2, 4.2.2 Representation of Waves**). Thereafter, the application of the calculation diagrams, the calculation of wave transformation, or the model experiment shown in **Part II, Chapter 2, 4.4 Wave Transformations** is performed in shallow waters, and the conditions of the waves that act on the facilities shall be determined.

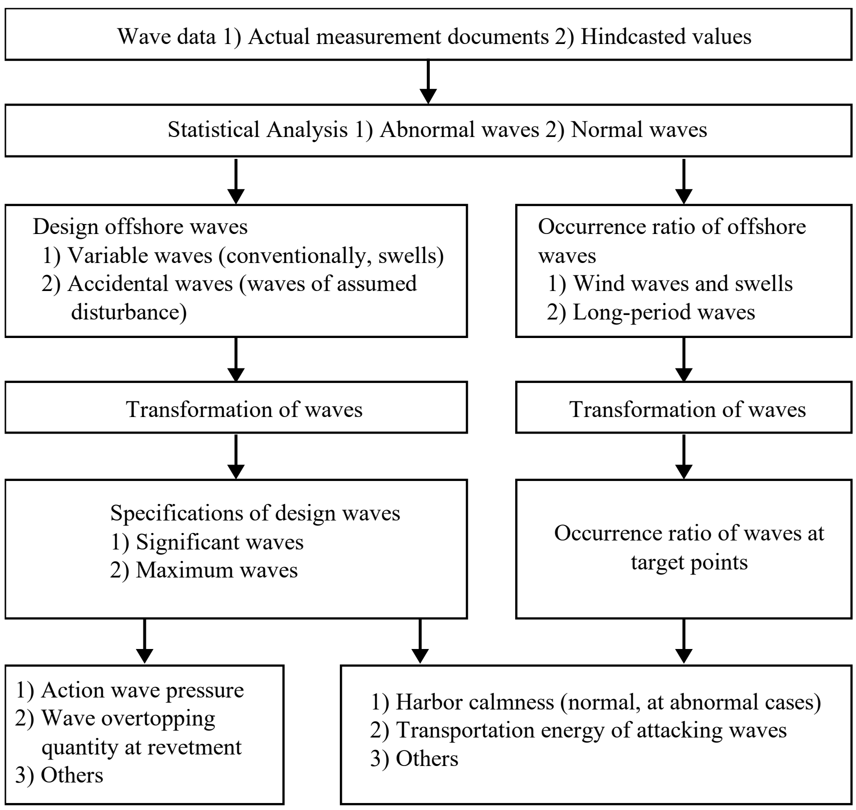

Fig. 4.2.1 Setting Procedure of Waves Used for the Design

(2) Linear dispersion relation of wave

The basic nature of waves generally varies according to the wave height, period (wave length), and water depth. These relations are called dispersion relations of water surface waves. The relation induced by the small amplitude wave theory, which assumes a small wave height as the first approximation, is called the linear dispersion relation and is expressed in the following equation.

$$\sigma^2 = gk \tanh kh \qquad \textbf{(4.2.1)}$$

where σ is the angular frequency (1/s), k is the wavenumber (1/m), h is the water depth (m), g is the gravitational acceleration (m/s^2). The angular frequency and the wavenumber are also expressed as $\sigma = 2\ \pi/T$ and $k = 2\pi/L$ using wave period T (s) and wave length L (m), respectively. Furthermore, by substituting and arranging these in **equation (4.2.1)**, the wave celerity C (m/s) is expressed as follows.

$$C = \frac{L}{T} = \sqrt{\frac{gL}{2\pi}\tanh 2\pi\frac{h}{L}} \qquad \textbf{(4.2.2)}$$

(3) Offshore Wave (Deepwater Wave) and Shallow Water Wave

The ratio of water depth to wavelength (h/L) may be called relative water depth. In waters where the relative water depth is at least one-half, the waves are hardly affected by the sea bottom and proceed without deforming. However, waves are gradually affected by the sea bottom when they invade waters where the relative water depth is less than one-half. Furthermore, the wave celerity becomes slower, the wavelength shortens, and the wave height also changes. Given this fact, waves in the relative water depth of at least one-half are called deepwater waves, and waves in waters shallower than this are called shallow water waves.

Here, when the relative water depth h/L is on the order of one-half or more, the value of tanh (hyperbolic tangent) function in **equation (4.2.2)** can be considered almost one. Thus, the length of deepwater waves is calculated by raising both sides of the equality to the second power and by arranging and specifically substituting the length and period of deepwater waves by L_0 and T_0.

$$L_0 \approx \frac{g}{2\pi}T_0^{\ 2} \approx 1.56T_0^{\ 2} \qquad \textbf{(4.2.3)}$$

As shown in **equation (4.2.3)**, the length of deepwater waves does not depend on the water depth; therefore, they are called offshore waves.

On the contrary, the length of shallow water waves, the relative water depth h/L of which is on the order of less than one-half, is calculated by **equation (4.2.2)**. As both sides of the equality include the wave length, a convergent calculation is generally required to obtain a solution. Therefore, the length and celerity of waves for a certain water depth and period may be estimated using **Reference (Part III), Chapter 4, 4 Linear Dispersion Relation of Waves**.

The value of the tanh function in **equation (4.2.2)** is almost equal to the value of the argument $2\pi h/L$ of the function when the relative water depth h/L is on the order of less than one-twenty-fifth. Thus, the following equations are obtained from the relation of both sides of the equality. The wave length can be calculated by multiplying the period.

$$C \approx \sqrt{gh} \quad L = CT \approx T\sqrt{gh} \qquad \textbf{(4.2.4)}$$

The shallow water wave in the sea area with a very shallow relative water depth indicating that these approximations are true is specifically called ultrashallow water wave or long wave. For example, a tsunami with a wavelength exceeding 100 km can be considered a long wave even if it propagates in the Pacific Ocean, where the mean water depth is 4 km. The propagation velocity can be estimated by **equation (4.2.4)**.

Moreover, concerning shallow water waves, it is necessary to take into consideration the fact that the shape of the spectrum and the frequency distribution of the wave height differ from the state of offshore waves because of the effects of wave transformation, such as refraction, wave shoaling, and wave breaking due to sea bottom topography.

(4) Wave Transformation in Shallow Waters

The phenomenon wherein the wave height or direction of progressive wave varies owing to the effects of water depth is called wave transformation, which should be taken into consideration in waters where the relative water depth to the wavelength L_0 of offshore waves is shallower than one-half and in waters where waves are affected by shielding due to land and other factors (refer to **Part II, Chapter 2, 4.4 Wave Transformations**). The wave transformation includes phenomena such as refraction, wave shoaling, and wave breaking due to sea bottom topography and diffraction, reflection, and partial penetration due to shielding by island, structures, etc. The calculation of these is performed by using the respective appropriate numerical calculation methods. Considering that these respective phenomena occur by mutually affecting one another, the application of a calculation method that can take all of them into consideration at once is preferable. However, at present, there is no calculation method that can simultaneously consider and perfectly reproduce all of these phenomena regardless of the space scaling in practical use. In principle, the waves that act on the port facilities are appropriate waves that are most disadvantageous for the stability of the structure of the port facilities or the utilization of the port facilities in view of transformations such as refraction, diffraction, wave shoaling, and wave breaking due to the propagation of offshore waves.

(5) Influence of finite amplitude of wave

Waves with heights that cannot be considered small are called finite amplitude waves. The difference from the property of small amplitude waves becomes apparent as the relative water depth decreases in shallow sea areas and wave forms with steep crests and flat troughs. These waves are called nonlinear waves. The influence of the nonlinearity of waves should be taken into consideration for wave shoaling where the wave height increases in shallow water depth as a kind of wave transformation.

Fig. 4.2.2 shows the change in the wave crest elevation of progressive waves obtained by arranging data in the hydraulic model experiment for water depth h = 100 to 150 cm. Moreover, **Fig. 4.2.3** was made on the basis of the site wave form records and shows the ratio of the maximum wave crest elevation $(\eta_c)_{max}$ read for each observation record to the maximum wave height H_{max} within the record in the $H_{1/3}/h$ relation. Actual wave crest elevation is slightly higher than the value of the model experiment. It is preferable to use the data in **Fig. 4.2.3**, which was obtained from the site records for the area $H_{1/3}/h$ < 0.5.

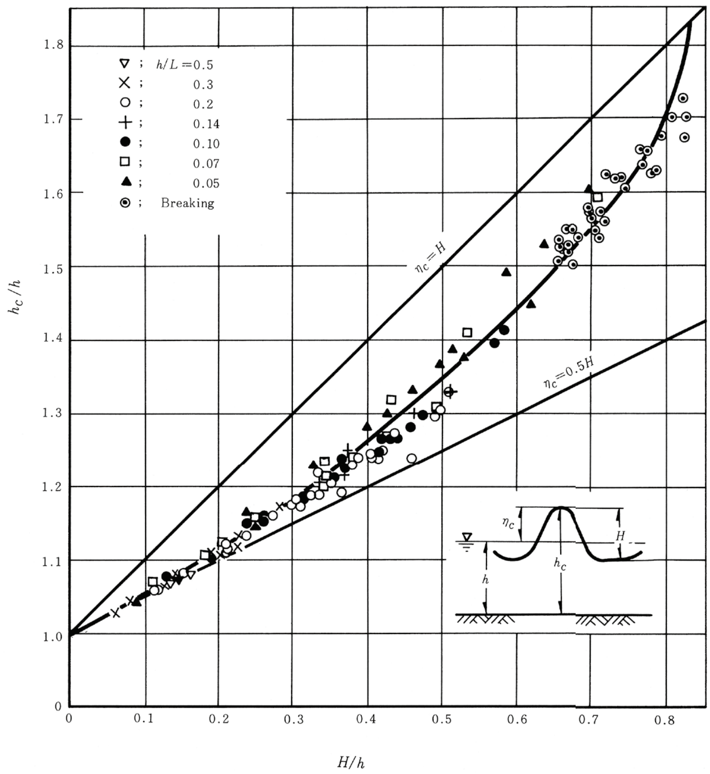

Fig. 4.2.2 Relative Wave Crest Elevation from the Sea Bed [21)]

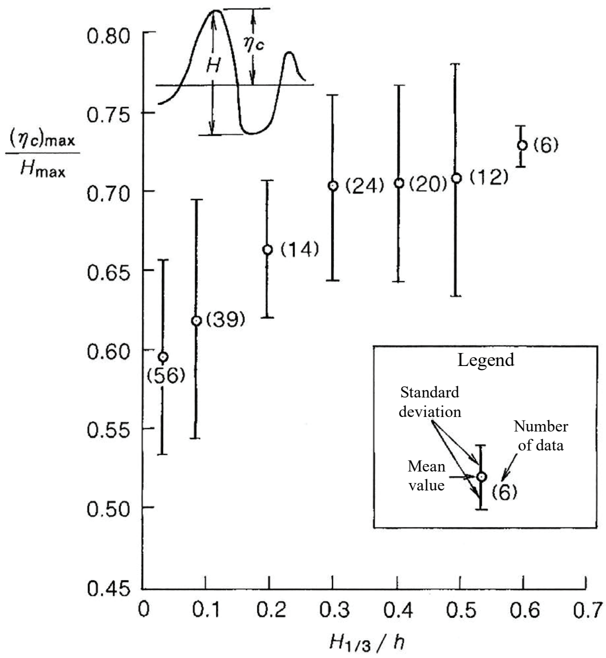

Fig. 4.2.3 Relation between the Maximum Wave Crest Elevation $(\eta_c)_{max}$ and $H_{1/3}/h$ [22)]

On the contrary, this effect can generally and practically be ignored because it is very small in deep sea areas and in shallow sea areas where relative water depth is sufficiently deep.

(6) Return period of offshore waves

Design waves are preferable to provide for the safety verification of the facilities after their completion and during their construction, respectively. When verifying safety during the service life and construction of port facilities, the offshore waves of proper return period must be selected according to the importance of the facilities. For general port facilities, which have a design service life of 50 years, a 50-year return wave may be used. However, although waves acting during construction (when facilities are left for a certain period with unfinished cross sections) need to be properly determined by considering the construction period of facilities and the natural conditions at the point concerned and others, waves on the order of a 10-year return wave may be used for the sake of convenience.

When reviewing design offshore waves as variable waves, it is a good idea to extract the peak wave height of the swell by focusing on period and wave steepness and by considering the return wave height obtained by statistically processing extreme waves as the design offshore waves of the swell as necessary, in addition to making the peak wave height in the past disturbance the peak wave data without any modification (see **Part II, Chapter 2, 4.1.1 (1) Setting of the variable wave conditions**). Moreover, when designing the port facilities that suffered from swell, performance verification shall be conducted together with the wave transformation calculation or model experiment for the design offshore waves of the swell for the design tide level.[6)]

(7) Utilization of the wave transformation calculation method

In the performance verification in the sea area where the relative water depth is roughly less than one-half of the offshore wave length, the design wave of facilities shall be calculated from the condition of offshore waves that is generally set by observation or wave hindcasting. When using the wave transformation calculation method, a calculation model should be properly selected according to the topography of the sea area where facilities are installed or on the basis of the importance of facilities.[23)] Although a graphic solution method that assumes regular waves as representative waves may be used in the sea area where it can be approximated by parallel bathymetric coast, the energy balance equation method,[24)] mild-slope equation method,[25)] and others can be used in the sea area with a complicated topography. Furthermore, a proper numerical calculation method should be used for the calculation in sea areas wherein water depth largely fluctuates or wherein refraction and diffraction occur simultaneously must be taken into consideration. For example, the energy balance equation method[26)] based on the small amplitude wave theory, which considers diffraction when the nonlinearity of waves can be ignored or handled separately; wave transformation calculation method,[27)] which uses the weakly nonlinear Boussinesq equation and is capable of simultaneously analyzing the reflection properties of wave-dissipating works when considering wave nonlinearity to some extent; and other methods can be used.

In the reliability design, it is necessary to properly provide the dispersion characteristics of calculation results from the real value by considering the errors in the wave transformation calculation method, referring to **Reference 28)**, etc.

(8) Utilization of the model experiment

When the shape of facilities is complicated, when wave transformation or nonlinearity is prominent, or when it is difficult to develop and utilize a proper numerical calculation method, it is preferable to conduct a hydraulic model experiment. In problems concerning waves, the effect of viscosity or surface tension of water is generally small; therefore, the Froude similarity law can be applied to the similarity between model and prototype for both the inertial and gravitational forces acting on the fluid. The Froude similarity law sets the scale reduction of time and velocity to the square root of the scale reduction of length. It is preferable to use a water tank that is 30 m or more wide and is equipped with a multidirectional random wave maker that can reproduce the multidirectional spreading waves in the hydraulic model test basin under consideration of the scale effect of a hydraulic model where the effect of viscosity and surface tension of water becomes relatively larger as the scale becomes smaller.[29)]

(9) Long-period waves and harbor resonance

Long-period waves, which have a water surface fluctuation with a frequency of several tens of seconds or longer, may exert a major effect on the mooring facilities or topography of the sea bottom. It is preferable to examine these waves on the basis of on-site observations and current analytical results if necessary (see **Part II, Chapter 2, 4.5 Long-Period Wave**). Long-period waves in a port not only excite the oscillation of large ships by resonance but also cause the elevation of water surface in front of facilities and increase wave overtopping rate and swash height. Given that they also exert a major effect on the littoral drift movement at the seaside, it is preferable to estimate the effect properly by field measurements. Moreover, the direction of long-period waves is difficult to restrict to one direction only. However, it may be practically possible to select the most dangerous wave direction in the range extending ten and several degrees to both sides of the wave direction which is assumed to be same as that of the wind waves and swells.[20)]

Harbor resonance, which is the natural resonance of harbors and bays, can affect not only moored ships but also the water level of the inner part of the bay; therefore, in the event that clear harbor resonance is found from the current tide records or in the event that the shape of the harbor is widely modified, it is preferable to examine the properties of the resonance with an appropriate numerical calculation method.[30)] (See **Part II, Chapter 2, 3.3 Harbor Resonance**.)

(10) Other items

A significant change of water depth due to dredging in navigation channels of a port necessitates the consideration of the variation in the navigation channels in the calculation of wave transformation. Considering that the reflection rate of upright wave-absorbing revetments largely changes according to the period of waves, the calculation of waves in a port should properly provide the reflection rate according to the wave period and should be verified using Computational Fluid Dynamics (CFD) method[31)] or model experiment as needed. Ship waves caused by navigating ships become bigger as ships grow larger and faster. The wave height may exceed 1 m. It is preferable to verify the influence of growing up of ship size on surrounding revetments, sand beaches, small fishing boats and small work ships.

In inner seas, such as in Tokyo Bay, the waves generated by strong wind and swells from the ocean become superposed. It is preferable to consider the effect of waves generated in the bay on the design wave by proper wave hindcasting or observation and to verify the effect of swells from the ocean and the increase of the swells in the bay.

At actual installation of facilities in shallow waters, transverse wave actions due to multidirectional spreading, wave amplification due to flows,[32)] effects of reflected waves, and so on must be considered in many cases. A more reasonable design can be achieved by considering these matters as a whole in the initial planning stage. The handling of waves during construction shall also be kept in mind.

(11) Concept of waves for the verification of stability in facilities

Acting waves need to be determined by keeping the following in mind in the performance verification of facilities:

① Random waves shall be used in principle.

② Offshore waves shall be determined by proper observation or wave hindcasting.

③ Offshore waves shall be set as probabilistic waves by considering the return period.

④ Wave transformation shall be calculated by considering the topography of target points.

⑤ Use a proper numerical calculation model for the estimation of design waves.

(a) Relatively deep sea area······································linear calculation model

(b) Shallow and topographically complicated sea area·········nonlinearity shall be preferably considered.

(c) Wave breaking or reflected waves occurs significantly····hydraulic model experiment is preferable

⑥ The tidal level that causes the severest action is basically employed as the design tidal level.

⑦ The stability of facilities during construction shall also be fully examined.

⑧ The return period of design waves during construction shall be properly set by considering the construction period.

⑨ Interaction between waves and flows shall be considered if the stream flow has a strong influence.

4.2.2 Representation of Waves

(1) Definition of Waves

The waves in the oceans are treated as random waves in principle and are set appropriately on the basis of past observation data and latest findings as far as possible. **Fig. 4.2.4** shows the definition of waves. Each wave is defined by the zero up-crossing method. Here, the height from the trough to the peak of the defined one wave is the wave height H, the spatial length is the wavelength L, and the wave propagation speed is the wave celerity C. The wave period T is defined as the time between two sequent zero-up crossing points in the time series of wave profiles observed at a fixed point. **Reference 33)** can be used as a reference for the specifics on the basic nature of waves.

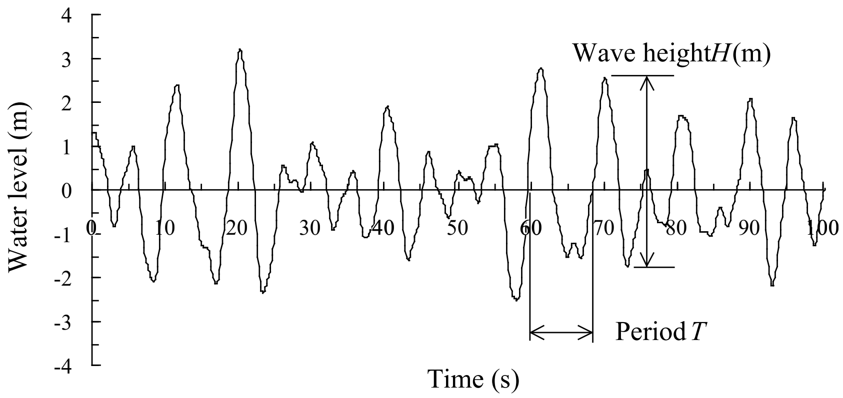

Fig. 4.2.4 Definition of Waves

(2) Waves Represented in Performance Verification

Considering that the wave height of random waves varies depending on time, representative waves shall be employed in the performance verification. Significant wave is normally employed as representative wave. For the representative wave, the waves in the record are counted and selected in descending order of wave height from the highest wave, until one -third of the total number of waves is reached. The height and period of the significant wave are calculated as the means of their heights and periods and denoted as $H_{1/3}$ and $T_{1/3.}$ The mean wave as a representative wave is calculated as the wave with mean height and period of all waves in the record. The highest wave refers to the wave having the height and period of the highest individual wave in the record. The height and period of the highest wave are denoted as H_{max} and T_{max}. The highest wave shall be employed for the stability verification of a breakwater.

On the assumption that wave energy is concentrated in the extremely narrow band of a certain frequency, the occurrence frequency of the wave heights included in a group of offshore waves follows the Rayleigh distribution, which is expressed in the following equation.

$$p(H/\overline{H}) = \frac{\pi}{2}\frac{H}{\overline{H}}\exp\left\{-\frac{\pi}{4}\left(\frac{H}{\overline{H}}\right)^2\right\} \quad \textbf{(4.2.5)}$$

where $\overline{H}$ denotes the height of the mean wave in the wave group. In the meantime, the period of actual sea waves fluctuates in a certain range; therefore, the wave height distribution tends to offset slightly from the Rayleigh distribution. However, it is known that the Rayleigh distribution consequently provides a very good approximate expression for the height distribution of individual waves defined in the zero up-crossing method.

In the event that the occurrence frequency of wave heights follows the Rayleigh distribution, the following relationship is derived between the heights of individual representative waves.

$$\left.\begin{array}{l} H_{1/10} = 1.27 H_{1/3} \\ H_{1/3} = 1.60 \overline{H} \end{array}\right\} \quad \textbf{(4.2.6)}$$

Here, $H_{1/10}$ is called the highest one-tenth wave height and is calculated using the highest one-tenth, similar to the calculation method for significant wave height.

Moreover, the mode and mean $H_{max}/H_{1/3}$, and the highest wave height $(H_{max})_\mu$, where μ denotes the value of the exceedance probability, are respectively given by the following equations, where the number of waves N_0 in the wave group is used as a parameter and γ is the Euler constant (0.5772…).

$$\left(H_{max}/H_{1/3}\right)_{mode} \approx 0.706\sqrt{\ln N_0} \quad \textbf{(4.2.7)}$$

$$\left(H_{max}/H_{1/3}\right)_{mean} \approx 0.706\left\{\sqrt{\ln N_0} + \gamma\big/\left(2\sqrt{\ln N_0}\right)\right\} \quad \textbf{(4.2.8)}$$

$$\left(H_{max}\right)_\mu\big/H_{1/3} \approx 0.706\sqrt{\ln\left[N_0/\ln\{1/(1-\mu)\}\right]} \quad \textbf{(4.2.9)}$$

The following equation is commonly employed as the relation between H_{max} and $H_{1/3}$. They are selected by considering the duration of waves subjected to design, i.e., the number of waves, reliability of the design wave estimation, accuracy of calculation methods, and importance and behavioral properties at the fracture limitation of structures. The relation H_{max}=1.8$H_{1/3}$ is often used in designing composite breakwaters.[34)]

$$H_{max} = (1.6 \sim 2.0) H_{1/3} \quad \textbf{(4.2.10)}$$

On the contrary, given that the period distribution is based on the correlation characteristic between the wave height and the period, there is no general form of the period distribution like the Rayleigh distribution for wave height. However, the following equation is true as an average relation among many observation records.

$$T_{max} \approx T_{1/3} = (1.1 \sim 1.3)\overline{T} \quad \textbf{(4.2.11)}$$

The ratio to $T_{1/3}$ varies to some extent according to the form of the frequency spectrum.

(3) Introduction of Random Waves

It is preferable in principle that random waves are employed in the performance verification. It is possible to consider random waves to be the superposition of regular waves with various periods, and the respective regular waves are called component waves. It is the frequency spectrum of a wave that indicates the degree of the energy of the component waves, and a spectrum shape corresponding to the properties of ocean should be employed in the performance verification. On Japan's seacoast, the Bretschneider–Mitsuyasu-type spectrum based on the observation data at the peak period $T_p \approx 1.05T_{1/3}$ or the modified Bretschneider–Mitsuyasu-type spectrum based on the relation $T_p \approx 1.13T_{1/3}$ obtained from the subsequent observation document is commonly employed.[35)]

The Bretschneider–Mitsuyasu spectrum shape is expressed by the following equation:

$$S(f) = 0.257 H_{1/3}^{\ 2} T_{1/3}^{\ -4} f^{-5} \exp\left\{-1.03 (T_{1/3} f)^{-4}\right\} \quad \textbf{(4.2.12)}$$

where

$S(f)$: frequency spectrum of the wave

$H_{1/3}$: significant wave height

$T_{1/3}$: significant wave period

f : frequency

The modified Bretschneider–Mitsuyasu-type spectrum shape is expressed by the following equation:

$$S(f) = 0.205 H_{1/3}{}^2 T_{1/3}{}^{-4} f^{-5} \exp\left\{-0.75(T_{1/3} f)^{-4}\right\} \qquad \textbf{(4.2.13)}$$

However, in inner bay areas, such as Tokyo Bay, the peak of the spectrum often becomes pointed; therefore, it is preferable to introduce a spectrum shape of the JONSWAP type[36] on the basis of observations to the greatest extent possible and to employ a spectrum that can reflect appropriately the observation results.

The spectrum shape of the JONSWAP type is shown by the following equations. Here, the peak enhancement factor γ takes a value between one and seven (3.3 in average), and the peak of the spectrum becomes steeper as the γ value increases. When $\gamma = 1$, **equation (4.2.14)** coincides with **equation (4.2.13)**.

$$S(f) = \beta_J H_{1/3}{}^2 T_p{}^{-4} f^{-5} \exp\left\{-1.25(T_p f)^{-4}\right\} \times \gamma^{\exp\left[-0.5\left\{(T_p f - 1)/\sigma\right\}^2\right]} \qquad \textbf{(4.2.14)}$$

$$\beta_J \approx \frac{0.0624}{0.230 + 0.0336\gamma - 0.185(1.9+\gamma)^{-1}}\left[1.094 - 0.01915 \ln \gamma\right] \qquad \textbf{(4.2.15)}$$

$$T_p \approx T_{1/3} \Big/ \left\{1 - 0.132(\gamma + 0.2)^{-0.559}\right\} \qquad \textbf{(4.2.16)}$$

$$\sigma \approx \begin{cases} 0.07 : f \le f_p \\ 0.09 : f > f_p \end{cases} \qquad \textbf{(4.2.17)}$$

where f_p is the peak frequency.

The representative wave height H_{m0} for these spectra is calculated as follows. If the wave spectra are concentrated within a narrow range of frequency band and if the wave height follows the Rayleigh distribution, H_{m0} equals to $H_{1/3}$ defined in the zero up-crossing method.

$$H_{m0} = 4.004\sqrt{m_0} \quad m_0 = \int_0^\infty S(f)df \qquad \textbf{(4.2.18)}$$

where m_0 is the total energy of waves.

Moreover, according to the statistic theory of random waves, the mean period T_{02} in the zero up-crossing method is calculated by the following equation.

$$T_{02} = \sqrt{m_0/m_2} \quad m_2 = \int_0^\infty f^2 S(f)df \qquad \textbf{(4.2.19)}$$

Furthermore, the mean period T_{01} is also used under the condition where the spectrum width is sufficiently small.

$$T_{01} = m_0/m_1 \quad m_1 = \int_0^\infty f S(f)df \qquad \textbf{(4.2.20)}$$

On the contrary, such cases are significantly increasing recently, particularly in Europe, that the representative period $T_{m-1,0}$ is hardly affected by the high-frequency component of spectrum and is almost equal to the significant wave period $T_{1/3}$ defined by the zero up-crossing method.

$$T_{m-1,0} = m_{-1}/m_0 \quad m_{-1} = \int_0^\infty f^{-1} S(f)df \qquad \textbf{(4.2.21)}$$

(4) Double-peaked spectrum

When two types of wave group having different dominant periods, such as wind waves and swells, are superimposed, double-peaked spectrum with peaks near each period may be observed. In such a case, the significant wave height used for the calculation of wave force may be obtained by energy synthesis (see **Part II, Chapter 2, 4.4.4 Reflection of Waves**), and the significant wave period $T_{1/3}$ may be calculated by the following equation.[37]

$$T_{1/3} = k\sqrt{\frac{(H_{1/3})_{\mathrm{I}}^{\ 2} + (H_{1/3})_{\mathrm{II}}^{\ 2}}{\dfrac{(H_{1/3})_{\mathrm{I}}^{\ 2}}{(T_{1/3})_{\mathrm{I}}^{\ 2}} + \dfrac{(H_{1/3})_{\mathrm{II}}^{\ 2}}{(T_{1/3})_{\mathrm{II}}^{\ 2}}}} \quad \textbf{(4.2.22)}$$

where

$$k = 1.0 + \alpha\left(R_H/\mu\right)^{-0.121A\ln(R_H/\mu)} \quad \textbf{(4.2.23)}$$

$$\alpha = 0.08\left(\ln R_T\right)^2 - 0.15\ln R_T \quad \textbf{(4.2.24)}$$

$$\mu = \begin{cases} 0.632 + 0.144\ln R_T & ; 0.1 \le R_T \le 0.8 \\ 0.6 & ; 0.8 \le R_T < 1.0 \end{cases} \quad \textbf{(4.2.25)}$$

$$A = \begin{cases} 13.97 + 4.33\ln R_T & ; 0.1 \le R_T \le 0.4 \\ 10.0 & ; 0.4 \le R_T < 1.0 \end{cases} \quad \textbf{(4.2.26)}$$

$$R_H = (H_{1/3})_{\mathrm{I}} \big/ (H_{1/3})_{\mathrm{II}} \quad \textbf{(4.2.27)}$$

$$R_T = (T_{1/3})_{\mathrm{I}} \big/ (T_{1/3})_{\mathrm{II}} \quad \textbf{(4.2.28)}$$

$(H_{1/3})_{\mathrm{I}}$, $(H_{1/3})_{\mathrm{II}}$: significant wave height (m) of wave groups I and II before superimposition

$(T_{1/3})_{\mathrm{I}}$, $(T_{1/3})_{\mathrm{II}}$: significant wave period (s) of wave groups I and II before superimposition

Wave group I has a shorter period.

(5) Introduction of the multidirectionality of Waves

In shallow waters, the wave height of the component waves becomes orthogonal to the shoreline owing to refraction effects, and the nature of the waves becomes closer to unidirectional random waves. Accordingly, a case in which the ratio of the water depth to the wavelength of offshore waves (h/L_0) becomes 0.1 or smaller is used as the benchmark; the waves in waters shallower than this may be approximated as waves that behave like unidirectional random waves and the approximation is limited to cases wherein the waves are employed as the variable action. In deeper waters, the character as multidirectional random waves whose component energy advances in various directions becomes stronger, and it is preferable to treat the waves as multidirectional random waves. Furthermore, given that the multidirectionality of the waves has a major effect in the stability at the head of a breakwater and the performance verification of floating facilities, the multidirectionality of the waves in waters should be examined beforehand with appropriate observation data. The wave direction has a major effect on the results in the calculation of the degree of calmness; thus, the waves are calculated as multidirectional random waves.

A directional wave spectrum is employed as an index for showing the multidirectionality of waves. The directional wave spectrum is the product of the abovementioned frequency spectrum $S(f)$ and the directional spreading function $G(f,\theta)$ and is expressed as $S(f,\theta) = S(f)G(f,\theta)$. The following Mitsuyasu-type directional spreading function is commonly employed in most cases as the directional spreading function.

$$G(f;\theta) = G_0 \cos^{2S}\left(\frac{\theta - \theta_0}{2}\right) \qquad \int_{-\pi}^{\pi} G(f;\theta)d\theta = 1 \quad \textbf{(4.2.29)}$$

where θ_0 signifies the principal wave direction. G_0 and S are expressed by the following equations, respectively.

$$G_0 = \left[\int_{\theta\min}^{\theta\max} \cos^{2S}\left(\frac{\theta - \theta_0}{2}\right)d\theta\right]^{-1} \quad \textbf{(4.2.30)}$$

$$S = \begin{cases} S_{\max}\left(f/f_p\right)^5 & : f \le f_p \\ S_{\max}\left(f/f_p\right)^{-2.5} & : f > f_p \end{cases} \quad \textbf{(4.2.31)}$$

Fig. 4.2.5 shows the distribution shape of the Mitsuyasu directional spreading function. The symbols of f, f_p, and l in the figure respectively denote the frequency, the peak frequency of the frequency spectrum, and the parameter in the function of $G(f,\theta) = G_0 \cos^{2l}(\theta - \theta_0)$ which is employed as the directional spreading function instead of **equation (4.2.29)**. The parameter of the directional wave function S_{max} is the directional spreading parameter introduced by Goda and Suzuki,[38)] and the following numerical values can generally be used.

Wind waves	$S_{\max} = 10$
Swell with a short attenuation distance	$S_{\max} = 25$
Swell with a long attenuation distance	$S_{\max} = 75$

However, the variance of the directional spreading parameter is large on-site. When the directional wave spectrum is observed on-site, these values should be used as a reference.

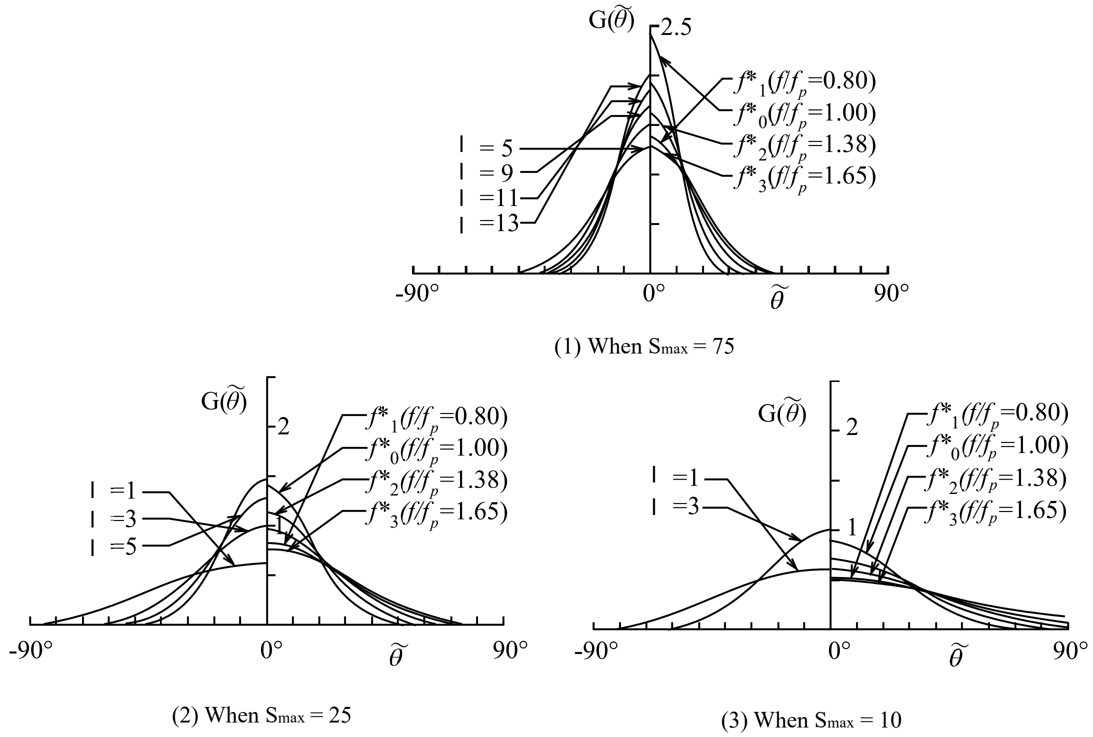

Fig. 4.2.5 Distribution Shape of the Mitsuyasu-Type Directional Spreading Function

The characteristics of the directional wave spectrum can also be expressed from the viewpoint of how the wave energy is distributed as a whole to each direction. To this end, the following curve $P_E(\theta)$ of the cumulative energy ratio shall be defined.

$$P_E(\theta) = \frac{1}{m_0}\int_{-\pi/2}^{\theta}\int_0^{\infty} S(f;\theta)dfd\theta \qquad m_0 = \int_0^{\infty}\int_{-\pi/2}^{\pi/2} S(f;\theta)d\theta df \tag{4.2.32}$$

Here, the range of component wave direction is set to [$-\pi/2$, $\pi/2$] because the components in the direction opposite to the principal one are commonly ignored in the calculation for the design.

Fig. 4.2.6 shows the cumulative curve of the wave energy obtained by using **equation (4.2.12)** as the frequency spectrum, **equation (4.2.29)** as the directional function, and **equation (4.2.31)** as the directional spreading parameter. The SWOP in the figure shows the cumulative curve of energy based on the directional function obtained from the stereo picture of the sea surface taken from two planes in the latter half of 1950s.

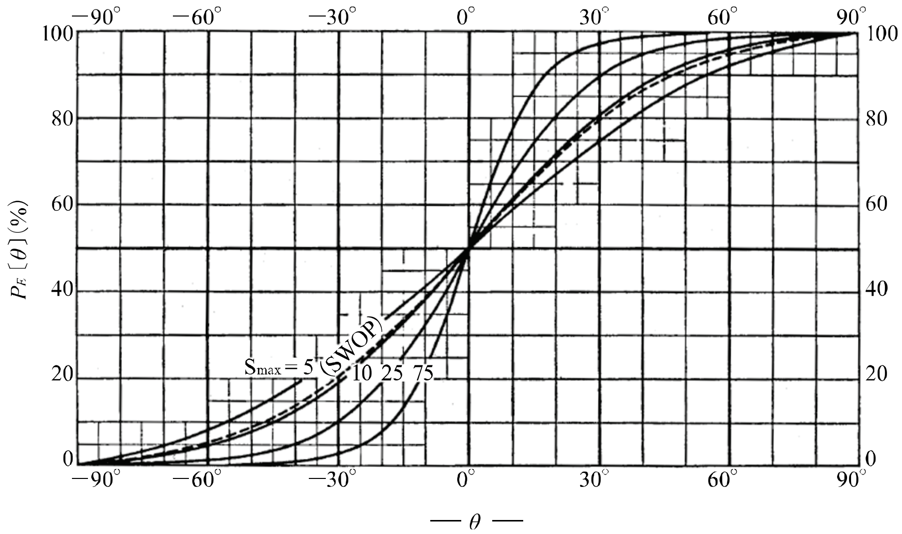

Fig. 4.2.6 Cumulative Curve of the Wave Energy

The directional spreading parameter S_{max} of offshore waves that expresses the directional spreading of wave energy varies depending on the wave steepness, and it can be estimated with **Fig. 4.2.7** in the event of inadequate observation data. Furthermore, in shallow waters, the value of directional spreading parameter varies depending on the sea bottom topography; therefore, it is preferable to estimate the parameter by a calculation of wave transformation. However, in cases wherein the coastline is close to linear with a simple topography and wherein the water depth contour is deemed parallel to the shoreline, the changes in S_{max} may be estimated by the diagram in **Fig. 4.2.8**.

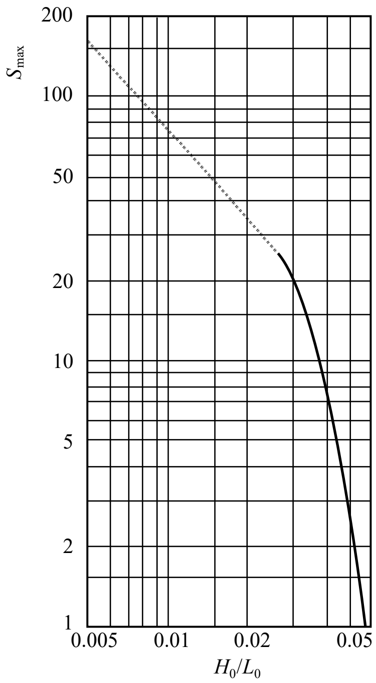

Fig. 4.2.7 Changes in S_{max} Due to Wave Shape Steepness

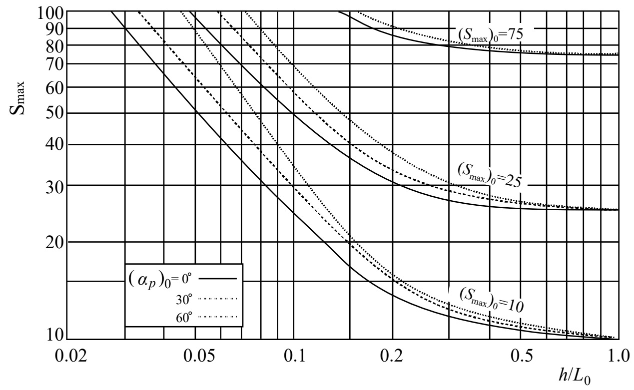

Fig. 4.2.8 Changes in S_{max} Due to Water Depth

(6) Wave direction

The wave direction is an important parameter for determining the direction of the forces acting on the facilities. It is preferable to determine the principal wave direction to the greatest extent possible by observing the directional wave spectrum or the flow speed of two components.[39] In the principal wave direction the crests in the wave train are distributed most densely, and the principal direction is considered an angle where the peak in the directional wave spectrum appears. However, when the swells from outside the bay and the wind waves that occur inside the bay overlap each other, bidirectional waves that have two peaks for the directional spreading function appear frequently.[40] In these cases, even if the principal wave direction is determined, it is seldom that this principal wave direction represents the direction in which the energy of the wave proceeds. Therefore, one should examine special measures, such as carrying out the performance verification of the facilities at the most dangerous wave direction, carrying out the performance verification for the respective wave directions, and setting the facilities to be stable for both.

4.3 Generation, Propagation and Attenuation of Waves

(1) Summary of the Wave Hindcasting Method

Wave hindcasting estimates the temporal and spatial changes in wind direction and wind velocity of the prescribed water area from the topographical and meteorological data and estimates the waves under the wind field. There are various methods for wave hindcasting based on the wind field data of the prescribed water area. In general, these methods can be divided roughly into the significant wave method and the spectrum method, which is the mainstream method at present.

(2) Wave Hindcasting by the Significant Wave Method

The modern wave hindcasting method that was first developed in the world treats the series of phenomena known as the generation, development, propagation, and attenuation of waves collectively and estimates the wave height $H_{1/3}$ (m) and period $T_{1/3}$ (s) with wind velocity U_{10} (m/s) value at 10 m above the sea surface, wind duration t (s), and fetch length F (m) as parameters. Its forerunner is the SMB method, which was proposed by Sverdrup and Munk[41] in the 1940s and was revised by Bretschneider.[42), 43)] Currently, the further improved Wilson IV formula [44)] is generally employed:

$$gH_{1/3} \Big/ U_{10}{}^2 = 0.30\left[1-\left\{1+0.004\left(gF/U_{10}{}^2\right)^{1/2}\right\}^{-2}\right] \quad \textbf{(4.3.1)}$$

$$gT_{1/3}/(2\pi U_{10}) = 1.37\left[1-\left\{1+0.008\left(gF/U_{10}^2\right)^{1/3}\right\}^{-5}\right] \quad \textbf{(4.3.2)}$$

where

$H_{1/3}$: significant wave height (m)

$T_{1/3}$: significant wave period (s)

U_{10} : wind velocity at 10 m above the sea surface (m/s)

F : fetch (m)

g : gravitational acceleration (m/s^2)

Fig. 4.3.1 illustrates these relational expressions (the unit of the fetch F is expressed by meter units in **equations (4.3.1)** and **(4.3.2)**, and it is expressed by kilometer units in **Fig. 4.3.1**). However, these relational expressions are for cases wherein the wind is continuously blowing constantly for an adequately long time; after the wind starts blowing, it does not reach this wave height or period. Waves generated at the upper extremity of the fetch propagate with growth and arrive at the fetch distance F(m) after the required time. The required time is called the minimum duration t_{min}(s) and is expressed by the following equation.

$$t_{\min} = \int_0^F \frac{1}{C_g(x)}dx \quad \textbf{(4.3.3)}$$

where

t_{min} : minimum duration (s)

$C_g(x)$: group velocity of the waves (m/s)

Furthermore, it is possible to make a rough estimate by using the following equation. [9)]

$$t_{\min}' = 1.0F'^{0.73}U_{10}^{-0.46} \tag{4.3.4}$$

where

$t_{\min}'$: minimum duration (hr)

F'' : fetch (km)

It is necessary to pay attention to the fact that the units of the symbols are different between **equations (4.3.3)** and **(4.3.4)**. When the wind duration is shorter than the minimum duration, the waves are in the state of full development and their magnitude is determined by the wind duration. On the other hand, when the wind duration is longer than the minimum one, the waves are in the process of developing with time and their magnitude depends on the fetch length. Therefore, in cases wherein the fetch and the duration are simultaneously provided, we must adopt the smaller wave of the two waves calculated by the wind duration and the fetch length.

The SMB method fundamentally applies to uniform wind field. However, in the event that the wind speed changes gradually, the waves can be hindcasted by using the equi-energy line (the line showing $H_{1/3}^2\ T_{1/3}^2$ = const).

In the event that the width is shorter than the fetch in a lake or bay or in the event that the fetch is determined by the opposite shore distance and varies widely to the minute fluctuations of the wind direction, **equations (4.3.1)** and **(4.3.2)** provide a wave height or period larger than real. In such cases, it is better to employ the effective fetch[45)] provided by the following formula.

$$F_{eff} = \sum F_i \cos^2\theta_i \Big/ \sum \cos\theta_i \tag{4.3.5}$$

where,

F_{eff} : effective fetch (km)

F_{i} : opposite shore distance in the ith direction from the hindcasting point of the wave (km)

θ_{i} : angle between the direction of the opposite shore distance F_{i} and the principal wind direction, -45° ≤ θ_{i} ≤ 45°

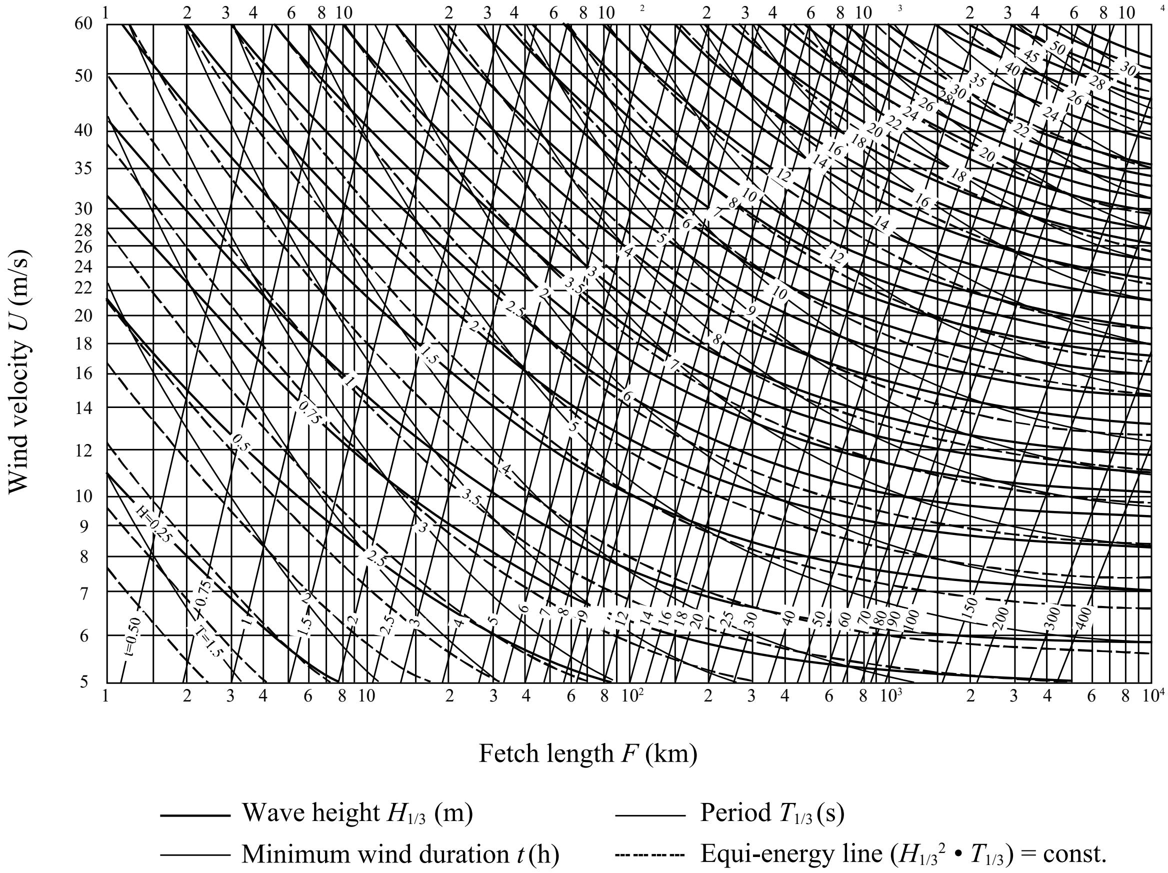

Fig. 4.3.1 Wind Hindcasting Diagram

Moreover, Mitsuyasu [46)] proposed the following equations for the wave hindcasting by assuming the finite fetch.

$$gH_{1/3}/U_{10}{}^2 = 2.15\times10^{-3}\left(gF/U_{10}^2\right)^{0.504} \quad \textbf{(4.3.6)}$$

$$gT_{1/3}/\left(2\pi U_{10}\right) = 5.07\times10^{-2}\left(gF/U_{10}^2\right)^{0.330} \quad \textbf{(4.3.7)}$$

where

$H_{1/3}$: significant wave height (m)

$T_{1/3}$: significant wave period (s)

U_{10} : wind velocity at 10 m above the sea surface (m/s)

F : fetch (m)

g : gravitational acceleration (m/s^2)

In the SMB method, when the wind field significantly varies like a typhoon or extra tropical cyclone, it is difficult to provide suitably the values for wind velocity U_{10}, fetch F, or wind duration t. As the methods that solve this problem, Wilson's graphical calculation method,[47)] and the methods of Ijima[48)] and Horikawa,[49)] which solve Wilson's equation numerically, are commonly employed.

As shown in **equations (4.3.1)** and **(4.3.2)**, the significant wave method is nothing more than a formula that links empirically the development of wind waves with the basic parameters and is not a formula that is constructed in line with the mechanisms of generation and development of waves. Owing to this nature, it leaves a number of vague points, such as how to handle cases wherein the wind gradually deflects, as well as the transition from wind waves to swells and the method for composing wind waves and swells. Furthermore, there is also the problem that the wave direction obtained by hindcasting agrees with the wind direction at the final step of calculation. However, under the condition that the wind field is simple in the sea and the effects of swells can be ignored, it is a practical estimation method that is simpler than the spectral method and has a short calculation time.

For swells that propagate away from the generation and development areas of wind waves, the Bretschneider equation[50)] was proposed on the basis of simple theoretical considerations and various empirical knowledge.

$$\frac{(H_{1/3})_D}{(H_{1/3})_F} = \left[\frac{k_1 F_{\min}}{k_1 F_{\min} + D}\right]^{\frac{1}{2}} \qquad \textbf{(4.3.8)}$$

$$\frac{(T_{1/3})_D}{(T_{1/3})_F} = \left[k_2 + (1-k_2)\ \frac{(H_{1/3})_D}{(H_{1/3})_F}\right]^{\frac{1}{2}} \qquad \textbf{(4.3.9)}$$

where

$(H_{1/3})_F$: significant wave height at the terminus of the fetch (m)

$(T_{1/3})_F$: significant wave period at the terminus of the fetch (s)

$(H_{1/3})_D$: wave height of a swell (m)

$(T_{1/3})_D$: wave period of a swell (s)

$F_{\min}$: minimum fetch that generates the wave (km)

D : attenuation distance of waves, i.e., distance between the end of wind area and the arrival position of swells (km)

Constant : $k_1 \fallingdotseq 0.4$, $k_2 \fallingdotseq 2.0$

Furthermore, the propagation time t of a swell is given by the following equation.

$$t = \frac{4\pi D}{g(T_{1/3})_D} \qquad \textbf{(4.3.10)}$$

where

t : propagation time of swells (s)

D : attenuation distance of waves, i.e., distance between the end of wind area and the arrival position of swells (km)

$(T_{1/3})_D$: wave period of swells (s)

G : gravitational acceleration (m/s^2)

A wave hindcasting method for shallow water area has also been proposed.[51)]

(3) Wave Hindcasting by the Spectral Method

In general, the following formula is employed for wave hindcasting by the spectral method.

$$\frac{\partial E(\omega,\theta)}{\partial t} + C_g \nabla E(\omega,\theta) = S_{net}(\omega,\theta) \qquad \textbf{(4.3.11)}$$

Here, C_g is the group velocity, the first term at the left stands for the local temporal change in wave spectral density $E(\omega, \theta)$, and the second term stands for the changes due to the transmission effect of the wave spectral density. Furthermore, $S_{net}(\omega, \theta)$ on the right side is the term expressing the total amount of change in energy related to the change of the wave spectral components and is provided by the following formula:

$$S_{net} = S_{in} + S_{n\ell} + S_{ds} \qquad \textbf{(4.3.12)}$$

Here, S_{in} is the energy transmitted from the wind to the waves. S_{nl} is the gain and loss of the energy that occurs between the four component waves with different wave numbers and is called the transport of wave energy by nonlinear interactions (hereinafter "nonlinear transport of wave energy"). The nonlinear interactions due to these four waves cause the shape of the directional wave spectrum to vary, with the total sum of energy that the waves have constant. S_{ds} stands for the effects where the energy of the waves dissipates owing to white-cap breaking waves or the internal viscosity of seawater.

Models based on the spectral method are classified into the disjoined propagation (DP) model, the coupled hybrid (CH) model and the coupled disjoined (CD) model, depending on how the nonlinear transport of wave energy term S_{nl} is treated. In the DP model, the nonlinear transport of wave energy term is not introduced directly, and the respective frequency and directional components are not coupled to each other. In the CH model, the nonlinear interactions between component waves are parameterized and introduced. In the CD model, the nonlinear interactions are introduced directly in one form or another.

On the contrary, the models are also classified by the period when they were developed. The DP model, which was developed from the 1960s to the beginning of the 1970s, is the first-generation model. The CH model and CD model, which were developed from the 1970s to the 1980s, are second-generation models, and the CD model, which was developed from the latter half of the 1980s to the present and handles the nonlinear interactions with a higher accuracy, is a third-generation model. In the third-generation model, the degree of flexibility of the scheme of the nonlinear transport of wave energy term is high, and it is possible to hindcast with good accuracy even in cases of waves wherein bidirectional waves, wind waves, and swells are all present.

The wave hindcasting model of the Japan Meteorological Agency started from MRI, [52] which is a first-generation model, and was developed into MRI-II[53] and MRI-II new,[54] which are second-generation models. MRI-III,[55] which is a third-generation model, is currently being employed. In addition to these, the Inoue model[56] and the Yamaguchi–Tsuchiya model[57] are known as a first-generation model, and the Tohoku model[58] is known as a second-generation model, and the WAM[59] is known as a third-generation model. Furthermore, in the first-generation models, a one-point method[60] wherein the waves at one spot are calculated along the wave ray of each component wave that arrives at one spot has been developed.

(4) First-generation model: MRI Model[52]

The MRI model, developed in 1973, was employed for the numerical wave forecast service of the Japan Meteorological Agency for approximately a decade from 1977.

In the MRI model, the linear and exponential developments of wind waves due to wind are taken into consideration as well as the physical mechanisms of energy dissipation due to the effects of breaking waves, internal friction and headwinds. The effects of nonlinear transport of wave energy S_{nl} are not considered formally, but the effects are expressed indirectly by employing the wave development equation[56], which does not separate the nonlinear transport of wave energy S_{nl} from the transport of wave energy S_{in} from the wind to the wave.

The total amount of change in energy S_{net} is divided into cases of tailwinds and headwinds and is expressed as follows.

$$
\begin{aligned}
S_{net} &= (A+BE)\left\{1-(E/E_{PM})^2\right\}\Gamma(\theta-\theta_w) && : E \le E_{PM}\,,\ \ |\theta-\theta_w| < \pi/2 \\
S_{net} &= -D f^4 E && : E > E_{PM}\,,\ \ |\theta-\theta_w| < \pi/2 \\
S_{net} &= -\left\{B\Gamma(\theta-\theta_w)+D f^4\right\}E && : |\theta-\theta_w| > \pi/2
\end{aligned}
\qquad \textbf{(4.3.13)}
$$

Here, f is the frequency, θ is the wave direction, θ_w is the wind direction, and $E = E(f,\theta)$ is the directional wave spectrum. E_{PM} is the Pierson–Moskowitz spectrum and is employed as the standard form of a saturated spectrum. Furthermore, Γ $(\theta-\theta_w)$ is the directional wave function that is proportionate to $\cos^2\theta$, A and B are the linear and exponential development rates[56] of wind waves per unit time, and D is the coefficient of internal friction (eddy viscosity).

In a DP model including the MRI model, the spectrum shape of the waves is expressed to gradually approximate a saturated spectrum by multiplying the term of the form $\{1-(E/E_{PM})^2\}$, and $-(E/E_{PM})^2$ expresses the formal energy dissipation. Furthermore, in the DP model, the calculation time is short, and it has practical accuracy with respect to wave height; therefore, it is employed currently as a wave model that can be used simply and conveniently.

(5) Third-generation model: WAM Model[59]

The WAM model is a representative third-generation wave hindcasting model that directly calculates the nonlinear interactions of four wave resonance, by the discrete interaction approximation[61] of S. Hasselmann and K. Hasselmann.

In the model of the spectral method, the transport of wave energy from wind to wave is generally provided by the following.

$$S_{in} = A + BE \tag{4.3.14}$$

Here, A corresponds to the Phillips resonance mechanism, and BE corresponds to the Miles instability mechanism. The Phillips resonance mechanism is a mechanism wherein the random pressure fluctuations of wind that blows over a still water surface and the component waves that have a spatial scale and phase velocity that matches the former cause resonance; owing to the phenomena, a wave is generated. On the contrary, the Miles instability mechanism is a mechanism wherein the airflow on the water surface is disturbed and becomes unstable owing to the unevenness of the water surface due to waves, and energy is efficiently transmitted from wind to waves owing to this phenomenon. In the WAM model, the following equation, from which the items related to the Phillips resonance mechanism are omitted, is adopted:

$$S_{in} = BE \tag{4.3.15}$$

However, in this method, if the initial value of the wave spectrum energy is assumed zero, no waves are generated; therefore, it is possible to provide a spectrum calculated from the fetch length and initial velocity as the initial value.

In the WAM model cycle 4, Janssen's quasilinear theory[62), 63] was incorporated in the calculation equation for the transport of wave energy term from wind to waves. Owing to this, even in the event that the conditions of the offshore winds are identical, it is possible to perform calculations that are closer to reality such that the amount of wave energy transported from wind is greater for waves with a younger age.

In the energy dissipation term of the WAM model, the effects of white-cap breaking waves and sea bottom friction have been taken into consideration.

In the nonlinear transport term of wave energy of the WAM model, the nonlinear interactions of the four wave resonance have been taken into account. Nonlinear interactions are a phenomenon wherein the component waves making up the spectrum exchange the energy that they respectively have. Although no change is imparted directly to the total energy of the wave, effects appear on the amount of energy transport from wind to waves and on the amount of energy dissipation due to the fact that the spectral shape changes. Thereafter, the nonlinear transport of wave energy of four wave resonance is expressed by the following equation. [64]

$$\begin{aligned} S_{n\ell} = \omega_4 \int_{-\infty}^{\infty}\int_{-\infty}^{\infty}\int_{-\infty}^{\infty} & Q(\mathrm{k}_1, \mathrm{k}_2, \mathrm{k}_3, \mathrm{k}_4)\delta(\mathrm{k}_1 + \mathrm{k}_2 - \mathrm{k}_3 - \mathrm{k}_4)\delta(\omega_1 + \omega_2 - \omega_3 - \omega_4) \\ & \times \{n_1 n_2 (n_3 + n_4) - n_3 n_4 (n_1 + n_2)\} d\,\mathrm{k}_1\, d\,\mathrm{k}_2\, d\,\mathrm{k}_3 \end{aligned} \tag{4.3.16}$$

Here, $n(\mathrm{k}) = E(\mathrm{k})/\omega$ stands for the wave action density, $Q(\ )$ is the joint function of the spectrum components, δ is the delta function, k is the wave number vector, and the subscripts are the four wave components. The delta function expresses the resonance conditions, and nonlinear interactions occur among the component waves that satisfy the following relations:

$$\mathrm{k}_1 + \mathrm{k}_2 = \mathrm{k}_a = \mathrm{k}_3 + \mathrm{k}_4, \quad \omega_1 + \omega_2 = \omega_a = \omega_3 + \omega_4 \tag{4.3.17}$$

However, the combinations of the resonance that satisfies these relations exist infinitely. Owing to this, an immense burden is involved in calculating all of these combinations; thus, in the actual model, one representative combination is chosen, and S_{nl} is approximated.

Third-generation wave hindcasting models other than WAM include SWAN[65] and Wave Watch III.[66] SWAN is based on WAM, and is expanded so that topographical breaking waves and wave setup can be considered. This model is employed for wave hindcasting in shallow waters. Furthermore, Wave Watch III has been improved by the recent upgrade[67] to increase the accuracy of the hindcasting for periods and swells.

Although wave hindcasting using the wave spectrum method basically uses a third-generation wave hindcasting model, it is preferable to select the wave hindcasting model which shows good results in the comparison with the observed waves.

4.4 Wave Transformations

In general, the waves for designing port facilities shall be appropriately set as waves that are most unfavorable in terms of structure stability or usage of port facilities. In this consideration, appropriate attention shall be given to wave transformations during the wave propagation from the deep water to the shore, including refraction, diffraction, shoaling, breaking, and others. In the calculation of wave transformations the waves should be regarded as multidirectional random waves, and the wave transformations have to be calculated after assigning the offshore waves with an appropriate directional wave spectrum[68]. However, when determining the rough wave height of the action, an approximate solution may be calculated using regular wave with the representative wave height and period (e.g., $H_{1/3}$ and $T_{1/3}$) of random waves.

Fig. 4.4.1 shows the outline of wave transformations near ports and shores, together with the structure of this chapter.

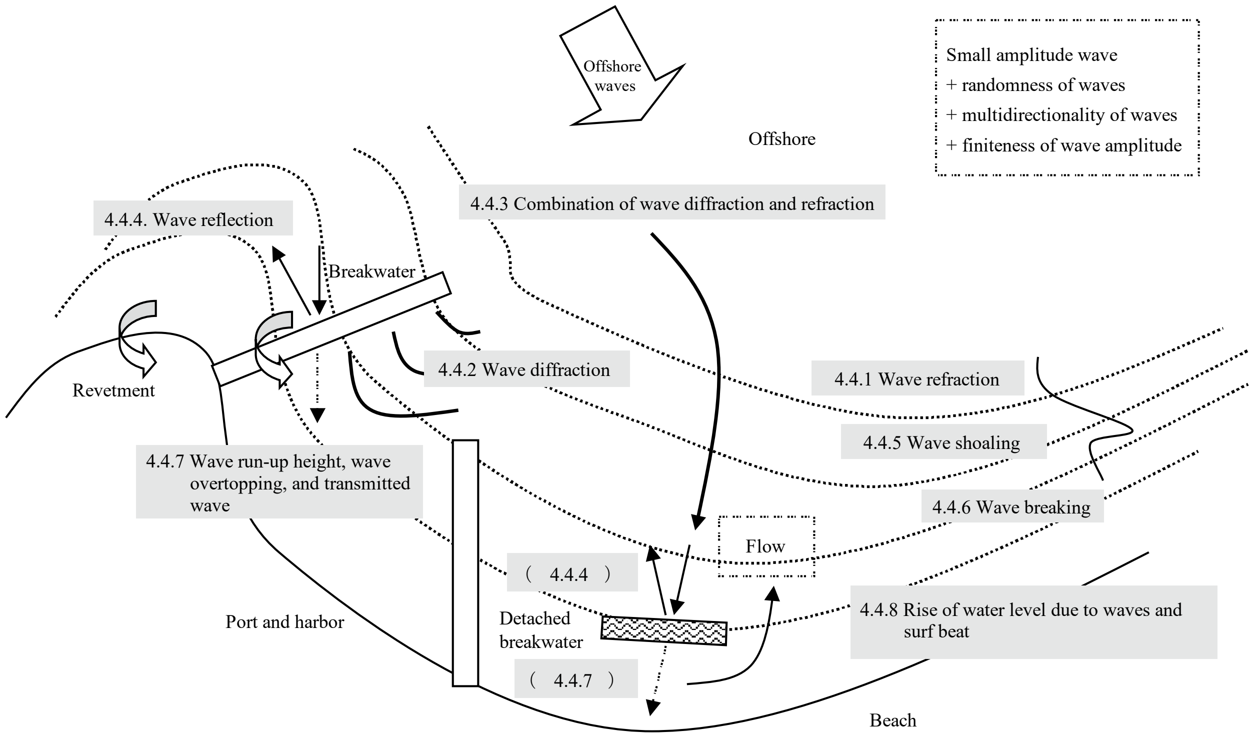

Fig. 4.4.1 Wave Transformations near Ports and Shores

4.4.1 Wave Refraction

(1) In shallow waters, the changes in wave celerity that depend on place accompanying the changes in water depth cause the wave refraction phenomenon. Therefore, the changes in wave height and wave direction due to refraction must be considered.

(2) Refraction is a phenomenon whereby the waves change their travel direction as the water depth becomes shallower. The travel direction generally changes perpendicular to the contour line in shallow sea areas. This is the phenomenon that must be verified in the performance verification of facilities when the wave height changes at the same time. For a beach that can be considered a simple one with a parallel contour line, the calculation results of regular wave refraction using the specifications of representative waves may be used as an approximate value. In principle, the effect of refraction in shallow sea areas is calculated by the numerical calculation.

(3) Wave refraction calculation of regular waves[69]

Figs. 4.4.2 and **4.4.3** show the refraction coefficient and refraction angle, which can be calculated from the wave refraction of regular waves, such as refraction drawing.

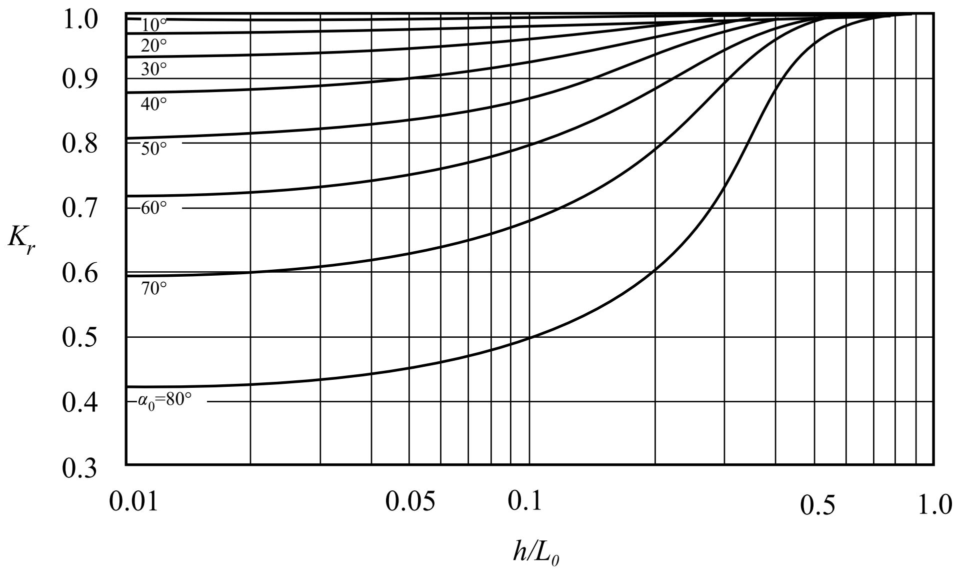

Fig. 4.4.2 Wave Refraction Coefficient of Regular Waves at a Coast with Straight, Parallel Contour Lines

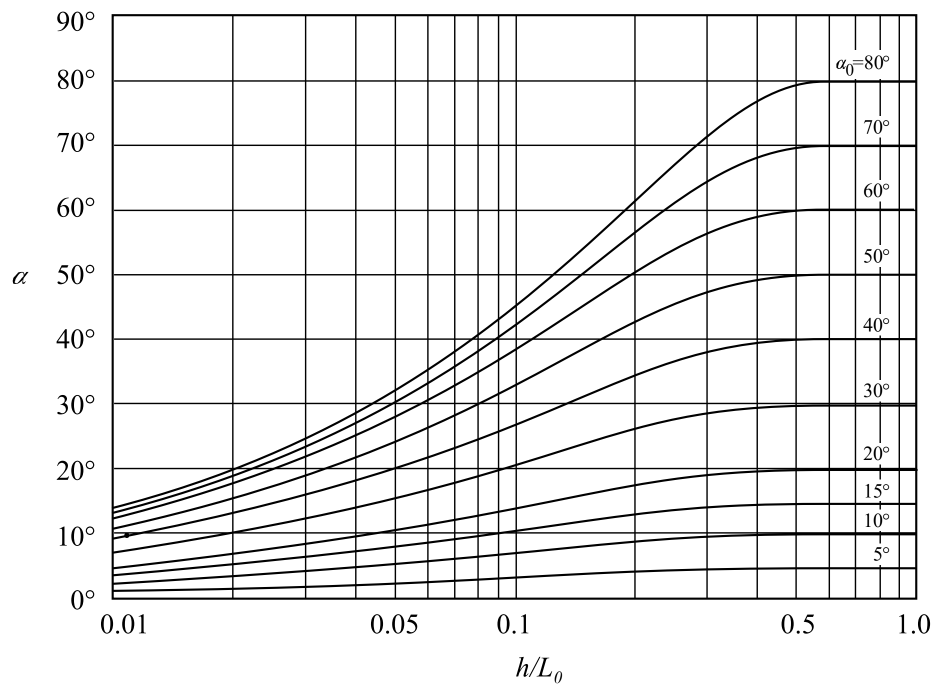

Fig. 4.4.3 Variation Diagram of Regular Wave Directions at a Coast with Straight, Parallel Contour Lines

(4) Refraction Calculation for Random Waves

① Calculation methods

The calculation method for refraction analysis for random waves includes the following: ① the component wave method,[70)] wherein the directional wave spectrum is divided into an appropriate number of component waves, a refraction calculation is performed for each component wave, and the wave refraction coefficient for the random wave is evaluated by making a weighted average of the component wave energies; ② methods in which the wave energy balance equation[24)] or the mild-slope equation[25)] for a wave is solved using a computer with finite difference schemes. Similar to the component wave method, the energy balance equation is derived by assuming that wave energy does not pass across wave rays and flow in/out. This means that the technique is basically the same in both cases. However, in the energy balance equation method, the refraction within a small section is calculated, i.e., the wave refraction coefficient does not become infinite even at a point in which two regular wave rays may converge. On the contrary, the mild-slope equation method for a wave is strictly analytical, but it is difficult to apply it to a large region. When determining the wave refraction coefficient for random waves, it is acceptable to use the component wave method, which involves the linear superposition of wave refraction coefficients for regular waves and is simple and convenient. However, when the intersections of wave rays occur during a refraction calculation for a component wave, the energy balance equation method may be used for practical purposes with the exception of a case wherein the degree of intersection is large.

② **Effects of diffraction**

When deepwater waves have been diffracted by an island or a headland, the wave spectrum becomes generally different from a standard form that has been assumed initially. Therefore, it is necessary to use the spectral form after diffraction when performing the refraction calculation.

③ **Diagrams of the wave refraction coefficient and angle for random waves at a coast with straight, parallel depth contours**[38)]

Figs 4.4.4 and **4.4.5** show the wave refraction coefficient K_r and the principal wave direction $(\alpha_p)_0$, respectively, for random waves at a coast with straight, parallel depth contours, with the principal direction of the deepwater waves $(\alpha_p)_0$ as the parameter. The direction $(\alpha_p)_0$ is expressed as the angle between the wave direction and the line normal to the boundary of the offshore sea. S_{max} is the maximum value of the parameter that expresses the degree of directional spreading of wave energy. (See **Part II, Chapter 2, 4.2.2 Representation of Waves**)

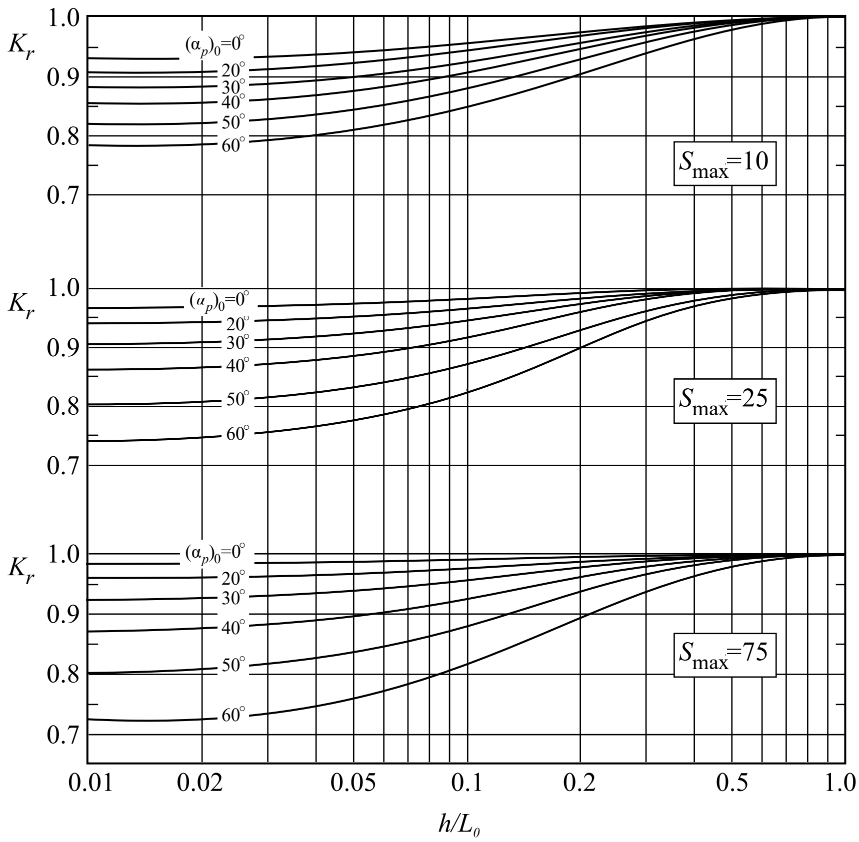

Fig. 4.4.4 Wave Refraction Coefficient of Random Waves at a Coast with Straight, Parallel Depth Contours

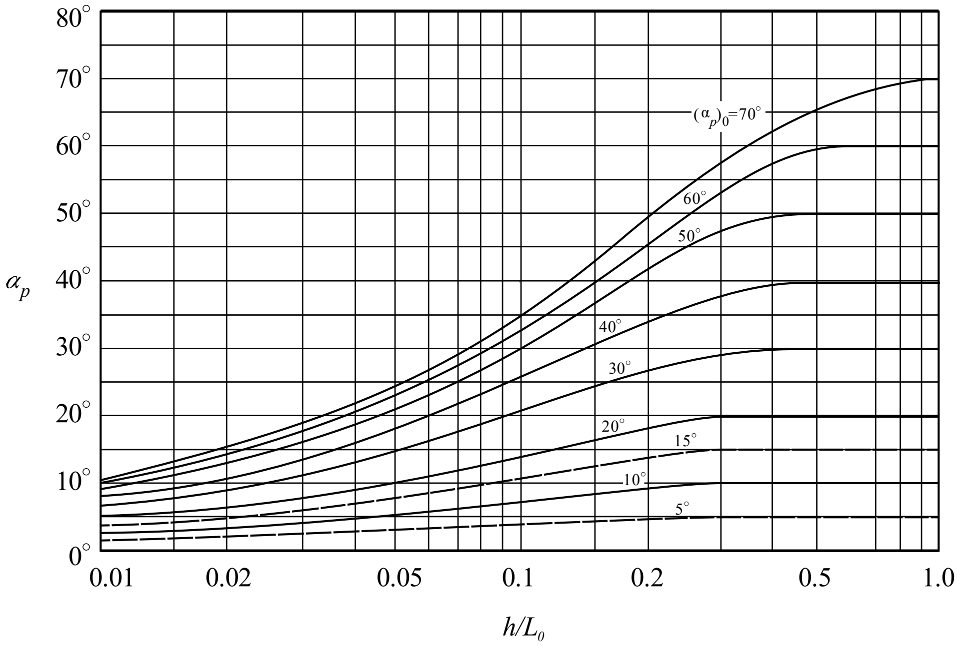

Fig. 4.4.5 Change Due to Refraction in the Principal Direction α_p of Random Waves at a Coast with Straight, Parallel Depth Contours

(5) Energy Balance Equation

The energy balance equation calculates the changes of the spectrum of random waves due to refraction and wave shoaling in the shallow waters and calculates the wave height change in shallow waters. **Equation (4.4.1)** shows the basic form of the energy balance equation.

$$\frac{\partial}{\partial x}(Sv_x)+\frac{\partial}{\partial y}(Sv_y)+\frac{\partial}{\partial \theta}(Sv_\theta)=0 \tag{4.4.1}$$

$$\begin{aligned} v_x &= C_g \cos\theta \\ v_y &= C_g \sin\theta \\ v_\theta &= \frac{C_g}{C}\left(\sin\theta\frac{\partial C}{\partial x}-\cos\theta\frac{\partial C}{\partial y}\right) \end{aligned} \tag{4.4.2}$$

Here, S is the directional spectrum of the wave, C is the wave celerity, C_g is the group velocity of the waves, and θ is the wave angle that is measured counterclockwise from the positive direction of the x axis. **Equation (4.4.1)** can be solved from offshore to the direction of the waves. In **equation (4.4.1)**, the right term is zero, and the total energy of the wave being propagated is not considered to vary. Takayama et al.[24] focused on the change in energy flux in the surf zone and added the energy loss due to wave breaking expressed in $-\varepsilon'_b S$ to the right side (where ε'_b is the dissipation factor of lost energy in a unit time due to wave breaking) to make improvements so that the effects of horizontally expanded wave breaking can be treated. Although it is not strict, it enabled the effects of reflected waves to be calculated. Therefore, the linear wave transformation due to a phenomenon other than diffraction can be calculated.

Fig. 4.4.6 shows an example of improved calculation by the energy balance equation.

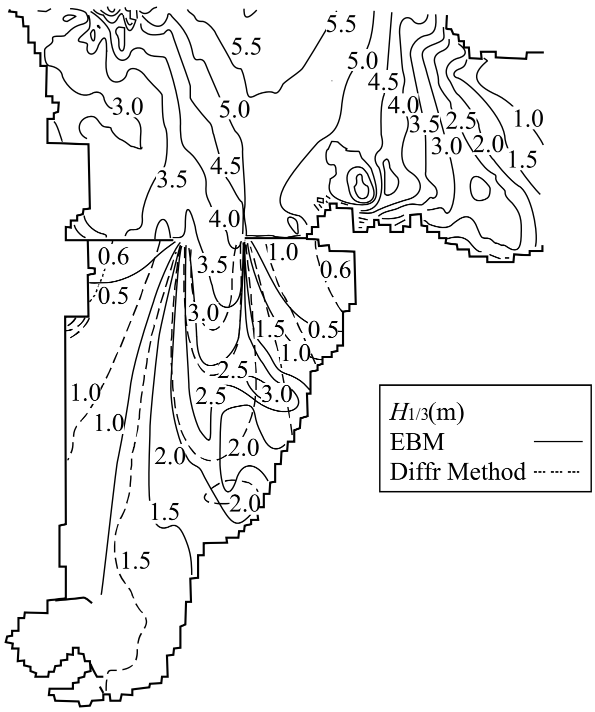

Fig. 4.4.6 Example of Calculation of the Wave Height Distribution by the Energy Balance Equation

In the figure, the solid line is the wave height distribution based on the energy balance equation, and the broken line is the wave height distribution calculated by taking into consideration only the diffraction inside the harbor. The energy balance equation is also applied to wave fields wherein the effects of refraction and diffraction are large. Considering that the shielding effect of structures to the directional dispersion of random waves are dominant compared with the invasion of wave energy due to diffraction, it is possible to examine the wave height inside a harbor that is shielded by a breakwater, excluding the area immediately behind it. The energy balance equation method,[26)] which considers that diffraction has been improved in the accuracy of the calculation of wave height distribution directly behind the breakwaters.

(6) At places wherein the water depth is 0.5 times less than the offshore wave height, the nature as a flow is more prominent than the nature as a wave; thus, the refraction calculation employed for computing the wave height and refraction coefficient is applied to the range where the water depth is 0.5 times deeper than the offshore wave height.

4.4.2 Wave Diffraction

(1) The wave height in regions where waves are anticipated to be greatly affected by the diffraction phenomenon caused by obstacles such as breakwaters or islands, needs to be calculated using an appropriate method.

(2) Diffraction is a phenomenon that waves invade into a water area sheltered by breakwaters or other obstacles. Since this phenomenon is important when determining the wave height in a harbor, the irregularity of waves should be considered in a diffraction calculation. For a harbor within which the water depth is assumed uniform, the diffraction diagrams for random waves with regard to a semi-infinite length breakwater or straight breakwaters with one opening are prepared. On the contrary, the cases that the regular wave diffraction diagram can be applied approximately to on-site waves are restricted to the diffraction of swells of which wave steepness are small (on the order of $H_0/L_0 \leq 0.005$) with the aligned wave crest line.

(3) Diffraction Calculation of Regular Waves

The change in wave heights due to diffraction can be calculated using the Sommerfeld solution in the velocity potential theory. **Reference (Part III), Chapter 4, 1. Wave Diffraction Diagram** shows the regular wave diffraction diagram by a semi-infinite breakwater and straight breakwaters with one opening.

(4) Diffraction Calculation of Random Waves

① **Types of Calculation Methods**

Although the wave diffraction calculation of random waves in harbors with relatively simple shapes can be performed by applying diffraction diagrams, it is generally conducted by numerical computation within a complex shape of harbor. The diffraction calculation methods include Takayama's method,[71)] which involves the linear superposition of analytical solutions for detached breakwaters, and calculation methods that use the Green functions.[72)] On the other hand, when the width of an island or the width of the entrance of a bay is at least ten times the wave length of the incident waves, the estimate by the directional spreading method[73)] using the amount of wave energy that arrives directly at the point of interest behind the island or in the bay can be approximately used.[74)] However, if the point of interest is just behind an island or headland, the effects of diffracted waves will be large; therefore, this method cannot be applied.

② **Effect of Refraction**

Diffraction diagrams and diffraction calculation methods assume that the water depth within the harbor is uniform. If there are large variations in water depth within the harbor, the errors will become large; in this case, it is preferable to examine the wave height in the harbor by either hydraulic model tests or numerical calculation methods that also take the effect of refraction into account.

③ **Diffraction Diagram**

The random wave diffraction diagram of a semi-infinite breakwater and straight breakwaters with one opening is shown in **Reference (Part III), Chapter 4, 1. Wave Diffraction Diagram**. S_{max} = 10 corresponds to the wind waves, S_{max} = 25 corresponds to the swells in the initial damping, and S_{max} = 75 corresponds to swell-like waves. However, in shallow water areas, the change in S_{max} due to refraction needs to be considered.

④ **Treatment of obliquely incident waves**

When waves are obliquely incident to breakwaters with opening, it is preferable to obtain the diffraction diagram by using a numerical calculation. When this is not possible or when the diffraction diagram is only required as a rough guideline, the following approximate method may be used instead. In the case of semi-infinite breakwaters, approximate values can be obtained by rotating the diffraction diagram for perpendicular incident waves to the principal direction of waves.

(a) Determining the axis of the diffracted wave

When waves are obliquely incident to breakwaters with opening, the direction θ' of the axis of the diffracted waves (see **Fig. 4.4.7**) varies slightly from the direction of incidence θ. **Tables 4.4.1 (a) to (c)** list the direction of the axis of the diffracted waves as a function of the breakwater opening width ratio B/L and the direction of incident waves. These tables are used to obtain the direction θ' of the axis of the waves after diffraction, and the virtual opening width ratio B'/L corresponding to θ' is obtained from **equation (4.4.3)**:

$$B'/L = (B/L)\sin\theta' \qquad \textbf{(4.4.3)}$$

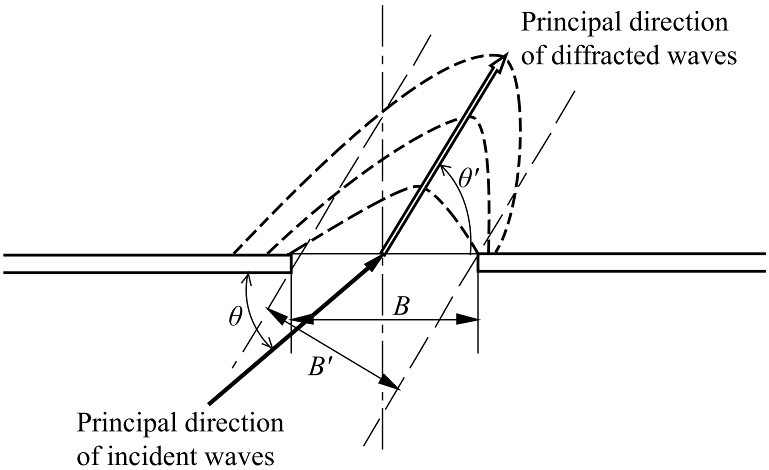

Fig. 4.4.7 Virtual Opening Width B' and Angle of Axis of Wave after Diffraction θ'

Table 4.4.1 Angle of Axis of Random Wave (θ') (The angle in parentheses is the angle of deflection relative to the angle of incidence.)

(a) S_{max} = 10

B/L	Angle between breakwater and wave direction θ			
	15 °	30 °	45 °	60 °
1.0	53 ° (38 °)	58 ° (28 °)	65 ° (20 °)	71 ° (11 °)
2.0	46 ° (31 °)	53 ° (23 °)	62 ° (17 °)	70 ° (10 °)
4.0	41 ° (26 °)	49 ° (19 °)	60 ° (15 °)	70 ° (10 °)

(b) S_{max} = 25

B/L	Angle between breakwater and wave direction θ			
	15 °	30 °	45 °	60 °
1.0	49 ° (34 °)	52 ° (22 °)	61 ° (16 °)	70 ° (10 °)
2.0	41 ° (26 °)	47 ° (17 °)	57 ° (12 °)	67 ° (7 °)
4.0	36 ° (21 °)	42 ° (12 °)	54 ° (9 °)	65 ° (5 °)

(c) S_{max}= 75

B/L	Angle between breakwater and wave direction θ			
	15 °	30 °	45 °	60 °
1.0	41 ° (26 °)	45 ° (15 °)	55 ° (10 °)	66 ° (6 °)
2.0	36 ° (21 °)	41 ° (11 °)	52 ° (7 °)	64 ° (4 °)
4.0	30 ° (15 °)	36 ° (6 °)	49 ° (4 °)	62 ° (2 °)

(b) Fitting of a diffraction diagram

Among the diffraction diagrams of normal incidence (see **Reference (Part III), Chapter 4, 1 Wave Diffraction Diagram**), the diffraction diagram that has a ratio of an opening width B to a wave length L nearly equal to the breakwater opening width virtual ratio is selected. This diffraction diagram is next rotated until the direction of incident waves matches the direction of the axis of the diffracted waves as determined from **Table 4.4.1**. The diffraction diagram is then copied and taken to be the diffraction diagram for obliquely incident waves. The errors in this approximate method are the largest around the opening in the breakwaters; in terms of the diffraction coefficient, the maximum error with the approximate method may amount to around 0.1.

⑤ **Notes on the diffraction calculation**

(a) If there is no diffraction diagram with the equal open width ratio B/L, it is common to use a diffraction diagram with an approximate value or to interpolate from two diffraction diagrams with approximate values.

(b) Given that the wave diffraction is more affected by the change in wave direction than by the change in period, diffraction by island or others, which is larger than the wave length, can be calculated by the directional spreading method by considering only the directional spread of wave energy.[59)]

(c) When the water depth changes significantly in the wave sheltered area, the wave refraction also needs to be considered with an appropriate method.

(d) It needs to be noted that the period of significant waves of diffracted random waves is different from the period before diffraction.

(e) When diffracted waves are reflected by quay walls and similar structures, the effect of reflection needs to be calculated by the superposition method for wave diffraction analysis[75)] or other proper methods.

(f) The broken waves may enter the port entrance in a storm with a significantly high wave height. Furthermore, in this case, the wave height in the port may be calculated by using a diffraction diagram. However, when the directional spreading of wave energy becomes concentrated when waves are broken, a high directional spreading parameter S_{max} of 75 or more or a regular wave diffraction diagram needs to be used.

⑥ **Studies by hydraulic model tests**

Owing to improvements of multidirectional random wave generators, it is easy to reproduce waves that have directional spreading in the laboratory nowadays, i.e., diffraction model tests can be performed relatively easily. When performing a model test, an opening in the harbor model is established within the effective wave generating zone, and the wave height is simultaneously measured at a number of points within the harbor. The diffraction coefficient is obtained by dividing the significant wave height in the harbor by the averaged significant wave height for at least two observation points at the harbor entrance.

4.4.3 Combination of Diffraction and Refraction (Equivalent Deepwater Wave Height)

(1) When performing diffraction calculations for waves in waters where the water depth varies greatly, wave refraction must also be considered.

(2) When the water depth within a harbor is more-or-less uniform by dredging, which is often seen in large harbors, the refraction of waves after diffraction can be ignored. To determine the wave height in the harbor in this case, it is acceptable to first perform a calculation by considering only refraction, wave shoaling, and breaking from the offshore wave hindcasting point to the harbor entrance. Thereafter, a diffraction calculation for the area within the harbor is performed by taking the incident wave height to be equal to the estimated wave height at the harbor entrance. In this case, the wave height H at a point of interest within the harbor is expressed using the following equation:

$$H = K_d K_r K_s H_0 \tag{4.4.4}$$

where

K_d : diffraction coefficient at the point of interest

K_r : refraction coefficient at the point of interest

K_s : shoaling coefficient at the point of interest (see **Part II, Chapter 2, 4.4.5 Wave Shoaling**)

H_0 : deepwater wave height

The energy balance equation method or the improved energy balance equation method,[24)] in which a term representing dissipation due to wave breaking is added, is appropriate as the calculation method for refraction analysis for the ocean. The harbor calmness calculation method of Takayama[71)], wherein diffraction solutions for detached breakwaters are superimposed to obtain the change in the wave height of random waves within the harbor due to diffraction and reflection, can be used for the diffraction calculation for the area within the harbor provided that there are no complex topographic variations within the harbor.

In **equation**(4.4.4), the assumed wave height by multiplying K_r and K_d by H_0 is used as the equivalent deepwater wave height H_0' and is calculated with the following equation.

$$H_0' = K_r K_d H_0 \tag{4.4.5}$$

The equivalent deepwater wave height is the assumed offshore wave used for the performance verification on the results obtained from 2D water tank experiments. The wave height H_0' is obtained by multiplying the effects of refraction and diffraction calculated in advance by H_0. By using wave height H_0', it is possible to make use of the calculation diagrams shown in **Part II, Chapter 2, 4.4.5 Wave Shoaling**, **4.4.6 Wave Breaking**, and **4.4.7 Wave Run-up Height, Wave Overtopping, and Transmitted Waves**.

(3) When there are large variations of water depth even in the area sheltered by breakwaters often seen in the case with relatively small harbors and coastal areas, it is necessary to simultaneously consider both diffraction and refraction within the harbor. If wave reflection is ignored and if only the approximate change in wave height is examined, it is possible to perform refraction and diffraction calculations separately; thereafter, the change in wave height can be estimated by multiplying together the refraction and diffraction coefficients obtained.

Calculation methods that allow the simultaneous consideration of the refraction and diffraction of random waves include the energy balance equation, which considers diffraction[26)]; a method that uses time-dependent mild-slope equations for wave[76)]; a method in which the Boussinesq equation is solved using the finite difference method;[77)] and the multicomponent coupling method of Nadaoka et al.[78)] There are also references in which other calculation methods are explained.[79)] The wave transformation calculation model using the Boussinesq equation has been modified, and NOWT-PARI (Nonlinear wave transformation model by Port and Airport Research Institute) has been proposed as one of the models that can be used at ports.[27)] Modified versions that allow the simultaneous consideration of run-up and seawall wave overtopping in shallow waters have also been proposed.[80)] Designers should use appropriate numerical calculation methods by taking into consideration water area characteristics and the application limit of the program.

4.4.4 Wave Reflection

(1) General

① In the performance verification of port facilities, examination shall be performed on the effects of reflected waves from neighboring structures on the facilities in question and on the effects of wave reflection from the facilities in question on neighboring areas.

② It is necessary to take note of the fact that the waves reflected from port facilities can exercise a large influence on the navigation of ships and cargo handling. For example, the waves reflected from breakwaters can cause disturbances in navigation water ways, and multiple-reflected waves from quay walls can cause agitations inside harbors.

③ **Composition of Reflected Waves and Incident Waves**

When incident waves and waves reflected from a number of reflective boundaries coexist, the wave height H_s can be calculated using **equation (4.4.6)**. Here, a train of incident waves and those of reflected waves from reflective boundaries are termed "wave groups."

$$H_s = \sqrt{(H_1^2 + H_2^2 + \cdots + H_n^2)} \tag{4.4.6}$$

where

H_s : significant wave height when all of the wave groups are taken together

$H_1, H_2, \ldots, H_n$: significant wave heights of individual wave groups

However, if the wave action varies with the wave direction, the differences in the wave directions of various wave groups must be considered. The calculated wave height is valid for places that are approximately more than 0.7 wavelengths away from a reflecting boundary. In a range within 0.7 wavelengths from the reflecting boundary, the remaining restraint condition for the phases of incident waves and reflected waves significantly changes the wave height.

Regarding the diffraction or refraction of waves, for which wave direction is an important factor, the significant wave height of each wave group is determined separately by performing the calculation necessary for that wave group when the wave directions are different among various wave groups. Thereafter, the composite wave height is calculated by putting these significant wave heights into **equation (4.4.6)**. Here, the composite period may be obtained by applying **equation (4.2.22)**. An acceptable alternative is to determine the spectrum for each wave group, add these spectra together to calculate the spectral form when the wave groups coexist, and then perform diffraction or refraction calculations by using this spectrum.

④ **Methods for Calculating the Effects of Reflected Waves**

The calculation methods for investigating the extent of the effects of waves reflected from a structure include the calculation method of wave height distribution around an island [81] and a simple method by means of diffraction diagrams.

(a) Calculation method of wave height distribution around an island[81]

In this calculation method, the theoretical solution that shows the wave transformation around a single convex corner is separated into three terms, namely, the incident, reflected, and scattered waves. The term for the scattered waves is progressively expanded to obtain an approximate equation so that the method can be applied to a case where there are a number of convex corners.

When there are a number of convex corners, it is assumed as a precondition that the lengths of the sides between convex corners are at least five times the wavelength of the incident waves so that the convex corners do not interfere with each other. It is necessary to pay attention to the fact that errors may become large if the sides are shorter than this.

Considering that another assumption is made such that the water depth is uniform, the refraction of reflected waves cannot be calculated. In general, it is sufficient for practical purposes if the lengths of the sides between convex corners are at least three times the wavelength of the incident waves. This calculation method can also be applied to the reflection of random waves by superposing component waves. Although the wave diffraction problems can also be analyzed with this calculation method, there will be large errors if it is applied to the diffraction of waves by thin structures, such as breakwaters.

(b) Simple method by means of diffraction diagrams

The example shown in **Fig. 4.4.8** is explained as follows. The wave height at point A on the front face of a detached breakwater is estimated when waves are incident on the detached breakwater at an angle α.

Instead of the detached breakwater, it is assumed that there are virtual breakwaters with opening (dashed lines in **Fig. 4.4.8**). Thereafter, one considers the situation whereby waves are incident on the virtual opening from both the wave direction of the incident waves and the direction symmetrical to this with respect to the detached breakwater (i.e., the direction shown by the dotted arrow in **Fig. 4.4.8**) and draws the diffraction diagram for the opening (dotted lines in **Fig. 4.4.8**). The range of influence of the reflected waves is represented by means of the diffraction diagram for the virtual breakwaters with opening. Accordingly, supposing that the diffraction coefficient at point A is read off as being 0.68, the wave height ratio with respect to the incident waves at point A is obtained by combining the value of 0.68 with a value of 1.0 representing the incident waves; given that the energies are added, the wave height ratio becomes $\sqrt{1+0.68^2}=1.21$. However, it should be noted that this value of 1.21 represents the mean value of the wave height ratio around point A. It is not preferable to use this method for points within 0.7 wavelengths away from the detached breakwater because the errors due to a phase coupling effect will be large.

For the case of wave reflection by a semi-infinite breakwater, the virtual breakwater also becomes a semi-infinite breakwater in the opposite direction; thus, the diffraction diagram for a semi-infinite breakwater is used. When the reflection coefficient of the front surface of the breakwater is less than 1.0 (e.g., owing to wave-dissipating work), the diffraction coefficient should be multiplied by the reflection coefficient before being used. For example, if the reflection coefficient of the detached breakwater is 0.4 in the previous example, the wave height ratio at point A becomes $\sqrt{1+(0.4\times 0.68)^2}=1.04$.

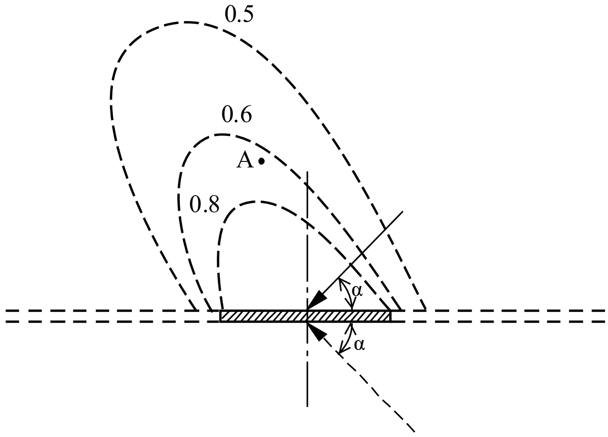

Fig. 4.4.8 Sketch Showing the Effect of Reflected Waves

(2) Estimation of Reflection Coefficient

① Reflection coefficients need to be determined appropriately on the basis of the results of field observations, hydraulic model tests, and past data.

② **Approximate Values for Reflection Coefficient**[82)]

It is preferable to calculate the value of a reflection coefficient by field observations. However, when it is difficult to perform observation or when the structure in question has not yet been constructed, it is possible to estimate reflection coefficient by referring to the results of hydraulic model tests. In this case, it is preferable to use random waves as test waves. The following is a list of approximate values for the wave reflection coefficients of several types of structures.

Upright wall	: 0.7–1.0 (0.7 is for the case of a low crown with much wave overtopping)
Submerged upright breakwater	: 0.5–0.7
Rubble mound slope	: 0.3–0.6
Deformed wave-dissipating blocks	: 0.3–0.5
Upright wave-dissipating structure	: 0.3–0.8
Natural beach	: 0.05–0.2

With the exception of the upright wall, the lower limits in the above ranges of reflection coefficient correspond to the case of steep waves and the upper limits to waves with low steepness. However, it should be noted that with the upright wave-dissipating structure, the wave reflection coefficient varies with the wavelength, and the shapes and dimensions of the structure. Furthermore, the reflection coefficients of swells with a period longer than 10 seconds or long period waves with a period of several tens of seconds become higher than the abovementioned values in the case of wave energy dissipating blocks or upright wave-dissipating structures. In recent years, there have been reports about calculation methods that incorporate a function that can reproduce the nature wherein the reflection characteristics of waves vary in accordance with the thickness and the porosity of the wave-dissipating layer in nonlinear wave transformation model, which can calculate a wave form temporally and spatially. [83)] See **Part II, Chapter 2, 4.5 Long Period Waves** for the wave reflection coefficient of long period waves.

③ **Calculation Method of Reflection Coefficient**

(a) Model experiment

It is best to obtain the reflection coefficient of facilities from the field wave height measurement. However, given that the field measurement is expensive and time consuming, the reflection coefficient of typical facilities may be determined by model experiments. The reflection coefficient of regular waves from the model or the edge of a water tank can be obtained by Healy's method which uses wave height records obtained by moving a wave gauge or by Goda–Suzuki's analysis method for separation of incident and reflected waves [84] using wave gauge records of a pair of stationary wave gauges. Furthermore, the latter method is mainly used for random waves.[85]

(b) Field measurement

The reflection coefficient measurement method in experimental flumes is difficult to apply to field measurement. However, Goda–Suzuki's analysis method for separation of incident and reflected waves may be applied if the wave direction is relatively stable in shallow sea area and is considered perpendicular to facilities. The estimation of the reflection coefficient by measuring the directional wave spectrum is possible if the waves acting on offshore breakwaters, etc. cannot be considered single directional waves.[86]

(3) Transformation of Waves at Concave Corners, near the Heads of Breakwaters, and around Detached Breakwaters

① Around the concave corners of structures, near the heads of breakwaters, and around detached breakwaters, the wave height becomes larger than the normal value of standing waves owing to the effects of diffraction and reflection. This increase in wave height shall be examined thoroughly. Moreover, the irregularity of waves shall be considered in the analysis.

② **Influence of Wave Irregularity**

When the wave height distribution near the concave corner, the head of a breakwater, or around a detached breakwater is calculated for regular waves, a distributional form with large undulations is obtained. However, when wave irregularity is incorporated into the calculation, the undulated form of the distribution becomes smoothed out, excluding the region within one wavelength of a concave corner, and the peak value of the wave height becomes decreases. Therefore, a calculation using regular waves overestimates the increase in wave height.

③ **Graphs for Calculating Wave Height Distribution around a Concave Corner**

Fig. 4.4.9 shows the wave height distributions for random waves near a concave corner. This figure exhibits the form of the distribution of the maximum value of the wave height, as obtained from numerical calculations for each principal wave direction. It has been assumed that waves are completely reflected by the breakwater. In the diagram, K_d is the ratio of the wave height at the front of the main breakwater to the incident wave height. The random waves used in the calculation has a spectral form with S_{max} = 75, which implies a narrow directional spreading. The long dash-dotted line in each graph shows the distribution of the maximum value of the wave height at each point, as obtained using an approximate calculation. l_1 is the length of the main breakwater, l_2 is the length of the wing breakwater, and β is the angle between the main breakwater and the wing breakwater. This figure may be used to calculate the wave height distribution near a concave corner. When it is not easy to use the calculation program, the approximate calculation method (a simple method with diffraction diagrams) may be used.

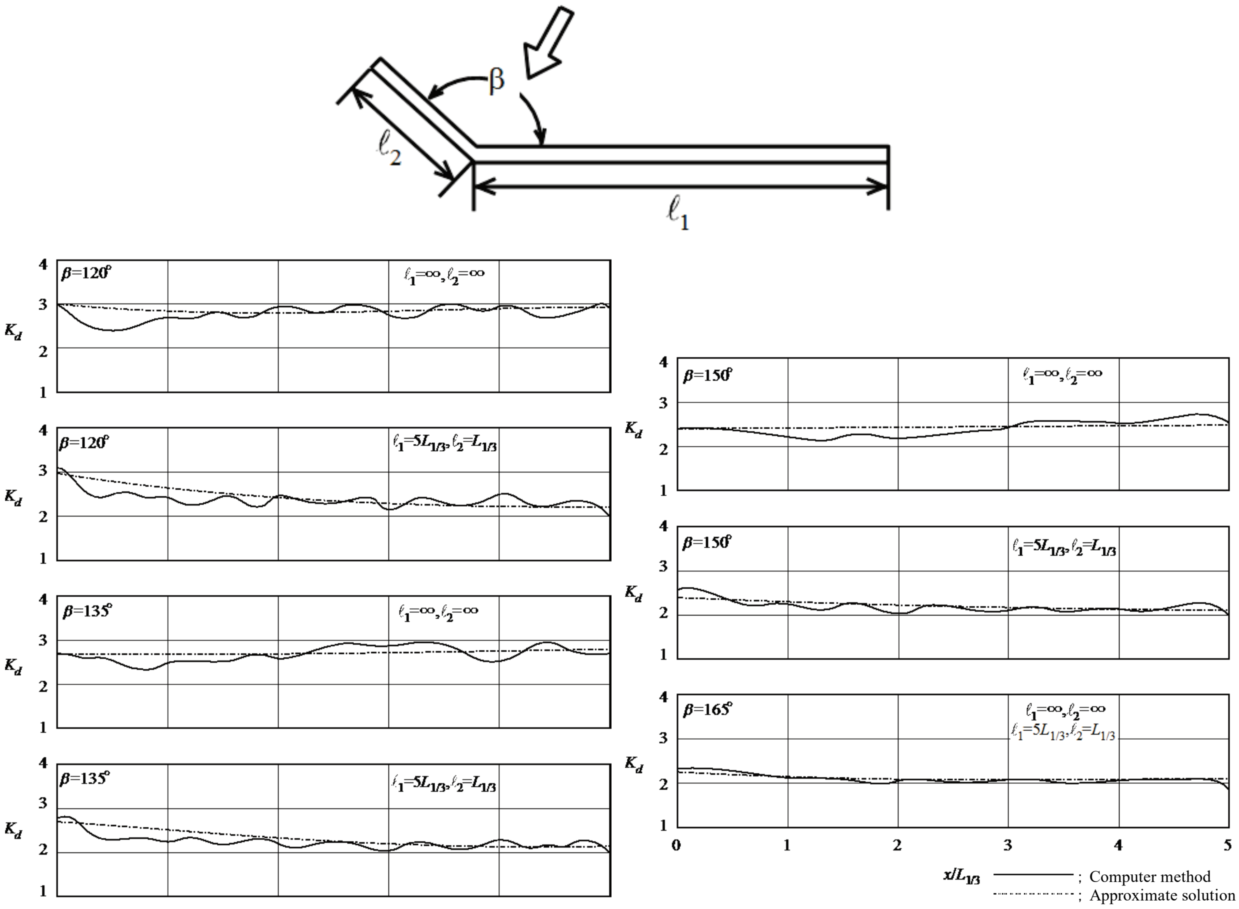

Note: Each diagram shows the distribution of the maximum values of wave height in the x axis direction along the principal breakwater (length: l_1) with the concave corner set to x = 0.

Fig. 4.4.9 Distribution of the Maximum Value of the Wave Height around Concave Corner[87)]

④ **Wave Height–Reducing Effects of Wave-Dissipating Work**

When a wave-dissipating work is installed to reduce the increase in wave height around a concave corner and if the wave-dissipating work is such that the reflection coefficient of the breakwater becomes no more than 0.4, it is quite acceptable to ignore the increase in wave height due to the presence of a concave corner. However, this is only the case when the wave-dissipating work extends along the whole of the wing breakwater. If the wing breakwater is long, one cannot expect the wave-dissipating work to be very effective unless it is installed along the entire length of the breakwater because the effect of waves reflected from the wing breakwater extend even to places that are at a considerable distance away from the concave corner. The same can be said for the influence of the main breakwater on the wing breakwater.

⑤ **Increase in Wave Height at the Head of a Breakwater**

Near the head of a semi-infinite breakwater or those of breakwaters with opening, specifically within a distance of one wavelength from the head, the waves diffracted by breakwaters cause local wave height increase over the normal standing wave heights. Given that the wave height distribution has an undulating form even at the back of a breakwater, it is necessary to pay attention to the fact that the difference in water level between the inside and outside of the breakwater causes a large wave force. **Fig. 4.4.10** shows an example of the results of a calculation of the ratio of the wave force to that of a standing wave near the head of a breakwater.

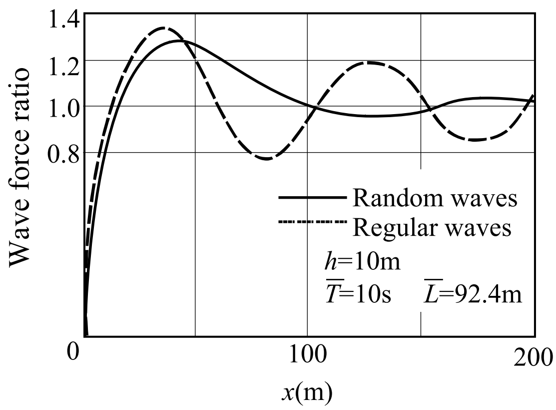

Fig. 4.4.10 Wave Force Distribution along a Semi-infinite Breakwater[88)]

⑥ **Increase in Wave Height around Detached Breakwater**

Along a detached breakwater, waves with a height greater than that of normal standing waves are produced, and the wave height distribution takes an undulating form even at the back of the breakwater because of the effect of wave diffraction at the two ends of the breakwater. The wave force also becomes large owing to the difference between the water levels in the front and back sides of the breakwater. In particular, it is necessary to pay attention to the fact that, with a detached breakwater, the place where the maximum wave force is generated can shift significantly with the wave direction and with the ratio of the breakwater length to the wavelength.

Fig. 4.4.11 shows an example of the calculation results of the wave force distribution along a detached breakwater for unidirectional random waves. In this calculation, the wave direction for which the largest wave force occurs is α = 30º of obliquely incident with a relatively shallow angle.

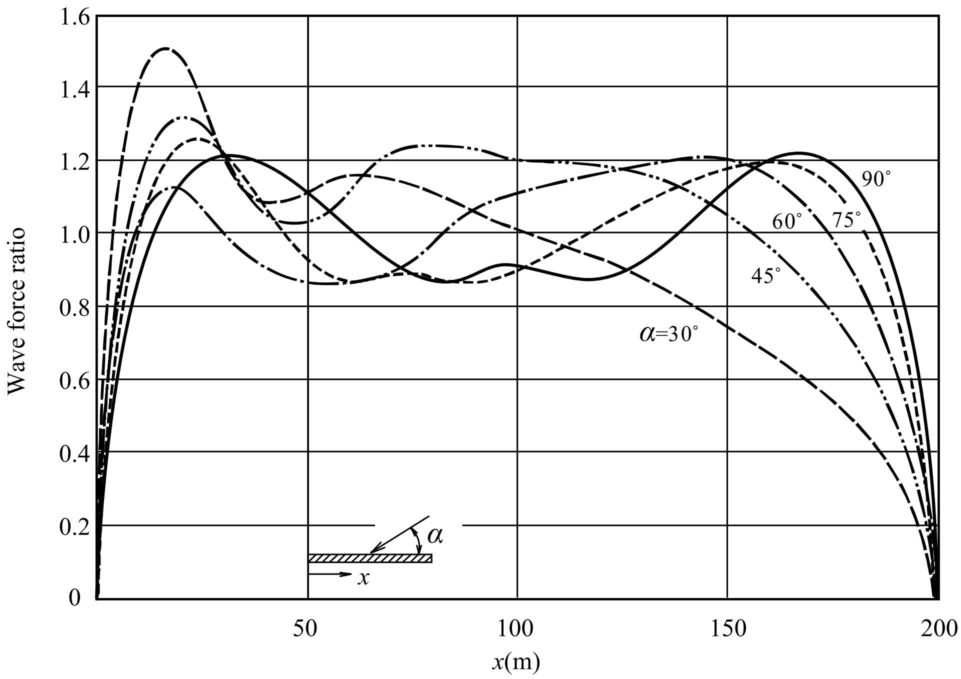

Fig. 4.4.11 Wave Force Distribution along a Detached Breakwater[89)]

4.4.5 Wave Shoaling

(1) When waves propagate in shallow waters, shoaling shall be considered, in addition to refraction and diffraction. In general, the nonlinearity of waves shall be considered when calculating the shoaling coefficient.

(2) Shoaling is one of the important factors that lead to the changing of wave height in coastal water areas. It exemplifies the fact that the wave height in shallow waters is also governed by the water depth and the wave period. **Fig. 4.4.12** was drawn on the basis of the nonlinear long wave theory of Shuto[90)]. It includes the linearized solution by the small amplitude wave theory and enables the estimation of the shoaling coefficient from deep to shallow waters.

In the diagram, K_s is the shoaling coefficient, H_0' is the equivalent deepwater wave height, H is the wave height at water depth h, and L_0 is the wavelength in the deep water.

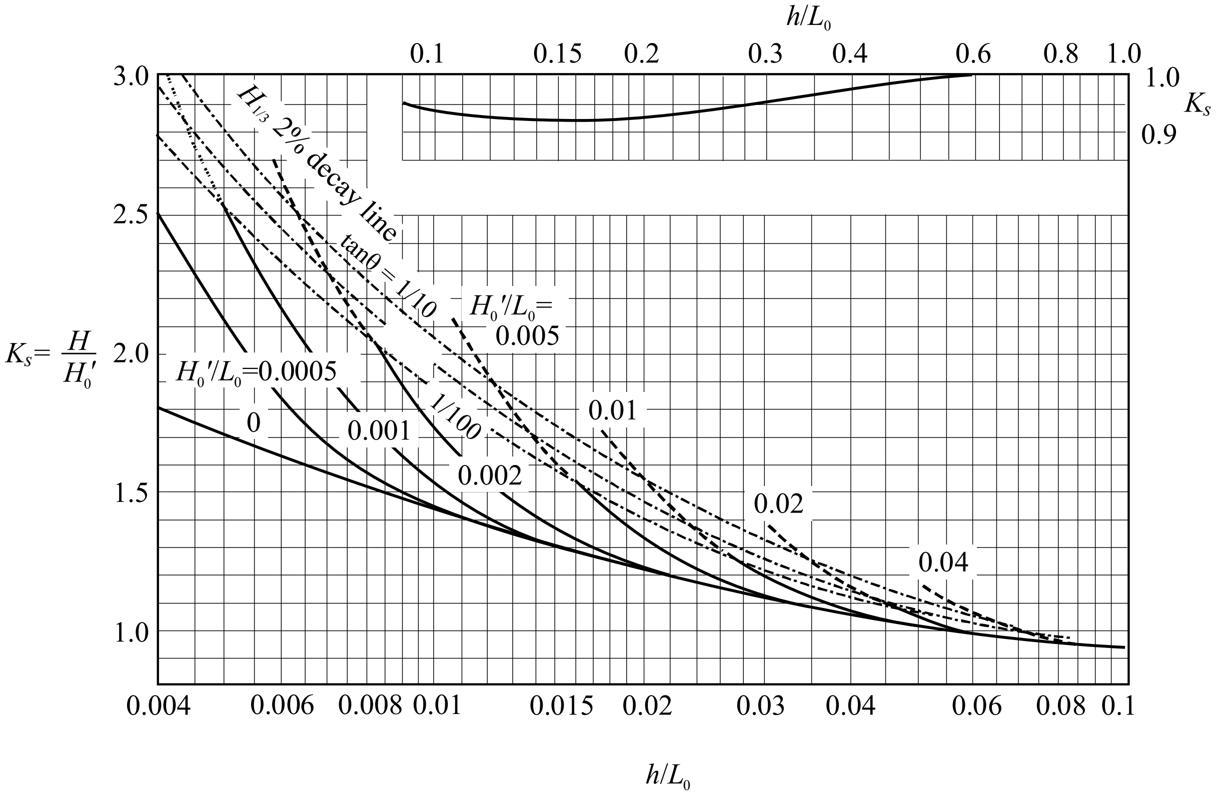

Fig. 4.4.12 Diagram for Evaluation of Shoaling Coefficient

4.4.6 Wave Breaking

(1) At places where the water depth is shallower than three times the equivalent deepwater wave height, the changing of the wave height due to wave breaking needs to be considered. It is standard to consider the irregularity of waves when calculating the change in the wave height due to wave breaking.

(2) After the height of waves has increased owing to shoaling, waves break at a certain water depth, and the wave height decreases rapidly. This phenomenon is called wave breaking. It is an important factor to be considered when determining the wave conditions exerting on coastal structures. For regular waves, the place at which waves break is always the same: this is referred to as the "wave breaking point." For random waves, the location of wave breaking depends on the height and period of individual waves, and wave breaking occurs over a certain distance (i.e., the "Surf Zone").

(3) Limiting Breaking Wave Height for Regular Waves

Fig. 4.4.13 shows the limiting breaking wave height[91)] for regular waves. This figure can be used to calculate the limiting breaking wave height in hydraulic model tests by using regular waves. The curves in the diagram can be approximated with **equation (4.4.7)**:

$$\frac{H_b}{L_0} = 0.17\left[1 - \exp\left\{-1.5\frac{\pi h}{L_0}\left(1 + 15\tan^{4/3}\theta\right)\right\}\right] \tag{4.4.7}$$

Where $\tan\theta$ denotes the seabed slope.

However, given that this approximation tends to give slightly higher breaking wave height at places where the seabed slope is steep, Goda[92] reduced the constant concerning $\tan\theta$ from 15 to 11 and modified it as follows. This modification provides an up to 11% less breaker index value H_b/h_b when the seabed slope is 1/10, but it is restricted to 2% when the seabed slope is 1/50.

$$\frac{H_b}{L_0} = 0.17\left[1 - \exp\left\{-1.5\frac{\pi h}{L_0}\left(1 + 11\tan^{4/3}\theta\right)\right\}\right] \quad \textbf{(4.4.8)}$$

Fig. 4.4.13 shows the limiting wave height at the point of first wave breaking. At places where the water is shallow, the water depth increases owing to the wave setup caused by wave breaking (see **Part II, Chapter 2, 4.4.8 (1) Rise of Mean Water Level Due to Waves**). When estimating the limiting wave height in the surf zone, it is necessary to consider this increase in water level.

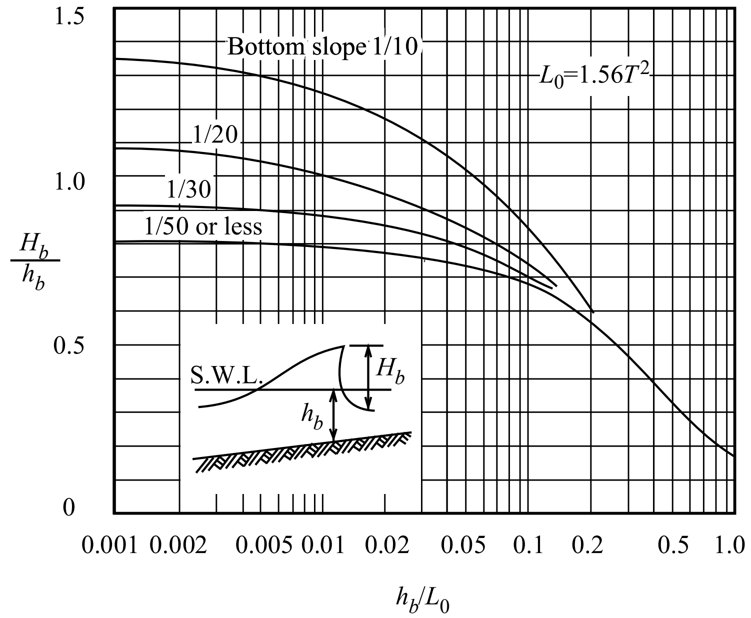

Fig. 4.4.13 Limiting Breaking Wave Height for Regular Waves[91]

(4) Change in Wave Height due to Wave Breaking

The change in wave height due to wave breaking may be determined using **Figs. 4.4.14 (a)–(e)** or **Figs. 4.4.15 (a)–(e)**. These figures show the change of the wave height which Goda[93] calculated by his theoretical model of random wave breaking. For the region to the right of the dash-dotted line on each diagram, the change of wave height is calculated using the shoaling coefficient (see **Part II, Chapter 2, 4.4.5 Wave Shoaling**). For the region to the left of this dash-dotted line, the change of wave height due to wave breaking dominates; therefore, the wave height must be determined using this diagram. For the seabed slope, it is appropriate to use the mean seabed slope over the region where the water depth to equivalent deepwater wave height ratio h/H_0' is in the range of 1.5 to 2.5.

Although the breaker index used in Goda's theoretical wave breaking model[93] was modified to **equation (4.4.8)**, **Reference 94)** indicates that this does not necessitate the modifications of **Figs. 4.4.14 (a) to (e)** and **Figs. 4.4.15 (a) to (e)**.

(5) Scope of Application of Graphs of Wave Height Change

At places where the water depth is shallower than approximately one-half of the equivalent deepwater wave height, a major portion of wave energy is converted to the energy of flows rather than to that of water level changes. Therefore, when calculating the wave force acting on a structure in very shallow water, it is preferable to use the wave height at the location where the water depth is one-half of the equivalent deepwater wave height if the facilities in question are highly important. However, it is necessary to estimate the wave force acting on facilities constructed on land areas from the shoreline with another proposed equation.[95]

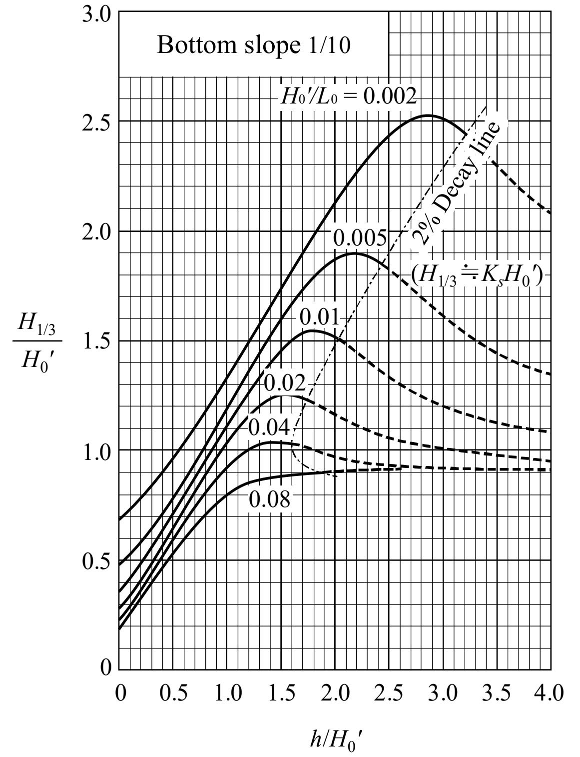

Fig. 4.4.14 (a) Diagram of Significant Wave Height in the Surf Zone for Seabed Slope of 1/10

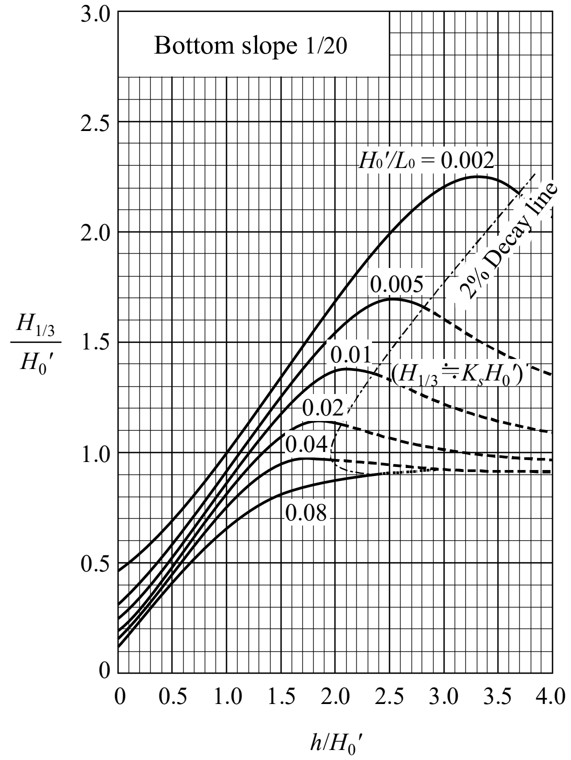

Fig. 4.4.14 (b) Diagram of Significant Wave Height in the Surf Zone for Seabed Slope of 1/20

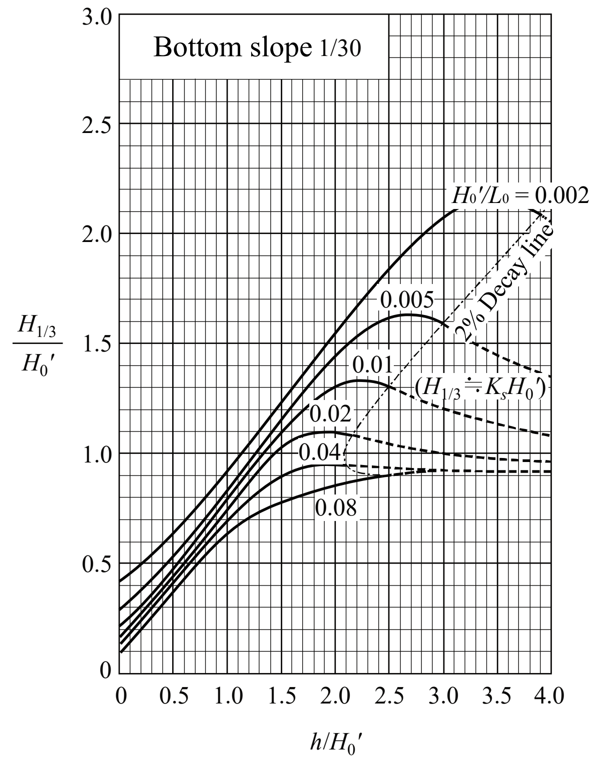

Fig. 4.4.14 (c) Diagram of Significant Wave Height in the Surf Zone for Seabed Slope of 1/30

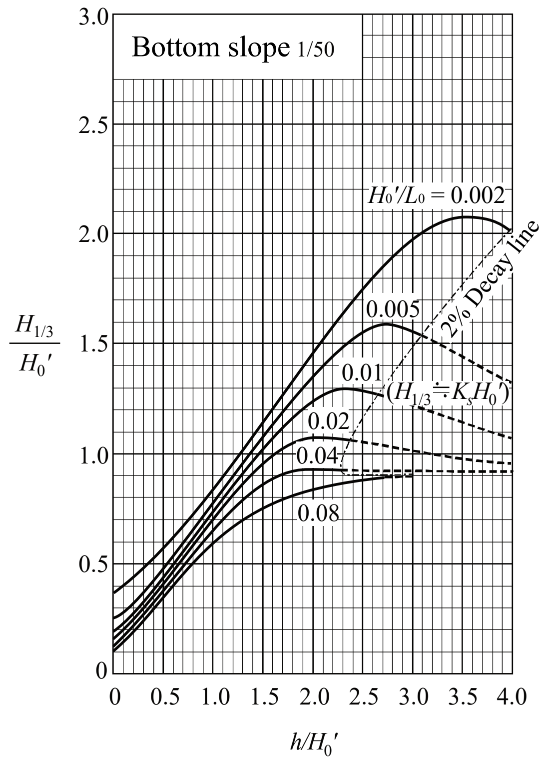

Fig. 4.4.14 (d) Diagram of Significant Wave Height in the Surf Zone for Seabed Slope of 1/50

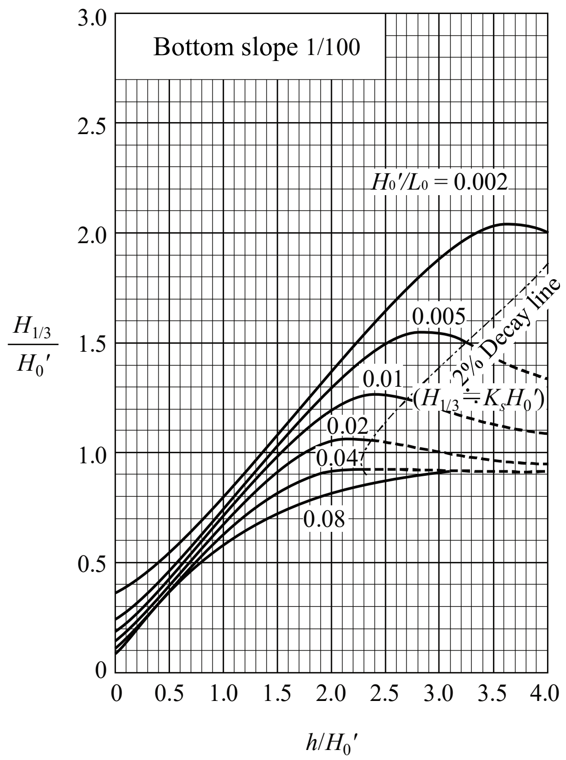

Fig. 4.4.14 (e) Diagram of Significant Wave Height in the Surf Zone for Seabed Slope of 1/100

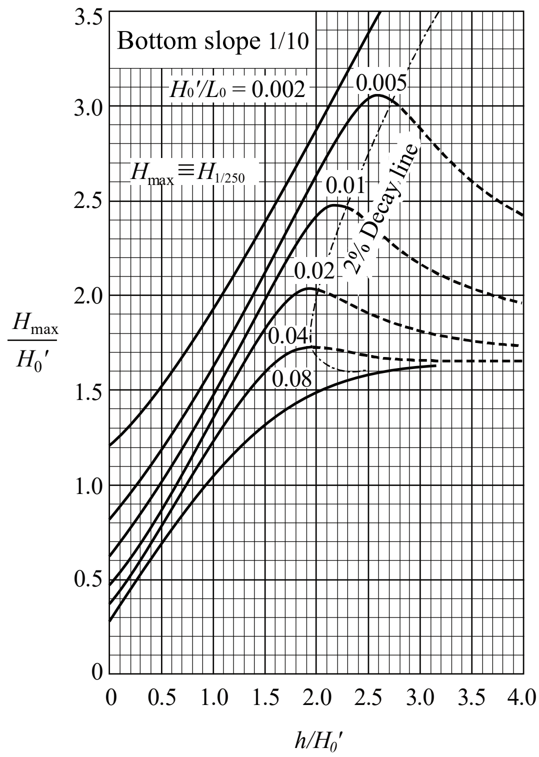

Fig. 4.4.15 (a) Diagram of Highest Wave Height in the Surf Zone for Seabed Slope of 1/10

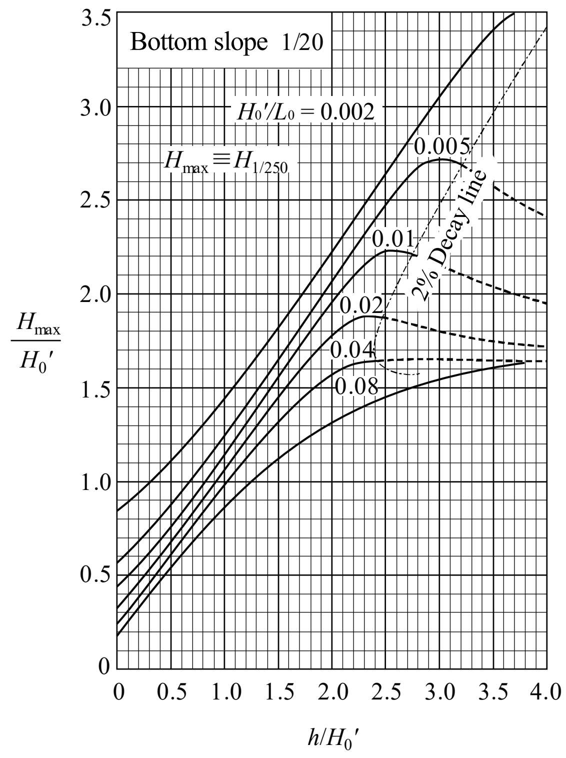

Fig. 4.4.15 (b) Diagram of Highest Wave Height in the Surf Zone for Seabed Slope of 1/20

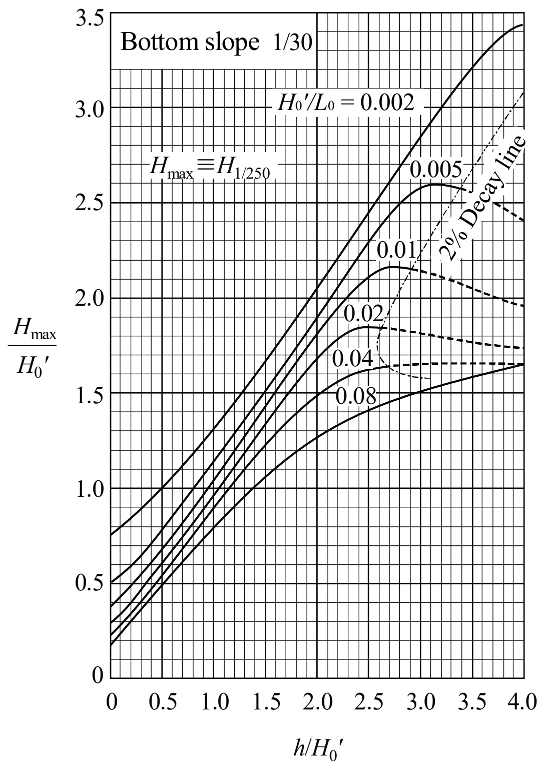

Fig. 4.4.15 (c) Diagram of Highest Wave Height in the Surf Zone for Seabed Slope of 1/30

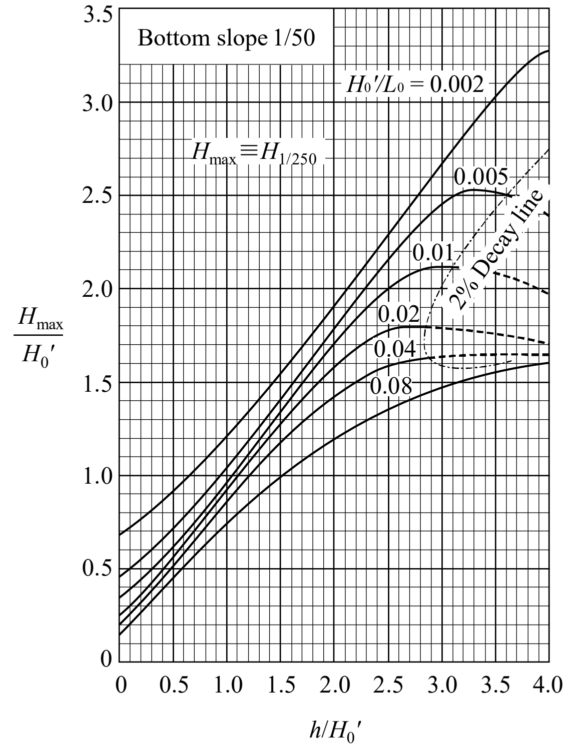

Fig. 4.4.15 (d) Diagram of Highest Wave Height in the Surf Zone for Seabed Slope of 1/50

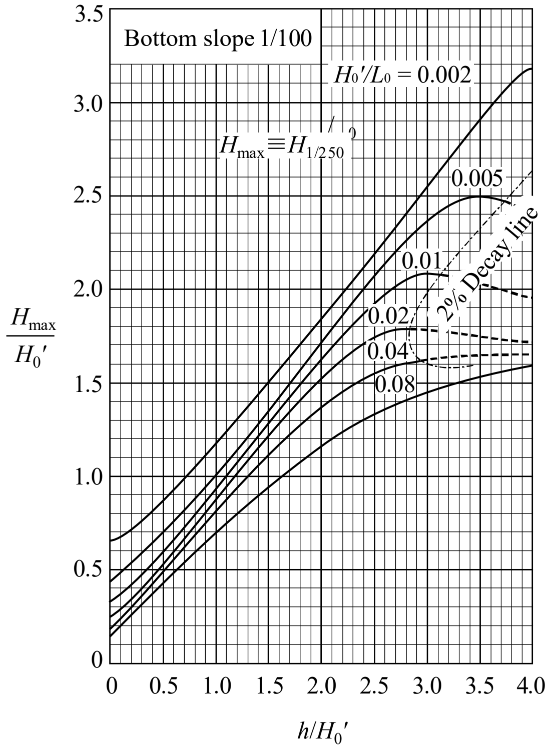

Fig. 4.4.15 (e) Diagram of Highest Wave Height in the Surf Zone for Seabed Slope of 1/100

(6) Approximate Calculation Formulas for Breaking Wave Height

The calculation of wave height changes based on a theoretical model for wave breaking generally requires the use of a computer. However, the wave breaking phenomenon is strongly affected by the individual wave height distribution of random waves and the condition of seabed topography. Therefore, considering the variability of the phenomenon and the overall accuracy, it is acceptable to calculate wave height changes by using the following simple formula in the case of a beach with constant seabed slope of approximately 1/10 to1/75.[93)]

The shoaling coefficient K_s is determined using **Fig. 4.4.12**, the operators min{ } and max{ } express the minimum and maximum value within the braces, respectively, and $\tan\theta$ is the seabed slope.

$$H_{1/3} = \begin{cases} K_s H_0' & (h/L_0 \geq 0.2) \\ \min\{(\beta_0 H_0' + \beta_1 h), \beta_{max} H_0', K_s H_0'\} & (h/L_0 < 0.2) \end{cases} \quad \textbf{(4.4.9)}$$

where

$$\begin{aligned} \beta_0 &= 0.028(H_0'/L_0)^{-0.38} \exp[20 \tan^{1.5} \theta] \\ \beta_1 &= 0.52 \exp[4.2 \tan \theta] \\ \beta_{max} &= \max\{0.92, 0.32(H_0'/L_0)^{-0.29} \exp[2.4 \tan \theta]\} \end{aligned} \quad \textbf{(4.4.10)}$$

Similarly, an approximate calculation formula for the highest wave height H_{max} is given as follows:

$$H_{max} = \begin{cases} 1.8 K_s H_0' & (h/L_0 \geq 0.2) \\ \min\{(\beta_0 H_0' + \beta_1 h), \beta_{max} H_0', 1.8 K_s H_0'\} & (h/L_0 < 0.2) \end{cases} \quad \textbf{(4.4.11)}$$

where

$$\beta_0 = 0.052(H_0'/L_0)^{-0.38} \exp[20 \tan^{1.5} \theta]$$
$$\beta_1 = 0.63 \exp[3.8 \tan \theta] \quad \textbf{(4.4.12)}$$
$$\beta_{max} = \max\{1.65, 0.53(H_0'/L_0)^{-0.29} \exp[2.4 \tan \theta]\}$$

(7) Diagram for Calculating Breaking Wave Height[93)]

If the maximum value $(H_{1/3})_{peak}$ of the significant wave height in the surf zone is taken as a representative of the breaking wave height, the breaker index curve becomes to be shown in **Fig. 4.4.16**. If the water depth $(h_{1/3})_{peak}$ at which the significant wave height is a maximum is taken as representative of the breaker depth, the diagram for calculating the breaker depth becomes to be shown in **Fig. 4.4.17**.

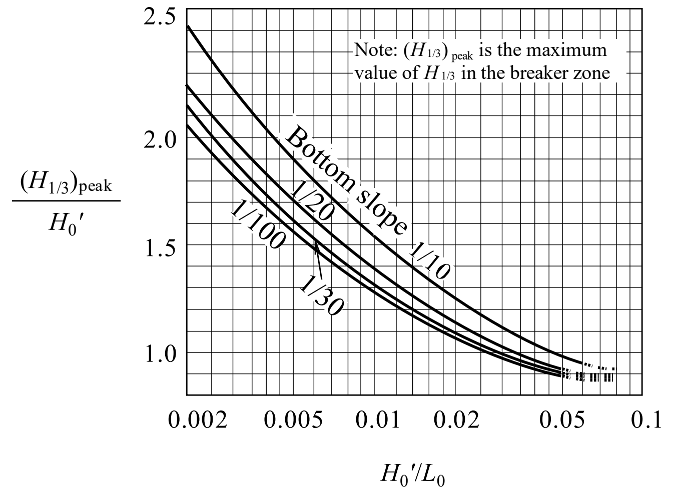

Fig. 4.4.16 Diagram of Maximum Value of the Significant Wave Height in the Surf Zone

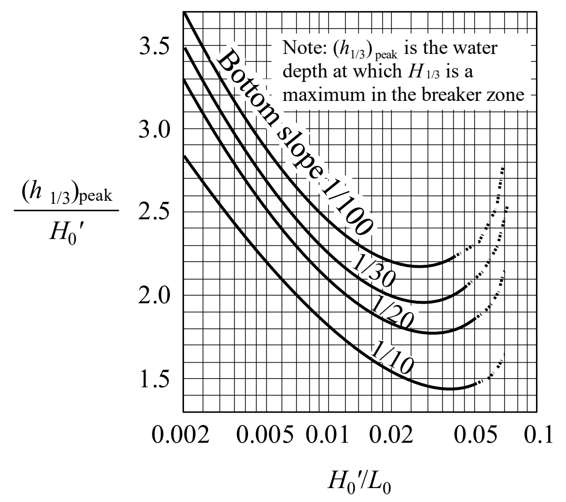

Fig. 4.4.17 Diagram of Water Depth at which the Maximum Value of the Significant Wave Height Occurs

(8) Change in Wave Height at Reef Coasts

At reef coasts where shallow water and a flat sea bottom continue over a long distance, the change in wave height cannot be calculated directly by using **Figs. 4.4.14 (a)–(e)** and **4.4.15 (a)–(e)**. Instead, the following empirical equation[96)] may be used:

$$\frac{H_x}{H_0'} = B \exp\left\{-A\left(\frac{x}{H_0'}\right)\right\} + \alpha \frac{h + \overline{\eta_\infty}}{H_0'} \quad \textbf{(4.4.13)}$$

where

H_0' : equivalent deepwater wave height

H_x : significant wave height at a distance x from the tip of the reef

h : water depth over the reef

$\overline{\eta}_\infty$: increase in the mean water level at a place sufficiently distant from the tip of the reef

Coefficients A and α are 0.05 and 0.33, respectively, according to the results of hydraulic model tests. However, it is advisable to use the following values that have been obtained from the data of field observations.[97)]

$$\left.\begin{aligned} A &= 0.089\frac{H_0'}{h+\overline{\eta}_\infty}+0.015 \\ \alpha &= \begin{cases} 0.20 & (4m > H_0' \geq 2m) \\ 0.33 & (H_0' \geq 4m) \end{cases} \end{aligned}\right\} \tag{4.4.14}$$

For coefficient B, using the diagram corresponds to the seabed slope at the front of the reef from **Figs. 4.4.14 (a)–(e)**, the significant wave height $H_{1/3}$ at water depth h is $H_{x=0}$. B is obtained as follows:

$$B = \frac{H_{x=0}}{H_0'} - \alpha\frac{h+\overline{\eta}_\infty}{H_0'} \tag{4.4.15}$$

The term $(h+\overline{\eta}_\infty)/H_0'$ is given by

$$\frac{h+\overline{\eta}_\infty}{H_0'} = \sqrt{\frac{C_0}{1+\frac{3}{8}\beta\alpha^2}} \tag{4.4.16}$$

Where β= 0.56.

From the continuity of the mean water level at the tip of the reef (x = 0), C_0 is given by

$$C_0 = \left(\frac{\overline{\eta}_{x=0}+h}{H_0'}\right)^2 + \frac{3}{8}\beta\left(\frac{H_{x=0}}{H_0'}\right)^2 \tag{4.4.17}$$

The term $\overline{\eta}_{x=0}$ represents the rise of mean water level at water depth h, which is controlled by the seabed slope in front of the reef. However, there are major localized variations in reef topography on actual coastlines. Wave height may increase behind circular reefs owing to the concentration due to the wave refraction; therefore, it is preferable to conduct model experiments by using multidirectional random waves wherever possible.[29)] See **Part II, Chapter 2, 4.4.8 Rise of Mean Water Level Due to Waves and Surf Beats** for more information on the concept of increased mean water level. The calculation method in the above has been derived under the assumption that the water depth h over the reef is small and that waves break over the reef. Therefore, it is not possible to apply the method when the water is deep and when wave breaking does not occur.

Considering the limiting breaking wave height criterion of a solitary wave, the highest wave height $H_{max,x}$ at the distance x from the tip of the reef may be obtained as follows.

$$H_{\max,x} = \min\{\,0.78(h+\overline{\eta}_x), 1.8H_x\} \tag{4.4.18}$$

where min$\{a,b\}$ is the smaller value of a or b, and $\overline{\eta}_x$ is the rise in the mean water level at the distance x and is given by the following equation:

$$\frac{\overline{\eta}_x+h}{H_0'} = \sqrt{C_0 - \frac{3}{8}\beta\left(\frac{H_x}{H_0'}\right)^2} \tag{4.4.19}$$

(9) Handling of wave breaking transformation in complicated seabed topography

In a topography where seabed slope abruptly changes, such as the bar trough topography, and water depth intricately changes, such as the actual coral reef, reef zone, and so on, the changes of wave height and their planar distribution can be obtained by using a numerical calculation model, which can directly calculate the wave breaking transformation of random waves. Goda[98)] proposed a phase-averaged type graded-wave breaking model that changes the wave breaking limit specified by water depth per the wave height of individual waves and indicated that a planar wave height distribution around an artificial reef can be calculated in a relatively short period. On the contrary, the Boussinesq model of time development type,[99)] which considers the wave height damping process by wave breaking, can calculate phenomena such as the rise of mean water level by waves and surf beat together with the planar wave breaking transformation on the complicated seabed topography.[100)]

4.4.7 Wave Run-up Height, Wave Overtopping and Transmitted Waves

(1) Wave run-up height

① Wave run-up needs to be calculated appropriately by taking into account the configuration and location of the seawall and the sea bottom topography.

② The phenomenon of wave run-up is dependent upon a whole variety of factors, such as wave characteristics, configuration and location of the seawall, and sea bottom topography; therefore, the run-up height varies in a complex way. Therefore, when the seawall and sea bottom are complex in form, it is preferable to confirm wave run-up heights by performing hydraulic model tests. It is important to consider that calculation diagrams or equations for regular waves proposed on the basis of the results of past research for restricted conditions are the mean values in experiments indicating significant dispersion. Moreover, it must be noted that the frequency of random waves exceeding the crown height set against the regular wave run-up height is high, and approximately half of the waves exceed this crown height in extreme cases even without considering the dispersion in experimental values. The report[101)] indicates that the run-up height of regular wave with the significant wave height corresponds to $R_{50\%}$ (i.e., the value averaged the wave run-up height with 50% of the number of incident waves) of random waves if the performance of the structural crown height is verified by using significant waves. When conducting the performance verification of sloping revetments, it is preferable to set the crown elevation of the revetment to be higher than the run-up height for regular waves. Therefore, the crown height of seawall, revetment, or others should not only be determined by wave run-up height but also by wave overtopping quantity (see **Part II, Chapter 2, 4.4.7 (2) Wave Overtopping Quantity**) should be considered. It is preferable to determine the ultimate crown height and the revetment form to prevent the wave overtopping quantity from exceeding the threshold value.

③ The results presented by Mase[102)] are simple, and the scope of application is wide for the wave run-up height of random waves to a uniform slope.

$$\frac{R_x}{H_0'} = a\xi^b,\ \frac{1}{30} \le \tan\beta < \frac{1}{5}\ \ and\ \ 0.007 \le \frac{H_0}{L_0} \qquad \textbf{(4.4.20)}$$

Here, x, a, and b stand for the coefficients of the statistical values and calculated values of the wave run-up height and are provided as follows.

Table 4.4.2 Coefficients of equation (4.4.20)

R_x	R_{max}	$R_{2\%}$	$R_{1/10}$	$R_{1/3}$	$\overline{R}$
a	2.32	1.86	1.70	1.38	0.88
b	0.77	0.71	0.71	0.70	0.69

Here, R_{max} is the maximum value of the wave run-up height. $R_{2\%}$ is the value at which the wave run-up height calculated in an experiment exceeds 2%. $R_{1/10}$, $R_{1/3}$, and $\overline{R}$ are the 1/10 maximum wave run-up height, 1/3 maximum wave run-up height, and mean value, respectively, which can be calculated by the same method as the case in which random waves are statistically analyzed. ξ is called the surf similarity parameter and is defined as $\xi = \tan\theta / \sqrt{H_0'/L_0}$, where $\tan\theta$ is the seabed slope, and H_0'/L_0 is the wave steepness of offshore waves.

It is possible to employ the following equation, which has been verified to accord well with experimental results, for the 1/3 maximum wave run-up height.[103)]

$$\begin{aligned} &R_{1/3}/H_s = 0.25 + 1.1\xi && (0 < \xi \le 2.2) \\ &R_{1/3}/H_s = 3.0 - 0.15\xi && (2.2 < \xi \le 9.0) \\ &R_{1/3}/H_s = 1.65 && (9.0 < \xi) \end{aligned} \qquad \textbf{(4.4.21)}$$

④ For the wave run-up height of random waves of a rubble slope, the equation of Van der Meer-Stam[104)] can be used.

$$\frac{R_x}{H_s} = a\xi_m \qquad (\xi_m \leq 1.5)$$
$$\frac{R_x}{H_s} = b\xi_m{}^c \qquad (\xi_m > 1.5) \tag{4.4.22}$$

Here, the coefficient is shown in the following table. Furthermore, in $\xi_m = \tan\theta / \sqrt{2\pi H_s / gT_m{}^2}$, H_s is the significant wave height at the water depth at the foot of a seawall (water depth at the foot of a slope), and T_m is the mean wave period.

Table 4.4.3 Coefficients of **equation (4.4.22)**

R_x	R_{max}	$R_{2\%}$	$R_{1/10}$	$R_{1/3}$	$\bar{R}$
a	1. 12	0. 96	0. 77	0. 72	0. 47
b	1. 34	1. 17	0. 94	0. 88	0. 60
c	0. 55	0. 46	0. 42	0. 41	0. 34
d	2. 58	1. 97	1. 45	1. 35	0. 82

The following equation is proposed for the wave run-up height of a slope that has permeability.

$$\frac{R_x}{H_s} = d \tag{4.4.23}$$

⑤ In the case of complex cross sections, the virtual slope method of Saville[105)] and the modified virtual slope method of Nakamura[106)] may be used for regular waves.

A "complex cross section" refers to the case where the sea bottom topography and the configuration and location of the seawall are shown in **Fig. 4.4.18**, where S.W.L. (Sea Water Level) denotes the still-water level.

(a) When the cross section can be considered complex, the run-up height of the seawall is obtained as follows (refer to **Fig. 4.4.18**).

1) Wave breaking point B is determined from the offshore wave characteristics.

2) Thereafter, the wave run-up height R (maximum run-up height from the S.W.L.) is assumed, and point A is set at the maximum run-up point. Points A and B are joined by a straight line, and the gradient of this line yields the virtual gradient cotα.

3) The wave run-up height for this virtual gradient is calculated using **Fig. 4.4.19**, and the calculated height is compared with the initially assumed run-up height. If the two do not agree, a new run-up height (i.e., virtual gradient) is assumed, and the estimations are repeated. This iterative process is repeated until convergence is achieved.

4) The value obtained is taken as the run-up height for the complex cross section in question.

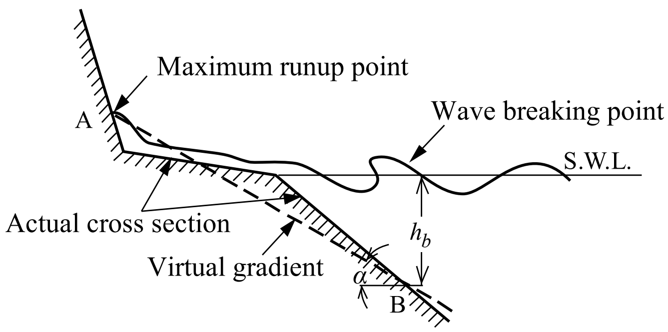

Fig. 4.4.18 Complex Cross Section and Virtual Gradient

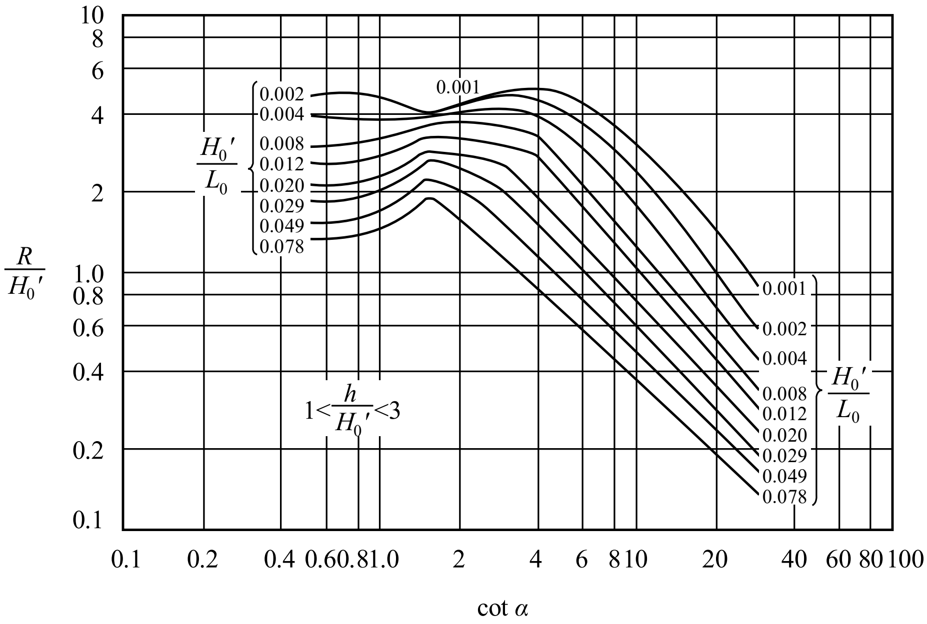

Fig. 4.4.19 Run-up Height on a Slope

(b) When the results obtained from this method are compared with the actual experimental results for a complex cross section, it is generally found that there is a good agreement between the two, with the error usually being not more than 10%. However, if the seabed slope is too gentle, the agreement between the two becomes poor; therefore, this method is should only be used when the seabed slope is steeper than 1/30.

(c) **Fig. 4.4.20** shows the experimental results[107)] obtained for a seabed slope of 1/70. This figure provides a useful reference when estimating the wave run-up height for a complex cross section with a gentle seabed slope.

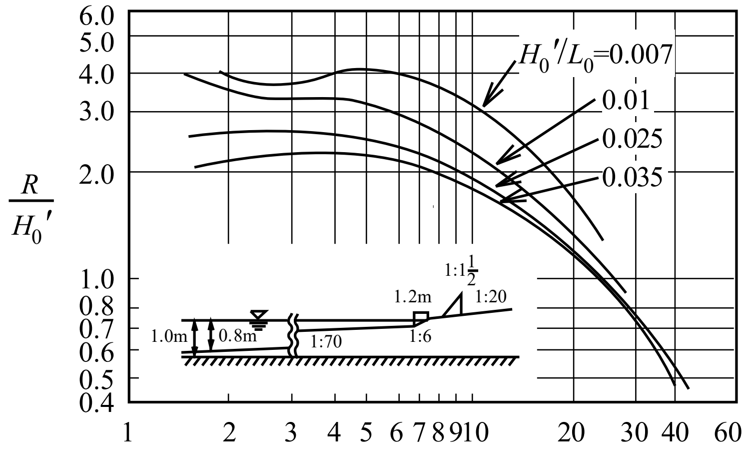

Fig. 4.4.20 Run-Up Height on Seawall Located Closer to Land than Wave Breaking Point

On the contrary, the wave run-up height of random waves for a complex cross section can be calculated with the following equation,[101)] which was proposed by arranging the experimental data following the concept of modified virtual slope method[106)] in the range satisfying $0 < \xi' < 6.0$, $0.009 < H_0'/L_0 < 0.06$ and $-0.37 < h_t/H_0' < 0.53$.

$$R_{2\%}/H_0' = 2.99 - 2.73\exp(-0.57\xi')$$
$$R_{1/10}/H_0' = 2.72 - 2.56\exp(-0.58\xi') \quad \text{where} \quad \xi' = \frac{\tan\alpha}{\sqrt{H_0'/L_0}} \tag{4.4.24}$$
$$R_{1/3}/H_0' = 2.17 - 2.18\exp(-0.70\xi')$$

Here, tan α is the virtual slope (tan α = 0.5 $(h_b + R)^2/A$) determined by area A of the actual cross section between two points, namely, wave run-up height R and breaker depth h_b; h_t is the water depth at the foot of a slope. Moreover, **Fig. 4.4.17** can be used in the calculation of the breaker depth used for the setting of wave breaking points in the range of 1/30 < tan θ < 1/10 (tan θ is the seabed slope) and $0.02 < H_0'/L_0 < 0.05$.

⑥ **Oblique Wave Incidence**[108)]

Fig. 4.4.21 shows the relationship between the incident angle coefficient K_β and the angle β. Here, β is the angle between the wave crest line of the incident waves and the face line of the seawall, and the incident angle coefficient K_β is the ratio of the run-up height for angle β to the run-up height when the waves are normally incident (i.e., when β = 0). This figure can be used to estimate the effect of wave incident angle on the run-up height in case of regular waves.

⑦ **Effects of Wave-dissipating Work**

The wave run-up height can be significantly reduced when the front of a seawall is completely covered with wave-dissipating blocks. **Fig. 4.4.22** shows an example for regular waves. However, the effect of the blocks varies greatly according to the way in which they are laid. Therefore, in general, it is preferable to determine the run-up height by means of hydraulic model tests.

⑧ **Use of Super Roller Flume for Computer Aided Design of Maritime Structure**

It is possible to use CADMAS-SURF, which is also used for wave-resistant design and the like, to perform a numerical simulation in calculating the run-up height on a slope. The calculation method and its applicability for the run-up height of regular waves on a uniform slope[31)] or an arbitrary slope[109)] has been identified by the study group on the application of CADMAS-SURF in wave-resistant design. Here, the special grid size for differential simulation should be determined carefully because it directly affects the accuracy of the calculation and the computation time, which have a trade-off relationship[110)]. Moreover, Sakuraba et al.[111)] proposed a numerical calculation method that uses unstructured spatial grid and examined its applicability.

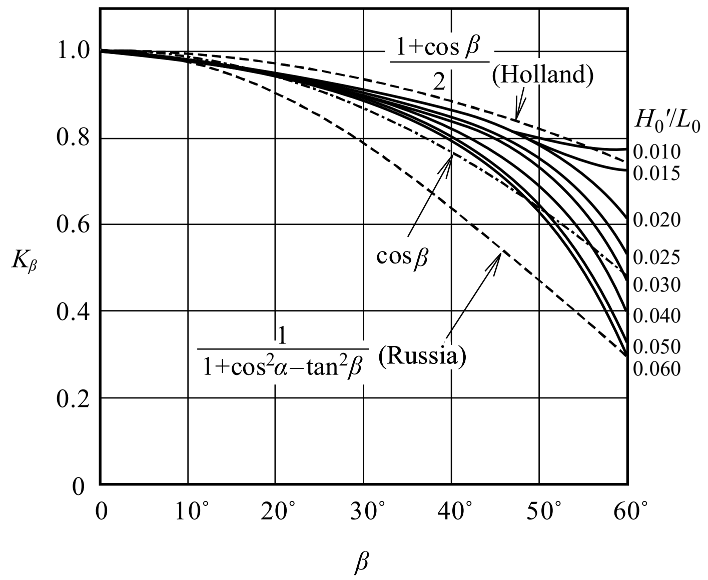

Fig. 4.4.21 Relationship between Wave Incident Angle and Run-Up Height
(Solid Lines: Experimental Values by Public Works Research Institute, Ministry of Construction)

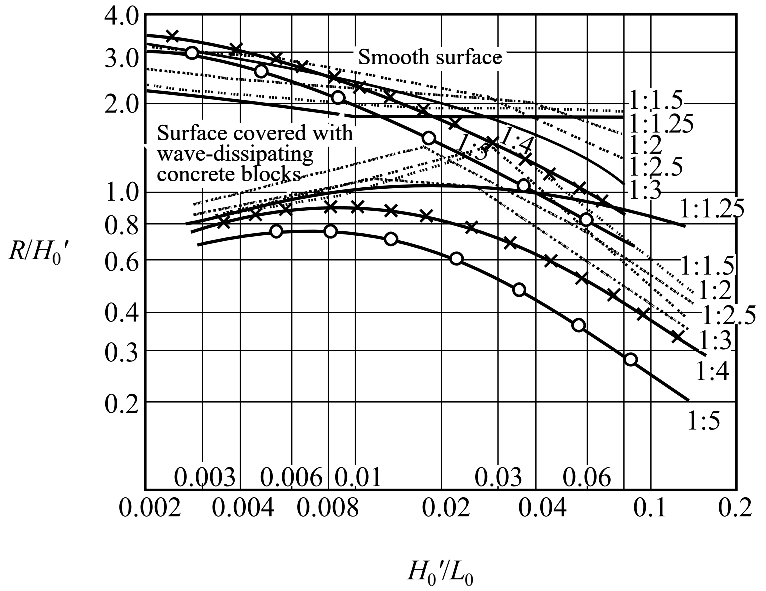

Fig. 4.4.22 Reduction in Wave Run-up Height Due to Wave-dissipating Work[208)]

(2) Wave Overtopping Quantity

① The "wave overtopping quantity" is the total volume of overtopped water. The "wave overtopping rate" is the average volume of water overtopping in a unit time; it is obtained by dividing the wave overtopping quantity by the time duration of measurement. The wave overtopping quantity and wave overtopping rate are generally expressed per unit width.

② For structures for which the wave overtopping quantity is an important performance verification factor, the wave overtopping quantity must be calculated by considering the irregularity of waves using hydraulic model tests or by using data from hydraulic model tests performed in the past. If the front sea bottom topography is complex, the revetment wave overtopping rate may be estimated[112)] by using the equivalent deepwater wave height which is calculated by estimating the wave transformation to obtain the progressive wave height at the front surface of the revetment. In the wave transformation calculation by using the Boussinesq model, the reproduction of the inundation process behind the revetment was also tried[113)] by calculating the planar distribution and its temporal variation of the wave overtopping rate by using the overflow formula. Moreover, the wave overtopping rate can be calculated for the revetment of slightly complicated cross-sectional shape by using CADMAS-SURF (the Super Roller Flume for Computer Aided Design of Maritime Structure)[114)], although its application range is restricted to the vicinity of revetments from the viewpoint of calculation capacity. However, it is preferable to conduct sufficient calibration for calculation model, spatial grid setting, and so on, e.g., examination of the accuracy of calculation in advance by performing reproduction calculation against the results of experiments in this case.

③ If the wave overtopping quantity is large, not only will there be damage to the seawall body itself but also damage by flooding to the roads, houses, and/or port facilities behind the levee or seawall even though the levee or seawall is intended to protect them. There is further a risk of drowning or injury to users of water frontage amenity-oriented facilities. When verifying performance, it is necessary to set the wave overtopping rate so that it is equal to or less than the permissible wave overtopping rate that has been determined in line with the characteristics of structures and the situation with regard to their usage. Furthermore, when estimating the wave overtopping quantity by means of experiments, it is preferable to consider changes in tidal water level, i.e., to perform experiments for different water levels.

④ **Estimation diagram of wave overtopping rate**[115)]

For an upright or wave-dissipating type seawall that has a simple form (i.e., does not have a toe protection mound or a crown parapet), the wave overtopping rate may be estimated using Figs. 4.4.23 to 4.4.26. These diagrams have been drawn on the basis of experiments employing random waves. From the results of a comparison between the experiments and field observations, it is thought that the accuracy of the curves giving the wave overtopping rate is within the range listed in Table 4.4.4. The wave overtopping rate for the wave-dissipating type seawall has been obtained under the condition that the upper armor layer at the crown consists of two rows of wave-dissipating concrete blocks.

Table 4.4.4 Estimated Range for the Actual Wave Overtopping Rate relative to the Estimated Value

$q/\sqrt{2g(H_0')^3}$	Upright seawall	Wave-dissipating type seawall
10^{-2}	0.7–1.5 times	0.5–2 times
10^{-3}	0.4–2 times	0.2–3 times
10^{-4}	0.2–3 times	0.1–5 times
10^{-5}	0.1–5 times	0.05–10 times

Note that when obtaining rough estimates for the wave overtopping rate for random waves using **Figs. 4.4.23 to 4.4.26**, the following should be considered:

(a) If the actual values of the seabed slope and the deepwater wave steepness do not match any of the values on the diagram, the diagram for which the values most closely match should be used or interpolation should be performed.

(b) The wave-dissipating concrete blocks in the figures are made up of two layers of tetrapods (upper armor layer at the crown consists of two rows). Even if the same kind of wave-dissipating concrete block is used, if there are differences in the crown width, in the placing way, or in the form of the toe, then there is a risk that the actual wave overtopping rate may considerably differ from the value obtained by the diagrams, as the different wave-dissipating block is used.

(c) If the number of rows of concrete blocks at the crown is increased, the wave overtopping quantity tends to decrease[116)].

(d) When there are difficulties in applying the diagrams for estimating the wave overtopping rate, the approximate equation of Takayama et al.[117)] may be used.

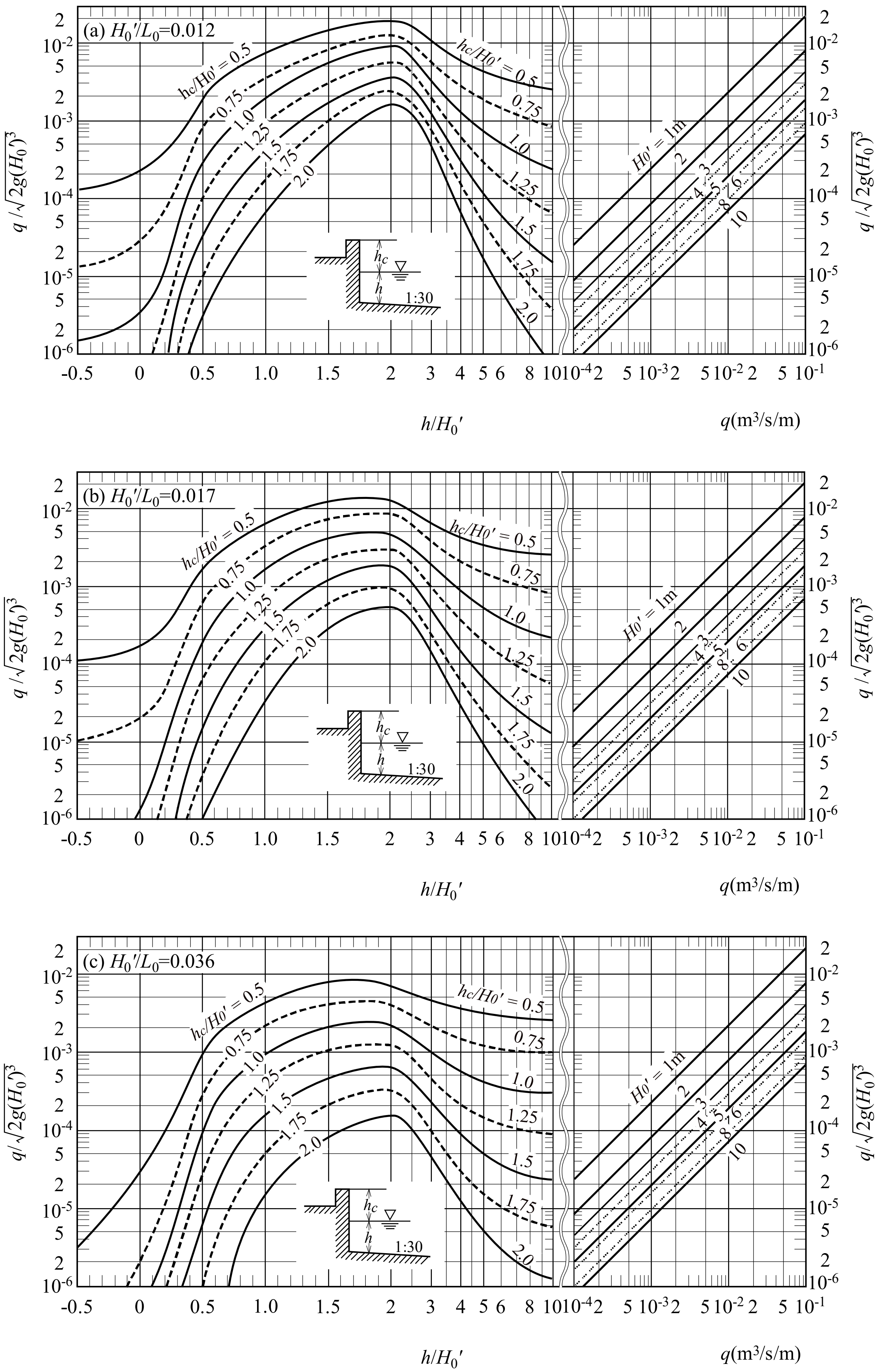

Fig. 4.4.23 Diagrams for Estimating Wave Overtopping Rate for Upright Seawall (Seabed Slope 1/30)

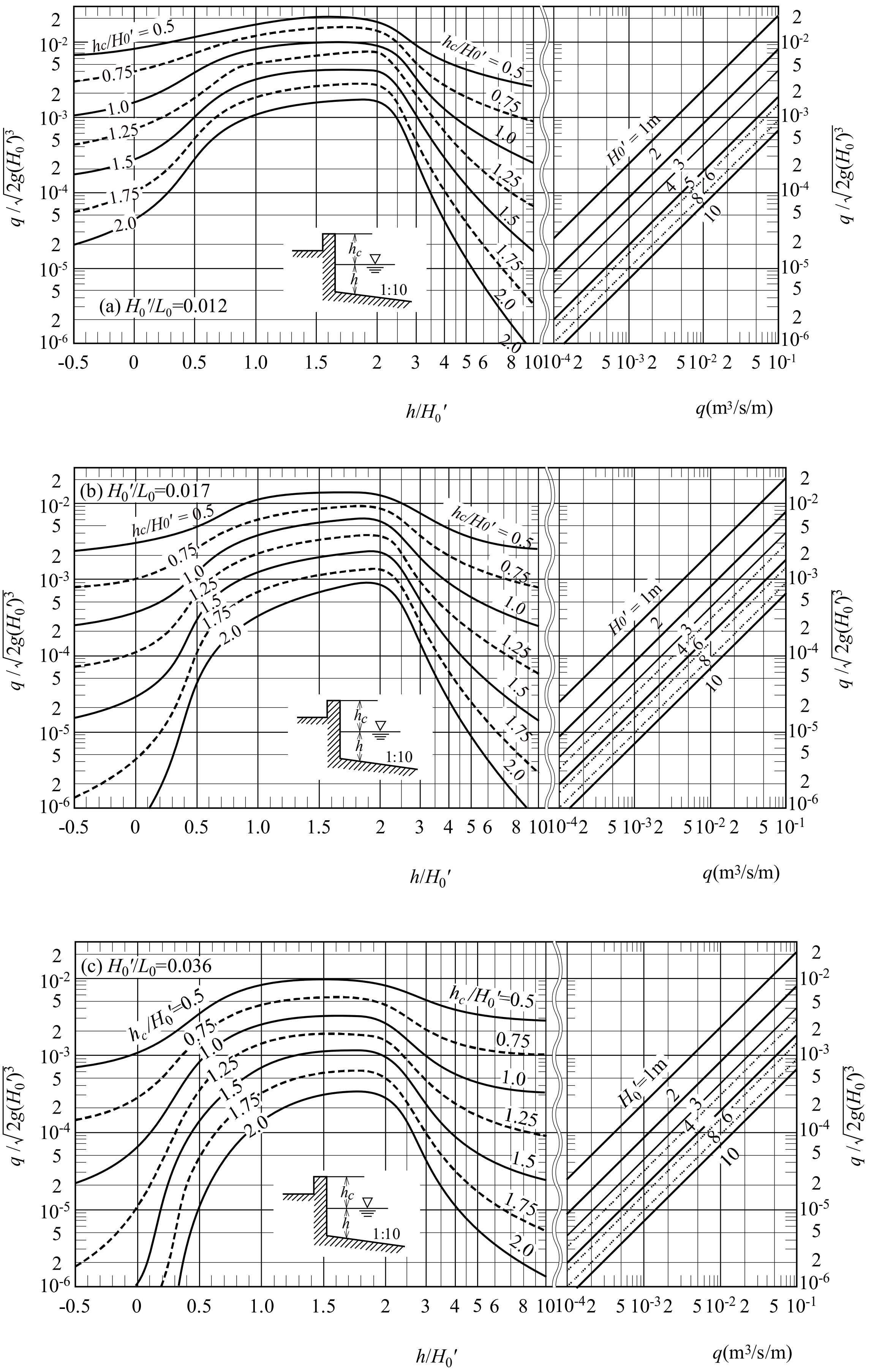

Fig. 4.4.24 Diagrams for Estimating Wave Overtopping Rate for Upright Seawall (Seabed Slope 1/10)

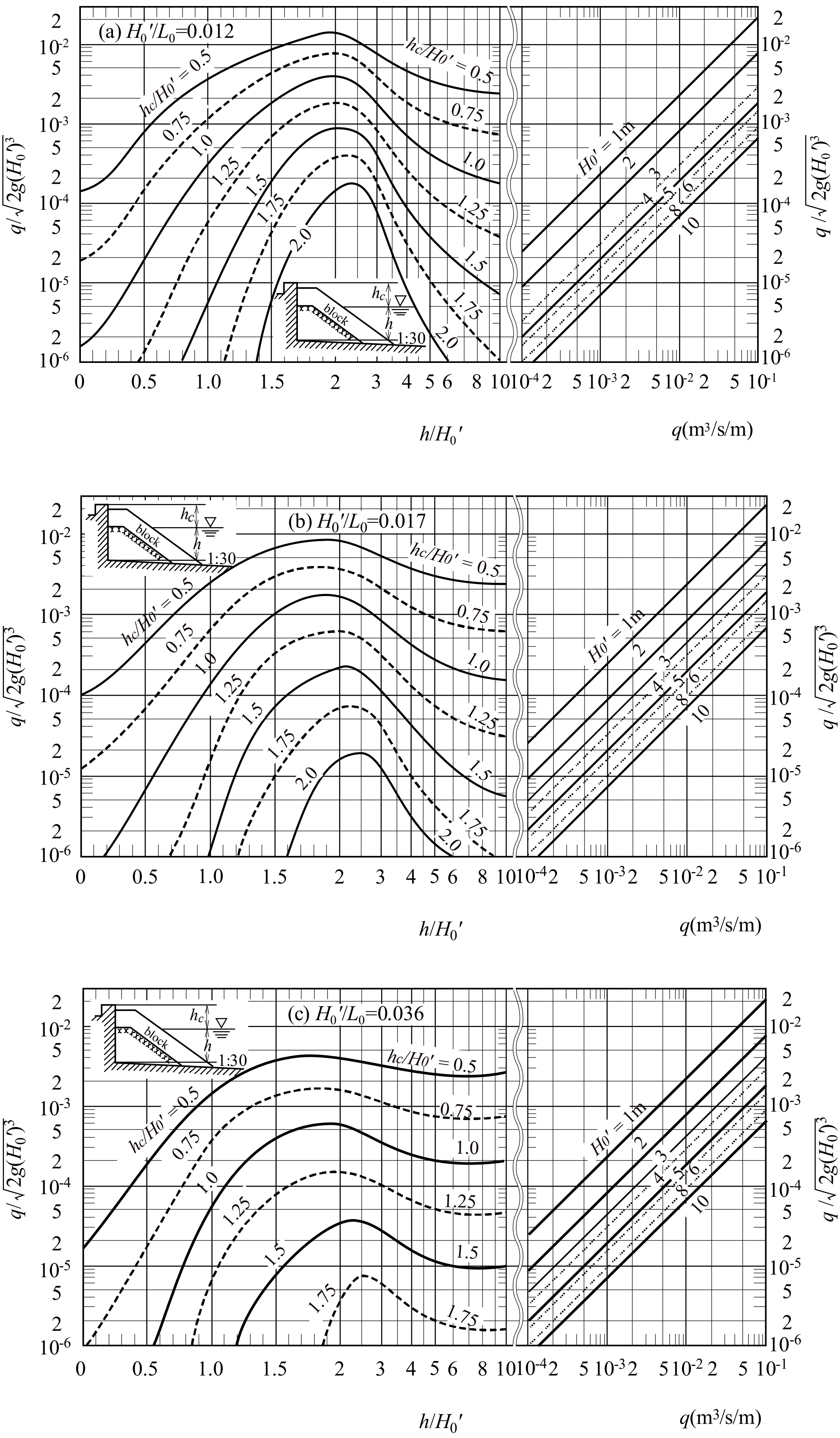

Fig. 4.4.25 Diagrams for Estimating Wave Overtopping Rate for Wave-dissipating Type Seawall (Seabed Slope 1/30)

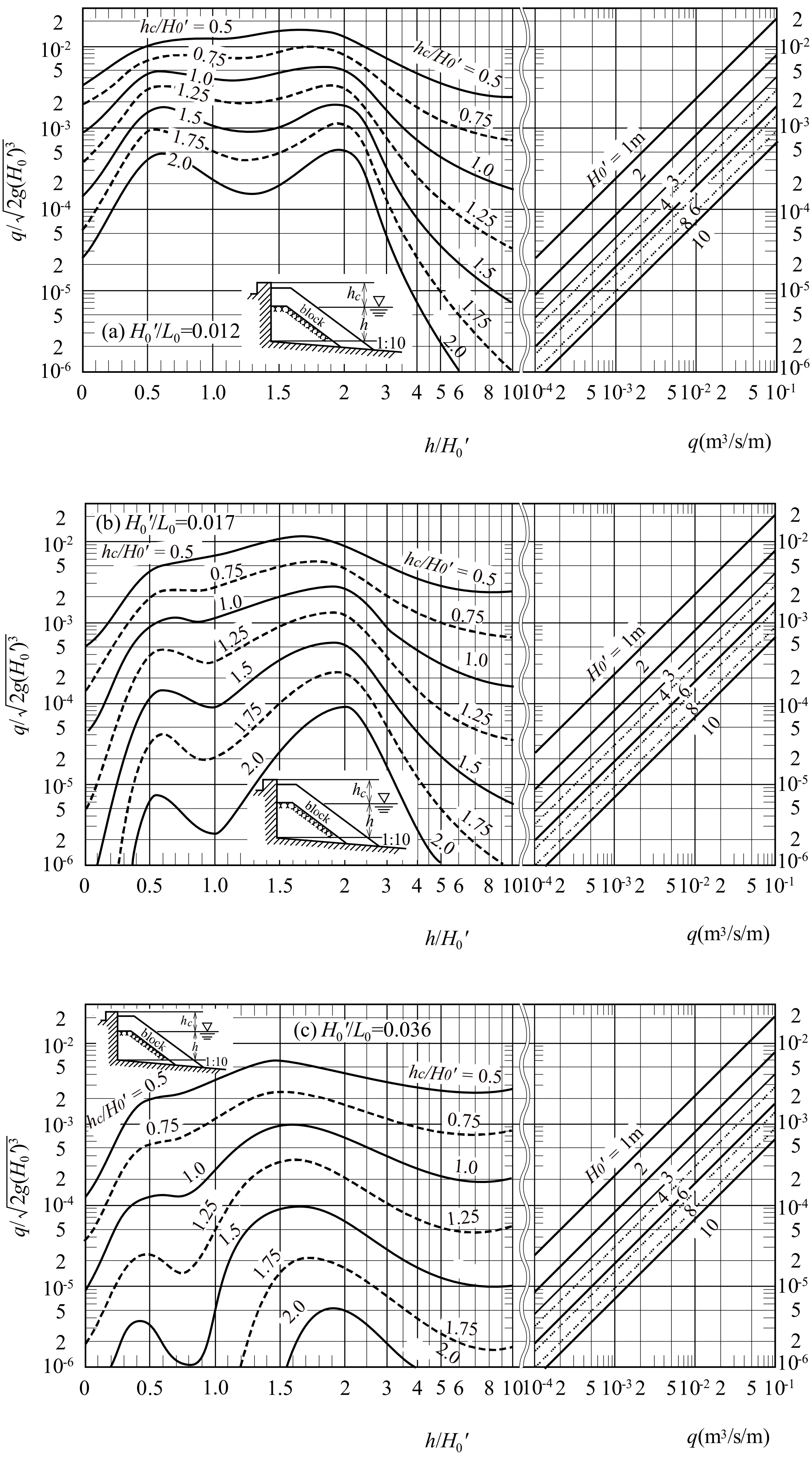

Fig. 4.4.26 Diagrams for Estimating Wave Overtopping Rate for Wave-dissipating Type Seawall (Seabed Slope 1/10)

⑤ **Equivalent Crown Height Coefficient**

The equivalent crown height coefficient can be used as a guideline when setting the wave overtopping rate for a seawall upon which wave-dissipating concrete blocks are laid or for a wave-dissipating type seawall with vertical slits. The equivalent crown height coefficient is the ratio of the height of the seawall in question to the height of an imaginary upright seawall that results in the same wave overtopping quantity, where the conditions in terms of waves and the sea bottom topography are taken to be the same for the both cases. If the equivalent crown height coefficient is less than 1.0, the crown of the seawall under study can be lowered below that of an upright seawall and still provide the same wave overtopping quantity; in other words, the seawall under study has a form that is effective in reducing the wave overtopping rate. Below are the reference values for the equivalent crown height coefficient β for typical types of seawalls.

Wave-dissipating block-type seawall [117]	:	$\beta = 0.9–0.7$
Vertical-slit type wave-dissipating seawall [117]	:	$\beta = 0.6$
Parapet retreating type seawall [116]	:	$\beta = 1.0–0.5$
Stepped seawall [116]	:	$\beta = 1.7–1.0$
When the waves are obliquely incident[118) 119]	:	$\beta = \begin{cases} 1-\sin^2\theta & \lvert\theta\rvert \le 30° \\ 1-\sin^2 30° = 0.75 & \lvert\theta\rvert > 30° \end{cases}$

(θ is the angle of incidence of the waves; it is 0º when the waves are incident perpendicular to the seawall face line)

⑥ **Wave Overtopping Quantity on the Revetments Installed on Reefs**

On a long reef topography, waves propagating on the reef are newly reproduced after the waves that broke at the tip of the reef were sufficiently damped. The wave overtopping rate over revetments on the reef where these waves act may be calculated by using the diagrams for estimating the wave overtopping rate [115] or the approximate calculation for wave overtopping rate[117] against the design tidal level by considering the risen mean water level owing to waves and surf beat (see **Part II, Chapter 2, 4.4.8 Rise of Mean Water Level due to Waves and Surf Beats**). Here, the equivalent deepwater wave height is conveniently calculated by dividing the front wave height (see **Part II, Chapter 2, 4.4.6 (8) Change in Wave Height at Reef Coasts in this chapter**) of the revetment above the reef by the shoaling coefficient considering that the wave reproduction point as offshore. However, if the shape of the reef is not uniform in the direction of shore, it is preferable to calculate the wave transformation by using the Boussinesq model in order to consider the refraction and diffraction at the reef cliff, deviation of water level on the reef, and the planar distribution of surf beat[112].

⑦ **Wave Overtopping Quantity of Sloping Revetments**

The calculation diagram made by Tamada et al.[120] can be used to calculate the wave overtopping rate at a sloping revetment that has a waterside slope of 30% (1:3) or more. For 30% slope, 50% slope, and 70% slope, this calculation diagram comprises four combinations: seabed slope of 1/10 and 1/30 and offshore wave steepness of 0.017 and 0.036. The wave overtopping rate of 30% slope revetments tends to be larger than the upright revetments, but it is smaller than the upright revetments in 50% slope revetments for the wind waves of wave steepness 0.036. The wave overtopping rate of 70% slope revetments is smaller than the upright revetments in every case. The wave overtopping rate decreases as the waterside slope becomes mild because the wave run-up height is proportional to the gradient of a slope (see **Part II, Chapter 2, 4.4.7 (1) Wave run-up height in this chapter**).

⑧ **Relations between the Wave Run-up Height and the Wave Overtopping Quantity**

Tamada et al.[121] and Mase et al.[122] proposed a wave overtopping rate calculation equation to link the wave run-up and wave overtopping and named it IFORM. The wave overtopping rate for complex cross-sectional seawalls and revetments near the shoreline (including onshore part) can be calculated using the following equation by considering the random wave run-up height.

$$\frac{q}{\sqrt{gH_0'^3}} = \begin{cases} C\left[0.018\left(\dfrac{R_{\max}}{H_0'}\right)^{1.5}\left\{1-\left(\dfrac{R_c}{H_0'}\right)\Big/\left(\dfrac{R_{\max}}{H_0'}\right)\right\}^{6.240}\right] & for \quad 0 \le R_c \le R_{\max} \\ 0 & for \quad R_{\max} \le R_c \end{cases} \tag{4.4.25}$$

Here, R_c is the crown height of seawalls and revetments, and R_{max} is the 99% probable maximum wave run-up height. Moreover, R_{max} is expressed as $R_{max} = 1.54R_{2\%}$ by using the $R_{2\%}$ calculated by **equation (4.4.24)** when the number of run-up waves is $N = 100$. Moreover, C is a parameter that is concerned with the waterside slope cot γ of a revetment (for example, cot $\gamma = 2$ denotes a 20% slope revetment) and is given by the following equation.

$$\begin{cases} C = 0.25\cot\gamma + 0.5 & for \quad 0 \le \cot\gamma < 2 \\ C = 1 & for \quad \cot\gamma \ge 2 \end{cases} \tag{4.4.26}$$

Tamada et al.[123] verified the applicability of IFORM by using a CLASH data set[124] that aggregates the wave overtopping quantity experimental data all over the world, and found that the estimation accuracy of the wave overtopping rate is ensured by IFORM for sloping revetments and upright revetments when the ratio of water depth at the foot of a seawall (water depth at the foot of a slope) h_t to the wave heights h_t/H_0' is less than 3.0 and when the seabed slope tanθ > 1/100. Consequently, they reported that IFORM covers the installation conditions of many seashore revetments in Japan.

The CLASH dataset was referred to in the EurOtop Wave Overtopping Quantity Evaluation Manual[125] published in July 2007 by the cooperation of England, Holland, and Germany and greatly contributes to the description of the wave overtopping rate estimation equation for sloping revetments and upright revetments. However, these estimation equations parameterize the significant wave height in front of the seawall, which is different from the wave overtopping rate calculation method in Japan that uses the equivalent deepwater wave height. On the contrary, Goda[126] extracted and analyzed the wave overtopping quantity data for upright revetments and impermeable smooth slopes among the CLASH data sets and proposed a wave overtopping rate estimation equation, which can treat the wave overtopping quantity of upright revetments, sloping revetments, and wave-absorbing revetments uniformly by calculating the significant wave height in front of the revetments using the approximated wave height calculation equation[93] in a surf zone.

⑨ **Effects of Parapet**

Parapet on a revetment is effective in reducing wave overtopping. **Reference 127)** can be referred for wave overtopping of sloping dikes with parapet. However, since the upward force acts on the wall body of parapet depending on the condition of waves and parapet structures, this upward force needs to be fully taken into consideration in examination of stability of a wall body.

⑩ **Wave Overtopping of Multidirectional Random Waves**

In waters where the multidirectionality of waves is well clarified, the wave overtopping rate may be corrected in accordance with S_{max}, as in Reference 119).

⑪ **Permissible Wave Overtopping Rate**

The permissible wave overtopping rate depends on factors such as the structural type of the seawall, the situation with regard to land usage behind the seawall, and the capacity of drainage facilities; therefore it needs to be set appropriately depending on the situations. Although it is impossible to give one standard value for the permissible wave overtopping rate, Goda[128] gave the values for the threshold rate of wave overtopping for inducing damage (**Table 4.4.5**) on the basis of the past cases of disasters. Furthermore, Fukuda et al.[129] gave the values shown in **Table 4.4.6**, and Allsop et al.[130] and Kimura et al.[131] gave the values shown in **Table 4.4.7** as values for the permissible wave overtopping rate in view of the land usage behind the seawall. Furthermore, Nagai and Takada[132] have considered the degree of importance of the facilities behind the seawall and have come up with the values for the permissible wave overtopping rate (**Table 4.4.8**) by using the results of experiments with regular waves. Suzuki et al.[133] proposed 0.01 $m^3/s/m$ as the permissible wave overtopping rate for amenity-oriented revetment. When conducting the performance verification, these must be set appropriately by considering the importance of the facilities and the capacity of drainage facilities.

CADMAS-SURF[31] or flooding analysis models, such as those that use the MARS method,[134] can be used when calculating wave overtopping precisely with the inclusion of items, such as the permeability of the soil behind the seawall and the characteristics of wave-dissipating work configurations.

Table 4.4.5 Threshold Rate of Wave Overtopping for Inducing Damage

Type	Armor Layer	Wave Overtopping Rate ($m^3/s/m$)
Seawall	Paved behind	0.2
	Not paved behind	0.05
Levee	Covered with concrete on three sides	0.05
	Crown paving/rear slope non constructed	0.02
	Crown not paved	0.005 or less

Table 4.4.6 Permissible Wave Overtopping Rate in View of the Usage Condition of Hinterland (1)

User	Distance from dike	Wave overtopping rate ($m^3/s/m$)
Pedestrian	Land right in back (50% degree of safety)	2×10^{-4}
	Land right in back (90% degree of safety)	3×10^{-5}
Automobile	Land right in back (50% degree of safety)	2×10^{-5}
	Land right in back (90% degree of safety)	1×10^{-6}
House	Land right in back (50% degree of safety)	7×10^{-5}
	Land right in back (90% degree of safety)	1×10^{-6}

Table 4.4.7 Permissible Wave Overtopping Rate in View of the Usage Condition of Hinterland (2)

User	Condition	Wave overtopping flow rate ($m^3/s/m$)
Pedestrian	• Those who are paying attention to wave overtopping	10^{-4}
	• Those who are paying no attention	3×10^{-5}
Automobile	• Stopping or driving at low speed	0.01 to 0.05
	• Normal driving, damage to vehicles	1.1×10^{-5}
Building	• Structural damage	3×10^{-5}
	• Damage to joinery	10^{-6} to 3×10^{-5}
	• No damage	10^{-6}

Table 4.4.8 Permissible Wave Overtopping Rate in View of the Degree of Importance of Hinterland ($m^3/s/m$)

Districts where significant damage is expected, particularly because of the invasion of wave overtopping and spray due to a dense concentration of residential houses and public facilities in the rear.	Around 0. 01
Other important districts	Around 0. 02
Other districts	0. 02–0. 06

Table 4.4.6 is a table created with the results where people who watch a wave overtopping observation video make a judgment and indicate a wave overtopping rate that at least that percentage of people judged safe. Moreover, **Table 4.4.7** does not indicate the values measured in the field but was estimated in the hydraulic model experiment after the occurrence of damages or by using the wave overtopping rate estimation diagram. Therefore, they were possibly affected by the model scale and care should be taken that much more wave overtopping rate might have been experienced in the field.

⑫ **Effect of Winds on the Wave Overtopping Quantity**

In general, winds have a relatively large effect on small wave overtopping quantity, although there is a lot of variation. However, the relative effect of winds decreases as the wave overtopping rate increases. **Fig. 4.4.27**[129] shows the results of an investigation on the wind effect on wave overtopping quantity based on field observations. The abscissa shows the spatial gradient of the horizontal distribution of the wave overtopping quantity, whereas the ordinate shows the wave overtopping quantity per unit area. As seen from the figure, when the wave overtopping quantity is small, a larger wind velocity corresponds to a smaller spatial gradient of the horizontal distribution of the wave overtopping quantity. When the wave overtopping quantity is large, the spatial gradient of the horizontal distribution of the wave overtopping quantity increases. This shows that when the wave overtopping quantity is small, the distance over which a mass of water splashes is strongly affected by the wind velocity, with a larger distance at a higher wind velocity; however, when the wave overtopping quantity is large, the difference in the splash distance becomes small. Moreover, Yamashiro et al.[135] rearranged the data at that time, added a wind tunnel water tank experiment, made a regression equation of the wind velocity effect, and reported that it was appropriate that the model wind velocity should be approximately 1/3 of the field wind velocity when reproducing the effect of wind in the wind tunnel water tank.

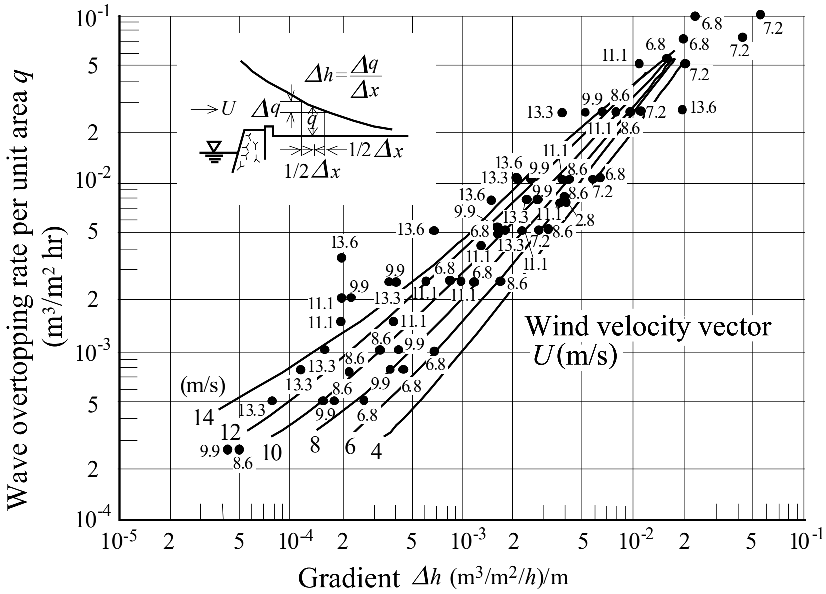

Fig. 4.4.27 Wind Effect on the Spatial Gradient of Horizontal Distribution of Wave Overtopping Quantity[129]

(3) Transmitted Wave Height

① The height of waves transmitted behind a breakwater by overtopping and/or permeation via the breakwater or the foundation mound of breakwater are calculated by referring to either the results of hydraulic model tests or the past data.

② It is necessary to appropriately estimate the transmitted wave height after waves have overtopped and/or passed through a breakwater because the transmitted waves affect the wave height distribution behind the breakwater. Transmitted waves include waves that have overtopped and/or overflowed, as well as waves that have permeated through a permeable rubble-mound breakwater or a foundation mound of composite breakwater. The latter in particular is sometimes referred to as permeated waves. Recently, several breakwaters have been built with caissons, which are originally not permeable, with through-holes to enhance the exchange of the seawater in a harbor. In this case, it is necessary to examine the wave coefficient of wave transmission (wave permeation) because the coefficient serves as an indicator of the efficiency of the exchange of seawater.

③ Coefficient of Wave Transmission to Inside of the Port at Breakwater

(a) **Fig. 4.4.28**[136] may be used to calculate the height of waves that are transmitted into a harbor when they overtop a composite breakwater or permeate through a foundation mound. Even when the waves are random, the coefficient of wave transmission agrees pretty well with that shown in **Fig. 4.4.28**. It has also been shown that **Fig. 4.4.28** is valid not only for the significant wave height but also for the highest one-tenth wave height and the mean wave height.[137] The period of the transmitted waves drops to approximately 50% to 80% of the corresponding incident wave period in both the significant wave and mean wave.[137] On the contrary, when wave overtopping transmitted waves dominate compared with waves permeating through a foundation mound, there is an example where an approximate value of coefficient of transmission was estimated using the wave overtopping rate on the breakwater crown.[138]

Moreover, there is a trial to calculate the overtopping transmitted waves behind the breakwater at the same time in wave transformation calculation for the targeting ports and harbors.[139)] Furthermore, Matsumoto[140)] indicated that CADMAS-SURF (the Super Roller Flume for Computer Aided Design of Maritime Structure) can be applied to the calculation of wave overtopping transmitted waves.

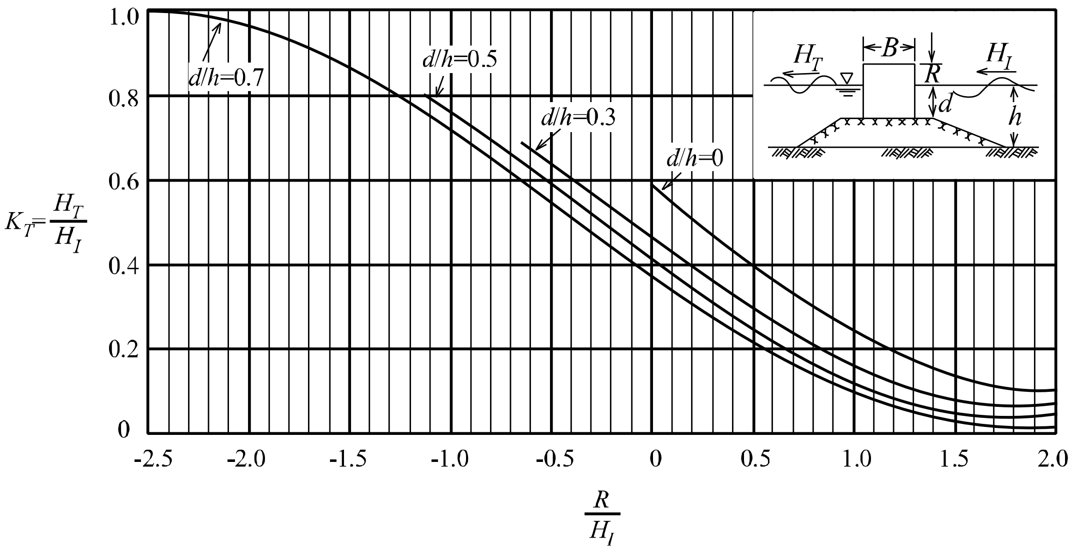

Fig. 4.4.28 Diagram for Calculating Coefficient of Wave Height Transmission[136)]

(b) The transmitted wave height for breakwater covered with wave-dissipating blocks was experimented by Kondo and Sato[141)] and Tanimoto and Oosato[142)]. Moreover, Sakamoto et al.[143)] experimented the wave-dissipating block-type sloping breakwater.

(c) A submerged breakwater is usually made by piling up crushed rock to form a mound and covers the surface with concrete blocks to prevent underlayers from sucking out. For wave transmission on a submerged breakwater of crushed rock, a diagram[144)] showing the relationship between the crown height of the breakwater and the coefficient of wave permeation is available.

④ **Coefficient of Wave Permeation at Breakwaters**

(a) For a porous and permeable structure, such as a rubble-mound breakwater or a deformed wave-dissipating concrete block-type breakwater, the theoretical analysis of Kondo and Takeda[145)] may be used as a reference. The following empirical equation may be used to obtain the coefficient of wave permeation of a typical structure.

Stone breakwater [146)] : $$K_T = 1\Big/\left(1 + k_t\sqrt{H/L}\right)^2 \qquad \textbf{(4.4.27)}$$

where

k_t : in the case of rubble-mound breakwater $k_t = 1.26\left(\dfrac{B}{d_t}\right)^{0.67}$,

in the case of deformed block-type breakwater $k_t = 1.184\left(\dfrac{B}{d_t}\right)^{0.895}$

B : crown width of the structure

d_t : nominal diameter of rubble or height of deformed block

H : height of incident waves

L : wavelength of incident waves

(b) For a curtain wall–type breakwater, the theoretical solutions of Morihira et al.[147)] may be used.

(c) For the coefficient of the wave transmission of an upright wave-dissipating breakwater of permeable type that has slits in both the front and rear walls, the experimental results are available.[148)]

(d) Types of breakwater aiming to promote the exchange of seawater include multiple-wing-type permeable breakwaters, multiple-vertical-cylinder breakwaters, horizontal-plate-type permeable breakwaters, and pipe-type permeable breakwaters. The coefficient of wave permeations of these types of breakwater is obtained.[148)]

4.4.8 Rise of Mean Water Level due to Waves and Surf Beats

(1) Wave Setup

① When constructing structures within the surf zone, it is preferable to consider the phenomenon of wave setup as necessary, which occurs in the surf zone owing to wave breaking as they approach the coast.

② **Rise of the mean water level due to breaking waves**

The phenomenon where the mean water level near the shoreline rises due to breaking waves (i.e., "wave set up") was known long ago via observations at the seashore and so on, but theoretical proof about the causes for the occurrence of this phenomenon has been lacking. In 1962, Longuet-Higgins and Stewart[149)] indicated that when a series of waves whose wave height varies approach the shore, this becomes the conveyance of a large momentum at the places where the wave height is large, and it becomes smaller at places wherein the wave height is small; therefore, apparent stress ends up being generated, and the mean water level changes. This apparent stress was called the radiation stress. This radiation stress is an amount proportionate to the square of the wave height and is an amount with the same order as the energy of a wave.

③ **Radiation Stress**

With the introduction of the concept of radiation stress, the change in the mean water level can be explained as follows.

When a wave approaching from offshore reaches shallow waters, the wave height increases owing to shallow water deformation as the water depth becomes shallower. When the wave height becomes larger, the conveyance of momentum becomes larger, and the mean water level begins to decrease (wave set down).

When the wave approaches the place where the water is even shallower, it breaks due to the wave height corresponding to the seabed slope and water depth. The wave height is suddenly diminished, the sudden decline of this wave height causes the conveyance of momentum to decrease suddenly, and the mean water level rises. The rise in the mean water level in the vicinity of the shoreline is viewed as a typical example of a phenomenon caused by such radiation stress.

④ **Diagrams for Estimating the Amount of Wave Setup**

Fig. 4.4.29 and **Fig. 4.4.30** show the changes in the mean water level by random wave breaking on the seabed slopes of 1/100 and 1/10, as calculated by Goda[93)]. A smaller wave steepness (H_0'/L_0) corresponds to a faster and larger rise in mean water level. Furthermore, a larger seabed slope corresponds to a larger rise in water level. **Fig. 4.4.31** shows the rise of mean water level at the shoreline. A smaller the wave steepness and steeper seabed slope leads to a larger rise of mean water level. When H_0'/L_0 is 0.01–0.05, with the exception of a very steep seabed slope, the rise of mean water level near the shoreline is 0.1–0.15 H_0', where H_0' is the equivalent deepwater wave height and L_0 is the wavelength of the deepwater wave. **Fig. 4.4.32** is a diagram for estimating the amount of wave setup that has been newly proposed by taking the directional wave spectrum into account. The values are slightly smaller than the values in **Fig. 4.4.31**, where the wave steepness is small.[150)]

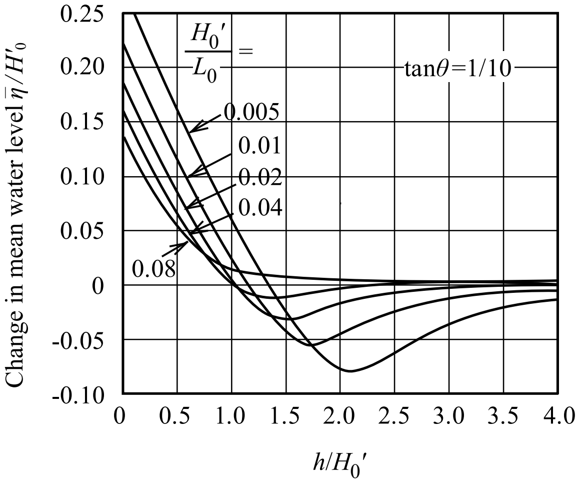

Fig. 4.4.29 Change in Mean Water Level (Seabed Slope 1/10)

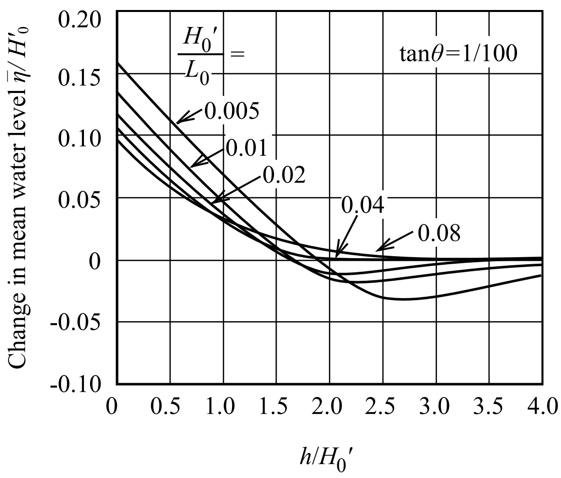

Fig. 4.4.30 Change in Mean Water Level (Seabed Slope 1/100)

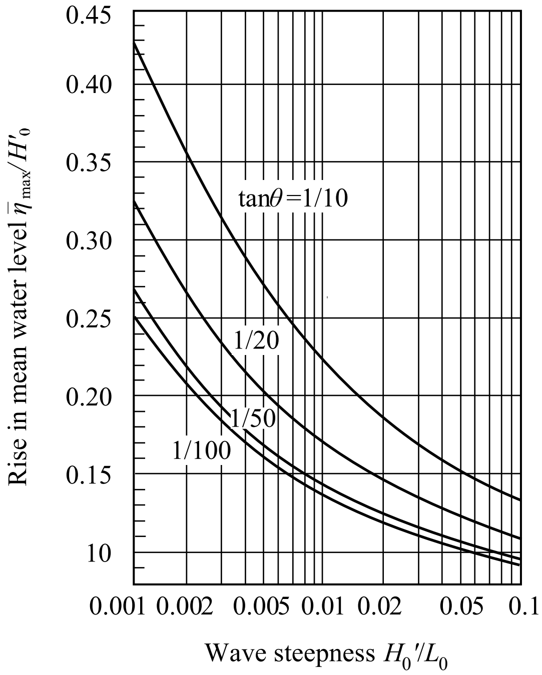

Fig. 4.4.31 Rise in Mean Water Level at Shoreline

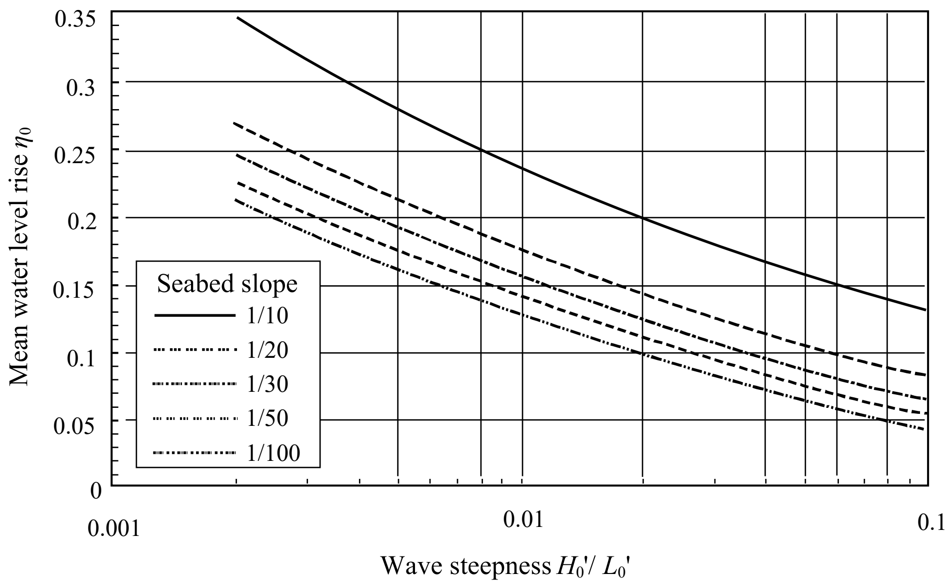

Fig. 4.4.32 Diagram of Water Level Rise at Shoreline considering the Multidirectionality of Waves

⑤ **Consideration of the rise in mean water level in the performance verification**

Given that the wave breaking point moves and that the breaking wave height becomes larger, owing to the rise of the mean water level, it is important to consider the rise in mean water level in performing an accurate computation of the design wave height in shallow waters.

(2) Surf Beats

① Surf beat with a period of one to several minutes, which occurs along with wave transformation in shallow waters, shall be examined as necessary in cases such as when using a numerical calculation model, which does not theoretically consider it, and when phenomenon exceeding what is implied by the calculation diagram based on the results of experiments.

② Random water level fluctuations lasting one to several minutes in the vicinity of the shoreline are called surf beat, and this has a major effect on the run-up height of waves, wave overtopping, and stability of beaches at the beach. The size of the surf beat should be estimated using either the approximation formulas of Goda[93] or on-site observations.

③ **Goda's Formulas for Estimating Surf Beat Amplitude**

On the basis of the results of field observations of surf beat, Goda[93] has proposed the following relationship:

$$\zeta_{rms} = \frac{0.04(\eta_{rms})_0}{\sqrt{\frac{H_0'}{L_0}\left(1+\frac{h}{H_0'}\right)}} = \frac{0.01H_0'}{\sqrt{\frac{H_0'}{L_0}\left(1+\frac{h}{H_0'}\right)}} \qquad \textbf{(4.4.28)}$$

where

ζ_{rms} : root mean square amplitude of the surf beat wave profile

$(\eta_{rms})_0$: root mean square amplitude of the deepwater wave profile

H_0' : equivalent deepwater wave height

L_0 : wavelength in deepwater

H : water depth

This equation shows that the amplitude of the surf beat is proportional to the equivalent deepwater wave height, that it falls as the water depth increases, and that it increases as the deepwater wave steepness (H_0'/L_0)

decreases. **Fig. 4.4.33** shows an example of the surf beat observation by Goda. **Fig. 4.4.34** compares **equation (4.4.28)** with the observation values.

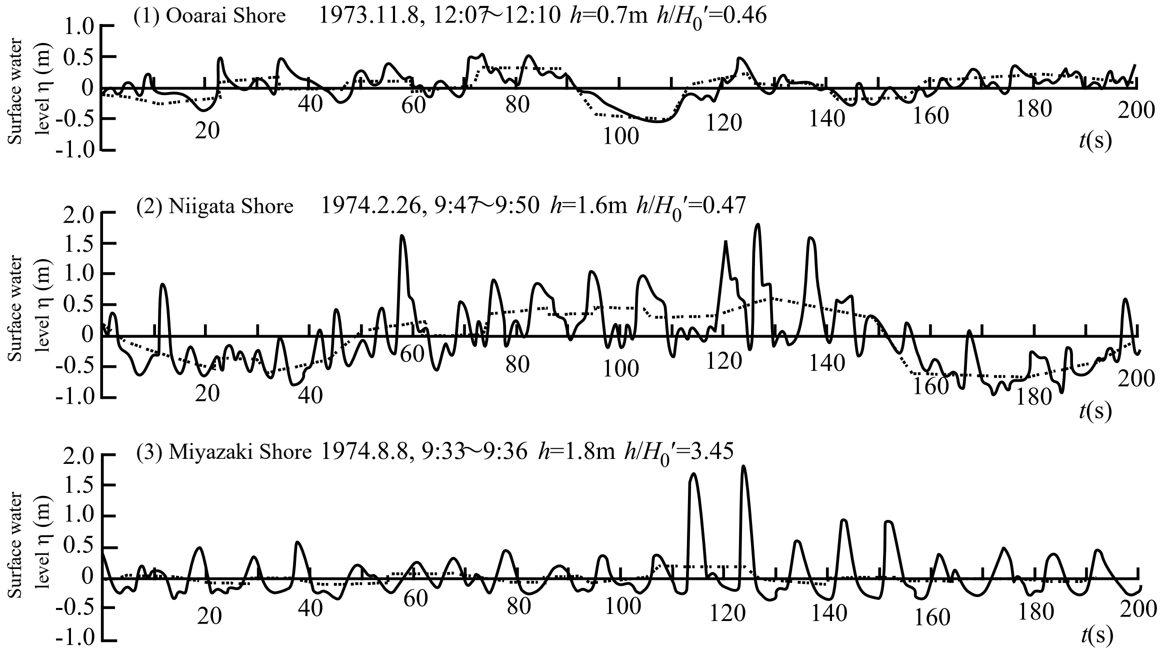

Fig. 4.4.33 Example of Waves and Surf Beats at Shores

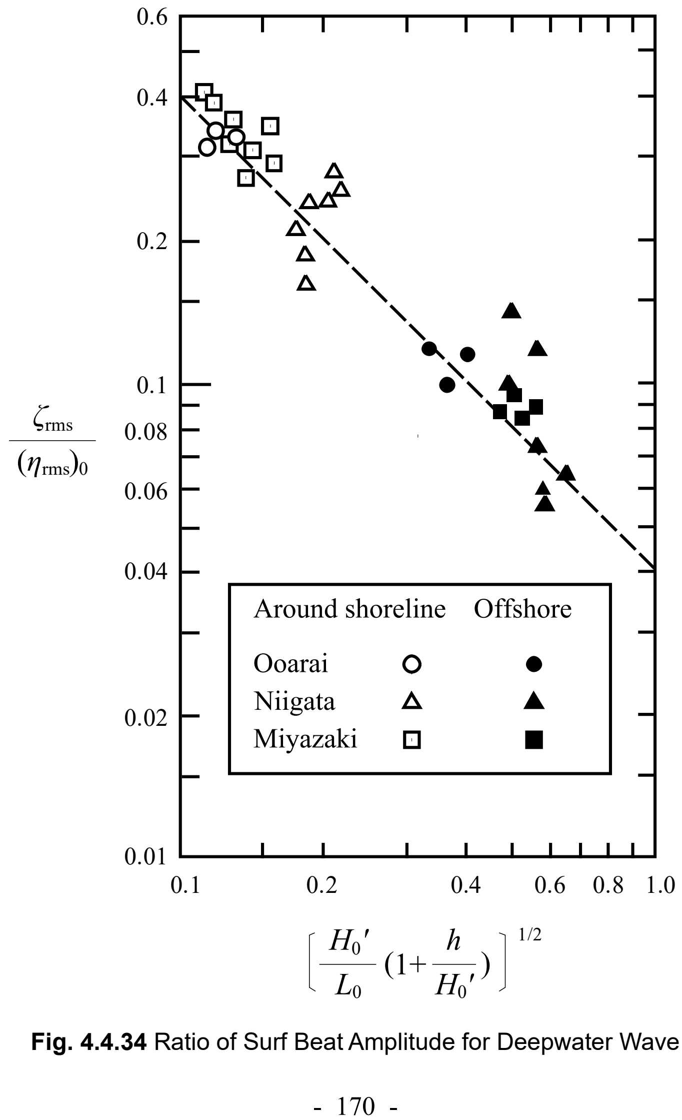

Fig. 4.4.34 Ratio of Surf Beat Amplitude for Deepwater Wave

4.5 Long-period Waves

(1) Setting Method of Long-Period Waves

① Definition of Long-Period Waves

With regard to long-period waves and harbor resonance, field observations should be performed as far as possible, and appropriate measures to control them must be taken on the basis of the results of these observations. Here, long-period waves are defined as waves composed of component waves with periods from 30 seconds to 300 seconds in the frequency spectrum analyzed from an uninterrupted wave record observed for the period more than 20 minutes.

② Distinction between Long-period Waves and Harbor Resonance

Water level fluctuations with the period between 30 seconds and several minutes sometimes appear at observation points in harbors and off the shore. Such fluctuations are generally called long-period waves. If the period of such long-period waves is close to the natural period in the surge motion of a ship moored at a quay wall by ropes, the phenomenon of resonance can give rise to a large surge motion with the amplitude of several meters even if the wave height is small, thus resulting in large effects on the cargo-handling efficiency of the port. The critical wave height for cargo handling affected by long-period waves differs by periods, specifications of ships, mooring conditions, loading conditions, and others. However, if it is clear that long-period waves of significant wave height 10–15 cm or more frequently appear in a harbor like the field observation results[151)] at Port of Tomakomai, it is advisable to investigate countermeasures from the hardware or software aspect[152)].

When conspicuous water level fluctuations with the period of several minutes or longer occur at an observation point in a harbor, it is highly likely that the phenomenon of harbor resonance is occurring. This phenomenon occurs when small disturbances in water level generated by changes of air pressure in offshore sea and amplifies the natural fluid motion in the harbor or bay by the resonance. If the harbor resonance becomes significantly large, the inundation at the innermost part of the bay or reverse outflow from municipal drainage channels may occur. Furthermore, high-current velocities may occur locally in a harbor, thus resulting in breaking of the mooring ropes of small ships. When drawing up a harbor plan, it is preferable to give consideration to making the shape of the harbor to minimize the harbor resonance motion as much as possible. The resonant period in small ports like marinas may be close to the period of long-period waves and the propagation of long-period waves from the open sea may excite the harbor resonance in the port. The two aspects of the long period wave and the harbor resonance are therefore highly correlated. If harbor resonance excitation by long-period waves becomes apparent from observations or numerical calculations, it is preferable to deliberate countermeasures while giving thought to these aspects.

In an ordinary harbor, the period of harbor resonance is several minutes or more, which is longer than that of long-period waves, and it is possible to distinguish the two from analysis of the oscillation period. However, the period of harbor resonance may become shorter to 2 to 3 minutes in the case of small craft basins and marinas, and this makes the discrimination difficult. In that case, it is preferable to make a judgment as suitable on the basis of the observation results for offshore waters and the circumstances in the surrounding harbor.

③ Occurrence Factor of Long-period Waves

The radiation stress[149)] indicated by Longuet Higgins and Stewart distributes unevenly for waves having prominent wave groups, and the long-period fluctuation of water level occurs. As this wave proceeds along with the wave group, it is called the bound wave. This wave theoretically proceeds at the wave group velocity C_G, and its amplitude is proportional to the square of the wave height of wind waves composing the wave group. Moreover, the amplitude increases as the water depth becomes shallower. If the wind waves are diffracted by a breakwater or a cape, the bound wave decreases because the diffracted wave height becomes smaller. However, given that the long period fluctuation induced so far does not disappear drastically, it is seemingly transformed to unbound long-period wave and propagated freely in the port. This wave is called a free progressive long wave, and its propagation velocity is expressed in $\sqrt{gh}$ as the long wave celerity.

Moreover, when waves with a wave group form break, the variation of their heights moves the wave breaking point onshore or offshore, the slope of the radiation stress is changed with time, and free progressive long waves are generated in the surf zone[153)]. Long-period waves invaded in a port as free progressive long waves are reflected by the quaywalls or beach, and some energies of the long waves propagate out of the port again. Therefore, long-period waves observed at an observation point outside a port include the component of bound waves, and the component of free progressive long waves advances onshore and offshore. However, some of the occurrence process of long-period waves are complicated and still unexplained. Here, countermeasures and others are presented by considering that the majority of long-period waves observed in a port is expressed as free progressive long waves advancing toward the shore. However, in reality, not only the component of free progressive long waves but also the component remaining as bound waves and the long-period wave induced by the change in wave height at the port entrance may exert some influence. Therefore, it is necessary to evaluate the effect of countermeasures against the long waves through the numerical analysis, model experiment, or others if any structures are constructed as the countermeasures.

(2) Representation of Long-Period Waves

① Standard Spectrum for Long-Period Waves

When there are insufficient field observation data of long-period waves in offshore sea and the property of the long-period waves are not sufficiently derived, the standard spectrum shown in **Reference** 154) or its approximate expression may be used for the long-period wave performance verifications. Here, the standard spectrum is proposed as the spectral form that superimposes uniform spectral density in the long-period wave side to the short-period wave spectrum represented by the Bretschneider–Mitsuyasu type.

Fig. 4.5.1 shows a comparison between an observed spectrum and an approximate form of the standard spectrum. The term α_l in the figure denotes a parameter that represents the energy level of the long-period waves. The parameter shows the relationship between the spectrum peak frequency f_p of short-period wave components and boundary frequency f_b for calculating the energy of long-period waves components. The parameter α_l is given as $\alpha_l = f_p / f_b$. The past observations show that the value of the parameter exists between 1.6 and 1.7. A smaller value of α_l leads to the larger energy of the long-period waves.

Given that the values of the parameter are determined as the mean values estimated from observation data with the significant wave heights of 3 m or more, the wave heights of the long-period wave components are prone to be overestimated for normal waves. Therefore, for the normal waves, it is needed to use the relations between the proper wave height ratio R_L (= $H_L/H_{1/3}$; where H_L is the significant wave height of the long-period wave component, and $H_{1/3}$ is the significant wave height of the whole frequency band) and α_l corresponding to the spectral form of short-period wave components. **References 155)** and **156)** are helpful because they propose the equation to directly calculate α_l from the height and period of the wind waves observed at the sea shallower than 50 m, in addition to the correlation equation between R_L and α_l for each frequency spectrum of the Bretschneider–Mitsuyasu type (**equation (4.2.12)**), modified Bretschneider–Mitsuyasu type (**equation (4.2.13)**), and JONSWAP type (**equation (4.2.14)**).

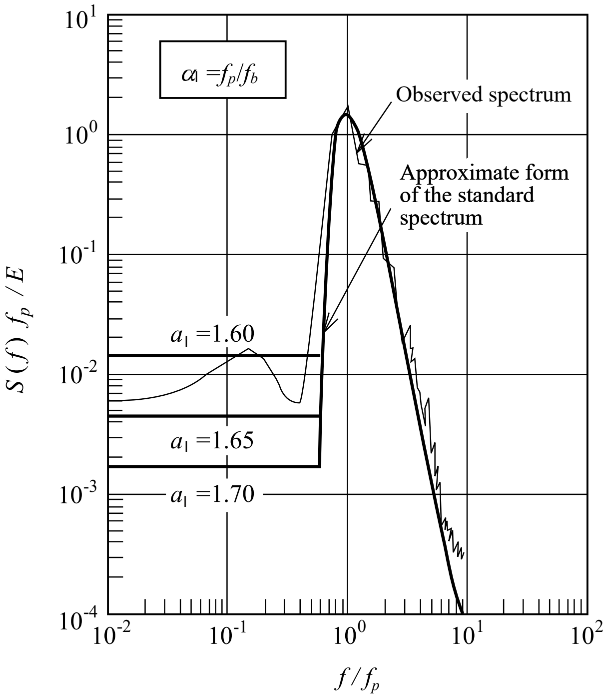

Fig. 4.5.1 Comparison between Standard Spectrum with Long-period Wave Components and Observed Spectrum

② **Direction of Long-period Waves**

At the propagation of the long-period waves they frequently overlap with the waves reflected from the longshore, and consequently it is difficult to determine their direction. However, if the main energy of the long-period waves advances toward the shore as the free progressive long waves, its wave direction may be conveniently assumed to be same as the principal direction of short-period waves (wind waves).

(3) Handling of Long-Period Waves

① **Calculating the Propagation of Long-Period Waves**

It is preferable to calculate the propagation of long-period waves into a harbor by setting up incident wave boundary in offshore sea and then by using either the Boussinesq equation or the linear long wave equations.[157) At this time, random waves for the calculation shall be the basic target. However, if there are any special circumstances such as the period restriction of the incident long waves to some specific period band, several calculation results for the regular waves with different periods may be synthesized in energy and used. See **Part II, Chapter 2, 3.3 Harbor Resonance** for the method for calculating harbor resonance.

② **Countermeasures against Long-Period Waves and Harbor Resonance**

In waters where long-period waves are marked, it is preferable to establish a breakwater layout plan to inhibit the ingress of long-period waves into the harbor. At this time, in the event that the particle diameter of the mound materials is large, almost all of the energy of the long-period waves is transmitted into the harbor; therefore, it is necessary to thoroughly examine the structures of the breakwater and mound.

To control the surge oscillation of ships, it is preferable to shift the resonant period of the ship mooring system from the period of the invading long-period waves. To this end, it is preferable to take such measures as changing the places and the initial tensions of the mooring ropes, as well as improvement of rope material and increase of the number of the mooring ropes by new installation of land winches. The effects of such measures should be examined beforehand, and appropriate measures should be devised on the basis of suitable numerical calculations.

The long-period waves are frequently amplified by the reflection from the facilities in a harbor; in particular, upright wave-dissipating revetments have almost no wave-dissipating functions for long-period waves and swells. Therefore, the review of the reflection coefficient of the facilities is necessary to accurately estimate the long-period wave heights inside harbors. **The Environment Assessment Manual of Long-Period Waves in Harbors**[158)] can be used as a reference for the rough order of magnitude and calculation method of the reflection coefficient.

Structures that control the reflection of long-period wave and lower the long-period wave height inside ports and harbors are called the long-period wave countermeasure construction, and many of them are installed behind the breakwater or in front of the revetment in ports and dissipate long-period waves by turbulence generated at the wave penetration through the permeable mound of gravel material and so on.[159)] In this case, if the width of the permeable mound is approximately 5% of the long-period wave length in the state of direct incidence, the reflection coefficient of the long-period waves is on the order of 0.8.[160)] Furthermore, long-period wave-dissipating revetments which are composed of a two-sided slit caisson and backfilling materials of large gravels have been developed to dampen the long-period waves in a harbor. It is preferable to set the width of the water transmitting layer, place of installation, and installation range through the hydraulic model test and numerical calculations to achieve the maximum effects.[161) 162)] Studies need to be conducted to examine the wave-dissipation effect by widening the virtual width of permeable mound for oblique incident long-period waves to the permeable mound[163)] and to examine the wave-dissipation performance of water-submerging-type long-period wave-dissipating works by expecting the friction effect on the permeable mound.[164)]

Considering that the distribution of long-period wave height is not uniform in the harbor, it is preferable to examine the modification of the berthing location at the planning stage in the event that the height of long-period waves in the target berth clearly exceeds the limit values.

4.6 Concept of Harbor Calmness

(1) Factors of Calmness and Disturbance

① The factors causing disturbances in the harbor need to be set appropriately for the evaluation of harbor calmness.

② The problem of harbor calmness is extremely complex. It involves not only physical factors such as waves, winds, ship motions, and wind- and wave-resistance of working machinery but also the factors requiring human judgment, such as the ease with which ships can enter and leave the harbor, ship refuge during stormy weather, and critical conditions of works at sea. Harbor calmness is further related with economic factors, such as the efficiency of cargo handling works, the operating rate of ships, and the cost of constructing the various facilities required to improve the harbor calmness. The factors that cause the harbor disturbances related to waves, which constitute the basis of the criteria for the evaluation of the harbor calmness, include the following:

(a) Invading waves from harbor entrance

(b) Transmitted waves into the harbor

(c) Reflected waves

(d) Long-period waves

(e) Harbor resonance

In large harbors, wind waves generated within the harbor may require attention, and the ship wake waves by larger ships may cause troubles for small ships.

(2) Points to remember for calculations of harbor calmness

It is necessary to bear the following points in mind when performing harbor calmness calculations.

① Set the wave height and period frequency distribution at the port entrance.

② In the event that the water depth in navigation channel differs significantly from the surrounding water depth, shoals exist inside the harbor, or the water depth changes suddenly in the port entrance, consider the water depth change in the calculation of wave height inside the harbor.

③ Introduce the effects of the period as concerns the permissible value of the wave height in the harbor.

④ Consider the future state of the port utilization to set up the target value for harbor calmness.

(3) Computation of Harbor Calmness for Normal Waves

Harbor calmness is generally set with the occurrence probability of the significant waves that does not exceed the critical wave height for cargo handling works or for ship anchoring. The critical wave height for cargo handling works means the upper limit of the significant wave height at which the ships moored at the quay wall or dolphin can safely perform cargo handling activities. The critical wave height for anchoring means the upper limit of the significant wave height at which ships can safely anchor in the berthing basin and moored at the buoy as well as at the mooring facilities. The occurrence probability of the significant waves that does not exceed the critical wave height for cargo handling works is called the cargo handling operating rate. In general, the harbor calmness is assessed by the cargo handling operating rate. The following methods may be used for computation of harbor calmness [165) 166)] (see **Fig. 4.6.1**).

① **Computation of the cargo handling operating rate for normal waves (wind waves and swells)**

(a) Prepare a frequency table of wind waves (wave height, period) by the wind direction outside the harbor.

(b) Set several representative waves outside the harbor for the computation

Set several representative waves (combination of wave height and period and wave directions) outside the harbor for the computation considering the topography of ports and referring to the frequency table of wind waves and swells by the wave direction at a point outside the harbor. If the waves' nonlinear transformation can be ignored inside and outside the harbor or if the wave direction and height at the harbor entrance are computed by using the linear models of the energy balance equation and others per combination of wave period and direction outside the harbor, the occurrence frequency of wave heights outside the harbor may not necessarily be considered in setting the height of representative waves.

(c) Compute the wave heights at points inside the harbor and prepare their occurrence frequency tables

If the wave transformation inside and outside the harbor can be computed at the same time by using a nonlinear wave model like the Boussinesq model, determine the ratio of the wave height at each point inside the harbor to the incident wave height outside the harbor per representative wave, and then, determine the ratio of the wave heights by interpolation to the class values of period and wave direction in the wind wave and swell frequency table at point outside the harbor or their original values of period and wave direction in the wave dataset observed at point outside the harbor. If the transformation of waves due to the seabed topography inside the harbor can be ignored because of the relatively small change of the water depth inside the harbor, it is possible to employ the ratios obtained by multiplying the wave height ratios inside the harbor, computed with Takayama or other methods for the incident wave at the harbor entrance, with the wave height ratio at the harbor entrance to the outside harbor previously computed with the energy balance equation and others. The wave height occurrence frequency table in front of the target facilities and inside the harbor can be computed by multiplying these ratios of wave heights with each of class values or original values of wave height. When the transmitted and permeated waves into the harbor are considered together as needed, these wave heights and the computed wave heights obtained above are squared individually, and the square root of their sum (mean wave of wave energy) may be considered as the wave height inside the harbor. In a harbor where the influence of the transmitted or the permeated waves is relatively small, the wave period inside the harbor may be represented by the wave period obtained from the above wave transformation computation inside the harbor. It was reported that the wave transmission rate becomes significant when the wave overtopping rate is at least $0.02m^3/s/m$ or more for a composite breakwater where transmitted waves caused by wave overtopping are more prominent than waves permeating through the foundation mound.[138)]

(d) Compute the cargo handling operating rate for normal wave (wind waves and swells) components

The cargo handling operating rate can be computed in the following procedures:

1) Setting the critical wave height for cargo handling works (if there is or may be a trouble in cargo handing due to swells and others, set by the type and deadweight tonnage of ships used and the wave direction, period, and the like per mooring facility as necessary). **The Environmental Assessment Manual of Long-Period Waves in Harbors**[167)] lists standard values of the critical wave height for cargo handling works, which can be used as a reference.

2) Accumulating the occurrence frequency of the wave heights which exceed the critical wave height for cargo handling works in front of the target facilities.

3) Determining the cargo handling non-operating rate (%) by dividing the cumulative frequency in 2) by the number of whole data and adding up by all periods and wave directions. Obtaining the cargo handling operating rate by subtracting the non-operating rate from 100%.

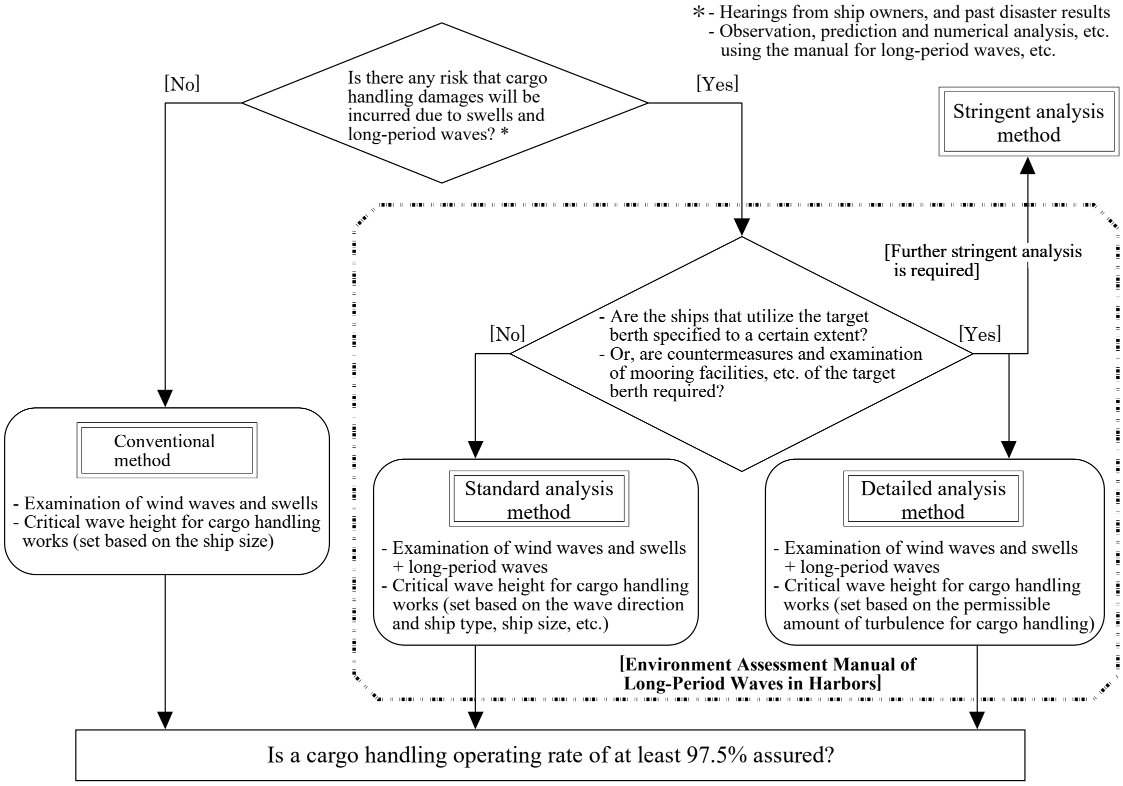

Fig. 4.6.1 Example of Performance Verification Steps Relating to Harbor Calmness

② **Calculation of the cargo handling operating rate for long-period waves**

Prepare a frequency table of long-period waves by the wave direction outside the harbor

If a frequency table of long-period waves measured in the field by the wave direction cannot be obtained, prepare a frequency table of long-period waves by the wave direction outside the harbor by utilizing the frequency table of the wind waves outside the harbor. In this case, the standard spectrum of the long-period waves may be used (see **Part II, Chapter 2, 4.5 Long-period Waves**).

(b) Set several wave directions and heights of long-period waves outside the harbor to compute

Set several wave directions and heights of long-period waves outside the harbor for the computation considering the topography of ports and referring to the frequency table of long-period waves by the wave direction at a point outside the harbor. In the application range of the linear theory, the heights of representative long-period waves outside the harbor may be set without considering the occurrence frequency. The period band of the component waves may be set from 30 s to 300 s according to the definition.

(c) Compute the wave heights inside the harbor and prepare the occurrence frequency table of long-period wave heights inside the harbor

By using a wave model like the Boussinesq model that can compute the wave transformation occurring inside and outside the harbor at the same time, determine the ratio of the wave height at each point inside the harbor to the incident long wave height outside the harbor per long-period wave direction, and then, determine the ratio of the wave heights by interpolation to the class values of wave direction in the long-period wave frequency table at point outside the harbor or their original values of wave direction in the wave dataset observed at point outside the harbor. It is preferable to consider the transformation of random waves at this time. The occurrence frequency table of wave heights in front of the target facilities and inside the harbor can be computed by multiplying these ratios of the wave heights with each of class values or original values of wave height.

(d) Compute the cargo handling operating rate for long-period wave components

The cargo handling operating rate for long-period wave components can be computed in the following procedures:

1) Setting the critical long-period wave height for cargo handling works. For this setting, it is preferable to consider the type of ship and the cargo handling system in question and to determine the wave heights separately based on a survey of the actual state of cargo handling. The critical wave height for cargo handling works for long-period waves is defined in **Table 4.6.1**.[168]

2) Accumulating the occurrence frequency of the wave heights which exceed the critical wave height for cargo handling works in front of the target facilities.

3) Determining the cargo handling non-operating rate (%) by dividing the cumulative frequency in 2) by the number of whole data and adding up for all wave directions. Obtaining the cargo handling operating rate by subtracting the non-operating rate from 100%.

Table 4.6.1 Critical Wave Height for Cargo Handling Works for Long-Period Waves [168]

Level of the significant wave height of long-period waves	Assumed conditions	Critical wave height for cargo handling works (m)
1	Ship classes for which the permissible amount of motions in cargo handling is relatively large for surging, or ships whose resonant period for surging is 1.5 minutes and under (medium sized ships: 1,000 to 5,000 DWT)	0. 20
2	Ship classes for which the permissible amount of motions in cargo handling is moderate for surging, and ships whose resonant period for surging is 1.5 minutes and under (general cargo ships: 5,000 to 10,000 DWT)	0. 15
3	Ship classes for which the permissible amount of motions in cargo handling is small for surging, or ships whose resonant period for surging is 2–3 minutes (container ships, mineral ore ships: 10,000 to 70,000 DWT)	0. 10

(4) Harbor calmness for abnormal waves

The harbor calmness for abnormal waves which is equivalent to a probabilistic wave with a return period of 50 years, for facilities with a design service life of 50 years in the case of waves as variable action can be generally assessed by considering the fact that the waves in an abnormal state have a major effect on the performance of the facilities in harbors. The evaluation of the harbor calmness can be performed by setting the critical value of the abnormal wave height inside the harbor and confirming that the wave heights computed inside the harbor in the abnormal state does not exceed this critical value.

It is preferable to set the critical wave height for ship refuge among the critical waves as 0.7 to 1.5 m for ships in the order of 5,000 to 10,000 GT class or less according to the type of ship and the refuge condition (mooring to a wharf, mooring to a buoy, anchoring). It may be on the order of 0.5 m in a small craft basin for small ships. A crown height of the wharf shall ensure no inundation behind owing to wave overtopping and others, and the critical wave height for that needs to be set properly.

(5) Harbor resonance

The period of the harbor resonance is approximately 5 minutes or more and is not a factor to extremely worsen the cargo handling works. However, a harbor shape that does not generate big harbor resonance is preferable because a large amplitude causes damage, such as troubles in mooring small ships, reverse flow from drains, flooding of quaywalls, etc. (See **Part II, Chapter 2, 3.3. Harbor Resonance**).

4.7 Ship Wake Waves

(1) It is preferable to consider ship wake waves due to ship navigation in canals and waterways.

(2) Ship wake waves are caused when ships navigate. A larger and faster ship leads to the greater ship wake waves. As the ship wake waves propagate longer, they attenuate gradually; therefore, they do not cause serious problems in wide water areas. However, they sometimes cause undesirable motions in moored small ships, floating piers, etc., inside harbors or in narrow waterways such as channels and canals. Furthermore, they infrequently affect wave overtopping, the scouring and stability of armored blocks at revetments on both sides of a waterway.

(3) Pattern of Ship Wake Waves

If the ship wake waves are viewed from air, they appear as shown in **Fig. 4.7.1**. It is composed of two groups of waves. One group spread out in a shape like "八" from a point slightly ahead of the bow of the navigation ship. The other group is behind the ship, and the wave crest is perpendicular to the ship's navigation line. The former waves are called "divergent waves," whereas the latter are called "transverse waves." The divergent waves form concave curves; the closer to the navigation line, the shorter the distance between the adjacent wave crests. On the contrary, the transverse waves are approximately arc-shaped, with the constant distance between the adjacent wave crests. In deep water, the area over which the ship wake waves extend is limited within the area bounded by the two cusplines, with the angles ±19º28' from the navigation line and starting from the origin lying somewhat in front of the bow of the ship. The divergent waves cross the transverse waves just inside the cusplines; this is where the wave height is the largest. Wave steepness is smaller for the transverse waves than for the divergent waves, thus implying that the transverse waves often cannot be distinguished from an aerial photograph.

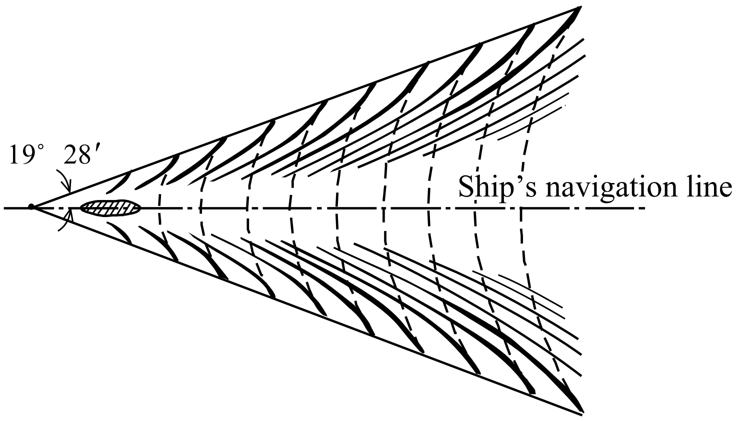

Fig. 4.7.1 Plan View of Ship Wake Waves (Solid lines show the crests of divergent waves, and dotted lines show the crests of transverse waves.)

(4) Wavelength and Period of Ship Wake Waves

The wavelength and period of ship wake waves are different between the divergent waves and the transverse ones, with the latter having both a longer wavelength and a longer period. Amongst the divergent waves, the wavelength and period are both the longest for the first wave and then become progressively shorter.

① The wavelength of the transverse waves can be obtained by the numerical solution of **equation (4.7.1)**, which is derived from the condition that the velocity of the transverse waves must be same as the speed of the ship navigation.

$$\frac{gL_t}{2\pi}\tanh\frac{2\pi h}{L_t} = V^2 \qquad (\text{when } V < \sqrt{gh}) \tag{4.7.1}$$

where

L_t : wavelength of transverse waves (m)

h : water depth (m)

V : ship navigation speed (m/s)

When the water is sufficiently deep compared with the wavelength of transverse waves, the wavelength of the transverse waves is given by the following equation:

$$L_0 = \frac{2\pi}{g}V^2 = 0.169{V_k}^2 \tag{4.7.2}$$

where

L_0 : wavelength of transverse waves at places where the water is sufficiently deep (m)

V_k : ship navigation speed (kt) ($V_k = 1.946\ V$)

② The period of the transverse waves is equal to the period of progressive waves with the wavelength L_t in water of depth h. It is given by **equations (4.7.3)** or **(4.7.4)**.

$$T_t = \sqrt{\frac{2\pi}{g} L_t \coth\left(\frac{2\pi h}{L_t}\right)} = T_0 \coth\left(\frac{2\pi h}{L_t}\right) \quad \textbf{(4.7.3)}$$

$$T_0 = \frac{2\pi}{g} V = 0.330 V_k \quad \textbf{(4.7.4)}$$

where

T_t : period of transverse waves in water of depth h (s)

T_0 : period of transverse waves at places where the water is sufficiently deep (s)

③ The wavelength and period of the divergent waves are given by **equations (4.7.5)** and **(4.7.6)**, which are derived from the condition that the component of the ship's speed in the direction of travel of the divergent waves must be equal to the velocity of the divergent waves.

$$L_d = L_t \cos^2\theta \quad \textbf{(4.7.5)}$$

$$T_d = T_t \cos\theta \quad \textbf{(4.7.6)}$$

where

L_d : wavelength of divergent waves as measured in the direction of travel (m)

T_d : period of divergent waves (s)

θ : angle between the direction of travel of the divergent waves and the navigation line (º)

According to Kelvin's theory of wave-generation at places where the water is sufficiently deep, the angle of travel θ of the divergent waves can be obtained, as shown in **Fig. 4.7.2**, as a function of the position of the place of interest relative to the ship. For actual ships, the minimum value of θ is generally approximately 40º, and θ is usually 50º to 55º for the point on a particular divergent wave at which the wave height is the maximum. The illustration in the figure shows that the angle θ directs the location of the source point Q where the divergent wave has been generated and α is the angle between the cuspline and the navigation line.

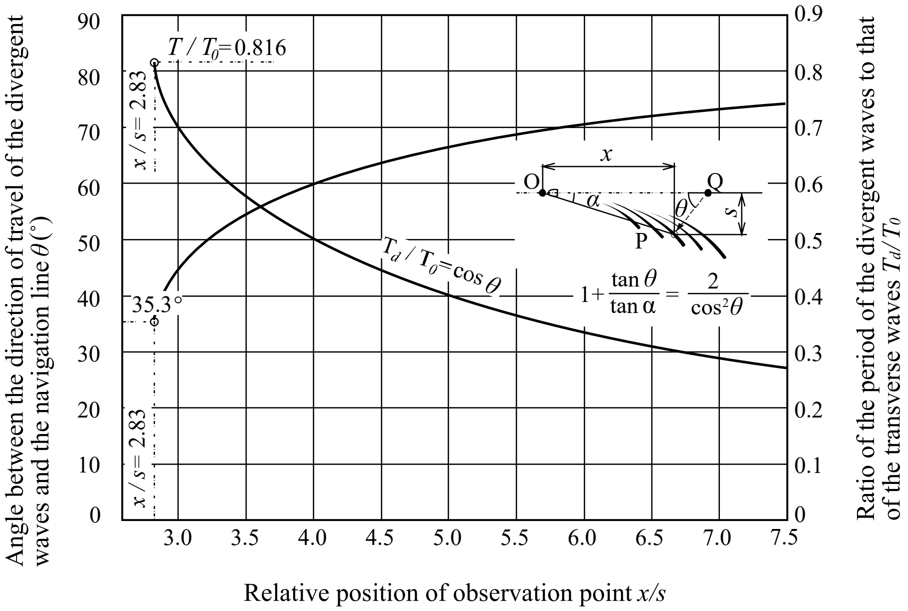

Fig. 4.7.2 Wave Direction and Period of Divergent Waves at Places where the Water is Sufficiently Deep

(5) Shoaling Effect on Ship Wake Waves

As same as normal water waves, ship wake waves are affected by the water depth, and their properties vary when the water depth decreases relative to their wavelength. This shoaling effect on the ship wake waves may be ignored if the condition defined by **equation (4.7.7)** is satisfied[169)]:

$$V \leq 0.7\sqrt{gh} \tag{4.7.7}$$

The critical water depth above which ship wake waves may be regarded as deepwater waves is calculated by **equation (4.7.7)**, as shown in **Table 4.7.1**. As can be seen from this table, the waves generated by ships in normal conditions can generally be regarded as deepwater waves. Situations in which they must be regarded as shallow water waves include the following cases: a high-speed ferry travels through relatively shallow waters, a motorboat travels through shallow waters, and ship wake waves propagate into shallow waters.

Note that ship wake waves generated in shallow water have a longer wavelength and period than those generated by the ship navigating in deep water at the same speed.

Table 4.7.1 Conditions under which Ship Wake Waves can be regarded as Deepwater Waves

Speed of ship	V_k(kt)	5.0	7.5	10.0	12.5	15.0	17.5	20.0	25.0	30.0
Water depth	h(m) ≥	1.4	3.1	5.5	8.6	12.4	16.9	22.0	34.4	49.6
Period of transverse waves	T_0(s)	1.7	2.5	3.3	4.1	5.0	5.8	6.6	8.3	9.9

(6) Height of Ship Wake Waves

The ship wake waves research committee of the Japan Association for Preventing Maritime Accidents has proposed the following **equation (4.7.8)** for giving a rough estimate of the height of ship wake waves[169)]:

$$H_0 = \left(\frac{L_{pp}}{100}\right)^{1/3} \sqrt{\frac{E_{\mathrm{HPW}}}{1620 L_{pp} V_K}} \tag{4.7.8}$$

where

H_0 : characteristic wave height of ship wake waves (m), or the maximum wave height observed at a distance of 100 m from the navigation line when a ship is navigating at its full-load cruising speed

L_{pp} : length between perpendiculars of the ship (m)

V_K : full-load cruising speed of the ship (kt)

E_{HPW} : wave-generation horsepower of the ship (W)

The wave-generating horsepower E_{HPW} of a ship is calculated as follows. For the ship dimensions necessary for these equations, reference 170) can be referred to.

$$E_{\mathrm{HPW}} = E_{\mathrm{HP}} - E_{\mathrm{HPF}} \tag{4.7.9}$$

$$E_{\mathrm{HP}} = 0.6 S_{\mathrm{HPm}} \tag{4.7.10}$$

$$E_{\mathrm{HPF}} = \frac{1}{2}\rho_0 S V_0^3 C_F \tag{4.7.11}$$

$$S = 2.5\sqrt{\nabla L_{pp}} \tag{4.7.12}$$

$$C_F = 0.075 \Big/ \left(\log\frac{V_0 L_{pp}}{\nu} - 2\right)^2 \tag{4.7.13}$$

where

S_{HPm} : continuous maximum shaft horsepower of the ship (W)

ρ_0 : density of seawater (kg/m^3) ρ_0=1030(kg/m^3)

V_0 : full-load cruising speed of the ship (m/s) $V_0 = 0.514 V_K$

C_F : frictional resistance coefficient

ν : coefficient of kinematic viscosity of water (m^2/s) $\nu \fallingdotseq 1.2 \times 10^{-6}$ (m^2/s)

∇ : full-load displacement of the ship (m^3)

Equation (4.7.13) has been obtained by assuming that the ship's energy consumed through wave-generation resistance is equal to the propagation energy of ship wake waves, whereas the values of the coefficients have been determined as averages of the data from ship towing tank tests. The characteristic wave height H_0 of ship wake waves depends on an individual ship, although for medium and large-size ships it is approximately 1.0 to 2.0 m. Tugboats sailing at full speed produce relatively large waves as well. The characteristic wave height H_0 shall be calculated by setting values of ship's length between perpendiculars L_{pp}, full-load displacement ∇, full-load cruising speed V_K, and continuous maximum shaft horsepower S_{HPm} in **equations (4.7.8)** to **(4.7.13)** from the documents describing ship specifications, such as reference 170). Here, the horsepower described in reference 170) can be used for the continuous maximum shaft horsepower S_{HPm}.

It can be considered that the wave height of ship wake waves attenuates in proportion to $S^{-1/3}$, where S is the distance of the observation point from the navigation line. It is also considered that the wave height is proportional to the cube of the cruising speed of the ship. Accordingly, the maximum wave height $H_{\max}$ of ship wake waves can be calculated by the following equation:

$$H_{\max} = H_0\left(\frac{100}{S}\right)^{1/3}\left(\frac{V_k}{V_K}\right)^3 \tag{4.7.14}$$

where

$H_{\max}$: maximum wave height of ship wake waves at any chosen observation point (m)

S : distance from the observation point to the navigation line (m)

V_k : actual cruising speed of the ship (kt)

Equation (4.7.14) cannot be applied if the distance S is too small. However, **equation (4.7.14)** can be applied to the smaller value of the ship's length between perpendiculars L_{pp} or 100 m.

The upper limit of the height of ship wake waves occurs when the wave steepness of the maximum wave height of the divergent wave reach to the breaking criterion of $H_{max}/L_t = 0.14$. If the angle between the wave direction and the navigation line is assumed to be $\theta = 50°$ at the point on a divergent wave where the wave height becomes largest, the upper limit of the wave height at any given point can be given by **equation (4.7.15)**. However, the conditions for deepwater waves shall be satisfied.

$$H_{\text{limit}} = 0.010 V_k^2 \tag{4.7.15}$$

where

H_{limit} : upper limit of the height of ship wake waves derived from the wave breaking conditions (m)

The ship wake waves are largely affected by the ship's conditions such as size, shape, and cruising speed and topographical conditions such as water depth. Therefore, it is practically preferable to consider these conditions in the estimation of the ship wake waves. The method described here is for quick calculation of the height of the ship wake waves. Other methods such as the numerical calculation method of the ship wake waves are also proposed.[171)]

(7) Propagation of Ship Wake Waves

① Among the two groups of ship wake waves, the transverse waves propagate in the direction of ship's navigation, and continue to propagate even if the ship changes course or stops. In this case, the waves have a typical nature of regular waves with the period given by **equation (4.7.3)**, and they propagate at the group velocity, undergoing transformation such as refraction and others. Takeuchi and Nanasawa[172)] gave an example of such transformations. As the waves propagate, the length of wave crest spreads out. Even when the water is of uniform depth, the wave height attenuates in a manner that is inversely proportional to the square root of the distance traveled.

② The direction of propagation of a divergent wave varies from point to point on the wave crest. According to Kelvin's theory of wave-generation, the angle between the direction of propagation and the navigation line is $\theta = 35.3°$ at the outer edge of a divergent wave. As one moves inwards along the wave crest, the value of θ approaches 90°. The first wave arriving at any particular point has the angle $\theta = 35.3°$, whereas the value of θ becomes gradually larger for subsequent waves. This spatial change in the direction of propagation of the divergent waves can be estimated by using **Fig. 4.7.2**.

③ The propagation velocity of a divergent wave at any point on the wave crest is the group velocity corresponding to the period T_d at that point (see **equation (4.7.6)**). In the illustration in **Fig. 4.7.2**, the time necessary for a component wave to propagate at the group velocity from point Q at wave source to point P is equal to the time taken for the ship to travel at the speed V from point Q to the point O. Considering that each wave profile propagates at the wave velocity (phase velocity), the waves pass beyond the cuspline and appear to vanish one after the other at the outer edge of the divergent waves.

(8) Generation of Solitary Waves

When a ship navigates through shallow waters, there are cases when solitary waves are generated in front of the ship if the cruising speed V_k approaches $\sqrt{gh}$. Around the river mouths, there is a possibility of small ships being affected by such solitary waves generated by other large ships. [173)]

4.8 Actions on Floating Body and its Motions

4.8.1 General

(1) The performance verification of a floating body shall be conducted under the appropriate consideration of the motions and mooring forces of the floating body due to wind, currents, and waves.

(2) In general, a floating body refers to a structure that is buoyant in water and makes allowable motions within a certain range.[174)] When verifying the performance of a floating body, both its required functions and its stability

shall be examined. It is necessary to pay attention to the matter that the required performance on each case is different in general.

(3) Mooring equipment includes a variety of types and is generally composed of a combination of mooring lines (ropes or chains), anchors, sinkers, intermediate weights, intermediate buoys, mooring piles, connection joints, and fenders. The mooring equipment has a large influence on the motions of a floating body; therefore, it is important to verify the stability of this equipment appropriately.

(4) The floating bodies used as port facilities can be classified into floating wharves, [175] offshore floating petroleum stockpiling bases,[176] floating breakwaters,[177] floating bridges,[178] [179] and floating disaster-prevention bases.[180] [181] Moreover, the investigation and development of very large floating type structures[182] [183] [184] [185] have been performed.

(5) Floating bodies can also be classified by the types of mooring methods. As described below, mooring methods include catenary mooring (slack mooring), dolphin mooring, taut mooring etc.

① **Catenary mooring (Fig. 4.8.1(a))**

This is the most common mooring method. With this method, the chains or other materials used in the mooring are given sufficient lengths to make them slack. This means that the force restraining the motions of the floating body is small, but the mooring system fulfills the function of keeping the floating body in more-or-less the same position. There are various types of catenary mooring depending on factors such as the material of the mooring lines, number of mooring lines, and presence or absence of intermediate buoys and sinkers.

② **Dolphin mooring (Fig. 4.8.1(b))**

With this method, mooring is maintained using either a pile-type dolphin or a gravity-type dolphin. In general, this method is suitable for restraining the motions of a floating body in the horizontal direction, but a large mooring force acts on the dolphin. This method has been used for mooring floating units of offshore petroleum stockpiling bases. Moreover, there is a pile mooring as a mooring method similar to the dolphin mooring. This mooring method is often used for relatively small floating piers and others. It generally uses a guide roller instead of a fender in the contact part with a floating body.

③ **Taut mooring (Fig. 4.8.1(c))**

This is a mooring method that reduces the motions of a floating body greatly; a Tension Leg Platform (TLP) is an example. With this method, the mooring lines are given a large initial tension so that they do not become slack even when the floating body moves. The advantages of this mooring method are as follows: The floating body does not move much, and only a small area is needed for installing the mooring lines. However, it is necessary to take note of the fact that because a large tensile force is generated in the mooring lines, the specifications of the lines become the critical factor on the stability of the floating body. This method is often used for mooring platforms for oil drilling and others in overseas.

④ **Mooring using a universal joint (Fig. 4.8.1(d))**

This is a mooring method with a mechanism that allows operation in every direction so as not to give the large restraining force to a floating body. The mooring equipment shown in the figure is an example of a mooring method that can be used to moor a large offshore floating body. The examples of mooring equipment that uses a universal joint on the sea bottom include a SALM (Single Anchor Leg Mooring) type single point mooring buoy[186] and the mooring of a MAFCO (MAritime Facility of Cylindrical Construction) tower.[187]

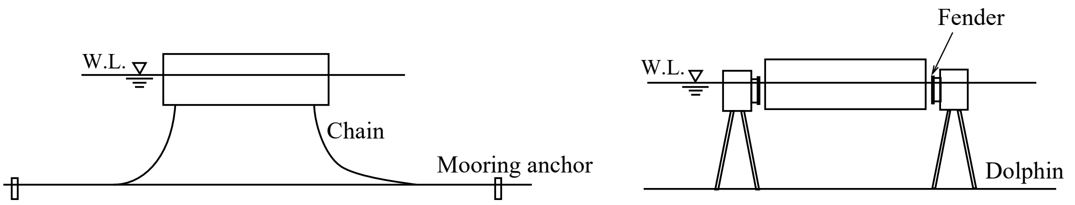

(a) Catenary mooring

(b) Dolphin mooring

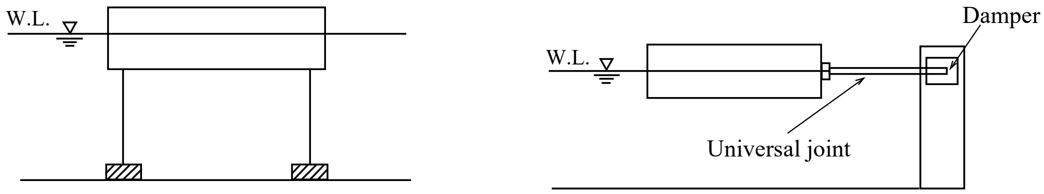

(c) Taut mooring

(d) Mooring by universal joint

Fig. 4.8.1 Examples of Mooring Methods for Floating Body

4.8.2 Action on Floating Body

(1) Types of Actions and Calculation Methods

When a port facility is made of floating structures, the forces acting on the floating structures and caused by their motions shall be composed of the following forces: wind drag force, drag force by currents, wave-exciting force, wave drift force, wave making resistance force, restoring force, and mooring force. These forces shall be estimated by an appropriate analytical method or hydraulic model tests, in accordance with the mooring method for the floating body and the size of facility.

(2) Wind Drag Force

With a structure for which a part of the floating body is above the sea surface, wind exerts an action on the structure. This action is called the wind drag force or wind pressure and is composed of a pressure drag and a friction drag. If the floating body is relatively small in size, the pressure drag is dominant. The pressure drag is proportional to the square of the wind velocity and is expressed as follows. The subscript *k* in the following equation refers to the characteristic value:

$$F_{W_k} = \frac{1}{2}\rho_a C_{DW} A_W \left|U_{W_k}\right| U_{W_k} \qquad \textbf{(4.8.1)}$$

where

F_W : wind drag force (kN)

ρ_a : density of air (t/m^3)

A_W : projected area of the part of the floating body above the sea surface as viewed from the direction in which the wind is blowing (m^2)

U_W : wind velocity (m/s)

C_{DW} : wind drag force coefficient

The wind drag force coefficient is proportionality constant and is also known as the wind pressure coefficient. It can be determined by wind tunnel tests and others. However, it is also acceptable to use a value that has been obtained in past experiments for a structure with a shape similar to the structure of interest.

Values such as those listed in **Table 4.8.1** have been proposed as the wind drag force coefficients of objects in the uniform flow. As can be seen from this table, the wind drag force coefficient varies with the shape of the floating body, but it is also affected by the wind direction and the Reynolds number. It is considered that the wind pressure acts in the direction of the wind flow and at the centroid of the projection of the part of the floating body above the water surface. However, it is necessary to pay attention to the fact that this may not necessarily be the case if the floating body is large. Moreover, the velocity of the actual wind is not uniform vertically. Therefore, the value of the wind velocity at the elevation of 10 m above the sea surface is generally employed as the representative wind speed U_W for the wind pressure calculation.

Table 4.8.1 Wind Pressure Coefficients

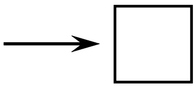	Square cross-section	2.0 [1.2] (0.6)
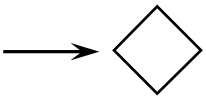	Square cross-section	1.6 [1.4] (0.7)
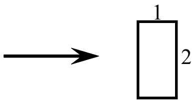	Rectangular cross-section (ratio of side lengths = 1:2)	2.3 [1.6] (0.6)
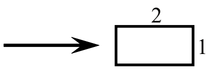	Rectangular cross-section (ratio of side lengths = 1:2)	1.5 (0.6)
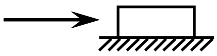	Rectangular cross-section (ratio of side lengths = 1:2, when one face is in contact with the ground)	1.2
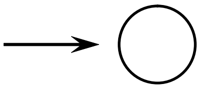	Circular cross-section (smooth surface)	1.2 (0.7)

[ ] is a value when chamfered with a diameter equal to 1/4 of one side
( ) is a numerical value equal to or more than the critical Reynolds number

(3) Drag Force by Currents

When there is a current, such as tidal currents, these currents exert forces on the submerged part of the floating body. These forces are referred to as the flow pressure or the drag force by currents. Similar to the wind drag force, they are proportional to the square of the flow velocity. Considering that the velocity of the current is generally small, the drag force by current is actually expressed as being proportional to the square of the relative velocity of the current to the motion of the floating body, as shown in the following equation. The subscript k in the following equation refers to the characteristic value:

$$F_{C_k} = \frac{1}{2}\rho_0 C_{DC} A_C \left| U_{C_k} - U_k \right| \left(U_{C_k} - U_k \right) \qquad \textbf{(4.8.2)}$$

where

F_C : drag force by currents (kN)

ρ_0 : density of fluid (t/m^3)

A_C : projected area of the submerged part of the floating body as viewed from the direction of the currents (m^2)

U_C : velocity of the currents (m/s)

U : velocity of motion of the floating body (m/s)

C_{DC} : drag coefficient with respect to the currents

The drag coefficient with respect to the current C_{DC} is a function of the Reynolds number. However, when the Reynolds number is large, the values for steady flow shown in **Table 7.2.1** may be used.

The drag coefficient for the currents generally varies with the shape of the floating body, the direction of the currents, and the Reynolds number. Similar to the wind pressure, the direction of the force exerted by the currents and the direction of the currents itself are not necessarily the same.[188] In general, the deeper the draft of the floating body relative to the water depth, the larger the drag coefficient for the currents becomes. This is referred to as the shoaling effect, and the drag coefficient increases because a smaller gap between the sea bottom and the base of the floating body increases the difficulty for water to flow through this gap.

(4) Wave-Exciting Force

The wave-exciting force is the force exerted by incident waves on the floating body when the floating body is considered to be fixed in the water. It is composed of a linear force that is proportional to the amplitude of the incident waves and a nonlinear force that is proportional to the square of the amplitude of the incident waves. The linear force is the force that the floating body receives from the incident waves as reaction when the floating body deforms the incident waves. The velocity potential for the deformed wave motion can be obtained by using wave diffraction theory. On the contrary, the nonlinear force is composed of a force that accompanies the finite amplitude nature of waves and a force that is proportional to the square of the flow velocity. The former force due to the finite amplitude effect can be analyzed theoretically; however, it is often ignored in practice. The latter force that is proportional to the square of the flow velocity becomes large, particularly when the diameter of the floating body is small relative to the wavelength; it is preferable to determine this force experimentally.

(5) Wave Drift Force

When waves act on a floating body, the center of the motion of the floating body gradually shifts in the direction of wave propagation. The force that causes this shift is called the wave drift force. If it is assumed that the floating body is 2-dimensional and the wave energy is not dissipated, the wave drift force is given by the following equations.[189] The subscript k in the equation refers to the characteristic value:

$$F_{d_k} = \frac{1}{8}\rho_0 g H_{i_k}^2 R \tag{4.8.3}$$

$$R = K_R{}^2\left\{1 + \frac{4\pi h / L}{\sinh(4\pi h / L)}\right\} \tag{4.8.4}$$

where

F_d : wave drift force per unit width (kN)

$\rho_0 g$: unit weight of seawater (kN/m^3)

H_i : incident wave height (m)

R : wave drift force coefficient

K_R : reflection coefficient

h : water depth (m)

L : wavelength (m)

If the dimensions of the floating body are extremely small relative to the wavelength, the wave drift force may be ignored as being much smaller than the wave-exciting force. However, the wave drift force becomes dominant as the floating body becomes larger.

When random waves act on a floating body moored at a system with only a small restraining force, such as a single-point mooring buoy designed for supertankers, the wave drift force becomes a dominant factor because it may give rise to slow drift oscillations. In this case, the long-period fluctuating wave drift force in the form of the wave drift force has a large effect on the slow drift oscillations of the floating body. For example, if random waves are comprised of waves with two different frequencies, the fluctuating wave drift force is given by the following equation.[190] The subscript k in the equation refers to the characteristic value:

$$F_{d_k} = \frac{1}{4}\rho_0 g H_{i_k}^2 R\left(\frac{\omega_1+\omega_2}{2}\right)\left\{1+\cos\left(\frac{\omega_1-\omega_2}{2}\right)t\right\} \quad \textbf{(4.8.5)}$$

where

F_d : wave (fluctuating) drift force per unit width (kN)

$\rho_0 g$: unit weight of seawater (kN/m^3)

H_i : incident wave height (m)

$R((\omega_1+\omega_2)/2)$: wave drift force coefficient by regular wave of $\cos((\omega_1+\omega_2)/2)$

ω_1 and ω_2 : wave frequency (rad/s)

t : time (s)

(6) Wave Making Resistance Force

When a floating body moves in still water, the floating body exerts a force on the surrounding water, and the floating body receives a corresponding reaction force from the water; this reaction force is called the wave making resistance force. This force can be determined by forcing the floating body to move through the still water and by measuring the force acting on the floating body. However, an analytical method is generally used wherein each mode of the floating body motions is assumed to be realized separately, and the velocity potential, which represents the motion of the fluid around the floating body, is obtained. Only forces that are proportional to the motion of the floating body can be determined analytically; the nonlinear forces that are proportional to the square of the motion cannot be determined analytically. Among the terms of the linear forces, i.e., those that are proportional to the motion of the floating body, the term that is proportional to the acceleration of the floating body is called the added mass term, whereas the term that is proportional to the velocity is called the linear damping term.

(7) Restoring Force

The static restoring forces make a floating body return to its original position when the floating body moves in still water. They are generated in the unbalance state of buoyancy and gravity when the floating body heaves, rolls, or pitches. They are generally treated as proportional to the amplitude of the motion of the floating body, although this proportionality is gradually lost as the amplitude becomes large. However, the static restoring force is often treated as proportional to the amplitude.

(8) Mooring Force

The mooring force is the force (restraining force) that is generated to restrain the motion of the floating body with mooring equipment such as mooring lines. The magnitude of this force depends greatly on the displacement-restoration characteristics of the mooring equipment. Reference 191) can be referred for the materials used in mooring equipment and their characteristic features.

(9) Analytical Method for Wave-Exciting Force and Wave Making Resistance Force by Using Velocity Potential

In the estimation of the wave-exciting force and the wave making resistance force, the velocity potentials which represent the motion of the fluid are derived first and then these two forces are calculated by using the velocity potentials. The derivation methods of the velocity potentials for both forces are fundamentally same except only difference in the boundary conditions. The velocity potentials can be obtained by using any of a number of methods, such as a domain decomposition method, an integral equation method, a strip method, or a finite element method. The outline of the abovementioned numerical calculation methods is introduced in references 192) 193) 194).

When a floating body is fixed in position, the wave force acting on the floating body can be calculated from the velocity potential that satisfies the boundary conditions at the sea bottom and around the floating body. For example, the wave force acting on a floating body with a long rectangular cross-section, such as a floating breakwater, can be determined using the approximate theory of Ito *et al.*[195)].

(10) Forces Acting on a Very Large Floating Type Structure

The external forces described in (2) to (9) above for relatively small floating body cannot be directly applied to a very large floating type structure, because its size is very large and its elastic response cannot be neglected. Therefore, it is necessary to perform sufficient examinations on their characteristics.[196)]

4.8.3 Motions of Floating Body and Mooring Forces

(1) Calculation Methods of Motions of Floating Body and Mooring Forces

The motions of a floating body and the mooring forces shall be calculated by an appropriate analytical method or hydraulic model tests, in accordance with the shape of the floating body and the characteristics of the external forces and mooring equipment.

(2) Motions of Floating Body

The motions of a floating body can be determined by solving the dynamic equilibrium equation, with the external forces due to wind and waves, the restoring force of the floating body itself, and the reaction forces of the mooring equipment. If the floating body is assumed to be a rigid body, then its motions comprise six motion components (**Fig. 4.8.2**): surging, swaying, heaving, pitching, rolling, and yawing. Among these, the horizontal motions of surging, swaying, and yawing, may show slow motions with the period of a few minutes or more in some cases. Such long-period motions have a large influence on the extension range of mooring lines and the performance verification of the mooring equipment. Thus, one may give separate consideration to the long-period motions, by taking only the wave drift force and the long-period fluctuating components of the wind and waves as the external forces when doing analysis. If the floating body is very long, elastic deformation may accompany the motions of the floating body and this should be examined if necessary.

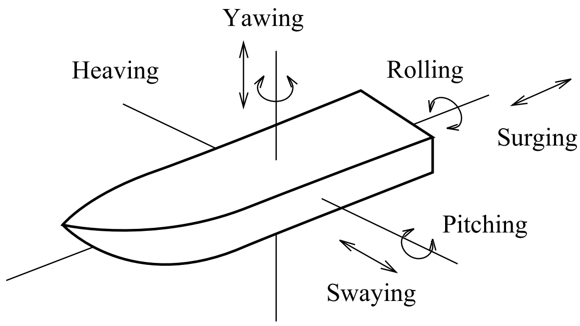

Fig. 4.8.2 Components of Motions of Floating Body

(3) Methods for Solving the Equations of Motion

① **Steady state solution method for the nonlinear equations of motion**

The equations of motion for a floating body are nonlinear. Therefore, it is not easy to solve the equations. Nevertheless, if the nonlinear terms in the equations of motion are linearized under the assumption that the motion amplitudes are small, the solutions can be obtained relatively easily. For example, the equations for the motions of a 3-dimensional floating body ends up with a system of six simultaneous linear equations for the amplitudes and phases of the six modes of motions. Note that if the floating body is assumed to be a rigid body and its motions are linear, the motions are proportional to the external forces. In particular, if there are no currents or wind, the motions are proportional to the wave height.

② **Numerical simulation of nonlinear motions**

The wind drag force and the drag force by currents are in general nonlinear, and the mooring force is also often nonlinear. In this case, an effective and general solution method is to use a numerical simulation where the equations of motion are progressively solved for a series of time steps. The equations of motion for the floating body can be divided into the constant coefficient method,[197)] in which the coefficient values of the added mass term and linear wave damping term within the equations of motion are fixed at a specific frequency, and the phase lag function method,[198) 199)] in which these terms are changed over time in a simulation using a phase lag function. The phase lag function method is also called the memory influence function method. In the numerical simulation, the time-series data of the wave-exciting force and the wave induced flow velocity are obtained from the incident wave spectrum, and data of the fluctuating wind speed are obtained from the wind spectrum. The external forces obtained from these time-series data are then placed into the equations of motion for the floating body, and the time-series of the floating body motions and the mooring forces are calculated.

Numerical simulations are applied to the analyses of the motions of various floating bodies. For example, Ueda and Shiraishi[197] performed numerical simulations on the motions of a moored ship, and Suzuki and Moroishi[200] analyzed the swinging motion of a ship moored at a buoy. The numerical simulation generally assumes as the preconditions that the fluid is ideal, that the motions of the floating body are small, and that the incident waves are linear and their superposition is allowed. If these assumptions cannot be held, it is preferable to perform hydraulic model tests.

The approximation theory of Ito *et al.*[195], which is relatively easy to handle, can be applied for calculating the motions and mooring forces for a rectangular cross-sectional floating body.

(4) Hydraulic Model Tests

Hydraulic model tests provide a powerful technique for determining the motions of a floating body and the mooring forces. Up to the present time, hydraulic model tests have been performed for various types of floating bodies. For examples, **References 201) 202) 203)** and **204)** can be used.

When conducting hydraulic model tests of a floating body, sufficient attention shall be paid to any similarities in the inertia moments of the floating body and the characteristics of mooring equipment. Given that the motion characteristics of the floating body vary significantly by the mooring method, it is particularly important to properly analogize the displacement-restoration characteristics of the mooring equipment. For example, considering that the similarity law for mooring line does not hold just by using the same materials at the site and analogizing the shape, it is necessary to reduce the elastic coefficients of the model materials just by the scale size from those at the site. However, it is practically difficult to look for such a material, and a variety of creative measures needs to be taken.

(5) Statistical Treatment of Motions of Floating Body and Mooring Forces

The motions and mooring forces for a floating body obtained by numerical simulation and hydraulic model tests for random waves vary irregularly with time. Therefore, the peak values of the motion amplitudes and mooring forces for the floating body also vary with time. Even if the wave spectrum is identical, the maximum values for these vary when the duration time or the wave run is different. In other words, given that the motion amplitudes and mooring forces for the floating body are probability variables, statistical treatment should be performed to estimate the expected values. In the usual statistical treatment, a normal distribution or a Rayleigh distribution is applied to the probability density distributions of the peak values of the obtained motion amplitudes and mooring forces, and the expected values are estimated.

(6) Methods for Estimating Expected Values of Motions of Floating Body

The expected values for the motions of a floating body can be estimated by taking into consideration its motion characteristics and by assuming either a normal distribution or a Rayleigh distribution.[201] The procedure is described below.

① **Simulation of oscillation**

A simulation of oscillation of a floating body is performed for adequate calculation time, and the values of double amplitudes of the motions are calculated for each wave. The motion double amplitude is defined as a sum of the maximum amplitude and the minimum one for a wave in the time series of the motion of a floating body, similar to the definition of the wave height to the surface wave. The number of waves needed to accurately estimate the expected value of the maximum motions is approximately 100 or more.

② **Assumption of the distribution shape of the motion double amplitude**

A suitable distribution shape for the double amplitudes of the motions obtained by the simulation of oscillation is assumed. A Rayleigh distribution or a normal distribution shown below may be adopted as the distribution shape.

Rayleigh distribution: $$P(x)dx = 2a^2 \exp\left(-a^2 x^2\right)dx \qquad \textbf{(4.8.6)}$$

Normal distribution: $$P(A) = \frac{1}{\sqrt{2\pi\sigma^2}} \exp\left\{-\frac{1}{2}\left(\frac{A-\overline{A}}{\sigma}\right)^2\right\} \qquad \textbf{(4.8.7)}$$

where

$x=A/A^*$

A : motSion double amplitude

A^* : arbitrary base motion double amplitude

$a = A^*/(8\, m_0)^{1/2}$

$(8\, m_0)^{1/2} = A_{rms}$ (root mean square of the motion double amplitudes)

σ : standard deviation of the motion double amplitudes

$\overline{A}$: mean value of the motion double amplitudes

However, the value of parameter a is 1.416 when the arbitrary base motion double amplitude A^* is the significant value $A_{1/3}$, and $\sqrt{\pi}/2$ when it is the mean value $\overline{A}$.

③ **Estimation method of the expected value of the maximum values**

Assuming that the number of waves is N and that the value at which the exceedance probability becomes $1/N$ is the expected value of the maximum values at that number of waves, the expected value of the ratios of double amplitudes of motions in a Rayleigh distribution is approximated by the following equation when N is sufficiently large.

$$x_N = \frac{1}{a}(\ln N)^{1/2} \tag{4.8.8}$$

On the contrary, in a normal distribution, the expected value of the motion double amplitudes is expressed by the following equation.

$$A_N = \overline{A} + \mu_N \sigma \tag{4.8.9}$$

The expected value of the maximum values varies depending on the number of waves N. **Table 4.8.2** shows the values of x_N and the values of μ_N, which is the parameter of the deviation of a standard normal distribution, relative to the representative values of N.

Table 4.8.2 Values for the Estimation of the Expected Value of the Maximum Values

Number of samples N relative to the expected value of the maximum values	100	200	500	1000	10000
Rayleigh distribution x_N	1.52	1.63	1.76	1.86	2.14
Normal distribution μ_N	2.33	2.58	2.88	3.09	3.96

④ **Calculation example of the expected value of the maximum values**

For example, assuming a Rayleigh distribution as the distribution shape, consider a case wherein the expected value of the maximum values for the number of waves of 1,000 is calculated. First, the significant value A^* of the double amplitudes of motions is calculated from the simulation results. Thereafter, a = 1.416 and N = 1,000 are substituted into **equation (4.8.8)**, and the value of x_N is calculated. Finally, the expected value A can be obtained from $x_N = A/A^*$.

4.9 Wave Observations and Investigation

(1) Overview

In shallow water, waves are transformed by processes such as refraction, breaking, and shoaling; therefore, offshore observations are necessary to understand their actual states. Notwithstanding its importance, it has been about 40 years only since the longshore wave observation using measuring instruments began as the routine in Japan. The volume of accumulated wave data is not necessarily enough at present compared with the observed data of tidal level or wind, and wave observation data must be accumulated further for a long time. See **Reference (Part II), 2.4 Observation and Examination of Waves** for details.

The objectives and items of wave observation need to be determined, and the types of observation instruments to use need to be selected depending on observation items. Moreover, with due consideration for the following points the observation point should be selected [3] so that the waves observed at the point can show the representative characteristics of waves in the sea area of interest:

① **A place where the principal wave direction can be observed**

A place that is open to the direction from which the most influential principal waves directly attack the target sea area.

② **Not affected by structures**

No affection of sheltering, reflection, diffraction, or others caused by existing or soon constructed structures such as breakwaters.

③ **Not complicated sea bottom topography**

Not near the steep sloping land or submarine escarpment but relatively flat sea bottom topography. A place where rapid tidal flows should also be avoided.

④ **Not affected by sailing ships and fish catching activities**

There is no frequent traffic of ships or activities of fish boats on the sea where wave observation instruments are installed.

⑤ **Others**

Select an observation point where the observation purpose is fulfilled as far as possible by coordinating with the jurisdictional Maritime Safety Agency, port and coast managing bodies (national government, autonomous bodies, etc.), and concerned parties of users (shipping lines, fishery cooperatives, etc.).

(2) Observation of Tsunamis and Long-period Waves with Offshore Wave Meters

Normally, 20-minute long sea surface observation data are used as a basis for analysis and arrangement of significant wave and so on, but a long-duration sea surface observation data also enable the analysis and arrangement of tsunamis and long-period waves.

① **Recording of offshore tsunami profile**

Previously, the only actual measured data at the sites of tsunamis were run-up traces and tide level recordings. Such data are important for clarifying the actual conditions of tsunamis, but it is not sufficient. In particular, the tidal level variations observed at tide measurement wells inside harbors were records of water level changes through inlet pipes; therefore, in actuality, it was extremely difficult to clearly measure vibration components with short periods less than 10 minutes. For this reason, the offshore tsunami wave profile recordings have a significant meaning.

② **Observation of long period waves**

Information concerning long-period waves from continuous observation data taken using offshore wave gauges is expected to be useful not just when tsunamis occur but also at normal times.

It is often impossible to correctly evaluate harbor calmness on the basis of significant wave height alone, as has been the custom to date. Even when the significant wave height is low and when the waves appear calm in the port, there have been many reports of cases where mooring ropes broke, which made cargo operations impossible, or where maritime construction work was unavoidably interrupted because of the large oscillations of ships and the operation of ships within the port owing to the effects of long-period waves. This is because they can cause resonance with the natural periods of the harbor associated with the port's topography on the order of several minutes to several tens of minutes or with the natural period of mooring systems generated by the mass of the ships and the spring constants of the mooring ropes on the order of several minutes to several tens of minutes.[205]

(3) Obtaining Wave Observation Documents

Longshore wave observation in Japan is conducted by the Ports and Harbours Bureau of the Ministry of Land, Infrastructure, Transport and Tourism; the Japan Meteorological Agency; electric power companies; local governments; and others. Among them, the **Nationwide Ocean Wave Information Network for Port and HarbourS (NOWPHAS)**, which is administered by Ports and Harbours Bureau of the Ministry of Land, Infrastructure, Transport and Tourism, has the most consummate observation network and data administration and analysis systems [206]. Since 1970, NOWPHAS wave observation data have been compiled and published in the Wave Observation Annual Report or Long-Term Statistical Report issued annually. [207] NOWPHAS wave observation information is also available on the following site: http://www.mlit.go.jp/kowan/nowphas/ (Real time wave information)

[References]

1) JSCE: Design Handbook for Shore Protection Facilities. JSCE, pp. 301-305, 2000
2) Coastal Development Institute of Technology (CDIT): Commentary on analysis and applications of Coastal Waves, Coastal Observation data, p. 181, 2000
3) Takayama, T. editorial supervisor, Study Group on Analysis and Utilization of Oceanographic Observation Data Edit: Overview of Waves-Waves, Tsunami, Storm Surge, GPS Ocean Wave Buoy, Coastal Wave Meter-, Coastal Development Institute of Technology (CDIT),318p,2013 (in Japanese)
4) Borgman, L. E.: Risk criteria, J. Wat. & Harb. Div., Proc. ASCE., Vol. 89, No. WW3, pp. 1-35, 1963
5) Hirayama, K, H. Kashima, M. Itsui and T. Naruke: Consideration for Probability of Extreme Swell Occurrences and Characteristics of their Regional Distribution; Journals of JSCE Division B2 (Coastal Engineering), Vol.71 No.2, pp.I_85-I_90, 2015 (in Japanese)
6) Matsufuji, E., T. Takayama, M. Miyata, K. Hirayama, H. Kawai, Y. Suzuki, Y. Utsunomiya and Y. Fukunaga: Estimation of Design Wave through Introduction of Swell Effect, Journals of JSCE Division B2 (Coastal Engineering), Vol.73 No.2, pp.I_1153-I_1158, 2017 (in Japanese)
7) Hirayama, K., Y. Minami, M. Okuno, K. Minemura, H. Kawai and T. Hiraishi: Case Study on Wave Disaster due to Typhoons in 2004, Technical Note of PHRI, No. 1101, p. 42, 2005
8) Takada, E., K. Morohoshi, T. Hiraishi, T. Nagai and S. Takemura: Distribution of wave, storm and tsunami design conditions on Japanese nationwide coastal structures, Technical Note of PARI No. 88, 2003
9) Goda, Y.: Revisiting Wilson's formula for simplified wind-wave prediction, J. Waterway, Port, Coastal and Ocean Eng., ASCE, Vol. 129, No. 2, pp. 93-95, 2003
10) Hirose, S. and T. Takahashi: Emergence Characteristics of Coastal Waves (Part 2), Proceedings of Coastal Eng. JSCE Vol. 30, JSCE, pp.168-172, 1983
11) Gringorten, I.I.: A plotting rule for extreme probability paper, J.Geophysical Res., Vol. 68, No. 3, pp. 813-814, 1963
12) Petruaskas, C. and P.M.Aagaard: Extrapolation of historical storm data for estimating design wave heights, Preprints 2nd OTC, No. 1190. 1970
13) Goda, Y.: Numerical Investigations on Plotting Formulas and Confidence Intervals of Return Values in Extreme statistics, Rept. of PHRI Vol. 27 No. 1, pp. 31-92, 1988
14) Goda, Y.: Wave-resistant Engineering (Wave-resistant design of port and coastal structures), Kashima Publishing, Chapter 13, pp.327-379, 2008
15) Goda, Y., O. Kohase and N. Nagai: Demonstrative study on Distribution generating function of extreme wave statistics, Proceedings of Coastal Eng. JSCE Vol. 45, JSCE, pp.211-215,1998
16) Utsunomiya, Y., M. Miyata, T. Takayama, H. Kawai, K. Hirayama, Y. Suzuki, M. Kimizuka and Y. Fukunaga: Estimation and Application of the Largest Class Storm Surge Predicted by Scenario Typhoons, Journals of JSCE Division B2 (Coastal Engineering), Vol.73 No.2, pp.I_1153-I_1158, 2017 (in Japanese)
17) NAGAI, T and H. OGAWA: Annual Report on Nationwide Ocean Wave information network for Ports and Harbors (NOWPHAS 2002), Technical Note of PARI, No. 1069, p. 336, 2004
18) Nagai, T: Long Term Statistics Report on Nationwide Ocean Wave information network for Ports and Harbors (NOWPHAS 1970-1999), Technical Note of PARI No. 1035, 2002
19) Bureau of Port and harbours: Design Manual for prestressed concrete port facilities, 1987
20) Coastal Development Institute of Technology (CDIT): Impact Evaluation Manual for long-period waves in ports, Coastal Technology Library No. 21, CDIT, pp.App.B-2-App.B-9, 2004 (in Japanese)
21) Goda, Y., "Wave forces on a vertical circular: Experiments and proposed method of wave force computation", Report of the Port and Harbour Research Institute, No. 8, p 24, 1964

22) Goda, Y. and K. Nagai: Investigation of the Statistical Properties of Sea Waves with Field and Simulation Data, Report of the Port and Harbour Research Institute, Vol.13, No.1, pp.3-37, 1974 (in Japanese)

23) JSCE: Design Handbook for Shore Protection Facilities. JSCE, pp. 31-68, 2000

24) Takayama, T., N. Ikeda and T. Hiraishi: Practical Computation Method of Directional Random Wave Transformation, Report of PHRI Vol. 30 No. 1, pp. 21-67, 1991

25) Coastal Engineering Committee, JSCE: Coastal waves, JSCE, pp. 46-50, 1994

26) Mase, H., T. Takayama, T. Kitano and S. Moriyasu: Study on the Modeling of Diffraction Effect in Phase Averaged Wave Deformation Analysis Model and its Applicability, Journals of JSCE Division B2 (Coastal Engineering), Vol.46, pp.66-70, 1999 (in Japanese)

27) HIRAYAMA, K.: Utilization of Numerical Simulation on Nonlinear Irregular Wave for Port and Harbor Design, Technical Note of PARI No. 1036, pp. 162, 2002

28) TAKAYAMA, T. and H. FUJI: Probabilistic Estimation of Stability of Slide for Caisson Type Breakwater Author Tomotsuka, Rept. of PHRI Vol. 30 No. 4, pp. 35-64, 1991

29) Hiraishi, T.: Generation and Application of Directional Random Waves in a Laboratory, Technical Note PHRI No, 723, p. 176, 1992

30) TAKAYAMA, T. and T. HIRAISHI: Amplification Mechanism of Harbor Oscillation Derived From Field Observation And Numerical Simulation, Technical Note of PHRI No. 636, P. 70, 1988

31) Coastal Development Institute of Technology (CDIT): Study and Development of Numerical wave channel (CADMAS-SURF), Coastal Development Technology Library No. 12, p 457, 2001

32) Hirayama, K and K. Minemura: Simple Estimation for Wave Shoring in an Estuary, Journals of JSCE Division B3 (Ocean Engineering), Vol.21, pp.313-318, 2005 (in Japanese)

33) JSCE: Design Handbook for Shore Protection Facilities. JSCE, pp. 9-25, 2000

34) Goda, Y.: Wave-resistant Engineering (Wave-resistant design of port and coastal structures), Kashima Publishing, Chapter 13, pp.11-18, 2008 (in Japanese)

35) ditto, p.20

36) ditto, p.21

37) Tanimoto, K., K. Kimura, A. P. dos Santos Pinto: Random Wave Forces and Design Wave Periods of Composite Breakwaters under the Action of Double Peaked Spectral Waves, Rept. Of PHRI, Vol. 25 No. 2, pp. 3-25, 1986

38) Goda, Y. and Y. Suzuki: Computation of refraction and diffraction of sea waves with Mitsuyasu's directional spectrum, Technical Note of PHRI, No. 230, p. 45, 1975

39) Hashimoto, N.: Study on Estimation Method of Directional Ocean Wave Spectrum, Technical Note of the Port and Harbour Research Institute, No.722, p.118, 1992 (in Japanese)

40) GODA, Y.: Numerical Examination of the Measuring Technique of Wave Direction with the 'Covariance Method', Rept. Of PHRI, Vol. 20, No. 3, pp.53-92, 1981

41) Sverdrup, H.U. and Munk, W.H.: Wind, sea, and swell; theory of relations for forecasting, U.S. Navy Hydrographic Of.ce, H.O.Pub. 601, pp.1-44, 1947

42) Bretschneider, C.L.: Revised wave forecasting relationships, Proc. 2nd Conf. Coastal Engg., ASCE, 1952

43) Bretschneider, C.L.: Revisions in wave forecasting, Deep and shallow water, Proc. 6th Conf. Coastal Engg., ASCE, pp. 30-67, 1958

44) Wilson, B.W.: Numerical prediction of ocean waves in the Nouth Atlantic for December, 1959, Deut, Hydrogr. Zeit, Jahrgang 18, Heft 3, pp. 114-130, 1965

45) JSCE: The Collected Formula of Hydraulics, JSCE, p. 508, 1971

46) Mitsuyasu, H.: Development of Wind Wave Spectrum (2)- wind wave spectrum form with finite fetch, Proceedings of Coastal Eng. JSCE Vol. 17, JSCE, pp.1-7, 1970 (in Japanese)

47) Wilson, B.W.: Graphical approach to the forecasting of waves in moving fetches, Tech. Memo. No. 73, Beach Erosion Board, U.S. Army Corps of Engrs., 1955

48) Ijima, T.: Numerical forecast of waves, JSCE Proceedings of Summer Training on Hydraulic Engineering A, pp. 2-1-2-30, 1968

49) Horikawa, K, H. Nishimura, Y. Ozawa and Y. Miyamoto: Wave hindcasting under typhoon in Beppu Bay, Proceedings of the 18th Conference on Coastal Eng. JSCE, pp. 7-12, 1971

50) Bretschneider, C.L.: Decay of ocean waves, Fundamentals of ocean engineering-Part 8b, Ocean Industry, pp. 45-50, 1968

51) Horikawa, K.: (New Edition) Coastal Engineering, Tokyo University Press, pp. 84-88, 1991

52) Isozaki, I. and Uji, T.: Numerical prediction of ocean wind waves, Report of Japan Meteorological Institute Vol. 24, No. 2, pp. 207-231, 1973

53) Uji, T.: A coupled discrete wave model MRI-II, J. Oceanogr. Soc. Japan, 40, pp. 303-313, 1984

54) Uji, T and Ueno K.: Wave Model MRI-II New, Japan Meteorological Institute Oceanography Division, p. 118, 1987

55) Ueno, K. and H. Takano: The third generation eave hindcasting model MRI-3 for on-site operation. Proceeding of Fall Term conference of Oceanographic Society of Japan, P. 153, 1998

56) Inoue, T.: On the growth of the spectrum of a wind generated sea according to a modified Miles-Philips mechanism and its application to wave forecasting, Dept. Meteorol. and Oceanogr., New York Univ., TR-67-5, p. 74, 1967

57) Yamaguchi, M. and Y. Tsuchiya: Numerical forecast method for waves in finite fetch, Proceedings of the 26th Coastal Engineering, JSCE, pp. 96-100, 1979

58) Joseph, P. S. Kawai, S. and Toba, Y.: Ocean wave prediction by a hybrid model-combination of single-parameterized wind waves with spectrally treated swells, Sci. Rept. Tohoku Univ., Ser. 5, Geophs., Vol. 28, No. 1, pp. 27-45, 1981

59) The WAMDI Group: The WAM model - A third generation ocean wave prediction model, J. Phys. Oceanogr., 18, pp. 1775-1810, 1988

60) Yamaguchi, M, Y. Hatada and Y. Utsunomiya: A shallow water prediction model at a single location and its applicability, Journal of the ASCE Vol. 381/II-7, pp. 151-160, 1987

61) Hasselmann, S and K. Hasselamann: Computations and parameterizations of the nonlinear energy transfer in a gravity wave spectrum, Part I, A new method for efficient computations of the exact nonlinear transfer integral, J. Phys. Oceanogr., 15, pp. 1369-1377, 1985

62) Janssen, P.A.E.M.: Wave-induced stress and the drag of air flow over sea wave, Journal of Physical Oceanography, vol. 19, pp. 745-754, 1989

63) Janssen, P.A.E.M.: Quasi-linear theory of wind wave generation applied to wave forecasting, Journal of Physical Oceanography, vol. 21, pp. 1631-1642, 1991

64) Hasselmann, K.: On the non-linear energy transfer in a gravity-wave spectrum, Part 1, General theory, J. Fluid Mech., 12, pp. 481-500, 1962

65) Booij, N., Holthuijsen, L. H. and R. C. Ris: The SWAN wave model for shallow water, Proceeding of 25th International Conference on Coastal Engineering, vol. 1, pp. 668-676, 1996.

66) Tolman, H. L., and D. V. Chalikov: Source terms in a third-generation wind wave model, J. Phys. Oceanogr., 26, pp. 2497-2518, 1996

67) Tolman, H. and the WAVEWATCH III Development Group: User manual and system documentation of WAVEWATCH III version 4. 18, 2014

68) Goda, Y: Standard wave spectrum and stochastic characteristics based on numerical simulation, Proceedings of Coastal Eng. JSCE, Vol. 34, pp. 131-135, 1987

69) JSCE: Design Handbook for Shore Protection Facilities. JSCE, pp. 33-36, 2000

70) Goda, Y.: Wave-resistant Engineering (Wave-resistant design of port and coastal structures), Kashima Publishing, pp.43-45, 2008 (in Japanese)

71) Takayama, T.: Wave Diffraction and Wave Height Distribution inside a Harbour, Technical Note of the Port and Harbour Research Institute, No.367, p.140, 1981 (in Japanese)

72) Coastal Engineering Committee, JSCE: Coastal waves, JSCE, pp. 27-37, 1994

73) Nagai, N., I Tamura and A. Toyoshima: Study on the Diffraction of Irregular Waves due to Breakwaters, Proceedings of the 30th Annual Meeting of JSCE Vol. II-12, pp.22-23, 1975 (in Japanese)

74) Goda, Y.: Wave-resistant Engineering (Wave-resistant design of port and coastal structures), Kashima Publishing, pp.49-59, 2008 (in Japanese)

75) Sato, S. and Y. Goda: Coast and Harbour, Easy-to-understand Civil Engineering Lecture, Shokokusha Publishing, pp. 72-75, 1971

76) Kubo, Y., Y. Kotake, M. Isobe and A. Watanabe: Time-dependent mild slope equation for random waves, Proceedings of Coastal Engineering JSCE No. 38, pp. 46-50, 1991

77) Hiraishi, T. I. Uehara and Y. Suzuki: Applicability of Wave Transformation Model in Boussinesq Equation, Technical Note of PHRI No. 814, p. 22, 1995

78) Nadaoka, K and Y Nakagawa: Derivation of fully-dispersive wave equations for irregular wave simulation and their fundamental characteristics, Journal of the JSCE, No. 467/II-23, pp. 83-92, 1993

79) Coastal Engineering Committee, JSCE: Coastal waves, JSCE, pp. 15-118, 1994

80) Hirayama, K.: Wave Transformation Calculation with Boussinesq Model and its Local Applicability, Text of the 43th Summer Workshop on Hydraulic Engineering, B-7, Conferences on Hydraulic Engineering and Coastal Engineering of JSCE, p.20, 2017 (in Japanese)

81) Nishimura, K., H. Kato, J. Inoue, I. Nakamura and S. Muratra: Numerical simulation and hydraulic model test on wave height distribution about an island, Proceedings of 27th Coastal Eng. JSCE, pp.65-69, 1980

82) Goda, Y.: Wave-resistant Engineering (Wave-resistant design of port and coastal structures), Kashima Publishing, p.83, 2008 (in Japanese)

83) Hirayama, K: Numerical Simulation of Nonlinear Partial Standing Waves using the Boussinesq Model with New Reflection Boundary, Rept. of PHRI Vol. 40, No. 4, pp. 3-48, 2001

84) Goda, Y., Y. Suzuki, Y. Kishira and O. Kikuchi, Estimation of incident and Reflected Waves in Random Wave Experiments, Technical Note of PHRI No. 248, p. 24, 1976

85) Sawaragi, T Edition: New Coastal Engineering for environmental sphere, Fuji Techno System, pp. 251-252, 1999

86) ditto, p.253

87) Kobune, K and M. Osato: A Study of Wave Height Distribution along a Breakwater with a Corner, Report of PHRI, Vol. 15 No. 2, 1976

88) Ito, Y. and K. Tanimoto: Meandering Damages of Composite Breakwaters, Technical Note of PHRI, No. 112, 1971

89) Goda, Y. and T. Yoshimura: Wave Force Computation for Structures of Large Diameter, Isolated in the Offshore, Report of PHRI Vol. 10, No. 4, pp. 3-52, 1971

90) Shuto, N.: Transformation of long wave- for the case of changing channel width and depth-, Proceedings of 21st Conference on Coastal Engineering JSCE, pp. 57-64, 1974

91) Goda, Y: Rearrangement of breaker indices, Journal of Civil Engineering No. 180, JSCE, pp. 39-49, 1970

92) Goda, Y.: Reanalysis of Breaking Wave Statistics for Engineering Applications, Proceedings of Coastal Eng. JSCE Vol. 54, JSCE, pp.81-85, 2007 (in Japanese)

93) Goda, Y.: Deformation of Irregular Waves due to Depth-controlled Wave Breaking, Report of the Port and Harbour Research Institute, Vol.14 No.3, 1975

94) Goda, Y.: Wave-resistant Engineering (Wave-resistant design of port and coastal structures), Kashima Publishing, p.73, 2008 (in Japanese)

95) JSCE: Design Handbook for Shore Protection Facilities. JSCE, pp. 90, 2000

96) Takayama, T., Y. Kamiyama and O. Kikuchi: Wave Transformation On a Reef, Technical Note of PHRI No. 278, pp. 32, 1977

97) Egashira, K, I. Fukuda, Y. Kishira and T. Nishimura: Field observation of transformation of waves on reefs, Proceedings of 32nd conference on Coastal Engineering, JSCE, pp. 90-94, 1985

98) Goda, Y.: Revision of 3-D Random Wave Transformation Model with Gradational Breaker Index, Journals of JSCE Division B3 (Ocean Engineering), Vol.19, pp.141-146, 2003 (in Japanese)

99) Uno, Y. and K. Hirayama: Characteristics of the Wave Breaking Model on the Production and Dissipation Process of Turbulence, Journals of JSCE Division B2 (Coastal Engineering), Vol.68 No.2, pp.I_026-I_030, 2012 (in Japanese)

100) Hirayama, K. and Y. Aida: Characteristics of Surf-beat Distribution on a Reef Estimated by Using Boussinesq Model, Journals of JSCE Division B3 (Ocean Engineering), Vol.72 No.2, pp.I_330-I_335, 2016 (in Japanese)

101) Tamada, T., H. Mase and T. Yasuda: Random Wave Runup Formulae for Seawall with Composite Cross Section, Journals of JSCE Division B2 (Coastal Engineering), Vol.B2-65 No.1, pp.936-940, 2009 (in Japanese)

102) Mase H.: Random wave runup height on gentle slope, J. Waterway, Port, Coastal and Ocean engineering, ASCE, Vol. 118, No. 5, pp. 649-664, 1989.

103) Mase, H., T.S, Hedges M. Share and S. Nagase: Study on wave overtopping rate of sloping coastal dikes considering wave up rush, Journals of JSCE Division B2 (Coastal Engineering), Vol.50, pp.636-640, 2003 (in Japanese)

104) Van der meer, J.W. and C.M.Stam: wave runup on smooth and rock slopes of coastal structures, J. Waterway, Port, Coastal and Ocean Engineering, ASCE, Vol. 118, No. 5, pp. 534-550, 1992

105) Saville, T. Jr.: Wave run-up on composite slopes, Proc.6th Conf. on Coastal Eng., pp. 691-699, 1958

106) Nakamura, A, Y. Sasaski and J. Yamada: Study on wave run-up on the composite slopes, Proceedings of 19th Conference on Coastal Eng., JSCE, pp. 309-312, 1972

107) Hosoi, M. and H. Mitsui: Wave up rush on the sea walls placed inner shore inside breaker line, Proceedings of 9th Coastal Eng., JSCE, pp. 143-148, 1962

108) Hosoi, M. and N. Shuto: Wave up rush for the case of diagonal incident wave, Proceedings of 9th Coastal Eng,. JSCE, pp. 149-152, 1962

109) Sakuraba, M., T. Sakakiyama, T. Arikawa, A. Inoue, J. Nakahira and M. Wada: An Investigation for Applicability of Wave Runup by CADMAS-SURF, Journals of JSCE Division B3 (Ocean Engineering), Vol.24, pp.867-872, 2008 (in Japanese)

110) Japan Society of Civil Engineers: Numerical Wave Flume- Deepening of Breaking Wave Calculation and Renovation of Wave Resistant Design, pp.43-53, 2012 (in Japanese)

111) Sakuraba, M, S. Hirosaki and K. Kashiyama: Numerical calculation of wave overtopping and wave run-up by CIVA/Level set method, Proceedings of Coastal Eng. No. 51, JSCE, pp. 36-40, 2004

112) Hirayama, K., K. Haruo and I Miyaszato: Evaluation of Design Wave Condition for Seawall on Coral Reef Calculated in Boussinesq-type Wave Transformation Model, Report of the Port and Airport Research Institute, Vol.48 No.3, pp.23-74, 2009 (in Japanese)

113) Hirayama, K., M. Moriuchi, M. Itsui, T. Kachi and T. Tamada: Evaluation for Distribution of Wave Overtopping Discharge along Coastal Seawall with H2D Boussinesq Model, Journals of JSCE Division B3 (Ocean Engineering), Vol.68 No.4, pp.I_780-I_785, 2012 (in Japanese)

114) Honda, T. and K. Ito: Study on Applicability of a Numerical Wave Flume for Overtopping by Irregular Waves, Journals of JSCE Division B2 (Coastal Engineering), Vol.55, pp.816-820, 2008 (in Japanese)

115) Goda, Y, Y. Kishira and Y. Kamiyama: Laboratory investigation on the overtopping rate of seawalls by irregular waves, Rept. Of PHRI Vol. 14, No. 4, pp. 3-44, 1975

116) GODA Y. and Y. KISHIRA: Experiments on irregular Wave Overtopping Characteristics of Seawalls of Low Crest Types, Technical Note of PHRI No. 242, p. 28, 1976

117) TAKAYAMA, T. T. NAGAI and K. NISHIDA: Decrease of Wave Overtopping Amount due to Seawalls of Low Crest Types, Rept. Of PHRI Vol. 21 No. 2, pp. 151-205, 1982

118) Takayama, T. T. Nagai, K. Nishida and T. Sekiguchi: Hydraulic Model Test for wave overtopping characteristics of sea walls against diagonal random incident waves, Proceeding of Coastal Eng. JSCE, Vol. 31, pp. 542-546, 1984

119) HIRAISHI, T. N. MOCHIZUKI, K. SATO, H. MARUYAMA, T. Kanazawa, 桝本達也: Effect of Wave Directionality on Overtopping at Seawall, Rept of PHRI Vol. 35 No. 1, pp. 39-64, 1996

120) Tamada, T., M. Inoue and T. Tezuka: Experimental Study on Wave Overtopping Discharge Calculation Chart of Gentle Slope Revetment and its Overtopping Wave Reduction Effects, Journals of JSCE Division B2 (Coastal Engineering), Vol.49, pp.641-645, 2002 (in Japanese)

121) Tamada, T., H. Mase and T. Yasuda: Prediction Formula of Wave Overtopping Discharge Including Wave Runup, Journals of JSCE Division B2 (Coastal Engineering), Vol.66 No.1, pp.926-930, 2010 (in Japanese)

122) Mase, H., T. Tamada, T. Yasuda and K. Kawasaki: Integrated Formula of Wave Overtopping and Runup Modeling for Seawalls, Journals of JSCE Division B2 (Coastal Engineering), Vol.72, pp.83-88, 2016 (in Japanese)

123) Mase, H., T. Tamada and T. Yasuda: Integrated Formula of Wave Overtopping and Runup Modeling for Vertical Seawalls Based on Clash Datasets, Journals of JSCE Division B2 (Coastal Engineering), Vol.71 No.2, pp.I_847-I_852, 2015 (in Japanese)

124) CLASH project: http://www.clash.ugent.be/, presented by De Rouck, J., H. Verhaeghe and J. Geeraets, Crest level assessment of coastal structures. General overview, J. Coastal Eng., Vol. 56, Issue 2, pp. 99-107, 2009

125) EurOtop: European manual for the assessment of wave overtopping, T. Pullen, N. W. H. Allsop, T. Bruce, A. Kortenhaus, H. Schuttrumpf and J. W. Van der Meer eds., HR Wallingford, Wallingford, U.K., 2007

126) Goda, Y.: Proposal of Unified Formulas for Wave Overtopping Rate of Seawalls Based on Clash Database, Journals of JSCE Division B3 (Ocean Engineering), Vol.24, pp.939-944, 2008 (in Japanese)

127) Miyajima, S. S. Ogura, Y. Ohashi, T. Morikawa and S. Okuda: Experimental Study on wave overtopping rate of sloping sea wall having parapet, Proceeding of Coastal Eng. JSCE, Vol. 51, pp. 636-640, 2004

128) GODA, Y: Estimation of the Rate of Irregular Wave Overtopping of Seawalls, Rept. Of PHRI Vol. 9, No. 4, pp. 3-41, 1970

129) Fukuda, N. T. Uno and I. Irie: Field observation of wave overtopping at sea walls (Second Report) Proceeding s of 20th Coastal Eng. JSCE, pp. 113-118, 1973

130) Allsop, N. W. H., L. Franco, G. Belloti, T. Bruce and J. Geeraerts: Hazards to people and property from wave overtopping at coastal structures, Coastlines, Structures and Breakwaters, (Proc. Int. Conf.) Inst. Civil. Engrs., Thomas Telford, pp. 153-165, 2005

131) Kimura, K., M. Hamaguchi, M. Okada and T. Shimizu: Characteristics of Wave Overtopping Splash due to Wave Dissipating Seawalls and its Effects on Roads at the Back of Seawalls, Journals of JSCE Division B2 (Coastal Engineering), Vol.50, pp.796-800, 2003 (in Japanese)

132) Nagai, S. and A. Takada: Effect of wave absorbing blocks on wave overtopping at coastal dikes, Proceeding of 11th Coastal Eng. JSCE, pp. 279-286, 1964

133) Suzuki, Y., T. Hiraishi, N. Mochizuki and T. Morikawa: Hearing Investigation on Wave Overtopping Damage to Seawalls, Journals of JSCE Division B2 (Coastal Engineering), Vol.41, pp.681-685, 1994 (in Japanese)

134) YASUDA, T and T. HIRAISHI: Highly Accurate Inundation Simulation by MARS Method on Compound Coastal Urban Area: Rept of PARI Vol. 43, No. 2, pp. 3-34, 2004

135) Yamashiro, M., A. Yoshida, H. Hashimoto, N. Kurushima and I. Irie: Conversion of the Wave Velocity in Wave-overtopping Experiment into the Wind Velocity of Real Coast, Journals of JSCE Division B3 (Ocean Engineering), Vol.20, pp.653-658, 2004 (in Japanese)

136) Goda, Y.: Wave-resistant Engineering (Wave-resistant design of port and coastal structures), Kashima Publishing, pp.91-96, 2008

137) Goda, Y. Y. Suzuki and Y. Kishira: Random wave model test and the characteristics, Proceedings of 21st Coastal Eng. JSCE, pp. 237-242, 1974

138) Hirayama, K. and J. Naganuma: Effects of Transmitted Waves through Breakwaters due to Wave Overtopping for Harbor Tranquility, Journals of JSCE Division B2 (Coastal Engineering), Vol.70 No.2, pp.I_761-I_765, 2013 (in Japanese)

139) Hirayama, K., H. Kashima, K. Hayashi and Y. Igarashi: Numerical Calculation of Observed Transmitted Waves by Using Boussinesq-type Wave Transformation Model, Journals of JSCE Division B3 (Ocean Engineering), Vol.69 No.2, pp.I_682-I_687, 2013 (in Japanese)

140) Matsumoto, A.: Numerical Analysis on Wave Transmission over Breakwaters Using VOF-type Numerical Wave Flume, Journals of JSCE Division B2 (Coastal Engineering), Vol.65 No.1, pp.781-785, 2009 (in Japanese)

141) Kondo, T. and I. Sato: A study on the crest height of breakwaters, Journal of Public Works Research Institute (PWRI), Hokkaido Regional Development Bureau (HRDB) No. 117, pp. 1-5, 1964

142) Tanimoto, K, M. Osato: An experiment on stability of breakwaters with wave-absorbing blocks against random waves, Proceedings of the 26th Coastal Eng., JSCE, pp, 309-313, 1979

143) Sakamoto, Y. Y. Miyaji T. Uenishi and H. Takeda: Experimental study on hydraulic characteristics of sloping sea walls, Journal of Public Works Research Institute, Hokkaido Regional Development Bureau Vol. 82, 1984

144) Tanaka, N.: Wave Reduction and Beach Stabilization Effects of Submerged Breakwaters with Wide Crown Widths, Proceedings of Coastal Eng. JSCE Vol. 23, JSCE, pp.152-157, 1976

145) Kondo, T. and H. Takeda: wave absorbing facilities, Motikita Publishing, pp. 70-114, 1983

146) Numata, A.: Experimental Study on Wave Dissipating Effect of Block Levees, Proceedings of Coastal Eng. JSCE Vol. 22, pp.501-505, 1975

147) MORIHIRA, M., S. KAKIZAKI and Y. GODA: EXPERIMENTAL INVESTIGATION OF A CURTAIN-WALL BREAKWATER, Rept. Of PHRI Vol. 3 No. 1, pp. 1-27, 1964

148) Sawaragi, T Edition: New Coastal Engineering for environmental sphere, Fuji Techno System, p. 258, 1999

149) Longuet-Higgins, M.S. and R.W. Stewart: Radiation stress and mass transport in gravity waves with application to surf beats, Jour. Fluid Mechanics Vol. 13, pp. 481-504, 1962

150) Goda, Y. Design diagram of wave set-up and longshore currents under directional random waves, Proceedings of Ocean Development Vol. 21, pp. 301-306, 2005

151) HIRAISHI, T, A. TADOKORO and H. FUJISAKU: Characteristics of Long Period Wave Observed in Port, Rept. Of PHRI Vol. 35 No. 3, pp. 3-36, 1996

152) Coastal Development Institute of Technology (CDIT): Impact Evaluation Manual for long-period waves in ports, Coastal Technology Library No. 21, CDIT, pp. 1-14, 2004

153) KATO, K., S. NAKAMURA and N. IKEDA: Estimation of Infragravity Waves in Consideration of Wave Groups (An Examination on Basis of Field Observation at HORF), Rept of PHRI Vol. 30 No. 1, pp. 137-163, 1991

154) Hiraishi, T., S. Kawano S. Tamaki and J. Hasegawa: Standard wave spectrum of long period wave employed in the design of port and habour facilities, Proceeding of Coastal Eng. JSCE No. 44, pp. 246-250, 1997

155) Hirayama, K., H. Kashima, J. Naganuma and Y. Uno: Harbor Tranquility Analysis for Long Period Waves Propagated from Offshore and Generated on Harbor Entrance, Journals of JSCE Division B3 (Ocean Engineering), Vol.70 No.2, pp.I_211-I_216, 2014 (in Japanese)

156) Hirayama, K. and H. Kashima: Estimation of Infragravity Wave Spectrum with Variable Parameter Related to Properties of Wind Wave, Journals of JSCE Division B2 (Coastal Engineering), Vol.70 No.2, pp.I_116-I_120, 2014 (in Japanese)

157) Coastal Development Institute of Technology (CDIT): Impact Evaluation Manual for long-period waves in ports, Coastal Technology Library No. 21, CDIT, pp. 48-52, 2004

158) ditto, p.49

159) Hiraishi, T, K. Hirayama, K. Ozawa and Y. Moriya: Wave Absorbing Capacity of Long Period Wave Countermeasures in Harbor, Technical Note of the Port and Airport Research Institute, No.1205, p.16, 2009 (in Japanese)

160) Yamada, A., H. Kunisu, T. Tamehiro, K. Kohirata and T. Hiraish: Examination of Wave Dissipating Structures to the Long Period Wave in the Ishinomaki Harbor, Journals of JSCE Division B3 (Ocean Engineering), Vol.21, pp.785-790, 2005 (in Japanese)

161) Ozawa, K, Y. Moriya, S. Yamamoto, K. Hirayama and T. Hiraishi: Harbor Tranquility Improvement Effect of Long Period Wave Countermeasure Facility in Akita Harbor, Journals of JSCE Division B3 (Ocean Engineering), Vol.25, pp.653-658, 2009 (in Japanese)

162) Matsuno, K., T. Yano, H. Kasai, T. Yamamoto, T. Hiraishi and K. Kimura: Field Observation of Long-period Wave Absorbers in Tomakomai Nishi Port, Journals of JSCE Division B2 (Coastal Engineering), Vol.67 No.2, pp.681-685, 2011 (in Japanese)

163) Hirayama, K., K. Kawauchi and I. Miyazato: Experimental Study on Wave Reflection Coefficients of Wave Dissipating Works for Oblique Incident Waves, Journals of JSCE Division B2 (Coastal Engineering), Vol.67 No.2, pp.I_686-I_690, 2011 (in Japanese)

164) Tanaka, M., A. Mtsumoto, M and Hanzawa: Experimental Study on Wave Absorbing Properties of Submerged Mound Type Long-period Wave Absorbing Structures, Journals of JSCE Division B3 (Ocean Engineering), Vol.68, pp.I_816-I_816, 2012 (in Japanese)

165) UEDA, S., S. SHIRAISHI, H. OSHIMA and K. ASANO: Allowable Wave Height and Wharf Operation Efficiency Based on the Oscillations of Ships Moored to Quay Walls, Technical Note of PHRI No. 779, p. 44, 1994

166) Hirayama, K.: Harbor Tranquility Analysis Method for Using Boussinesq-type Nonlinear Wave Transformation Model, Technical Note of the Port and Airport Research Institute, No.1159, p.90, 2007 (in Japanese)

167) Coastal Development Institute of Technology (CDIT): Impact Evaluation Manual for long-period waves in ports, Coastal Technology Library No. 21, CDIT, pp.17-18 and App.A-2-App.A-7, 2004

168) ditto, p.19

169) Japan Association of Marine Safety: Survey and Study on Fundamental Elements of Sea Transport Safety (Report 3) - Effect of Ship Waves on Small Crafts, p.83, 1976. (in Japanese)

170) Japan Shipping Exchange, Inc.: Register of Ships (2017), 2017. (in Japanese)

171) Shiotani, S.: On comparison of estimation methods of ship waves, Journal of Japan Institute of Navigation, Vol.106, pp.271-277, 2002. (in Japanese)

172) Takenouti, Y. and K. Nanasawa: About “GUNKAN-NAMI” (warship wave) which reaches on the Imabari Beach as significant breakers, Journal of the Oceanographical Society of Japan, Vol.17, No.2, pp.80-90, 1961. (in Japanese)

173) Ertekin, R. C., W. C. Webster and J. V. Wehausen: Ship-generated solitons, Proc. of the 15th Symposium on Naval Hydrodynamics, pp.347-364, 1985.

174) Coastal Development Institute of Technology: Technical Manual for Floating Structure, p.115, 1991. (in Japanese)

175) Kanda, K., N. Shiraishi and Y. Takino: About oscillation characteristics of floating type wharves, Proceedings of Civil Engineering in the Ocean, Vol.2, pp.163-168, 1986. (in Japanese)

176) Toyoda, S.: Floating oil storage system, The 4th Ocean Engineering Symposium, Society of Naval Architects of Japan, pp.25-50, 1979. (in Japanese)

177) Kogure, K., Y. Suzuki, M. Katagiri and T. Yakuwa: Design and construction of floating breakwater, Proceedings of Coastal Engineering, Vol.30, pp.435-439, 1983. (in Japanese)

178) Maruyama, T.: Construction of movable floating bridge, The 14th Ocean Engineering Symposium, Society of Naval Architects of Japan, pp.327-334, 1998. (in Japanese)

179) Public Works Bureau, Osaka City: Record of Construction of YUMEMAI Bridge, Osaka City, 2002. (in Japanese)

180) Miyamoto, T.: Floating disaster prevention basis, Cargo-handling, Vol.44, No.3, Japan Association of Cargo-handling Mechanization, 1999. (in Japanese)

181) Kozawa, T., Y. Miyachi, T. Koizumi, K. Wada and Y. Matsushita: Provision of Floating Disaster Prevention Basis, Proceedings of Techno-Ocean 2000 International Symposium, Techno-Ocean Network, pp.623-628, 2000.

182) Coastal Development Institute of Technology and Floating Structures Association of Japan: Study Report of Large Scale Floating Structure, p.638, 1995. (in Japanese)

183) Technological Research Association of Mega-Float: Fiscal Year 1997 Study Report of Very Large Floating Offshore Structure (Mega-Float), p.350, 1998. (in Japanese)

184) Floating Structures Association of Japan: Large Scale Floating Structure, Kajima Institute Publishing, p.172, 2000. (in Japanese)

185) Technological Research Association of Mega-Float: Demonstrative Study on Utilization of Mega-Float as Airport (Mega-Float Technology Study Report) -Summary of the Results of Phase II and the Results in Fiscal Year 2000-, p.228, 2001. (in Japanese)

186) Takayama, T., T. Hiraishi, M. Furukawa, K. Sao and S. Tachino: Field Observation of Motions of a SALM Buoy and Tensions of Mooring Hawsers, Technical Note of PHRI, No.542, p.38, 1985. (in Japanese)

187) Iwatani, F., S. Miyai and K. Mishina: Wave observation at Sakata Port utilizing new structural type, Proceedings of Civil Engineering in the Ocean, Vol.2, pp.97-102, 1986. (in Japanese)

188) Tsuji, T., N. Mori and Y. Yamanouchi: On the Force Acting on a Ship in Oblique Flow, Rept. of Ship Research Institute, Vol.6, No.5, pp.15-28, 1969. (in Japanese)

189) Nojiri, N. and K. Murayama: Study on drift force acting on 2-dimensional floating body in regular waves, Transactions of the West-Japan Society of Naval Architects, Vol.51, pp.131-152, 1976. (in Japanese)

190) Motora, S., T. Koyama, M. Fujino and H. Maeda: (Revised Edition) Dynamics of Ships and Offshore Structures, Seizando-Shoten Publishing, pp.220-224, 1997. (in Japanese)

191) Port and Harbour Research Institute and Ports and Harbours Bureau, Ministry of Transport: Study Report on Development of Construction Methods of Floating Structures, p.171, 1985. (in Japanese)

192) Coastal Engineering Committee, JSCE: Coastal Waves, JSCE, pp.291-429, 1994. (in Japanese)

193) Akishima Laboratories (Mitsui Zosen): Akishima Laboratories 15th Anniversary -Trace of Research and Development-, pp.105-130, 1995. (in Japanese)

194) Performance Working Group, Ocean Engineering Committee, Society of Naval Architects of Japan: Practical Guide for Hydrodynamics of Floating Body (First Part) Numerical Calculation Methods for Oscillation Problems, Seizando-Shoten Publishing, p.291, 2003. (in Japanese)

195) Itou, Y. and S. Chiba: An Approximate Theory of Floating Breakwaters, Rept. of PHRI, Vol.11, No.2, pp.15-28, 1972. (in Japanese)

196) Ocean Engineering Committee, Society of Naval Architects of Japan: Mega-Float Offshore Structure, Seizando-Shoten Publishing, p.351, 1995. (in Japanese)

197) Ueda, S. and S. Shiraishi: Method and its Evaluation for Computation of Moored Ship's Motions, Rept. of PHRI, Vol.22, No.4, pp.181-218, 1983. (in Japanese)

198) Cummins, W. E.: The impulse response function and ship motions, Schiffstechnik, Bd.9, Heft 47, pp.101-109, 1962.

199) Kubo, M. and S. Okamoto: Study on precision improvement of time series analysis of a moored floating body in front of a quaywall using retarded function, Proceedings of Coastal Engineering, Vol.34, pp.611-615, 1987. (in Japanese)

200) Suzuki, Y. and K. Moroishi: On the Slow Motions of Ships Moored to Single-Point Mooring Systems, Rept. of PHRI, Vol.21, No.2, pp.107-150, 1982. (in Japanese)

201) Ueda, S.: Analysis Method of Ship Motions Moored to Quay Walls and the Applications, Technical Note of PHRI, No.504, p.372, 1984. (in Japanese)

202) Suzuki, Y.: Study on the Design of Single Point Buoy Mooring, Technical Note of PHRI, No.829, p.48, 1996. (in Japanese)

203) Shiraishi, S., K. Nazato and H. Kawahara: A Study on the Characteristics of Motions of Pleasure Boats and Floating Piers in a Marina, Technical Note of PHRI, No.950, p.63, 1999. (in Japanese)

204) Yoneyama, H., K. Ohgaki, M. Tsuda, A. Kurihara, T. Hiraishi and T. Aono: Model Experiments and Numerical Simulation on Tsunami Impact to a Moored Ship, Technical Note of PARI, No.1213, p.27, 2010. (in Japanese)

205) Coastal Development Institute of Technology (CDIT): Impact Evaluation Manual for long-period waves in ports, Coastal Technology Library No. 21, CDIT, p. 86, 2004

206) Nagai, T: Study on Japanese Coastal Wave Characteristics Obtained from the NOWPHAS Wave Observation Network, Technical Note of PHRI No. 863, p. 113, 1997 (in Japanese)

207) Kawaguchi, K., S. Sakuraba and T. Fujiki : Annual Report on Nationwide Ocean Wave Information Network for Ports and Harbours (NOWPHAS2014), Technical Note of PHRI,No.1319, p.126, 2016 and so on (in Japanese)

208) JSCE: The Collected Formula of Hydraulics (1971 Edition), JSCE, p. 533, 1971

5 Tsunamis

[Public Notice] (Design Tsunami)

Article 9

Design tsunamis shall be appropriately defined in terms of the tsunami height and others based on historical tsunami records or numerical analyses.

[Interpretation]

7. Setting of Natural Conditions, etc.

(3) Items related to waves (Article 6 of the Ministerial Ordinance and the interpretation related to Article 8 and 9 of the Public Notice)

④ **Setting of the design tsunami**

The design tsunami and the excess design tsunami used to performance verification shall be larger than the frequent tsunami of several ten year- to one hundred and several ten year-return period and be properly set according to the importance of the facilities concerned.

(1) **Definition of Terminology Related to Tsunamis**

Most of tsunamis are a series of waves that are generated as vertical fluctuation of the sea surface by the uplift and subsidence of sea bottom due to submarine earthquakes and propagate to the coast. Other causes of the tsunamis are large landslides into or in sea, the undersea volcano eruptions, etc.

The sea bottom displacement may extend in a horizontal direction for several tens of kilometers but water depth is several kilometers at most. As the range of a crustal movement is considerably wider than the range to which surface waves propagate during crustal movement, sea surface fluctuation occurs. This sea surface fluctuation becomes the initial tsunami profile. The sea surface fluctuation due to crustal movement can be treated as the sum of vertical amount of sea bottom displacement and the vertical amount of sea bottom displacement due to horizontal movement of undulating topography of the sea bed [1]. As an initial tsunami profile has an extremely long wavelength compared to the water depth, the sea surface fluctuation propagates outward as a long wave.

Terminology of the tsunamis is as shown in **Fig. 5.1.1**.

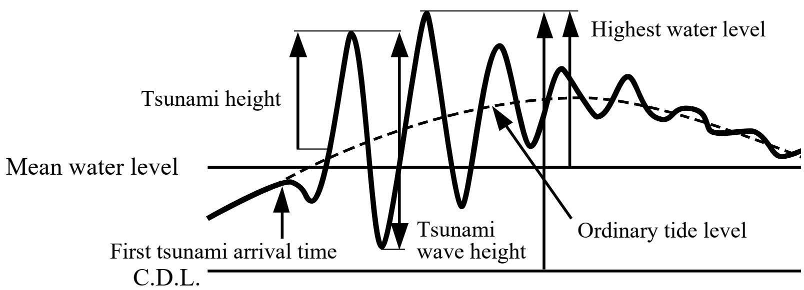

Fig. 5.1.1 Tsunami Terminology

① **Ordinary tide level**

Ordinary tide level is the level of the sea surface when there is no tsunami. It is expressed in height relative to the mean sea level (M.S.L.) in Tokyo Bay (T.P.) or the lowest astronomical tide (D.L.). It may be deviated from the astronomical tide level calculated from harmonic components of tide due to factors such as atmospheric pressure changes, winds, and changes in ocean currents.

② **Tsunami height**

The value of the difference between the actual tidal level and the ordinary tidal level is referred to as deviation. The maximum value of the deviation when the actual tidal level is higher than the estimated tidal level is referred to as the maximum deviation or the tsunami height. It is necessary to recognize that the tsunami height is different from the tsunami wave height as described later.

③ **Highest water level**

The maximum value of the tidal level that is measured during a tsunami is called the highest water level. It is indicated by the sea-surface height relative to the mean sea level (M.S.L.) in Tokyo Bay (T.P.) or the lowest astronomical tide (D.L.).

④ **Tsunami wave height and period**

Wave profiles of tsunami are irregular. In the same way as analysis of wind waves, the tsunami can be analyzed by the zero up-crossing method to define the tsunami wave height and period for an individual wave. An individual wave is defined to extend from a point where the observed sea surface water level crosses over the ordinary tide level from the negative side to the positive side, to the next such point. The difference between the highest water level and the lowest water level within the individual wave is defined as the tsunami wave height, while the time duration of the individual wave is defined as the tsunami period. Finally, the highest value within a series of tsunami wave heights is called the highest tsunami wave height.

⑤ **Initial movement**

Initial movement refers that the detaching of observed tidal level from the ordinary tidal level. When the first observed level is higher than the ordinary tidal level, such initial motion is referred to as the pushing initial motion; when it is lower than the ordinary tidal level, the initial motion is called the drawing initial motion.

⑥ **Run-up height and tsunami trace height**

Run-up height of tsunami is the maximum water level on land or facilities. It is expressed in the height relative to the mean sea level (M.S.L.) in Tokyo Bay (T.P.) or the lowest astronomical tide (D.L.). The run-up height is often determined by the trace that the tsunami leaves at that location, and the height of that trace is also called the tsunami trace height.

(2) Tsunami Period

The predominant period of a tsunami depends on factors such as the size of the source area of the tsunami and the distance from the epicenter. A tsunami may have components whose periods are the same as the natural periods of the bay or harbor and which are amplified through resonance. Therefore, it is preferable to investigate not only tsunamis caused by expected earthquakes but also tsunamis with the periods that are the same as the natural periods of bays and harbors by numerical simulation etc.

(3) Tsunami wave celerity

Tsunami wave celerity is usually well approximated by the celerity of long wave that is a function only of the water depth, as in the following formula:

$$C = \sqrt{gh} \tag{5.1.1}$$

where

C : wave celerity (m/s)

g : gravitational acceleration (m/s^2)

h : water depth (m)

For example, the tsunami wave celerity would be 198 m/s (713 km/h) in the average depth of the Pacific Ocean which is about 4,000 meters. In 1960, the tsunami that formed off the coast of Chile reached Japan about one day later. At the shore, with a depth of 20 m, the wave celerity decreases to 14 m/s (50 km/h).

If the time when a tsunami arrives at various coastal locations is known from the tide observation record or others, the tsunami wave source area can be estimated by reverse propagation calculation toward offshore from observation points.

(4) Tsunami Transformation

① **Wave shoaling, refraction, and diffraction**

In the deep sea, the common wavelength of a tsunami is several tens of kilometers or more, while the wave height is only about several meters. Therefore, tsunami is not distinguishable at the deep sea. However, in the process of propagation to the coast, the tsunami is transformed by wave shoaling and refraction in the same way as wind waves. This process provides the increase of tsunami wave height and the wave height can exceed 10 m. In addition, the affection of the local topological features along the shore, on a scale of several hundreds of meters, occasionally makes it possible for the tsunami to runup the shore several tens of meters in height. For example, the tsunami by the 1993 Hokkaido-oki earthquake (the 1993 Okushiri Tsunami) ran up 32 m high at the V-shaped cliff of Okushiri Island. [2) 3)] A 40 m wave run-up height was recorded at a V-shape valley on the Sanriku ria coast also in the 2011 Tohoku District off the Pacific Ocean Earthquake tsunamis [4)]. Also, a tsunami can be concentrated at a cape due to refraction induced by bathymetry change off the cape. Further, due to diffraction, a tsunami wave may reach the opposite side of an island or cape to the direction of approach of the tsunami. For example, the 1993 Okushiri tsunami approached Okushiri Island from the west side, but tsunami caused damages even on the east side as well as the west side of the island, and the 2004 Indian Ocean tsunami by the Sumatra-Andaman earthquake reached Sri Lankan Island from the east side but the tsunami of about 5 m high also hit the southwest shore.

② **Transformation of tsunamis in a bay**

A tsunami increases its wave height and fluid velocity if it propagates into a bay where the water depth becomes shallower and the width of the bay becomes narrower. The wave height can be calculated from Green's law, as shown in **equation (5.1.2)**:

$$\frac{H_2}{H_1} = \left(\frac{b_1}{b_2}\right)^{1/2} \left(\frac{h_1}{h_2}\right)^{1/4} \qquad \textbf{(5.1.2)}$$

where

H_1 : the tsunami wave height for a cross-section of width b_1 and water depth h_1

H_2 : the tsunami wave height for a cross-section of width b_2 and water depth h_2

Equation (5.1.2) only holds if one assumes that the ratio of the wave height to the water depth is small, the width and water depth change gradually, there is no energy loss due to sea bottom friction, and there is no reflected wave. It cannot be applied in places such as shallow water area and the inner portion of a bay where there is a strong effect of the reflected wave.

(5) Bore Type Tsunamis [5)]

The tsunami by the 1983 Nihonkai-Chubu earthquake (the 1983 Sea of Japan Earthquake) attacked along the northern shore of Akita prefecture where the shore has a mild bottom slope of about 1/200 that extends for 30 km. The tsunami was greatly deformed into a bore, accompanied by short periodic waves of about 5 to 10 seconds. On the other hand, when this same tsunami hit a shore with a relatively steep slope of about 1/50, such as the western shore of Oga peninsula, it became rather similar to standing waves. A bore type tsunami tends to have a greater run-up height than a standing-wave type tsunami, even if the heights of two tsunami are same.

(6) Edge Waves

If a tsunami approaches a coast obliquely, the wave refraction can make the tsunami reflected from a coast propagate along the coast and consequently part of energy of the tsunami can be trapped near the coast. For example, in the 2003 Tokachi-oki earthquake in the sea off Tokachi in Hokkaido, a tsunami that could be considered an edge wave was detected along the coast from Cape Erimo to Kushiro in the southeastern coast of Hokkaido, Japan. The fact that a tsunami can continue for a long time due to formation of edge waves means the increase of possibility that the tsunami can meet a high tide resulting in inundation in coastal areas. [6)]

(7) Tsunami Wave Force

Part II, Chapter 2, 6.7 Tsunami Wave Force may be referred to for the tsunami wave force.

(8) Fluid Velocity of Tsunami

For a tsunami different from a wind wave, the movement of the sea water is uniform from the sea surface to the sea bottom. The fluid velocity u may be given by **equation (5.1.3)** and it is faster in the shallower water.

$$u = \frac{C\eta}{h} = \eta\sqrt{\frac{g}{h}} \qquad \textbf{(5.1.3)}$$

where

η : sea surface deviation due to the tsunami (m)

C : wave celerity (m/s)

h : water depth (m)

g : gravitational acceleration (m/s^2)

(9) Tsunamis in Tide Records

Tide records are extremely useful as records of tsunamis. However, when using such data, it is necessary to keep in mind the following items. [2)]

① Tsunami records measured at a tide station in a harbor may indicate different characteristics of tsunami, from those outside the harbor, because they are affected by harbor facilities such as breakwaters.

② A tsunami with a relatively short period will be measured to be smaller than the tsunami around tide station because of an energy loss due to the tsunami water flows through the tide station's inlet pipe. **Table 5.1.1** shows the tidal levels of the Middle Japan Sea Earthquake tsunami recorded in each harbor, the flood trace height obtained near tide observatories, or the estimated height from the visual observation. Comparing these levels shows that the tide records are somewhat lower than the flood trace height and others.

(10) Impact of Crustal Movement on Water Level Records of Tsunamis

In addition to the tidal observation records, water level records of tsunamis obtained from the ocean bottom pressure gauge, GPS wave buoy, and other instruments are very efficient as tsunami records.

However, when the vertical displacement of observation benchmarks, due to crustal movement, cannot be ignored, data should be handled carefully. **Part II, Chapter 5, 2 Crustal Movement due to Earthquake** may be referred to for this. The water level data in this case records superimposed changes in the water level, due to the tsunami itself, and in the observation benchmark accompanied by vertical displacement of the crust. To extract the change in the water level due to tsunamis, the impact of crustal movement needs to be deducted. The vertical displacement of the observation benchmark accompanied by crustal movement can be calculated from the difference in the mean value of tide levels before and after the earthquake [7)].

Table 5.1.1 Ratio of Tide Observation Records to the Flood Trace Heights (Based on Level) [5)]

	A Level recorded in tide observation records (m)	*B* Level recorded in trace or visual observation (m)	*A*/*B*
Ishikari Bay Shinko	0.56	0.63	0.89
Iwanai Port	1.25	1.3	0.96
Esashi Port	0.75	1.1	0.68
Fukaura Port	0.61	3.2	0.19
Noshiro Port *	1.94	2.8	0.69
Funagawa Port	0.32	0.7	0.46
Sakata Port	0.81	1.3	0.62
Iwafune Port *	0.73	0.7	1.04
Niigata Higashi Port	0.78	1.0	0.78
Niigata Nishi Port	0.50	1.0	0.50
Ryotsu Port	1.17	1.5	0.78

	A Level recorded in tide observation records (m)	*B* Level recorded in trace or visual observation (m)	*A/B*
Teradomari Port	0.59	0.6	0.98
Kashiwazaki Port	1.01	1.0	1.01
Naoetsu Port	0.72	0.7	1.03

* The first wave reached the highest water level.

(11) Model Experiments of Tsunamis

In model experiments, a water area including a harbor or the sea bottom topography around a structure is reproduced. And then, around that, by reproducing tsunami waveforms determined by numerical simulations, it is possible to investigate the stability and protective effect of tsunami breakwaters[8)] and the effect of topological alterations such as reclamations on tsunamis. The scouring of a breakwater entrance mound by the 1993 Okushiri tsunami has been investigated in the model experiments. [9)]

(12) Numerical Simulations of Tsunamis

① Numerical simulations of tsunamis must use appropriate numerical models which are based on fundamental equations that can reproduce the subject tsunamis. The following two types of theories are mainly used for regional tsunamis that occur near the coast:

(a) Non-dispersive theories [10)]: There are the linear long wave theories that apply to waves whose wavelengths are long compared to the water depth, and also the ratio of wave height to water depth is small, and nonlinear long wave theories that apply to long waves when the ratio of wave height to water depth is not small. According to Shuto[11)], the linear long wave theory may be applied in the water 200 meters or deeper.

(b) Dispersive theories: Dispersion of tsunami, such as observed near the coast for the tsunami by the 1983 Nihonkai-Chubu earthquake, can be reproduced with a nonlinear dispersed-wave theory[12) 13)]. This theory includes factors that take wave dispersion into account (dispersion terms) to a nonlinear long wave theory.

For a distant tsunami (teletsunami) that originates from a faraway source, it is possible to use linear dispersive wave theories, which add dispersion terms to the linear long wave theory. Since a tsunami in general is a series of waves whose components have various periods and a wave component with longer period has slightly faster wave celerity in deep water, wave components with shorter periods delay and the waves disperse while traveling long distance like the Pacific Ocean. Further, accurate calculation of a distant tsunami generally needs to consider the Coriolis force and to use the spherical coordinates.

② In numerical simulations of tsunami, a tsunami incident waveform shall be provided at the boundary of the calculation region[14)]. Otherwise, displacement of the sea bottom shall be calculated by an earthquake fault model [15)] and then the sea level displacement at the initial stage of the tsunami is calculated to provide the initial spatial waveform of the tsunami. In calculating the displacement from an earthquake fault model, the elastic theory solution of Mansinha and Smylie[16)] and Okada[17)] may be used. The sea surface movement due to the crustal movement can be treated as the sum of vertical amount of sea bottom movement and the vertical movement generated by horizontal displacement of uneven bottom. [1)]. Moreover, there are some cases where spatiotemporally uneven fault slip distribution is given considering the asperity in the fault or a large slip near the trench axis confirmed at the 2011 off the Pacific coast of Tohoku Earthquake[1)].

③ In order to calculate the tsunami runup on the land, the method of Iwasaki and Mano, [18)] or improvements on it[19)] can be used. If the tsunami overflows structures such as breakwaters or seawalls, it is possible to use the Honma formula[20) 21)] to calculate the amount of overflow for a unit width. In order to evaluate tsunami reduction effect of breakwaters and other structures, momentum loss at the opening section should be considered. The momentum loss, which is proportional to the mean flow velocity calculated by the long wave theory models, includes the sea bottom friction that can be evaluated by Manning's roughness coefficients and others, and the momentum loss due to abrupt narrowing and widening of the cross-section as seen in the opening section of breakwater. Comparing model experiments[22)] with numerical simulations for the breakwaters at the entrance to Kamaishi Bay provided a value of 0.5 for the coefficient of the momentum loss due to the breakwaters.[10)] Recently it has also become possible to calculate the flows near submerged breakwaters in the opening section of tsunami breakwater as well as the tsunami wave force that acts on the submerged breakwaters[23) 24) 25)] by using non-hydrostatic and three-dimensional numerical models.

(13) "Design Tsunami" and "Excess Design Tsunami"

When constructing tsunami countermeasures, two levels of tsunamis shall be considered; one is the "design tsunami," the other is the "excess design tsunami," used to performance verification. They are set between high-frequency tsunamis and maximum-class tsunamis according to the importance of the facilities concerned[26) 27)].

The high-frequency tsunamis shall be set by properly considering the highest past tsunami in the target region, tsunamis of the scale deemed appropriate in terms of disaster prevention among recent tsunamis, of which relatively large amounts data are available, and tsunamis based on the scenario earthquake in the seismic gap. “A setting method of the water level of design tsunami[28)],” can be referred to. In the method, high-frequency tsunami with some specific return period (e.g. once in several ten years to one hundred and some ten years) can be set in consideration of the record of past tsunamis, revealed by flood trace heights, and investigating historical documents, such as historical records and literature, and data based on the simulation conducted as needed.

In order to set the maximum-class tsunamis a scientific comprehensive survey on past tsunamis and earthquakes is required. It shall be composed of the analysis of historical materials, sedimentary records, coastal topography, etc. The result of physical survey shall be summarized from the viewpoint of disaster prevention and the maximum-class tsunami is set in consideration of all possibilities[29)]. The tsunami fault model published by the Central Disaster Prevention Council may be referenced.

These tsunamis shall be properly set in consideration of the regional disaster prevention plan under the careful coordination among persons concerned.

(14) Determination of Tsunami for the Performance Verification of Facilities

Two grade tsunamis, "design tsunami" and "excess design tsunami" is considered in the design of port facilities. "Design tsunamis" is utilized to verify the facilities' stability and "Excess design tsunami" is considered in the design process of contingency-prepared facilities (e.g. breakwaters, seawalls, water gates, locks, revetments, dikes, parapets, and waste disposal sites) in order to maximize the stability and resilience of facilities, to minimize the damage of disaster and to maintain the calmness of the harbor for promotion of early recovery and reconstruction.

It seems that high-frequency tsunamis are generally set to the "design tsunami." When protecting significantly important facilities, like electric power stations and others, or regions where people, property, industry, and others are present in large numbers, it is necessary to set the tsunami magnitude properly even in consideration of maximum-class tsunami, according to the importance of facilities concerned.

A proper magnitude of tsunami needs to be set to the "excess design tsunami" in the range up to the maximum-class tsunami, from the view point of the cost and benefit of additional structural treatment to stabilize the facilities and the importance of facilities concerned[27)].

Moreover, it is important to consider the effects of settlement, deformation, remaining bearing force and others of facilities due to earthquake ground motion and crustal movement in performance verification by tsunami actions, as the facilities are often influenced by the earthquake before the attack of tsunamis.

[References]

1) Nankai trough giant earthquake research committee of the central disaster management council: Seismic intensity distribution and tsunami heights of Nankai trough mega earthquake (first report), p. 44, 2012.3.31

2) Takayama, T., Y. Suzuki, H. Tsuruya, S. Takahashi, C. Gotoh, T. Nagai, N. Hashimoto, T. Nagao, T. Hosoyamada, K. Shimosako, K. Endo and T. Asai: Field investigations of the tsunami caused by 1993 HokkaidoNnansei-oki Earthquake, Technical Note of PHRI No. 775, p. 225, 1994

3) Shuto, N. H. Tomimatsu and M. Ubana: Characteristics of Off-Hokkaido Southwest Earthquake and outstanding issues towards future, Proceedings of Coastal Eng. JSCE Vol. 41, pp. 236-240, 1994

4) The 2011 Tohoku Earthquake Tsunami Joint Survey (TTJS) Group: Field survey report, URL: http://www.coastal.jp/ttjt/, 2012

5) Tanimoto, K., T. Takayama, K. Murakami, S. Murata, H. Tsuruya, S. Takahashi, M. Morikawa, Y. Yoshimoto, S. Nakano and T. Hiraishi: Field and laboratory investigations of the tsunami caused by 1983, Nihonkai Chubu Earthquake, Technical Note of PHRI No. 470, pp. 299, 1983

6) Tomita, T., H. Kawai and T. Kakinuma: Tsunami disasters and tsunami characteristics due to the Tokachi-oki Earthquake in 2003, Technical Note of PHRI No. 1082, pp. 30, 2004

7) Kawai, H., M. Satoh, K. Kawaguchi, K. Seki: Characteristics of the 2011 off the Pacific Coast of Tohoku Earthquake Tsunami, Report of PARI, Vol. 50, No. 4, pp. 3-63, 2011

8) Takayama, T. and T. Hiraishi: Hydraulic model tests on tsunamis at Suzaki-port, Technical Note of PHRI, No. 549, pp. 131, 1986

9) Tsuruya, K. and Y. Nakagawa: Model experiment for reproduction of disaster at Okushiri-higashi breakwater by Hokkaido-Nansei-oki Earthquake Tsunami, Technical Note of PHRI, No. 789, pp. 20, 1994

10) Goto, C. and K. Sato: Development of tsunami numerical simulation system for Sanriku coast in Japan, Rept of PHRI, Vol. 32, No. 2, pp. 3-44, 1993

11) Shuto, N: Tsunami and countermeasures, Jour. of the JSCE, No. 369/II-5, pp. 1-11, 1986

12) Iwase, H, T. Mikami and C. Goto: Practical tsunami numerical simulation model by use of non-linear dispersive wave theory, Jour. Of JSCE, Vol. 600/11-44, pp. 119-124, 1998

13) Iwase, H. K. Fujima. T. Mikami, H. Shibaki and C. Goto: Calculation of Central Japan Sea Earthquake Tsunami run-up considering wave number dispersion effect., Proceedings of Coastal Eng. JSCE Vol. 49, pp. 266-270, 2002

14) Arikawa, T., M. Sato, K. Shimosako, T. Tomita, D. Tatsumi, G. Yeom and K. Takahashi: Investigation of the failure mechanism of Kamaishi breakwaers due to tsunami – initial report focusing on hydraulic characteristics –, Technical Note of PARI, No. 1251, p. 53, 2012

15) Sato, R., K. Abe, Y. Okada, K. Shimazaki and Y. Suzuki: Parameter handbook of seismic faults in Japan, Kajima Institute Publishing, pp. 10-27, 1989

16) Mansinha, L. and D. E. Smylie: The displacement fields of inclined faults, Bulletin of the Seismological Society of America, Vol. 61, No. 5, pp. 1433-1440, 1971

17) Okada Y.: Internal deformation due to shear and tensile faults in a half-space, Bulletin of the Seismological Society of America, Vol. 82, No. 2, pp. 1018-1040, 1992

18) Iwasaki, T. and A. Mano: Numerical calculation of 2-dimensional tsunami run-up in Euler coordinates, Proceedings of 26th Conference on Coastal Eng. JSCE, pp. 70-74, 1979

19) Kotani, Y., F. Imamura and N, Shuto: Calculation of Tsunami Run-up and damage estimation utilizing GIS, Proceedings of Coastal Eng. JSCE Vol. 45, pp. 356-360, 1998

20) Honma, M. and K. Akishiro: Mononobe Hydraulics, Iwanami Publishing, pp. 232-237, 1962

21) JSCE: The Collected Formula of Hydraulics (1999 Edition), Maruzen Publishing, p. 713, 1999

22) Tanimoto, K., K Kimura and K. Miyazaki: Study on stability of submerged dike at the opening section of tsunami protection breakwaters, Rept of PHRI, Vol. 27, No. 4, pp. 93-122, 1988

23) Masamura, K., K. Fujima, C. Goto, K. Iida and T. Shigemura: Numerical analysis of tsunami by using 2D/3D hybrid model, Jour. of JSCE, No. 670/II-54, pp. 49-61, 2001

24) Tomita, T., T. Kakinuma and A. Shimada: Numerical calculation of effect of Tsunami breakwater utilizing 3-dimensional wave model, Proceedings of Coastal Eng. JSCE Vol. 51, pp. 296-300, 2004

25) Tomita, T., K. Honda and Y. Chida: Numerical simulation on tsunami inundation and debris damage STOC Model, Report of PARI Vol. 55, No. 2 pp. 3-33, 2016

26) Transportation Policy Council Harbor Disaster Prevention Subcommittee: The way of earthquake and tsunami countermeasures in harbors - to maintain the lifeline of island country Japan, p. 20, 2012.6.13

27) MLIT Ports and Harbours Bureau: Guideline for Tsunami-Resistant Design of Breakwaters, p. 37, 2015

28) MAFF and MLIT: About setting method of water level of design tsunami, 2011.7.8

29) Central Disaster Management Council: Report of the committee for technical investigation on countermeasures for earthquakes and tsunamis based on the lessons learned from the “2011 off the Pacific coast of Tohoku Earthquake, 2011.9.28

6 Wave Force

6.1 General

6.1.1 Wave Forces due to Waves and Tsunamis and Wave Forces at Storm Surges

Wave forces are classified roughly as due to waves, tsunamis, or storm surges. As shown in **Figs. 6.1.1**, **6.2**, **6.3**, **6.4**, and **6.5** deal with wave forces due to waves, **6.6** deals with wave forces due to tsunamis, and **6.7** deals with wave forces due to storm surges.

6.1.2 Classification of Wave Forces by Structure Type

Wave forces can be generally classified by the type of structure. Wave forces acting on upright walls are described in **6.2**, wave forces acting on submerged members in **6.3**, wave forces acting on structures near the water surface in **6.4**, and wave forces acting on armor stones or concrete blocks in **6.5**.

The wave forces are different for each type of structure. It is thus necessary to use an appropriate calculation method in accordance with the conditions including structural type. Wave forces and resistance forces acting on armor stones and concrete blocks in **6.5** differ greatly depending on their shapes and positions in addition to conditions of the waves acting on them. Therefore, when verifying performance, the required mass for the armor stones and concrete blocks are usually determined directly from wave conditions rather than calculating the acting wave force.

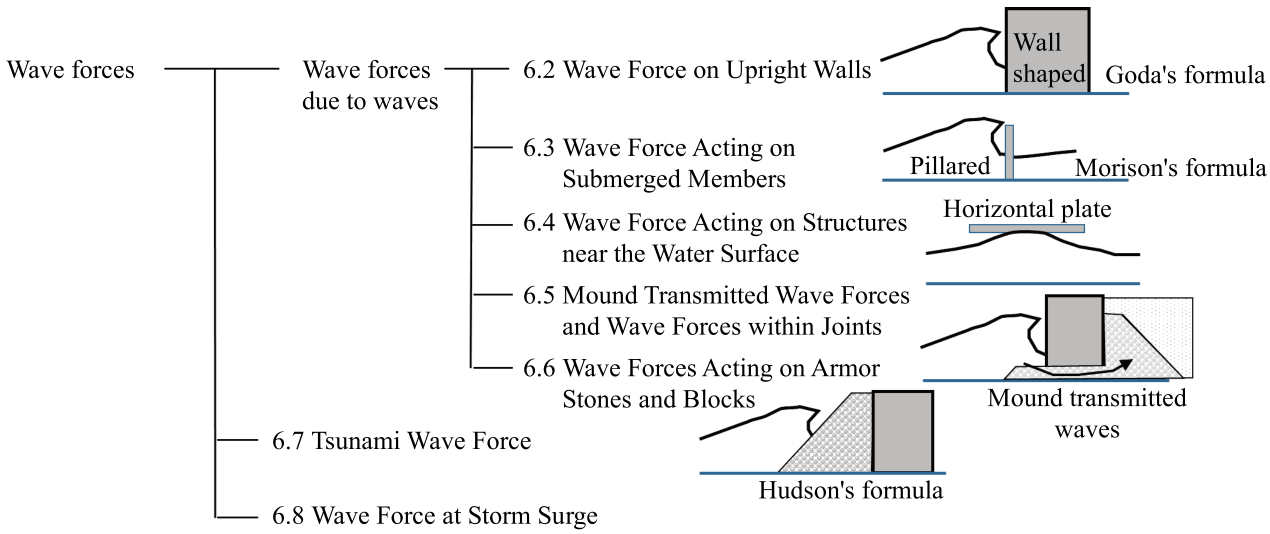

Fig. 6.1.1 Classification of Wave Forces

6.1.3 Examination of Wave Force by Hydraulic Model Tests

In the case of structures in which there is a lack of construction experience, wave actions have not been sufficiently resolved, and therefore it is preferable to carry out studies including hydraulic model tests for such structures. When examining wave force by hydraulic model tests, it is necessary to give sufficient consideration to the failure process of the structure and to use an appropriate measurement method. It is also preferable to give sufficient consideration to the irregularity of waves in the field concerned. In particular, when carrying out experiments using regular waves, an examination against the highest wave should be included in principle.

6.1.4 Examination of Wave Force by Numerical Calculation

A great deal of labor and expense is required for examining the wave force with hydraulic model tests, and usually there are limits to the experimental cases and the measurement items. On the other hand, in recent years it has become possible to employ numerical calculations. If the accuracy of the calculation models is verified by the comparison with on-site observations and hydraulic model tests at the employment of the numerical calculation in actual design, the computation of wave force can save labor and expense more than the hydraulic model test. The CADMAS-SURF [1] is a numerical computation program developed for the purpose of assisting the structurally resistive design against wave action and with the program it is possible to examine the interactions among waves, ground and structures and the impulsive breaking wave pressure. In addition, numerical models, such as OpenFOAM [2] or the particle method, [3] can be used. However, it is essential to verify the calculated results in spite of the calculation methods with the hydraulic model experimental data, and others, when applying to complicated phenomena such as impulsive breaking wave pressure.

6.2 Wave Force on Upright Walls

6.2.1 General Characteristics of Wave Force on Upright Walls[4) 5) 6) 7)]

(1) Parameters affecting wave force on upright walls

The major parameters that affect the wave force acting on an upright wall are wave period, wave height, wave direction, tidal level, water depth, bottom slope, water depth of the crown of the foundation mound, the front berm width of foundation mound, slope of foundation mound, the crown height of upright wall, and water depth at base of the upright wall. In addition, it is also necessary to consider the effect of the wall alignment. The wave force on an upright wall with a concaved alignment may be larger than that on an upright, straight wall of infinite length. Furthermore, if the front of upright wall is covered with wave-dissipating concrete blocks, the characteristics of these blocks and the crown height and width will affect the wave force.

(2) Types of wave force

The wave force acting on an upright wall can be classified according to the type of waves such as a standing wave force, a breaking wave force, or a wave force after breaking. It is considered that the changes of wave forces are continuous. A standing wave force is produced by waves whose height is small compared with the water depth, and the change in the wave pressure over time is gradual. As the wave height increases, the wave force also increases. In general, the largest wave force is generated by the waves breaking just a little off the upright wall. Accordingly, with the exception of very shallow water conditions, the force exerted by waves breaking just in front of an upright wall is larger than the wave force by higher waves that have already broken offshore. It is necessary to note that especially when breaking waves act on an upright wall on a steep seabed, or on an upright wall set on a high mound even on a mild slope, a very strong impulsive breaking wave force may appear.

(3) Wave Irregularity and Wave Force

Sea waves are irregular with the wave height and period. Depending on the water depth where facilities are to be installed and the topography of the sea bottom, wave forces such as non-breaking, breaking or after breaking act on the structure. When calculating the wave force, it is important to include the waves that cause the severest effect on the structure. It is necessary to give sufficient consideration to wave irregularity and to the characteristics of the wave force in accordance with the type of structure.

In general, it may be assumed that the larger the wave height, the greater the wave force becomes. It is thus acceptable to focus on the wave force of the highest wave among a train of random waves attacking the structure. However, with regard to the stabilities of concrete blocks or armor stones on the slope and wave force acting on the floating structures and cylindrical structures with small rigidity, it is preferable to consider the effect of the successive action of the random waves.

6.2.2 Wave Forces of Standing Waves or Breaking Waves when the Peak of Waves is on the Wall Surface

(1) Goda's formula (General)

The maximum horizontal wave force acting on an upright wall and the simultaneous uplift is generally calculated using Goda's formula as shown below. Goda's formula[8)] takes into consideration results of wave pressure experiments and application of the formula to the existing breakwaters and has been modified to include the effects of wave direction[9)]. Its single-equation formula enables one to calculate the wave force from the standing to breaking wave conditions without making any abrupt transition. However, where the upright wall is located on a steep seabed, or built on a high mound, and is subjected to a strong impulsive wave pressure due to breaking waves, the formula may underestimate the wave force. It should therefore be applied preferably with consideration of the possibility of occurrence of impulsive wave pressure due to breaking waves (see **Part II, Chapter 2, 6.2.4 Impulsive Breaking Wave Force**). The wave pressure given by Goda's formulas takes the hydrostatic pressure at the still water condition as the reference value. Any hydrostatic pressure before wave action should be considered separately. Further, the formula aims to examine the stability of the whole body of an upright wall. When breaking wave actions exist, the formula does not necessarily express the local maximum wave pressure at the respective positions; thus, such should be considered during examination of the stress of structural members.

(2) Wave pressure on the front face according to the Goda's formulas

The wave pressure on the front face of an upright wall in the Goda's formula is a linear distribution. Wave pressure is 0 at the height expressed as η^* in **equation (6.2.1)**, maximum value expressed as p_1 in **equation (6.2.2)** at still water level, and expressed as p_2 in **equation (6.2.3)** at the sea bottom. The formula considers wave pressure from the bottom to the crown of the upright wall (see **Figs. 6.2.1** and **6.2.2**).

$$\eta^* = 0.75(1+\cos\beta)\lambda_1 H_D \tag{6.2.1}$$

$$p_1 = 0.5(1+\cos\beta)\left(\alpha_1\lambda_1 + \alpha_2\lambda_2\cos^2\beta\right)\rho_0 g H_D \tag{6.2.2}$$

$$p_2 = \frac{P_1}{\cosh(2\pi h/L)} \tag{6.2.3}$$

$$p_3 = \alpha_3 p_1 \tag{6.2.4}$$

In this equation, η^*, p_1, p_2, p_3, $\rho_0 g$, β, λ_1, λ_2, h, L, H_D, α_1, α_2, and α_3 respectively represent the following values:

η^* : height above still water level at which intensity of wave pressure is 0 (m)

p_1 : intensity of wave pressure at still water level (kN/m^2)

p_2 : intensity of wave pressure at sea bottom (kN/m^2)

p_3 : intensity of wave pressure at toe of the upright wall (kN/m^2)

ρ_{0g} : unit weight of water (kN/m^3)

β : angle between the most dangerous direction within the range of ±15° from the main wave direction and the line perpendicular to the faceline of the upright wall (°)

λ_1, λ_2 : wave pressure correction coefficient (1.0 is the standard value)

h : water depth in front of the upright wall (m)

L : wavelength at water depth h used in calculation as specified in the item (4) below (m)

H_D : wave height used in calculation as specified in the item (4) below (m)

α_1 : value expressed by the following equation

$$\alpha_1 = 0.6 + \frac{1}{2}\left\{\frac{4\pi h/L}{\sinh(4\pi h/L)}\right\}^2 \tag{6.2.5}$$

α_2 : value expressed by the following equation

$$\alpha_2 = \min\left\{\frac{h_b - d}{3h_b}\left(\frac{H_D}{d}\right)^2, \frac{2d}{H_D}\right\} \tag{6.2.6}$$

α_3 : value expressed by the following equation

$$\alpha_3 = 1 - \frac{h'}{h}\left\{1 - \frac{1}{\cosh(2\pi h/L)}\right\} \tag{6.2.7}$$

In this equation, h_b, d, and h' respectively represent the following values:

h_b : water depth at an offshore distance of 5 times the significant wave height from the front face the upright wall (m)

d : water depth at the crest of either the foot protection works or the mound armoring units of whichever is higher (m)

h' : water depth at toe of the upright wall (m)

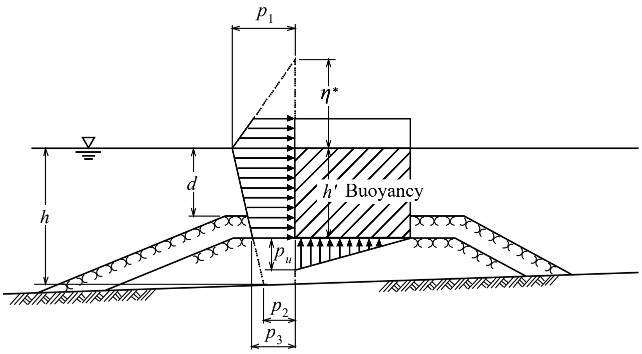

Fig. 6.2.1 Wave Pressure Distribution Used in Design Calculation

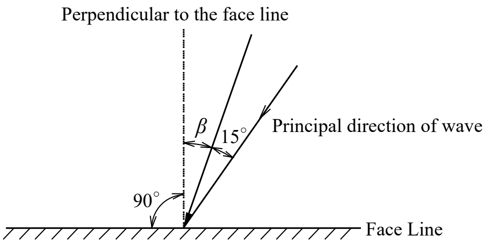

Fig. 6.2.2 Way of Obtaining Incident Wave Angle β

(3) Uplift on the bottom of upright wall

In Goda's formulas, the uplift acting on the bottom of an upright wall is described by a triangular distribution, with the pressure intensity at the front toe p_u given by the following equation and 0 at the rear toe.

$$p_u = 0.5(1+\cos\beta)\alpha_1\alpha_3\lambda_3\rho_0 g H_D \tag{6.2.8}$$

In this equation, p_u and λ_3 respectively represent the following values:

p_u : uplift pressure acting on the bottom of the upright wall (kN/m^2)

λ_3 : uplift pressure correction coefficient (1.0 is the standard value)

(4) Wave height and wavelength used in the wave pressure calculation

In Goda's formulas, the wave height H_D and the wavelength L are the height and wavelength of the highest wave. The wavelength of the highest wave is that corresponding to the significant wave period, while the height of the highest wave is as follows:

① **When the highest wave does not have effect of wave breaking:**

$$H_D = H_{\max} = 1.8H_{1/3} \tag{6.2.9}$$

In this equation, $H_{\max}$ and $H_{1/3}$ respectively represent the following values:

$H_{\max}$: highest wave height of incident waves as a progressive wave at the water depth of the upright wall (m)

$H_{1/3}$: significant wave height of incident waves as a progressive wave at the water depth of the upright wall (m)

② **When the highest wave has effect of wave breaking:**

H_D : maximum wave height considering transformation due to the breaking of random waves (m)

(5) Highest wave

Since Goda's formulas represents the wave force on an individual wave, in the breakwater performance verifications in general, it is necessary to use the wave parameters of the severest wave force from a wave group. The highest wave shall be subject to consideration. The occurrence of the highest wave in a random wave group is probabilistic, and so it is not possible to determine the parameters of the wave explicitly. Nevertheless, after examination of the results of applying the current method to breakwaters in the field, it is standard to use 1.8 times the significant wave height as the height of the highest wave where no transformation of breaking wave is observed. It has also become standard to use the wavelength corresponding to the significant wave period as the wavelength of the highest wave.

In order to determine whether or not the highest wave is subject to wave breaking, the diagrams for determining the highest wave height (**Figs. 4.4.15 (a)–(e)** in **Part II, Chapter 2, 4.4.6 Wave Breaking**) should be used by referring to the location of the peak wave height in the zone in the onshore side of the 2% attenuation line. It is acceptable to consider that the highest wave is not subject to wave breaking when the water is deeper than that at the peak height, but that it is subject to wave breaking when the water is shallower than this. If the highest wave height is to be obtained using the approximate **equation (4.4.11)** in **Part II, Chapter 2, 4.4.6 Wave Breaking** h_b should be substituted as h in the first term in the braces { } on the right-hand side of the equation.

If using a value other than 1.8 as the coefficient on the right-hand side of **equation (6.2.9)**, it is necessary to conduct sufficient examinations into the occurrence of the highest wave and then choose an appropriate value (see **Part II, Chapter 2, 4.2 Handling of Waves Used for Design**).

(6) Wave pressure correction coefficient λ_1, λ_2, λ_3

Equations (6.2.1) to **(6.2.8)** are the generalized version of Goda's formulas. They contain three correction coefficients so that they can be applied to walls of different conditions. For an upright wall, the correction coefficients are of course 1.0. The wave pressure acting on other types of wall such as a caisson covered with wave-dissipating concrete blocks or an upright wave-dissipating caisson may be expressed using the generalized Goda's formulas with appropriate correction coefficients (see **Part II, Chapter 2, 6.2.5 Wave Force Acting on Upright Wall covered with Wave-dissipating Concrete Blocks** and **Part II, Chapter 2, 6.2.7 Wave Force Acting on Upright Wave-absorbing Caisson**).

(7) Features and application limits of the Goda's formulas

The first feature of Goda's formulas is that the wave force from standing waves to breaking waves can be calculated continuously, including the effect of surrounding conditions. The parameter α_1 given by **equation (6.2.5)** expresses the effect of the period (strictly speaking h/L); it takes the limiting values of 1.1 for shallow water waves and 0.6 for deepwater waves. The effect of period also appears when determining the maximum wave height to be used in the calculation; for a constant deepwater wave height, the longer the period, the larger the maximum wave height in a shallow sea. Goda's formulas incorporate the effect of period on the wave pressure as well as on the maximum wave height.

Another feature of Goda's formulas is that the change in the wave force with the foundation mound height and the bottom slope is considered by means of the parameter α_2. As can be seen from **equation (6.2.6)**, as the foundation mound height is gradually increased from zero (i.e., $d = h$) with constant H_D, α_2 gradually increases from zero to its maximum value. After reaching its limit value, α_2 then decreases until it reaches zero again when $d = 0$. The limit value of α_2 is 1.1; combining this with the limit value of α_1 of 1.1, the intensity of the wave pressure p_1 at the still water level is given $2.2\rho_0 g H_D$.

With regard to the effect of the bottom slope, h_b within the equation for α_2 is taken as the water depth at the distance of 5 times the design significant wave height from the upright wall. Because of this artifice, a steep bottom slope results in the same effect as having a high foundation mound. The highest wave height at $5H_{1/3}$ apart was used to calculate regions affected by wave breaking because it was considered that the waves that break slightly offshore, as progressive waves exert the largest wave force on upright walls. The effect of the bottom slope also appears when determining the maximum wave height to be used in the calculation. In the wave breaking zone, the steeper the bottom slope, the larger the wave height, because the wave height used in the calculation is the maximum wave height at a distance $5H_{1/3}$ offshore from the upright wall. The bottom slope thus has a strong influence on the wave force.

As explained above, Goda's formulas consider the effects of the foundation mound height and the bottom slope on the wave pressure. Nevertheless, for an upright wall on a high mound or a steep seabed, a large impulsive breaking wave force may act, and under such conditions Goda's formulas may underestimate the wave force. When applying the Goda's formulas, it is thus preferable to pay attention to the risk of an impulsive breaking wave force arising. In particular, with a high mound, it is necessary to consider not only α_2 in **equation (6.2.6)** but also the impulsive breaking wave force coefficient α_I by Takahashi et al. [10] (see **Part II, Chapter 2, 6.2.4 (6) Impulsive breaking wave forces acting on composite breakwater**), and to use α_I in place of α_2 when α_I is the larger of the two.

One more problem with Goda's formulas concerns its applicability to extremely shallow waters, for example near to the shoreline. The applicable range of Goda's formula is rigidly where the waves that break slightly offshore on the side of the upright walls exert the maximum wave force. It is difficult, however, to clearly define where the limit of applicability lies. For cases such as the wave force acting on an upright wall near the shoreline, it is advisable to use other calculation equations together with the Goda formula. (See **Part II, Chapter 2, 6.2.11 Wave Force Acting on Upright Wall Located Considerably Toward the Landside from the Breaker Line**.)

(8) Effect of wave direction in Goda's formula

Although a number of experiments have been carried out for the effect of wave direction on the wave force, there are still many points unclear. Traditionally, for standing waves, no correction has been made for wave direction to the wave force. The effects of wave direction have been considered only for breaking waves, by multiplying the wave force by $\cos^2\beta$. However, it is irrational that the breaking wave force is assumed to decrease as the wave angle increases, reaching zero at the limiting value β = 90°, and on the other hand the standing waves are assumed to remain at the perfect standing wave condition. In other words, when the incident wave angle is large (i.e., oblique wave incidence), it takes a considerably large distance from the tip of breakwater until the wave height becomes twice the incident height. At the limiting value of β = 90°, it becomes an infinite distance. In this case, because actual breakwaters are finite in extension, it is appropriate to consider that the wave pressure of progressive waves acts on the upright wall. Furthermore, even in cases where the breakwater can be taken to extend infinitely, when using second-order approximation finite amplitude wave theory, the wave pressure from oblique incident waves decreases slightly in comparison to incidence at right angles and its degree becomes proportionate to the wave steepness. Considering these points and application to the breakwaters in the field, **equation (6.2.2)** for wave direction has been corrected by multiplying α_2 which represents mound effects with $\cos^2\beta$, and then multiplying the whole term by $0.5(1 + \cos\beta)$.

(9) Application of other theory and formulas

Goda's formula enables continuous determination of wave forces with considerable precision from standing waves to breaking waves without categorizing them by their application limits. But when the ratio of the wave height to the water depth is small and a standing wave force is obviously exerted on an upright wall, a high-accuracy standing wave theory may be applied. In this case, however, it is necessary to give sufficient consideration to the irregularity of waves in the field, and preferable to examine the force for the highest wave. Moreover, the Sainflou formula [11)] and Hiroi's formula [12)] may also be used for wave force calculations[13)]. When applying these methods, adequate care is needed in determining applicability.

(10) Wave force and significant wave period for waves composed of two wave groups with different periods

An example of two wave groups with different periods being superimposed is the superimposition of waves entering a bay from the outer sea and another group of waves generated within the bay. Another case is the superposition of waves diffracted at the entrance of a harbor and waves transmitted by wave overtopping. In such cases, the spectrum is bimodal (i.e., having two peaks) [14)]. Tanimoto, Kimura et al. [15)] carried out experiments on the wave force acting on the upright section of a composite breakwater by using waves with a bimodal spectrum, and verified that Goda's formulas can be applied even in such a case. They also proposed a method for calculating the significant wave period to be used in the wave force calculation (see **Part II, Chapter 2, 4 Waves**). If each frequency spectrum of the two wave groups before superimposition can be considered to be a Bretschneider-Mitsuyasu type, the significant wave period after superimposition may be obtained by the method proposed by Tanimoto et al. Then this significant wave period may be used in wave force calculation.

(11) Wave force for low crested upright wall

If the crown height of the upright wall is low, the reduction in resistance force due to the weight fall owing to the crest lowering becomes greater than the reduction in wave force resulting from the decrease in the range of wave pressure acting on the wall. Therefore, in general, the wall needs to be widened. However, there are cases that the stability of an upright wall increases as the crown height is reduced. Nakata, Terauchi et al. [16)] have proposed a method for calculating the wave force for a breakwater with a low crown height. In the method, the terms of the front wave pressure and the uplift in the Goda's formulas are multiplied by a reduction coefficient λ_h, thus reducing the wave force.

(12) Wave force for high crested upright wall

When the crown of the upright wall is considerably higher than that for a normal breakwater, there will be no wave overtopping, meaning that the wave force may be larger than that given by Goda's formulas. Mizuno, Sugimoto et al. [17)] carried out experiments on the wave force acting on a breakwater with a high crown.

(13) Wave force on inclined walls

When the wall is slightly inclined, such as a trapezoidal caisson, the horizontal wave force is more-or-less the same as that for an upright wall. However, it is necessary to consider the vertical component of the wave force acting on the inclined surface, along with the reduction in uplift. Tanimoto and Kimura [18)] have carried out experiments on the wave force for slightly inclined walls, and have proposed a method for calculating the wave force.

(14) Uplift on caisson with footing

When a caisson has a footing, a wave force acts downwards on the upper surface of the footing on the seaside, and an uplift of p_u' acts at the front toe, while the uplift at the rear toe is zero. Nevertheless, in general the resultant force is not significantly different to the uplift without the footing. It is thus acceptable to ignore the footing, and to assume that the uplift has a triangular distribution as shown in **Fig. 6.2.3**, with the uplift p_u at the front toe being given by **equation (6.2.8)**, and the uplift at the rear toe being zero. If the footing is extremely long, however, it is necessary to calculate the uplift appropriately, considering the change in the uplift p_u' at the front toe of the footing. Esaki et al. [19), 20)] have proposed a calculation equation of uplift and others acting on large footing based on the hydraulic model.

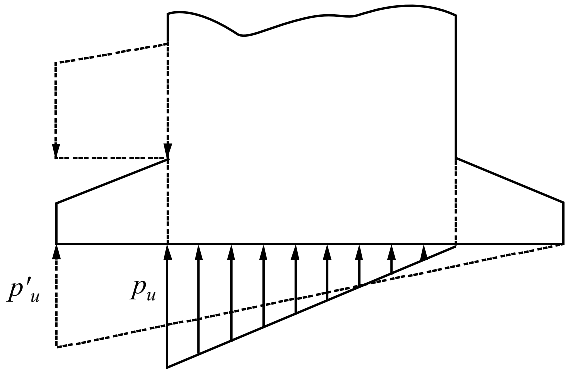

Fig. 6.2.3 Uplift when there is a Footing

(15) In case of wide mound berm in front of upright wall

The wave force acting on the upright wall of a composite breakwater varies not only with the mound height but also with the berm width and the front slope of foundation mound (see **Part II, Chapter 2, 6.2.4 Impulsive Breaking Wave Force**). As explained, of these three coefficients, Goda's formulas incorporates only the effect of the mound height. Consequently, if the width and/or slope of the foundation mound are considerably different from normal, it is preferable to carry out examination using hydraulic model tests. Note however that if the berm is sufficiently wide, it may be considered as a part of the topography of the sea bottom. Even with the standard formula, if the width is more than one half of the wavelength, it is possible to use the water depth on the mound for calculation of both the wave height and the wavelength.

(16) Wave force acting on an upright wall comprised of vertical cylinders

Nagai, Kubo et al. [21)] as well as Hayashi, Karino et al. [22)] have carried out studies on the wave force acting on an upright wall comprised of cylinders such as a pile breakwater. Through their researches, it has been verified that the wave force is not greatly different from that acting on an upright wall with a flat face. It is thus acceptable to treat an upright wall comprised of cylinders as having a flat face and calculate the wave force using Goda's formulas.

6.2.3 Negative Wave Force of Wave Troughs on Wall Surfaces

(1) General

When the trough of a wave is at a wall, a negative wave force acts corresponding to the trough depth of the water surface from the still water level. A negative wave force is a wave force that is obtained through suitable hydraulic model tests or through appropriate calculations. It is a force directed seaward and may be comparable in magnitude to a positive wave force when the water is deep and the wavelength is short.

(2) Negative wave pressure distribution

The negative wave pressure acting on the front side of an upright wall at the wave trough can be approximately estimated as shown in **Fig. 6.2.4**. Specifically, it can be assumed that a wave pressure acts toward the sea, with the magnitude of this wave pressure being zero at the still water level and having a constant value of p_n from a depth $0.5H_D$ below the still water level right down to the toe of the wall. Here p_n is given as follows:

$$p_n = 0.5\rho_0 g H_D \qquad \textbf{(6.2.10)}$$

where

p_n : intensity of wave pressure in constant region (kN/m^2)

$\rho_0 g$: unit weight of seawater (kN/m^3)

H_D : wave height used in performance verification (m)

In addition, the negative uplift acting on the bottom of the upright wall can be assumed to act as shown in **Fig. 6.2.4**. Specifically, it can be assumed that an uplift acts downwards with its intensity being p_n as given by **equation (6.2.10)** at the front toe, zero at the rear toe, and having a triangular distribution in-between. Incidentally, it is necessary to use the highest wave height as the wave height H_D used in the performance verification.

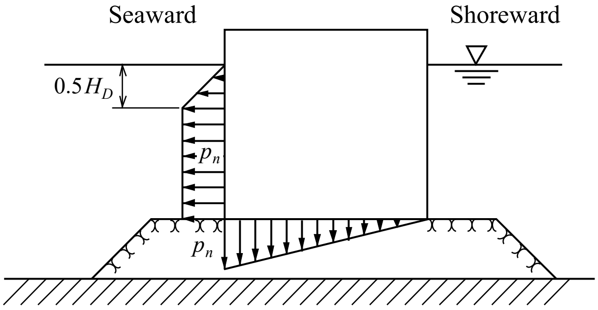

Fig. 6.2.4 Negative Wave Pressure Distribution

(3) Negative wave force by finite amplitude wave theory

Goda and Kakizaki [23] have carried out a wave force calculation based on the fourth order approximate solutions of a finite amplitude standing wave theory, and presented calculation diagrams for negative wave pressure. It has been verified that their calculation results agree well with experimental results. When the water is deep and standing waves are clearly formed, it is acceptable to use the results of this finite amplitude standing wave theory of higher order approximation. It should be noted that, for a deepwater breakwater, the negative wave force at the wave trough may become larger than the positive wave force at the wave crest, and that the upright wall may slide toward offshore.

6.2.4 Impulsive Breaking Wave Force

(1) General

An impulsive breaking wave force is generated when the steep front of a breaking wave strikes a wall surface. Hydraulic model tests have shown that under certain conditions the maximum wave pressure may rise as much as several tens of times the hydrostatic pressure corresponding to the wave height ($1.0\rho_0 g H_D$). However, such a wave pressure acts only locally and for a very short time, and even slight changes in conditions lead to marked variation in the wave pressure. Because of the impulsive nature of the wave force, the effects on stability and the stress in structural elements vary according to the dynamic properties of the structure. Accordingly, when there is a risk of a large impulsive force due to breaking waves being generated, it is necessary to take appropriate countermeasures by understanding the conditions of the impulsive breaking wave force generation and the wave force characteristics by means of hydraulic model tests. It is preferable to avoid the use of cross-sectional shapes and structures that may give rise to a strong impulsive breaking wave force. Where generation of strong impulsive breaking wave force is unavoidable due to steep sea bottom or other reasons, it would be preferable to arrange ways of mitigating wave forces such as by installing appropriate wave-dissipating works.

(2) Conditions of Generation of Impulsive Breaking Wave Forces

A whole variety of coefficients contribute to generation of an impulsive breaking wave force, and so it is difficult to describe the conditions in general. Nevertheless, based on the results of a variety of experiments, it can be said that an impulsive breaking wave force is liable to occur in the following cases when the wave incident angle β (see **Fig. 6.2.2**) is less than 20°.

① **In the case of steep bottom**

When the three conditions, such that the bottom slope is steeper than about 1/30; there are waves that break slightly off the upright wall; and their equivalent deepwater wave steepness is less than 0.03, are satisfied simultaneously, then an impulsive breaking wave force is liable to be generated.

② **In the case of high foundation mound**

Even if the bottom slope is mild, the shape of the rubble mound may cause an impulsive breaking wave force to be generated. In this case, in addition to the wave conditions, the crown height, the berm width, and the slope gradient of the mound all play a part, and so it is hard to determine the conditions under which such an impulsive breaking wave force will be generated. In general, an impulsive breaking wave force will be generated when the mound is relatively high, the berm width is relatively wide or the slope gradient is gentle, and breaking waves form a vertical wall of water at the slope or at the top of the mound.[24)]

When the seabed slope is gentler than about 1/50 and the ratio of the water depth above the top of the mound including armor units to the water depth above the seabed is greater than 0.6, it may be assumed that a large impulsive breaking wave force will not be generated.

(3) Countermeasures

If a large impulsive wave force due to breaking waves acts on an upright wall, the wave force can be greatly reduced by sufficiently armoring the front with wave-dissipating concrete blocks. In particular, with a high mound, a sufficient covering with wave-dissipating concrete blocks can prevent the generation of the impulsive breaking wave force itself. In some cases, the action of an impulsive wave force can also be avoided by using special caissons such as perforated-wall caissons or sloping-top caissons.[24)] The wave direction also has a large effect on the generation of an impulsive breaking wave force, and therefore, one possible countermeasure is to ensure that the wave direction is not perpendicular to the breakwater alignment.

(4) Examining wave force using hydraulic model tests

When examining the wave force using hydraulic model tests for the case that an impulsive force due to breaking wave acts, it is necessary to give consideration to the response characteristics of the structure. For example, the examination of the stability of upright wall as a whole is preferably conducted by sliding experiment and the strength of members such as parapets by stress measurement experiment.

(5) Impulsive breaking wave force due to breaking waves acting on an upright wall on a steep seabed

① **Water depth of upright wall inducing maximum wave pressure and the mean intensity of wave pressure**

Mitsuyasu[25)], Hom-ma, Horikawa et al.[26)], Morihira, Kakisaki et al.[27)], Goda and Haranaka[28)], Horikawa and Noguchi[29)], and Fujisaki, Sasada et al.[30)] have all carried out studies on the impulsive breaking wave force due to breaking waves acting on an upright wall on a steeply sloping sea bottom. In particular, Mitsuyasu carried out a wide range of experiments using regular waves whereby he studied the breaking wave force acting on an upright wall on uniform slopes of gradient 1/50, 1/25, and 1/15 for a variety of water depths. He investigated the change in the total wave force with the water depth at the location of the upright wall, and obtained an equation for calculating the water depth h_M at the upright wall for which the impulsive wave force is largest. When the Mitsuyasu equation is rewritten in terms of the deepwater wavelength, it becomes as **equation (6.2.11)**:

$$\frac{h_M}{H_0} = C_M \left(\frac{H_0}{L_0} \right)^{-1/4} \qquad \textbf{(6.2.11)}$$

where

$$C_M = 0.59 - 3.2 \tan\theta \qquad \textbf{(6.2.12)}$$

H_0 : deepwater wave height (m)

L_0 : deepwater wavelength (m)

$\tan\theta$: gradient of uniform slope

Hom-ma and Horikawa et al.[28] have proposed a slightly different value for C_M based on the results of experiments with a gradient of 1/15 and other data. In any case, the impulsive breaking wave pressure is largest when the structure is located slightly shoreward of the wave breaking point for progressive waves.

Fig. 6.2.5 shows the total wave force when the impulsive breaking wave force is largest for a number of slope gradients, as based on the results of Mitsuyasu's[25] experiments. In this figure, the mean intensity of the wave pressure $\bar{p}$, determined by assuming that wave pressure acts from the sea bottom to the height of 0.75 times limiting breaker height H_b above the still water surface, has been obtained and then divided by $\rho_0 g H_b$ to make it dimensionless; it has then been plotted against the deepwater wave steepness. Specifically, it can be seen that the smaller the wave steepness i, the larger the impulsive breaking wave force is generated. Also, as the slope gradient becomes smaller, the intensity of the maximum impulsive breaking wave force decreases.

② **Conditions for generation of impulsive breaking wave force**

The conditions for the occurrence of an impulsive breaking wave force on a steep seabed, as described in **Part II, Chapter 2, 6.2.4 (2) ① In the case of steep sea bottom**, have been set by primarily employing **Fig. 6.2.5** as a gross guideline. For random waves in the sea, the equivalent deep water wave steepness can be calculated as the ratio of the equivalent deepwater wave height corresponding to the highest wave height H_{max} to the deepwater wavelength corresponding to the significant wave period: where the wave height H_{max} is to be calculated at the distance $5H_{1/3}$ from the upright wall taking into account of wave transformation due to random wave breaking. One may refer to **Fig. 6.2.5** in order to obtain an approximate estimate of the mean intensity of the wave force for this equivalent deepwater wave steepness. In this case, H_b should be taken to be the aforementioned H_{max}. One can also envisage an installation of a breakwater at a place where the risk of impulsive breaking wave force generation is not large for the design waves. However, when placing an upright wall closer to the shore where waves already broken act upon, it becomes important to carry out examination for waves with a height lesser than that of the design waves because it is possible that the waves breaking in front of the upright wall exert more wave force than the design waves that lower the wave height, due to wave breaking, among waves of lower height than design waves.

③ **Impulsive breaking wave force acting on an upright wall on a horizontal floor adjoining a steep slope**

Takahashi and Tanimoto et al.[31] have carried out studies on the impulsive breaking wave force acting on an upright wall on a horizontal floor joining to a steep slope. They employed a horizontal berm connected to a slope of uniform gradient 1/10 or 3/100 in a water tank, and then measured the wave pressure that acts on an upright wall at a variety of positions on the horizontal berm with regular waves. They have proposed an equation valid for certain wave conditions for calculating the upright wall position at which the wave force is largest and the maximum wave force in that condition.

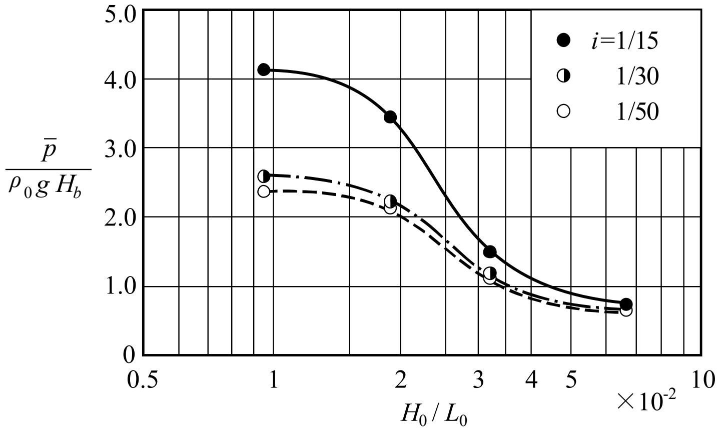

Fig. 6.2.5 Mean Intensity of Wave Force for the Severest Wave Breaking (Upright Wall on a Steep Slope)

(6) Impulsive breaking wave force acting on composite breakwater

① **Effect of the mound shape (impulsive breaking wave pressure coefficient)**

Takahashi et al. [10] have proposed, based on the results of sliding experiments[24], the impulsive breaking wave force coefficient α_I. This is a coefficient that represents the extent of the impulsive force due to breaking waves when the foundation mound is high. It is expressed as the function of the ratio of the wave height to the depth of water above the mound in front of the caisson H_D/d, the ratio of the depth of water above the mound to the original water depth at the upright wall d/h, and the ratio of the front berm width of the mound to the wavelength at this place B_M/L. Note that the wave height H_D is the design wave height, namely highest wave height. The impulsive breaking wave force coefficient α_I is expressed as the product of α_{I0} and α_{I1} as in the following equations:

$$\alpha_I = \alpha_{I0}\alpha_{I1} \tag{6.2.13}$$

$$\alpha_{I0} = \begin{cases} H_D/d & (H_D/d \le 2) \\ 2 & (H_D/d > 2) \end{cases} \tag{6.2.14}$$

Fig. 6.2.6 shows the distribution of α_{I1}. It attains the maximum value of 1 when d/h is 0.4 and B_M/L is 0.12. The impulsive breaking wave force coefficient α_I takes values between 0 and 2; the larger the value of α_I, the larger the impulsive breaking wave force is. When calculating the wave force using conventional Goda's formulas, among α_I and α_2, whichever larger shall be used. The equation for α_I has been formulated based mainly on the results of sliding experiments when H_D/h is relatively large and may be used when examining the sliding of an upright wall on the condition of $H_D/h \ge 0.5$. When $H_D/h < 0.5$, $h = 2H_D$ may be used, for the sake of convenience, in the calculation of α_{I1}. [32]

② **Effect of the crown height of the upright wall**

The higher the crown height, the greater the risk of an impulsive breaking wave force being generated. This is because the steep front of a breaking wave often takes a nearly vertical cliff of water above the still water level, and if there is an upright wall at this place, the impact of the wave front results in the generation of an impact load. For example, Mizuno, Sugimoto et al. [17] have pointed out the tendency that, when the crown is high, an impulsive breaking wave force is generated even when the mound is relatively low.

③ **Effect of the wave direction**

According to the results of the sliding experiments of Tanimoto et al.[24], even if conditions are such that a large impulsive breaking wave force is generated when the wave angle β is 0°, there is a rapid drop in the magnitude of the wave force as β increases to 30° or 45°. When the alignment of breakwater is oblique at the direction of incident waves, the impulsive breaking wave force will not generate or actually be neglected because of the weak effect of it against sliding, even if generated. By considering the fluctuation in the wave direction, it is reasonable to assume that the condition for the generation of an impulsive wave force is that β is less than 20°.

④ **Dynamic response of the upright section to an impulsive breaking wave force and the sliding of upright section**

When an impulsive breaking wave force due to breaking waves acts on an upright section, the instantaneous local pressure can rise up to several tens of times the hydrostatic pressure corresponding to the wave height, although the fluctuation of the impulse is not large and the duration time of the strong impulsive breaking wave force is very short. It is necessary to evaluate the contribution of the impulsive breaking wave force to sliding of the upright section in terms of the dynamic response, considering deformation of the mound and the subsoil. Goda[33] as well as Takahashi and Shimosako[33] have carried out calculations of the shear force at the bottom of an upright section using dynamic models. Judging from the results of these calculations and the results of various sliding experiments, it would seem reasonable to take the mean intensity of the wave pressure of the extreme impulsive breaking wave force statically equivalent to the sliding of the upright wall on the mound to be (2.5–3.0) $\rho_0 gH$. The impulsive breaking wave force coefficient has been introduced based on the results of sliding experiments with consideration of such dynamic response effects to a certain extent.

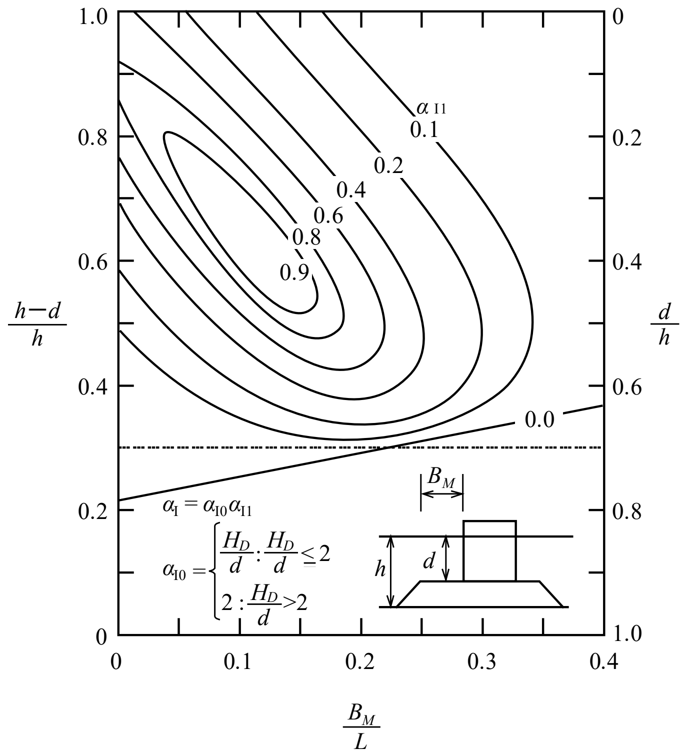

Fig. 6.2.6 Impulsive breaking wave force coefficient

6.2.5 Wave Force Acting on Upright Wall Covered with Wave-dissipating Concrete Blocks

(1) General

If the front of an upright wall is covered with wave-dissipating deformed concrete blocks, the features of wave force acting on the wall varies. The extent of this variation depends on the characteristics of incident waves, along with the crown height and width of the wave-dissipating work, the size and the type of wave-dissipating concrete blocks used, and the composition of the wave-dissipating work including the presence or non-presence of core materials such as rubble. In general, when standing waves act on an upright wall, the wave force does not change drastically by introducing wave-dissipating works. However, when a large impulsive breaking wave force acts, the wave force can be reduced significantly by covering the upright wall with wave-dissipating blocks. Nevertheless, such a reduction in the wave force is only achieved when the wave-dissipating work has a sufficient width and crown height; in particular, it should be noted that if the crown of the wave-dissipating work is below the design tide level, the wave-dissipating work often causes an increase in the wave force.

(2) Wave force calculation formula for upright wall sufficiently covered with wave-dissipating concrete blocks

The wave force acting on an upright wall covered with wave-dissipating concrete blocks varies depending on the composition of the wave-dissipating work, and therefore it should be evaluated using the results of hydraulic model tests. However, if the crown elevation of the wave-dissipating work is as high as the crown of the upright wall and the wave-dissipating concrete blocks are sufficiently stable against the wave actions, the wave force acting on the upright wall may be calculated by applying the extended Goda's formulas. In this method with the standard formula given in **Part II, Chapter 2, 6.2.2 Wave Forces of Standing Waves or Breaking Waves when the Peak of Waves is on the Wall Surface,** the values of η^*, p_1, and p_u given by **equations (6.2.1)**, **(6.2.2)**, and **(6.2.8)** are used respectively, but it is necessary to assign appropriate values to the wave pressure correction coefficients λ_1, λ_2, λ_3 in accordance with the design conditions.

When in the surf zone where the significant wave height lowers by the effect of wave breaking and fully covered with wave-dissipating blocks, the method proposed by Morihira et al. [27] may be referred to.

(3) Wave pressure correction coefficients to the extended Goda's formulas

The method using the extended Goda's formulas can be applied for not only breaking waves but also non-breaking waves by assigning appropriate wave pressure correction coefficients λ_1, λ_2, and λ_3. Studies about the wave pressure correction coefficients for the wave-dissipating blocks have been carried out by Tanimoto et al. [35) 36)], Takahashi et al. [37)], Sekino, Kakuno et al. [38)], and Tanaka, Abe et al. [39)] They have revealed the following:

① Wave-dissipating concrete blocks result in a considerable reduction in the breaking wave pressure, and so it is generally acceptable to set the breaking wave pressure correction coefficient λ_2 to zero.

② The larger the wave height, the smaller the correction coefficient λ_1 for standing wave pressure and the correction coefficient λ_3 for uplift become.

③ The larger the ratio of the width of covering block section to the wavelength, the smaller the correction coefficients λ_1 and λ_3 become.

④ If even a small portion of the upper part of the upright section is left uncovered, there is a risk of the wave force of the uncovered portion becoming an impulsive breaking wave force.

Based on these, Takahashi et al. [37)] have proposed that in general, when the upright wall is sufficiently covered with wave-dissipating concrete blocks, the wave pressure reduction coefficient λ_2 may be taken to be zero, while the values of λ_1 and λ_3 depend primarily on the wave height H (the highest wave height). They have thus proposed the following equations:

$$\lambda_1 = \begin{cases} 1.0 & (H/h \le 0.3) \\ 1.2 - 2(H/h)/3 & (0.3 < H/h \le 0.6) \\ 0.8 & (H/h > 0.6) \end{cases}$$
$$\lambda_3 = \lambda_1$$
$$\lambda_2 = 0 \qquad \textbf{(6.2.15)}$$

In the surf zone, where breakwaters covered with wave-dissipating concrete blocks are generally used, the above equations give $\lambda_1 = \lambda_1 = 0.8$.

(4) Wave force acting on the superstructure of a sloping breakwater covered sufficiently by wave-dissipating blocks

Tanimoto and Kojima [40)] have proposed a calculation equation for the wave pressure correction coefficient λ for cases where the foundation ground exists near the still-water surface, and where it is covered sufficiently with wave-dissipating blocks similar to the superstructure of a sloping breakwater.

(5) Block load due to wave action

Wave force as the direct action of waves and the action due to the leaning of the blocks act on an upright wall that is covered with wave-dissipating blocks. The latter is called the block load. Research on the block load has been carried out by Hiromoto, Nishijima, et al. [41)], Tanaka, Abe, et al. [39)], and Takahashi, Tanimoto, et al. [37)], and the results have been summarized as follows.

① The block load in still water when waves are not acting is small immediately after installation, but increases along with the action of waves, and approaches the constant value. It is possible to consider the same distribution as the earth pressure for that load, but the value differs depending on the wave forces that act on.

② The block load during wave action can be ignored in ordinary cases. This is because the upright wall is displaced, albeit slightly, by the action of the waves, and the block load decreases, and becomes almost 0 when the wave height becomes larger. However, in the event that the wave height is small, or when the water depth is large and the block load in still water is large, it can no longer be ignored.

(6) Impact force of wave-dissipating blocks

Immediately after installation of the blocks or in the event that settlement of the blocks has occurred, when they are subjected to the action of waves in a state where the interlocking between blocks is loose, there are cases where the blocks move due to the waves, and strike the upright wall. In particular, when a wave-dissipating block is large, a powerful impact force acts. This collision of blocks may result in local failure on the caisson's side wall, which makes a bore. Kawabata et al. [40)] indicated a design and verification method of local failure on the caisson's side wall.

(7) Wave force on the discontinuous part of wave-dissipating block covering

In those cases where wave-dissipating blocks are placed partially at corners of breakwater alignment, a discontinuous part of a wave-dissipating block covering appears at the end of wave-dissipating works. In cases where the crest height of a wave-dissipating work is lower than the design tide level, care is required since the wave force may increase greatly from when it is not armored, and a similar large increase in the wave force may occur also at the discontinuous part of the wave-dissipating block covering. [43)]

Shiomi, Yamamoto, et al.[44)] have conducted a 3-D experiment for the wave force at the discontinuous part of the wave-dissipating block armoring and examined the calculation method shown in **Fig. 6.2.7**. The target range for wave force calculation of the discontinuous part is set as from the slope toe end of the wave-dissipating work to the point where H.W.L. crosses the slope. The target range is divided into unit lengths l. For each divided section, water depth of the wave-dissipating work is assumed to be the water depth d on the mound armored work crest, and the wave-dissipating work crest width is assumed to be the mound crest width B_M. The wave pressure and uplift intensity is calculated by Goda's formulas (employing the impulsive breaking wave force coefficient α_I) in **Part II, Chapter 2, 6.2.2 Wave Forces of Standing Waves or Breaking Waves when the Peak of Waves is on the Wall Surface**, and the wave pressure of each divided section is determined. The wave force is calculated such that the mean wave pressure intensity (p_1, p_3, p_4) and the uplift pressure intensity (p_u) of the one caisson act on the entire caisson located in the discontinuous portion. The division length l is determined such that the full wave force over the length of one caisson becomes maximum, but in general it is set at 1/4 to 1/1 of the partition wall interval of the caisson.

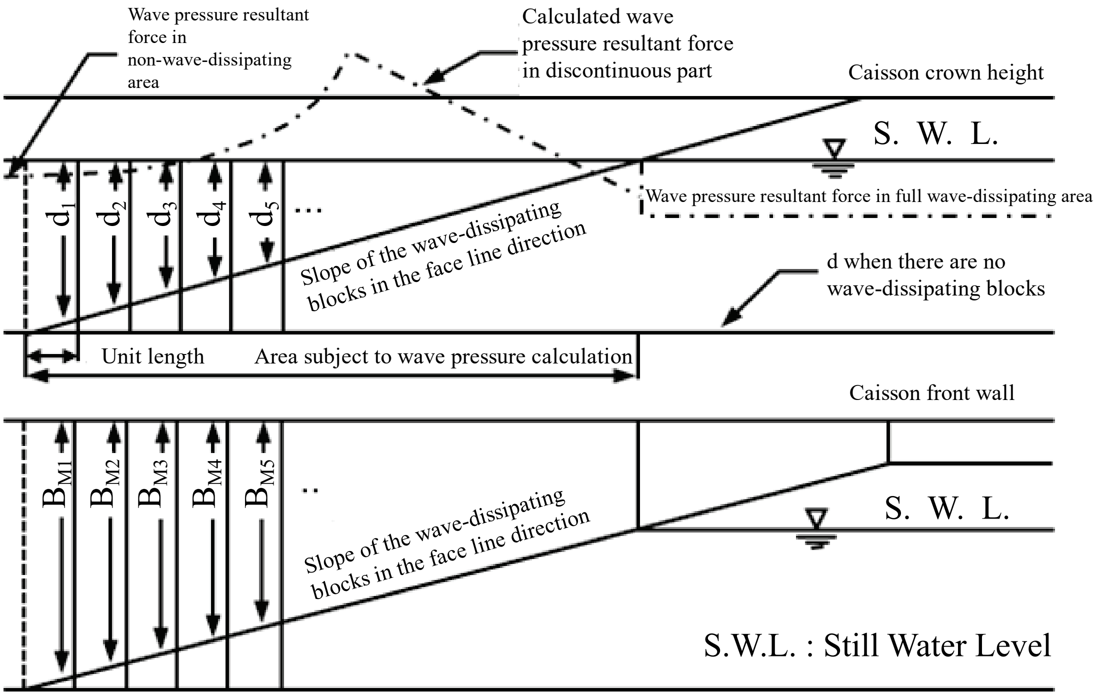

Fig. 6.2.7 Calculation Method of Wave Force at Discontinuously Covered Part of the Wave-Dissipating Blocks (Shiomi et al. [44)])

(8) Wave force on the cross section incompletely covered with wave-dissipating blocks

Even if the crown height of wave-dissipating blocks is higher than the still water level, the wave force may become larger than when there are no wave-dissipating works, provided that the wave-dissipating works provide insufficient cover and the upper part of the upright walls in the front side is not covered with wave-dissipating works. When wave-dissipating works do not completely cover the front side of the upright walls of the breakwater, revetment, and seawall that are covered with the wave-dissipating blocks, the simultaneous action of the storm surge and high waves may exert a strong wave force on upright walls or parapets.

Takahashi et al. [45)] conducted an experiment on an incompletely covered cross section of these wave-dissipating works to obtain a calculation method of wave pressures. This calculation method divides the wave pressure correction coefficient expressed in **equation (6.2.15)** into three regions, as shown in **Table 6.2.1** and **Fig. 6.2.8**. Region 1 is the area not covered with the wave-dissipating works, region 2 is the area covered with wave-dissipating works, on which the impulsive breaking wave exerts a force, and region 3 is the area covered with the wave-dissipating works and on which the impulsive breaking wave does not exert a force. Region 2 extends down by d_p below from the crown height of the wave-dissipating works. The value of d_p can be calculated by the following equation.

$$d_P = \min[H_{1/3}/3, (h_c - h_B)] \quad \textbf{(6.2.16)}$$

where

h_c is the crown height of the superstructure above the still water level, and h_B is the crown height of the wave-dissipating works above the still water level.

Table 6.2.1 Wave Pressure Correction Coefficient on Incompletely Covered Cross Section, λ_1, λ_2

	λ_1	λ_2	
Region 1	1.0	1.0 1.0–10 / 7(h_B / H) 1.0–10h_B / 7H 0.0	(h_B / H < 0.0) (0.0 ≤ h_B / H ≤ 0.7) (0.7 < h_B / H)
Region 2	$\lambda_{10}\,\lambda_{11}$	1.0 1.0–10 / 7(h_B / H) 0.0	(h_B / H < 0.0) (0.0 ≤ h_B / H ≤ 0.7) (0.7 < h_B / H)
Region 3	$\lambda_{10}\,\lambda_{11}$	0.0	

where, λ_{10} is the reduction coefficient of the standing wave pressure component on the cross section fully covered with wave dissipating blocks and λ_{11} is expressed by the following equation.

$$\lambda_{10} = 0.8 \sim 1.0 \quad \textbf{(6.2.17)}$$

$$\lambda_{11} = \begin{cases} 1.0/\lambda_{10} & (h_B/H < 0.0) \\ \left\{1.0 - \dfrac{1.0-\lambda_{10}}{0.35}\left(\dfrac{h_B}{H}\right)\right\}\Big/\lambda_{10} & (0.0 \le h_B/H \le 0..35) \\ 1.0 & (0.35 < h_B/H) \end{cases} \quad \textbf{(6.2.18)}$$

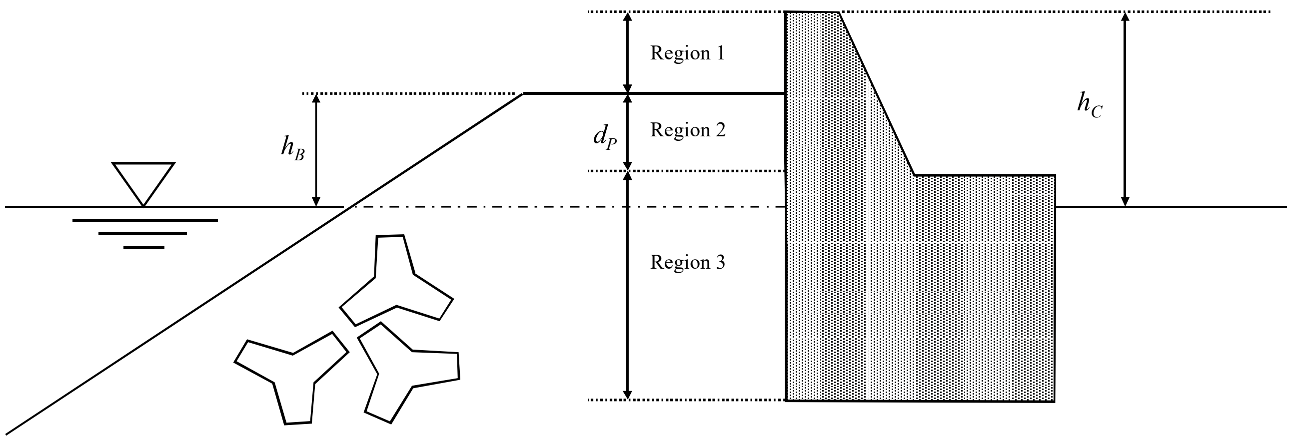

Fig. 6.2.8 Three Regions Distinguishing the Wave Pressure Correction Coefficients on Incompletely Covered Cross Section, λ_1, λ_2

6.2.6 Wave Force on Sloping-top Caisson Breakwaters

(1) Wave force calculation equation of the sloping-top caisson breakwaters not covered with wave-dissipating blocks

The wave force on sloping-top caisson breakwaters should be calculated based on the hydraulic model test results that are suited to the conditions. However, it is possible to use the following calculation equations, if the conduct of the model test is difficult. [46)] (See **Fig. 6.2.9**)

$$F_X = F_{SH} + F_V = \lambda'_{SL} F_1 \sin^2\alpha + \lambda_V F_2 \quad \textbf{(6.2.19)}$$

$$F_Z = -F_{SV} + F_U = -\lambda'_{SL} F_1 \sin\alpha\cos\alpha + 0.5 p_u B \quad \textbf{(6.2.20)}$$

$$\lambda'_{SL} = \min\left[\max\left\{1.0, -23(H/L)\tan^{-2}\alpha + 0.46\tan^{-2}\alpha + \sin^{-2}\alpha\right\}, \sin^{-2}\alpha\right] \quad \textbf{(6.2.21)}$$

$$\lambda_V = \min\left[1.0, \max\left\{1.1, 1.1 + 11 d_c/L\right\} - 5.0(H/L)\right] \quad \textbf{(6.2.22)}$$

Here,

F_X : total horizontal wave force acting on the sloping-top breakwater (kN/m)

F_Z : total vertical wave force acting on the sloping-top breakwater (kN/m)

F_{SH} : horizontal component of the wave force acting on the sloping part (kN/m)

F_{SV} : vertical component of the wave force acting on the sloping part (with the upwards direction being positive) (kN/m)

F_V : wave force acting on the upright part (kN/m)

F_U : uplift acting on the bottom surface (kN/m)

F_1 : component corresponding to the sloping part out of the horizontal wave force acting on the upright wall calculated by Goda's formulas (kN/m)

F_2 : component corresponding to the upright part out of the horizontal wave force acting on the upright wall calculated by Goda's formulas (kN/m)

λ_{SL}' : correction coefficient for the wave force acting on the sloping part

λ_V : correction coefficient for the wave force acting on the upright part

α : angle of the sloping part (°)

p_U : uplift pressure at the front toe of an ordinary caisson calculated by Goda's formulas(kN/m^2)

B : caisson width of a sloping-top breakwater (m)

H : wave height (m)

L : wavelength (m)

d_c : height from the still-water surface to the lower end of the slope (with a case where it is located above the still-water surface taken to be positive) (m)

λ_{SL}' is defined by the following three areas.

① **Where *H/L* is relatively small**

$\lambda_{SL}'=\sin^{-2}\alpha$, that is, $F_{SH}=F_1$, $F_{SV}=F_1\cdot\tan^{-1}\alpha$

② **Where *H/L* is large**

$\lambda_{SL}'=1.0$, that is, $F_{SH}=F_1\cdot\sin^2\alpha$, $F_{SV}=F_{SV}\cdot\sin\alpha\cdot\cos\alpha$

③ **Where *H/L* is between ① and ②**

λ_{SL}' decreases as *H/L* becomes larger

In addition, with respect to λ_V, λ_V=1.0 when H/L is relatively small, and λ_V decreases as H/L becomes larger. However, this wave force calculation equation is applied in the cases where the water depth is relatively deep and the period of the design wave is long, and the value of λ_V should be set at a lower limit of around 0.75.[32] Before this calculation equation was proposed, it had been calculated as $\lambda_{SL}' = \lambda_V = 1.0$ as a convenient and simple method.[47] In this case, the calculated results are somewhat on the safe side in those cases other than when H/L is relatively small.

(2) Wave force acting on sloping-top caisson breakwaters covered with wave-dissipating concrete blocks

The research of Sato, et al.[48] can be referenced as concerns the wave force acting on sloping-top caisson breakwaters covered with wave-dissipating blocks. In addition, Katayama, et al.[49] have proposed a wave force calculation equation for the semi-submerged type, as when the lower end of the sloping part is under the water surface.

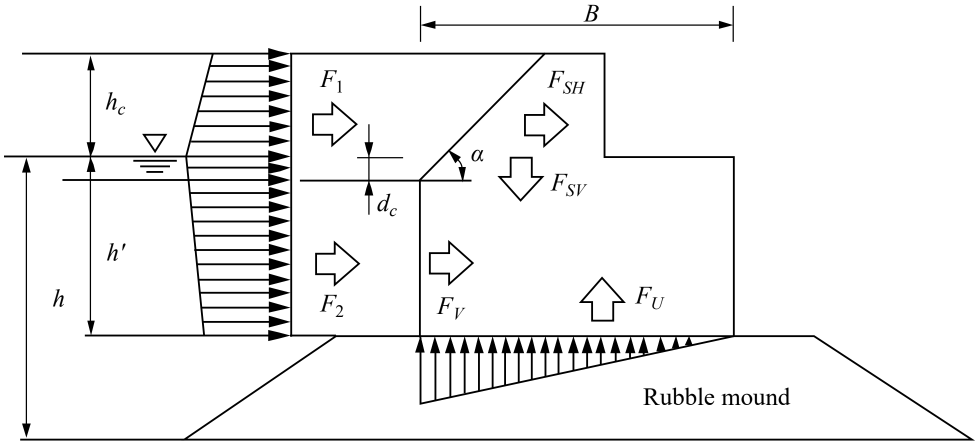

Fig. 6.2.9 Wave Force Acting on Sloping-top Caisson Breakwater

6.2.7 Wave Force Acting on Upright Wave-absorbing Caisson

(1) General

The wave force acting on an upright wave-absorbing caisson varies in a complex way. Specifically, it varies with the wave characteristics, the water level, the water depth, the topography of sea bottom and the shape of the foundation mound as with the case of an ordinary upright wall, but it also varies with the structure of the wave-dissipating structure. It is thus difficult to designate a general calculation method that can be used in all cases. Consequently, if the calculation method that is sufficiently reliable for the structure in question is not proposed, it is necessary to carry out the hydraulic model tests matched to the individual conditions. It is preferable to sufficiently examine not only the wave force to be used in the stability examination but also the wave force acting on structural members. Moreover, it should be noted that the wave force varies significantly according to whether or not the top of wave chamber is covered with a ceiling slab.

(2) Wave force without a ceiling slab in the wave chamber

For the ordinary case where there is no ceiling slab in the wave chamber, one can apply the extended Goda's formulas to calculate the wave force. Takahashi, Shimosako, et al.[50] have carried out experiments on a vertical-slit wall caisson, and have presented a method for calculating the wave pressure acting on the slit and rear walls for four representative phases, where the wave pressure given by the Goda's formulas is multiplied by a correction coefficient λ. They give specific values for the correction coefficient for the slit and rear walls for each phase. This method can be used to give not only the wave force that is severest in terms of the sliding or overturning of the caisson, but also the wave force that is severest in terms of the performance verification of the structural members for each wall. Note, however, that the experiments which form the basis for this calculation method were conducted under limited structural conditions. Discretion should therefore be exercised in the scope of application for this method.[32]

(3) Simplified method to examine the stability of a wave chamber without a ceiling slab

A simpler form of the Goda's formulas can similarly be applied when examining the stability of a caisson. In this method, it is assumed that the wave pressure acts on the main body of the caisson disregarding the wave-dissipating structure (see **Fig. 6.2.10**), and then the wave force is calculated using η^* obtained using **equation (6.2.1)**, p_1 from **equatin (6.2.2)** and p_u from **equation (6.2.8)**, as described in the Goda's formulas in **Part II, Chapter 2, 6.2.2 Wave Force of Standing Waves or Breaking Waves when the Peak of Waves is on the Wall Surface**. In this case, with respect to the wave-dissipating structure, buoyancy of the entire section should be taken into account. With regards the main body of the caisson, on the other hand, buoyancy under the still water should be considered. However, the wave pressure correction coefficient λ_1, λ_2 and λ_3 should be assigned appropriately according to structural conditions. There are examples of examinations [24] on the correction coefficients λ_1 and λ_2 on curved-slit caissons, [51] perforated-wall caissons and vertical-slit wall caissons.

(4) Wave force used for the examination of the stability with a ceiling slab in the wave chamber

When the top of the wave chamber is closed off with provision of a ceiling slab, an impulsive breaking wave force is generated at the instant when the air layer in the upper part of the wave chamber is trapped in by the rise of water surface. It is thus necessary to give consideration to this impulsive breaking wave force in particular with regard to the wave pressure used in the performance verification of structural elements. This impulsive breaking wave force can be reduced by providing suitable air holes. However, it should be noted that if these air holes are too large, the rising water surface will directly strike the ceiling slab without air cushion, meaning that the wave force may actually increase. [52) 53]

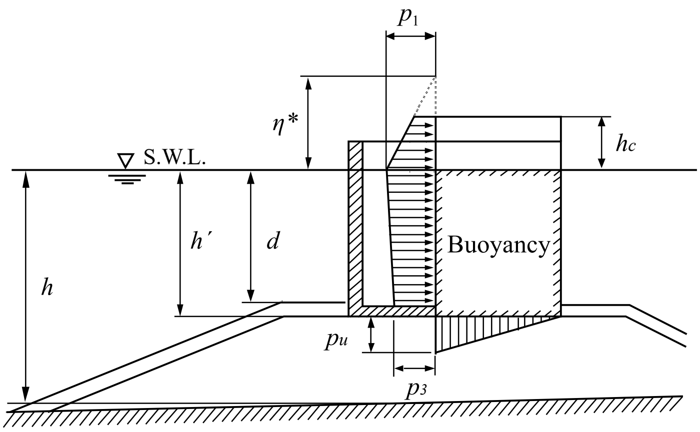

Fig. 6.2.10 Wave Pressure Distribution Employed for Examining Stability
(In case no ceiling slab is installed for wave chamber)

6.2.8 Calculation of Wave Force considering Effect of Alignment of Breakwater

(1) General

When the alignment of breakwater is discontinuous, the distribution of the wave height along the alignment of breakwater becomes non-uniform due to the effects of wave reflection and diffraction. Ito and Tanimoto [54] have pointed out that most breakwaters having been damaged by storm waves show a pattern of meandering distribution of sliding distance. They have termed this "meandering damage," and pointed out that one of the causes of this type of damage is the differences in the local wave forces induced by the non-uniform wave height distribution. The variation of wave heights along the breakwater is particularly prominent when the breakwater alignment contains a concave corner with respect to the direction of wave incidence (see **Part II, Chapter 2, 4.4.4 (3) Transformation of Waves at Concave Corners, near the Heads of Breakwaters, and around Detached Breakwaters**). This should be considered in the calculation of the wave forces. [55) 56] Variations in wave heights along the breakwater alignment may also occur near the head of the breakwater. In particular, for a detached breakwater that extends over a short length only, diffracted waves from the two ends may cause large variations in wave heights. [56] These aspects should be considered in the calculation of the wave forces, as necessary.

(2) Wave force calculation method taking increase in wave height into consideration

Wave force calculation methods that consider the effects of the shape of the breakwater alignment have not reached to the level of reasonable reliability yet. It is thus preferable to carry out an examination using hydraulic model tests suited to the conditions. Nevertheless, there is a good correlation between the increase in the wave height owing to the shape of the breakwater alignment and the increase in the wave force. It is thus acceptable to increase the wave height for the performance verifications in accordance with the effect of the shape of the breakwater alignment as in **equation (6.2.23)**, and then calculate the wave force based on the standard calculation equation.

$$H_D' = \min\{K_c H_D, K_{cb} H_b\} \qquad \textbf{(6.2.23)}$$

where

H_D' : wave height to be used in the wave force calculation in consideration of the effect of the shape of breakwater alignment (m)

K_c : coefficient for the increase in wave height due to the effect of the shape of breakwater alignment; $K_c \geq 1.0$

K_{cb} : limit value of increase coefficient for limiting breaking wave height; $K_{cb} \fallingdotseq 1.4$

H_D : wave height used in the wave force calculation when the effects of the shape of breakwater alignment are not considered (m)

H_b : limiting breaking wave height at the offshore location with the distance of 5 times the significant wave height of progressive waves from the breakwater (m)

The wave height increase coefficient K_c in **equation (6.2.23)** is generally expressed as in **equation (6.2.24)**. It can be appropriately determined based on the distribution of the standing wave height (see **Part II, Chapter 2, 4.4.4 (3) Transformation of Waves at Concave Corners, near the Heads of Breakwaters, and around Detached Breakwaters**) along the alignment of breakwater as determined under the condition that the waves do not break.

$$K_c = H_s / \{H_I (1 + K_R)\} \qquad \textbf{(6.2.24)}$$

where

H_s : standing wave height along the wall of breakwater (m)

H_I : incident wave height (m)

K_R : reflection coefficient for the breakwater in question

If the waves are treated as regular waves, then the coefficient for wave height increase varies considerably along the breakwater. Moreover, the height increase coefficient is very sensitive to the period of the incident waves and the direction of waves. It is thus reasonable to consider the irregularity of the period and the direction of waves. It should be noted that the value of K_c obtained in this way varies along the breakwater and that there may be regions where K_c < 1.0. In that case, K_c = 1.0 shall be applied.

The second term in the braces { } on the right-hand side of **equation (6.2.23)** was introduced in view of the fact that the increase in wave height from the effects of the shape of the breakwater alignment is limited by the water depth. The height of limiting breaking wave H_b can be taken to be the highest wave height H_{max} in **Part II, Chapter 2, 4.4.6 Wave Breaking** when there is an upright wall in a region where the highest wave would be affected by breaking waves. If it is further offshore, values of limiting breaking wave height of regular waves provided in the breaker index diagram (see **Fig. 4.4.13**) in **Part II, Chapter 2, 4.4.6 Wave Breaking** can be applied. The limit value K_{cb} of increase coefficient for limiting breaking wave height has not been clarified in detail. Nevertheless, it may be considered to be about 1.4 based on experimental results up to the present time.

6.2.9 Wave Force acting on Upright Wall in Abrupt Depth Change

For an upright wall located in a place where the water depth changes abruptly owing to the presence of reefs and others, waves transform significantly and strong impulsive breaking wave force or wave force after breaking act on the upright wall in accordance with the conditions such as the location of the breakwater. Therefore, it is preferable to calculate the wave force acting on the upright wall based on hydraulic model tests, by taking the rapid transformation of waves into consideration.

Ito et al. [58] have carried out experiments on the wave force acting on an upright wall located on or behind a reef with the uniform water depth and with the offshore slope of about 1/10.

6.2.10 Wave Force acting on Upright Wall Located Toward the Landside from the Breaker Line and Near the Shoreline

(1) Wave force acting on an upright wall located at the seaside of the shoreline near the shoreline

① General

When the changes in wave force due to the installation depth of an upright wall on a uniform slope are examined under conditions of the specified waves, in general the wave force reaches a maximum when the upright wall is located somewhat to the shore side from the breaker point as the progressive wave, and the wave forces decrease as the installation depth becomes shallower than that. Given such a tendency, it is considered that the wave force due to the smaller waves that break somewhat at the offing of the upright wall is greater than wave force after the breaking of a large wave that breaks considerably toward the offing from the upright wall, when it has a certain degree of water depth.

Goda's formula, which are stipulated in **Part II, Chapter 2, 6.2.2 Wave Force of Standing Waves or Breaking Waves when the Peak of Waves is on the Wall Surface**, provide a wave force based on the waves breaking somewhat in the offing of such an upright wall. However, in those places where the water depth in the vicinity of the shoreline is shallow, not only does the breaking wave height vary greatly depending on the changes in water level due to surf beat and so on, but also the breaking wave force varies greatly due to the sea bottom gradient, the wave steepness of offshore waves and the irregularity of the waves, so it is not appropriate to employ Goda's formulas, and it should be calculated with an equation suited to the conditions or the results of a hydraulic model test. In addition, the fact that the water depth itself changes due to the littoral drift, or that the effects of storm surge are great, should also be taken into consideration.

② Calculation method of wave force acting on an upright wall at the seaward side of shoreline near the shoreline

A number of different wave force formulas have been proposed for upright walls near the shoreline. It should be necessary to carry out an appropriate wave force calculation in line with the design conditions. Very roughly speaking, the standard formula in **Part II, Chapter 2, 6.2.2 Wave Forces of Standing Waves and Breaking Waves when the Peak of Waves is on the Wall Surface** are applicable in the regions where the seabed slope is mild and the water is relatively deep. The formula of Tominaga and Kutsumi [59] is applicable in the regions near the shoreline. The formula of Hom-ma, Horikawa and Hase [26] is applicable in the regions where the seabed slope is steep and the water is of intermediate depth. When applying Goda's formula to the places where the water depth is less than one half the equivalent deepwater wave height, it may be preferable to use the values for the wavelength and wave height at the water depth equal to one half the equivalent deepwater wave height in the calculation.

(2) Wave force acting on an upright wall located at the land side of the shoreline

① General

Since the wave force acting on an upright wall located at the land side of the shoreline varies greatly depending on the rise in the water level due to surf beat or the runup of the waves, it should be calculated with an equation suited to the conditions or the results of a hydraulic model test. In addition, the fact that the topology in the vicinity of the shoreline changes due to the littoral drift, or that the effects of storm surge are great, should also be taken into consideration.

② Calculation method of wave force acting on an upright wall at the landward side of shoreline near the shoreline

For an upright wall located on the landward side of the shoreline, the formula by the US Army Coastal Engineering Research Center (CERC) [60] is available. Moreover, one may refer to the research that has been carried out by Tominaga and Kutsumi [59] on the wave force acting on an upright wall located on the landward side of the shoreline.

6.3 Wave Force Acting on Submerged Members and Large Isolated Structures

6.3.1 Wave Force Acting on Submersed Members [61)]

(1) Morison's Formula

① General

Structural members such as piles that have a small diameter relative to the wavelength hardly disturb the propagation of waves. The wave force acting on such members can be obtained using the Morison's formula as shown in **equation (6.3.1)**, in which the wave force is expressed as the sum of a drag force that is proportional to the square of the velocity of the water particles and an inertia force that is proportional to the acceleration.

$$\vec{f}_n = \frac{1}{2} C_D \rho_0 |\vec{u}_n| \vec{u}_n D \Delta S + C_M \rho_0 \vec{a}_n A \Delta S \tag{6.3.1}$$

where

$\vec{f}_n$: force that acts on a small length ΔS (m) in the axial direction of the member, where the direction of this force lies in the plane containing the member axis and the direction of motion of the water particles and is perpendicular to the member axis (kN)

$\vec{u}_n$, $\vec{a}_n$: components of the water particle velocity (m/s) and acceleration (m/s^2), respectively, in the direction perpendicular to the member axis that lies within the plane containing the member axis and the direction of motion of the water particles (i.e., the same direction as $\vec{f}_n$) (these components are for incident waves that are not disturbed by the presence of member)

$|\vec{u}_n|$: absolute value of $\vec{u}_n$ (m/s)

C_D : drag coefficient

C_M : inertia coefficient

D : width of the member in the direction perpendicular to the member axis as viewed from the direction of $\vec{f}_n$ (m)

A : cross-sectional area of the member along a plane perpendicular to member axis (m^2)

ρ_0 : density of seawater (normally 1.03 t/m^3)

Equation (6.3.1) is a generalized form of the equation presented for mooring posts by Morison et al. [62)], to give the wave force acting on a section of a very small length ΔS of a member orientated in any given direction. The arrows on top of symbols indicate that the force, velocity and acceleration are the components in the direction perpendicular to the member. The first term on the right-hand side represents the drag force, while the second term represents the inertia force. The water particle velocity and acceleration components in the equation both vary in time and space. It is preferable to pay sufficient attention to these variations, and to examine the distribution of the wave force that is severest to the member or structure in question. Because of the phase deviation between velocity and acceleration, the inertia force does not become highest when the drag force is highest. When a member's diameter is quite small compared to the wavelength, the drag force is dominant and the inertia force can be ignored, but it cannot be ignored as the member's diameter becomes larger. It should be also necessary to appropriately evaluate the drag coefficient and the inertia coefficient by hydraulic model tests or field measurement results.

② Water particle velocity and acceleration components

The components of water particle velocity and acceleration ($\vec{u}_n$, $\vec{a}_n$) in **equation (6.3.1)** represent the component of the water particle motion at the center axis of the member. These components are in the direction perpendicular to the member axis, and are evaluated under the assumption that waves are not disturbed by the presence of the structure in question. When calculating the wave force, it is necessary to estimate these components as accurate as possible, based on either experimental data or theoretical prediction. In particular, the water particle velocity component contributes to the wave force with its square, meaning that when the wave height is large, an approximation using small amplitude wave theory becomes insufficient to yield reliable estimate. Moreover, when the member extends above the water level, it is necessary to give sufficient consideration to the range over which the wave force acts, i.e., the elevation of wave crest. When calculating these terms using theoretical values, it is preferable to use the finite amplitude wave theory that agrees with the characteristics of the design waves, based on **Part II, Chapter 2, 4.2.1 Setting Procedure of Waves**. Note also that it is necessary to take full account of wave irregularity with regard to the wave height and period used in the wave force calculation, and to study the wave characteristics that are severest to the safety of member or structure in question. In general, the highest wave height and the significant wave period may be used in the analysis for rigid structures.

③ **Drag coefficient C_D**

In general, the drag coefficient C_D for steady flow can be used as the drag coefficient C_D for wave force. Note, however, that the drag coefficient varies with the shape of the member, the surface roughness, the Reynolds number Re, and the separation distance between neighboring members. It also varies with the Keulegan-Carpenter number (KC number). It is necessary to consider these conditions when setting the value of drag coefficient. For a circular cylindrical member, it is standard to set C_D = 1.0 if the finite amplitude properties of the waves are fully considered. A lower value may be used according to the importance of the facilities if its value is based on the results of hydraulic model tests. Even in this case, however, C_D should not be set below 0.7. Note also that when estimating the water particle velocity by an approximate equation, it is preferable to use a value for the drag coefficient that has been adjusted for the estimation error in the water particle velocity. If the velocity of the water particle motion can be calculated accurately, drag coefficient values for steady flow in **Table 7.2.1** in **Part II, Chapter 2, 7.2 Fluid Force due to Current** may be used with necessary modifications.

④ **Inertia coefficient C_M**

The value by the small amplitude wave theory may be used for the inertia coefficient C_M. Note, however, that the inertia coefficient varies with the shape of the member and other coefficients such as the Reynolds number, the KC number, the surface roughness, and the separation distance between neighboring members. The value of the inertia coefficient should be set appropriately in line with the given conditions.

When the diameter of the object in question is no more than 1/10 of the wavelength, it is standard to use the value listed in **Table 6.3.1** for the inertia coefficient C_M. However, when estimating the water particle acceleration by an approximate equation, it is necessary to adjust the value of C_M for the error in the estimate of water particle acceleration. The values of inertia coefficient shown here are mostly from the study by Stelson and Mavis. [63] According to the experiments of Hamada, Mitsuyasu et al. [64], the inertia coefficient C_M for a cube is in the range of 1.4 to 2.3.

Table 6.3.1 Inertia Coefficient

Shape of the object	Basic volume	Inertia coefficient
Cylinder 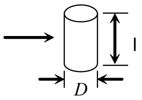	$\frac{\pi}{4}D^2 l$	2.0 ($l > D$)
Regular prism 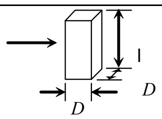	$D^2 l$	2.19 ($l > D$)
Cube 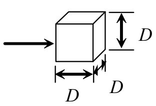	D^3	1.67
Sphere 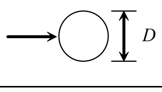	$\frac{\pi D^3}{6}$	1.5
Flat plate 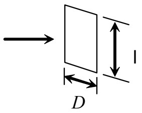	$\frac{\pi}{4}D^2 l$	When D/l =1, 0.61 When D/l =2, 0.85 When D/l =∞, 1.00

⑤ **Experimental values for drag coefficient and inertia coefficient of cylinder**

There are many experimental values for the drag coefficient and inertia coefficient of a vertical cylinder; for example, those of Keulegan and Carpenter, [65] Sarpkaya, [66] [67] [68] Goda, [69] Yamaguchi, [70] Nakamura, [71] Chakrabarti, [72] [73] and Koderayama and Tashiro. [74] There are many variations between these values. However, there is not sufficient data in the region of high Reynolds number, which is subject to the actual performance verification. Oda [75] has produced a summary of these researches which may be referred to.

⑥ **On-site measurement values for drag coefficient and inertia coefficient of cylinder**

The drag coefficient and inertia coefficient of a cylinder is also obtained by measuring the wave force at on-site facilities. For example, Mizuno et al. [76] obtained C_D = 0.60 ± 0.17, C_M = 1.23 ± 0.34 for a steel pipe structure. Many other on-site measurement results, such as Kim's, [77] have been reported, but they are not coincident, partly because of restrictions on accuracy in the on-site experiments, etc.

⑦ **Effects of neighboring members**

When structural members neighbor one another, the values of the drag coefficient and inertia coefficient vary due to the effects of the other structural members. According to experiments on cylindrical columns, the drag coefficient increases in the event that two columns are arranged in a row perpendicular to the direction of the flow, but it has been known that if the net space between the columns (s) is at least 2.5 times its diameter (D), its effects are small. In addition, in the event that they are arranged in a row in the direction of the flow, the drag coefficient for the column in back exhibits a tendency to decrease over a considerable range (s/D = about 9). However, it cannot be recognized that its effects have been phenomenaadequately solved already, and in general it is better not to consider this as a decrease in the drag coefficient due to the neighboring effect.

In addition, the value of the inertia coefficient considering the effects of neighboring columns has been calculated by diffraction theory, and an increase or decrease has been known compared with the case of a single column depending on the values of s/D and D/L, [78] but when D/L is small, its effects are small. Nakamura and Abe [79] have investigated experimentally the increase in the inertia coefficient in a range of $D/L < 0.1$, and have pointed out that although the results are scattered, the upper limit of the coefficient value is extremely large in the vicinity of s/D = 2 to 3, and it is better to avoid a situation where the interval between the two columns matches such conditions.

⑧ **Facilities composed of many structural members**

The wave force that acts on an entire facility composed of upright columns, slanted members and/or horizontal members is calculated by **equation (6.3.1)** considering the phase difference of the wave force acting on each structural member, and by compounding the vector sums of these. In the case of facilities composed of many of structural members, there is a risk that the whole might collapse due to the failure of one point in the structural member, so the distribution of the wave force that is most severe for the individual structural members and the entire facility should be considered in particular.

⑨ **Resonance with waves and random wave force**

In the event that the rigidity of the facilities is low, and the natural frequency period is long, it is preferable to consider the effects of the dynamic response on the wave force that acts periodically. The wave force in this case may be calculated for the temporal changes of $\vec{u}_n$, $\vec{a}_n$ based on **equation (6.3.1)**. However, since only the specific dynamic effects are reflected in the examination for waves with a constant period, it is reasonable to view this as the continuous action of random waves. When calculating the wave force for random waves, suitable measures may be devised for the way to provide the height of the wave crest and the drag coefficient, and the water particle movement component may be calculated based on small amplitude wave theory.

(2) Wave force when breaking waves act

When breaking waves act on facilities on a steep sea bottom surface, there are cases when an impulsive wave force similar to the impulsive breaking wave pressure that acts on upright walls acts in addition to the drag and inertia forces given by **equation (6.3.1)**. Since the response characteristics of the facilities become the dominant effective factor for such an impulsive action, not only a calculation of the wave force but also an examination that includes the behavior of the entire facility as well as the structural members should be carried out. [80] [81]

(3) Uplift

In addition to the drag and inertia forces of **equation (6.3.1)**, wave force acting on submerged members is the uplift acting in the direction perpendicular to the plane containing the member axis and the direction of the water particle motion. In general, it is acceptable to ignore this uplift, but it is necessary to pay attention to the fact that the uplift may become a problem for horizontal members that are placed near to the seabed. [82) 83) 84) 85) 86) 87)] Moreover, for long and thin members, it is necessary to pay attention to the fact that the uplift may induce vibrations.

(4) Wave force due to random waves

Of the wave force components acting on structural members in the sea, the inertia force is linear, so the spectrum of the wave force can be calculated easily from the spectrum of the waves, but when the drag force is included this becomes difficult owing to its nonlinearity. Borgman [88)] has introduced a theoretical equation for the wave force spectrum that includes drag force based on probability theory. The first approximation of this drag force corresponds to something where the nonlinear drag force is made linear in a form in which the root-mean-square value of the water particle speed is incorporated in the coefficient, and this is employed occasionally in spectrum analysis of on-site observational data and other cases. In addition, Hino [89)] has introduced a theory of a case where waves and a uniform flow co-exist by using the characteristic function method. A simulation method where the random wave forms and water particle movement are simulated based on a prescribed wave spectrum, and its time series is inputted and the wave force is calculated, is also being employed commonly as a method for studying the statistical nature of random waves including the nonlinear drag and the dynamic response of the facilities. Borgman [90)] has explained this method, and there is the calculation example of Ito et al. [91)]. These are simulations based on linear theory, but recently nonlinear simulation calculations that consider everything up to the second-order interference terms between component waves have also been carried out, [92)] and in addition, nonlinear simulation calculations of multi-directional random waves have also been tried. [93)] As for the probability distribution of the wave force, the wave height exhibits a Rayleigh distribution, whereas the distribution of its local maximum value may become considerably different from the Rayleigh distribution owing to the nonlinearity of the drag force etc. and the incidence rate of large maximum values may become considerably high. Tickell-Elwany [94)] has calculated the theoretical value of the wave force distribution based on three-dimensional random waves. In addition, Kimura et al. [95)] has calculated the probability distribution of the wave force acting on a single cylindrical column based on the joint distribution of the wave height and period of random waves, and shown a method for calculating the anticipated values for the maximum wave force.

(5) Equation for calculating the breaking wave force acting on slanted columns

Tanimoto, Takahashi, et al. [81)] have developed the research of Goda et al. [80)], and have proposed a method for calculating the breaking wave force acting on cylindrical columns based on experimental results. The calculation of the impulsive breaking wave force acting on upright cylindrical columns or slanted cylindrical columns installed on a sea bottom with a uniform slope may be carried out based on this method. In the experiments both regular and random waves were employed, and the experiments were carried out with a cylindrical column with a D/h = 1/5, for gradients i = 1/100 and 1/30, and θ = −30°, −15°, 0°, +15° and +30°. The position of the impulsive wave force that acts and the changes over time can be calculated by the proposed calculation method, and the response of the cylindrical column member to the impulsive wave force can also be calculated by applying appropriate methods.

(6) Breaking wave force acting on small diameter cylindrical columns on a reef

Goda et al. [96)] have proposed a method for calculating the breaking wave force that acts on upright cylindrical columns on reefs, where the water depth changes suddenly, and it is possible to carry out calculations of the wave force based on this method for waves like those that break on the slope of reefs.

(7) Effects of multi-directionality of waves

As the multi-directionality of waves becomes stronger, the components of the wave force other than the principal direction of the waves becomes larger. Therefore, the multi-directional dispersion of the waves should be considered in facilities constructed in deep waters where the multi-directionality is strong. [97)]

6.3.2 Wave Force Acting on Large Isolated Structures

(1) General

The wave force acting on a large isolated structure whose dimensions are comparable to the wavelength can be calculated using the velocity potential, because it is generally possible to ignore the drag force. In particular, for structures of a simple shape, analytical solutions obtained by diffraction theory are available. However, it is necessary to calculate the breaking wave force by hydraulic model tests if there is a possibility of breaking wave force exerted on structure.

(2) Diffraction theory

MacCamy-Fuchs [98] have determined the velocity potential of waves around an upright cylindrical column of large diameter using diffraction theory, and calculated the wave force from the water pressure distribution at the surface of cylinder. Goda and Yoshimura [99] have applied diffraction theory to an upright elliptic cylinder, and presented their results in terms of the inertia coefficient C_M. Yamaguchi [100] has examined the effect of the wave nonlinearity on the wave force acting on an upright cylindrical column of large diameter by nonlinear diffraction theory, and pointed out that it is necessary to consider these effects when the water is shallow.

(3) Isolated structure of arbitrary shape

For a structure that is complex in shape, it is difficult to obtain the wave force analytically, and so it is necessary to carry out a numerical calculation. Various methods are available, such as integral equation methods (see **Part II, Chapter 2, 4.8 Action on Floating Body and its Motions**).

6.4 Wave Force Acting on Structures near the Water Surface

6.4.1 Uplift Acting on Horizontal Plates near the Water Surface

(1) General

In the case of facilities near still water surface, such as the superstructure of piled piers or pile-type dolphins, and in particular those facilities that are roughly parallel to the water surface, there is a risk that a rising wave surface will strike on the bottom surface of the facilities and an impulsive wave force (uplift) will act on. In particular, it becomes a large impact load when the wave height is large and the clearance with the still water surface is small. In addition, in a case where there is a reflecting wall at the rear as in the case of open type wharf, and the waves become standing waves and act on this, the wave surface rise rate increases and so does the impact load. If there is a risk of an impact load, the impulsive uplift should be calculated by a suitable method such as a hydraulic model test. Due attention should also be paid to the fact that ordinary uplift that is not an impact load also acts on the bottom surface of such structures, in addition to the impulsive uplift.

(2) Characteristics of impulsive uplift

If the bottom surface of the plate is flat, the impulsive uplift acting on a horizontal plate near the still water surface level varies with the impact velocity of the wave surface and the angle between the wave surface and the plate. As shown in **Fig. 6.4.1 (a)**, when there is an angle between the wave surface and the plate, the wave surface runs along the bottom surface of the plate and the wave pressure distribution becomes as shown there. The distinct feature of the wave pressure in this case is its rapid rise in time. On the other hand, when the angle between the wave front and the plate is close to 0, as shown in **Fig. 6.4.1 (b)**, a layer of air is trapped between the wave surface and the plate, and compression of this layer of air results in the almost uniform wave pressure distribution. The distinct feature of the wave pressure in this case is its oscillation in time with having a short-period damping vibration.

In case of a piled pier with a deck plate supported by horizontal beams, the wave surface is disturbed by the beams, and the uplift becomes of complex nature. With beams, a layer of trapped air is often formed and this layer of air is compressed by the uprising wave surface. It is thus necessary to give consideration to the change in the uplift with respect to the shape of the bottom face of the horizontal plate. The shape of the impacting wave surface varies greatly according to the condition whether the wave is progressive or standing in nature. With standing waves, the shape of the impacting wave front varies with the distance between the position of wave reflection and the horizontal plate. It is thus necessary to consider such differences.

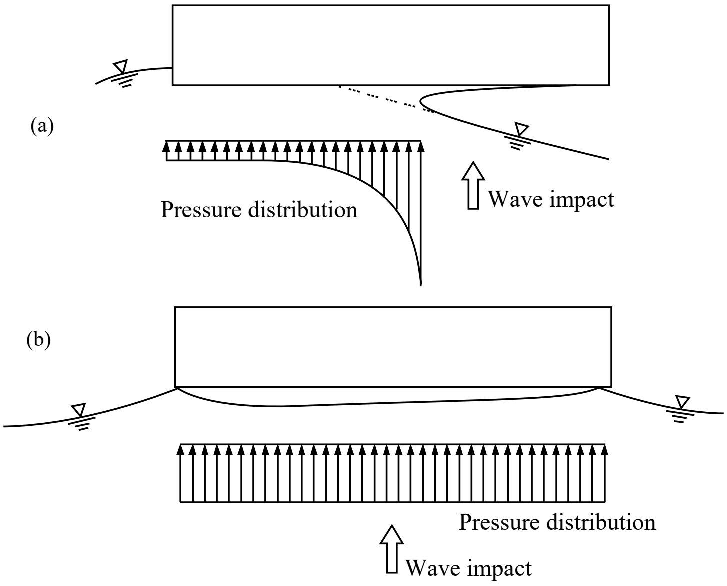

Fig 6.4.1 Impact between Wave Front and Horizontal Plate

(3) Calculation of uplift from standing waves

① **Uplift acting on horizontal plate with flat bottom surface**

Goda [6] considered the uplift acting on a horizontal plate as being the force resulted from the sudden change in the momentum of wave by its impact on the plate. Using von Karman's theory, he obtained the following formulas for calculating the uplift of standing waves acting on a horizontal plate.

$$P = \zeta \frac{\rho_0 g}{4} HLB \tanh \frac{2\pi h}{L} \left(\frac{H}{s'} - \frac{s'}{H} \right) \tag{6.4.1}$$

$$s' = s - \pi \frac{H^2}{L} \coth \frac{2\pi h}{L} \tag{6.4.2}$$

where

P : total uplift (kN)

ζ : correction coefficient

$\rho_0 g$: unit weight of seawater (kN/m^3)

H : wave height of progressive waves, generally the highest wave height H_{max} (m)

L : wavelength of progressive waves (m)

B : width of plate (m)

H : water depth (m)

s : clearance of the plate above the still water surface (m)

s' : clearance of the plate above the level corresponding to the middle of the wave crest and trough (m)

It is necessary to pay attention to the fact that the uplift in the above equations does not depend on the length of the horizontal plate l.

The impact force has the magnitude given by the above equations and takes the form of a pulse that lasts for a time τ from the moment of the impact, that is given as follows:

$$\tau = \frac{\pi T l^2}{L^2} \frac{s'}{\sqrt{H^2 - s'^2}} \tag{6.4.3}$$

Where T is the wave period and l is the length of the horizontal plate. Provided the length of the horizontal plate is sufficiently short compared with the wavelength L and the bottom surface of the horizontal plate is flat, **equation (6.4.1)** well represents the features of the uplift well with simple equation. Comparing calculated values with $\zeta = 1.0$ to experimental values, agreement is relatively good provided H/s' is no more than 2.

Tanimoto, Takahashi et al. [101] have proposed another method for calculating the uplift acting on horizontal plate based on Wagner's theory. With this calculation method, the angle of contact β between the wave surface and the horizontal plate as well as the impact velocity V_n are given by Stokes' third order wave theory, making it possible to obtain the spatial distribution of the impact pressure and its change over time. Note, however, that the use of Stokes' third order wave theory makes the calculation rather complex. This calculation method is intended for use when the bottom face of the horizontal plate is flat. It cannot be applied directly to structures of complicated shape such as an ordinary piled pier that have beams under the floor slab; the impact between the wave surface and the floor slab is disturbed by the beams. In general, the presence of beams causes air to become trapped in and the wave surface to be disturbed, the result being that the impact force is less than for a horizontal plate with a flat surface. Accordingly, the value obtained from this calculation method may be considered as being the upper limit of the uplift for an ordinary piled pier.

② **Uplift Acting on Piled Pier**

Ito and Takeda[102] have conducted scale model tests of piled pier to obtain the uplift acting on an access bridge, and its vibration threshold weight and falling threshold weight. The peak value of the uplift obtained by the experiment varied considerably from wave to wave even under the same conditions. Nevertheless, the mean of these peak values is given approximately by the following **equation (6.4.4)**:

$$p = \rho_0 g(8H - 4.5S) \tag{6.4.4}$$

where

p : mean peak value of uplift (kN/m^2)

$\rho_0 g$: unit weight of seawater (kN/m^3)

H : incident wave height (m), (highest wave height)

S : distance from the water level to the underside of access bridge (m)

Note however that the peak value of the intensity of the uplift given by **equation (6.4.4)** acts only for an extremely short time, and that the phase of this uplift varies from place to place. This means that even if the uplift p exceeds the self weight of the access bridge, the bridge will not necessarily move or fall down immediately. Based on this perspective, Ito and Takeda have obtained the threshold weight at which the access bridge vibrates and that at which the deck slab falls down. The relationship between the vibration threshold weight and the wave height is given below:

$$q = \rho_0 g(1.6H - 0.9S) \tag{6.4.5}$$

The vibration threshold weight given by **equation (6.4.5)** is one fifth of the intensity of the uplift as given by **quation (6.4.4)**. The falling threshold weight was found to be 1/2 to 1/3 of the vibration threshold weight.

In these access bridge experiments, Ito and Takeda also tested the access bridge with holes or slits of various sizes, and investigated how the threshold weights changed when the void ratio was changed. In general, the change in the vibration threshold weight by the void ratio is only slight compared to access bridges without holes, when the void ratio is small i.e., around 1%, air escapes easily and the water surface strikes the access bridge impulsively. The falling threshold weight, on the other hand, drops noticeably when the void ratio exceeds 20%. Note that the bridge weight referred to here is the weight per unit area of the substantial part i.e., the weight per unit area excluding the voids. In this way, since there is little change to the vibrating threshold weight, namely the stable weight per unit area of the substantial part of the access bridge, the weight of an entire surface area can be reduced by boring holes. What is more, the falling threshold weight decreases with the increase in the void rate. From these two reasons, it can be concluded that it is best to raise the void rate.

Furthermore, Ito and Takeda [102] have attached a strain gage to the deck slab in the superstructure of the model of piled pier and measured the stress. Based on their results, they proposed the following equation for the equivalent static load (kN/m^2) assumed to act with uniform distribution on the deck slab.

$$p = 4\rho_0 gH \tag{6.4.6}$$

Note, however, that the value given by this equation corresponds to the upper limit of the experimental values and should, thus, be considered corresponding to the case that the distance s from the water level to the underside of the superstructure is almost 0. The equivalent static load, given by **equation (6.4.6)**, is generally lower than the uplift acting on a horizontal plate with a flat bottom face. It is considered that this is partly because the beams disturb the impacting wave front, trapping air. Experimental research into the uplift acting on a piled pier has also been carried out by Murota and Furudoi, [103] Nagai and Kubo et al. [104], Horikawa and Nakao et al. [105], and Sawaragi and Nochino. [106]

(4) Calculation of uplift from progressive waves

① Uplift acting on horizontal plate with flat bottom surface

An impulsive uplift also acts when progressive waves act on a horizontal plate that is fixed near to the still water level. Tanimoto and Takahashi et al. [107] have proposed a method for calculating this impulsive uplift, based on the same theory that was used for impulsive uplift by standing waves.

② Uplift acting on superstructure of detached pier

(a) Ito and Takeda [102] have also carried out studies on the uplift of progressive waves acting on a detached pier. Specifically, they measured the stress occurring in the deck slabs of a detached pier model. Based on the upper limits of their experimental results, they proposed the following equation for the uniformly distributed equivalent static load.

$$p = 2\rho_0 gH \tag{6.4.7}$$

(b) Allsop and Cuomo, et al. [108] [109] [110] [111] have undertaken a systematic examination of the uplift due to progressive waves that act on detached pier by hydraulic model tests based on random waves and theoretical analysis. They have proposed calculation equations concerning the ordinary uplift that is not an impact load. [109]

6.4.2 Horizontal Wave Force Acting on the Vertical Plate near the Water Surface

A horizontal wave force acts on thin, vertical plates, such as curtain walls installed near the water surface, or the vertical surface of the horizontal plates, such as the dolphin superstructure of the stationary offshore berth. The water surface location and the wave making resistance force, due to the existence of the free surface, should be considered when calculating this horizontal wave force.

Tanimoto, Takahashi et al. [107] proposed a calculation equation for the horizontal wave force acting on the stationary structure near the water surface, primarily targeting the dolphin superstructure, and also proposed to use this horizontal wave force calculation equation for the horizontal wave force acting on the curtain walls fixed near the water surface. Moreover, Kubou, Takezawa et al. [112] also proposed a calculation equation for curtain walls with a shallow submersion depth.

Morihira, Kakizaki et al. [113] experimentally obtained the horizontal wave force acting on curtain walls used as breakwater. Also, Sekimoto et al. [114] indicated a calculation method for the wave force acting on curtain walls, considering the incidence angle.

6.5 Mound Transmitted Wave Pressure of Caisson Type Seawall and Wave Pressure within Joints of Caissons

6.5.1 General

In the caisson-type seawalls, waves may transmit rubble mounds and back fill stones, as in **Fig. 6.5.1**, and act on the reclaimed sand. As the rubble and reclaimed sand significantly differ in grain size, sand leakage prevention sheets and joint plates between caissons are installed to prevent the leakage of reclaimed sand. However, these sand leakage prevention sheets and joint plates are frequently damaged by the mound transmitted waves during and after construction to result in the leakage of the reclaimed sand.

Here, the mound transmitted waves and the wave pressure generated in the joint of caissons are explained.

6.5.2 Mound Transmitted Wave Pressure

After installation of impermeable sand leakage prevention sheets or reclaimed soil behind the backfill stones as in **Fig. 6.5.1**, the inside of the rubble mound or backfill stones becomes sealed. In this condition, the pressure exerted to the front toe of the caisson acts on the sand leakage prevention sheets or the reclamation gravel without attenuation [115]. The wave pressure p_w acting on the front toe can be calculated by Goda's formula (**equation (6.2.4)**) [116], and the pressure almost equal to the wave pressure is generated inside the backfill stones

The uplift of the sand leakage prevention sheets due to this wave force, needs to be prevented because it causes damage of the sheets during construction.

Moreover, even after construction period, mound transmitted strong waves may blow off the reclaimed soil if it is thin at the back. Depressurizing works may be installed in the upper part of the mound to reduce such strong mound transmitted waves. See "Design, construction and control manual for the controlled type waste disposal site (Revised)" [116] for the pressure calculation method inside the mound with depressurizing works.

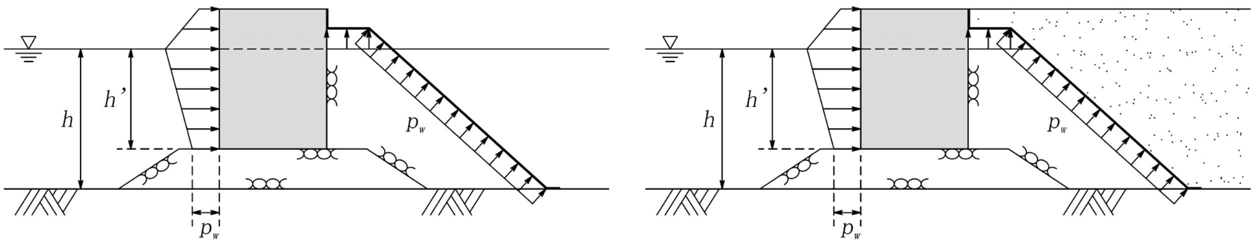

Fig. 6.5.1 Mound Transmitted Wave Pressure Applied behind the Caisson Type Seawall
(left: during construction, right: after completion)

6.5.3 Wave Pressure within Joints

The joint plates are installed behind the joints, between the caissons, to prevent the leakage of backfill stones or reclaimed soil. The impulsive wave pressure may be generated inside the joints, as shown in **Fig. 6.5.2**, when the wave surface acts on the joint plates. This wave pressure is often larger than the one acting on the front side of caisson and is expressed by **equation (6.5.1)** [115].

The stability and tensile strength of the sand leakage prevention plate can be obtained by using Takebe et al's method. [117]

Moreover, as the joint plate deforms even slightly by such wave force after construction of the seawall, sediment with small grain sizes, like sand, may leak out. Therefore, it is necessary to avoid putting reclaimed sand just behind the joint plate, but to install the back fill stones just behind the joint plate or in other ways.

$$p=2\rho_0 gH \quad \textbf{(6.5.1)}$$

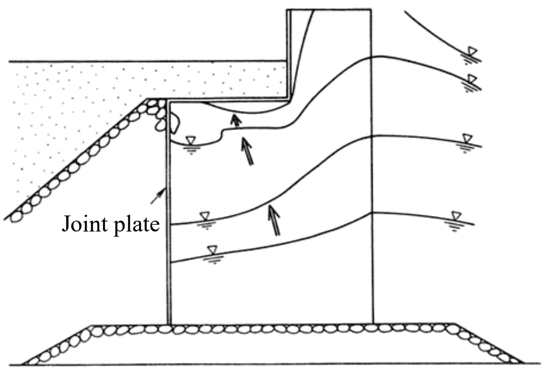

Fig. 6.5.2 Behavior of Wave Surface inside the Joint

6.6 Stability of Armor Stones and Blocks against Waves

6.6.1 Required Mass of Armor Stones and Blocks on Slope[118) 119)]

(1) General

The armor units for the slopes such as sloping breakwaters are placed to protect the rubble stones inside; it is necessary to ensure that an armor unit has a mass sufficient to be stable so that it is not scattered itself. This stable mass (the required mass) can generally be obtained by hydraulic model tests or calculations using appropriate equations.

(2) Basic Equation for Calculation of Required Mass

When calculating the required mass of rubble stones and concrete blocks covering the slope of a sloping structure which is affected by wave forces, Hudson's formula with the stability number N_S, which is shown in the following equation, may be used. [120)]

$$M = \frac{\rho_r H^3}{{N_S}^3 (S_r - 1)^3} \qquad \textbf{(6.6.1)}$$

where

M : required mass of rubble stones or concrete blocks (t)

ρ_r : density of rubble stones or concrete blocks (t/m^3)

H : wave height used in stability calculation (m)

N_S : stability number determined primarily by the shape, slope, damage rate of the armor, etc. of the armor units

S_r : specific gravity of rubble stones or concrete blocks relative to water

(3) Stability Number and Nominal Diameter

The stability number directly corresponds to the size (nominal diameter) of the armor required for a certain wave height H. Assume the nominal diameter $D_n = (M/\rho_r)^{1/3}$ and $\Delta = S_r - 1$ and substitute into **equation (6.6.1)**, a simple equation

$$H / (\Delta D_n) = N_S \qquad \textbf{(6.6.2)}$$

is obtained to show that the wave height and the nominal diameter are proportional with ΔN_S as its proportional constant.

(4) Design Wave Height *H* Used in the Performance Verification

Hudson's formula was proposed based on the results of experiments in regular waves. When applying it to the action of actual waves which are random, there is thus a problem of which definition of wave heights shall be used. However, with structures that are made of rubble stones or concrete blocks, there is a tendency for damage to occur not when one single wave having the maximum height H among a random wave train attacks the armor units, but rather for damage to progress gradually under the continuous action of waves of various heights. Considering this fact and past experiences, it has been decided to make it standard to use the significant wave height of progressive waves at the place where the slope is located as the wave height H in **equation (6.6.1)**, because the significant wave height is representative of the overall scale of a random wave train. Note however that for places where the water depth is less than one half of the equivalent deepwater wave height, the significant wave height at the water depth equal to one half of the equivalent deepwater wave height should be used.

(5) Parameters Affecting the Stability Number N_S

As shown in **equation (6.6.1)**, the required mass of armor stones or concrete blocks varies with the wave height and the density of the armor units, and also the stability number N_S. The N_S value is a coefficient that represents the effects of the characteristics of structure, those of armor units, wave characteristics and other factors on the stability. The main coefficients that influence the N_S value are as follows.

① Characteristics of the structure

(a) Type of structure; sloping breakwater, breakwater covered with wave-dissipating concrete blocks, and composite breakwater, etc.

(b) Gradient of the armored slope

(c) Position of armor units; breakwater head, breakwater trunk, position relative to still water level, front face and top of slope, back face, and berm, etc.

(d) Crown height and width, and shape of superstructure

(e) Inner layer; permeability coefficient, thickness, and degree of surface roughness

② **Characteristics of the armor units**

(a) Shape of armor units (shape of armor stones or concrete blocks; for armor stones, their diameter distribution)

(b) Placement of armor units; number of layers, and regular laying or random placement, etc.

(c) Strength of armor material

③ **Wave characteristics**

(a) Number of waves acting on armor layers

(b) Wave steepness

(c) Form of seabed (seabed slope, where about of reef, etc.)

(d) Ratio of wave height to water depth as indices of non-breaking or breaking wave condition, breaker type, etc.

(e) Wave direction, wave spectrum, and wave group characteristics

④ **Extent of damage (damage ratio, deformation level, relative damage level)**

Consequently, the N_S value used in the performance verification must be determined appropriately based on hydraulic model experiments in line with the respective design conditions. By comparing the results of regular waves experiments with those of random wave experiments, [121)] it was found that the ratio of the height of regular waves to the significant height of random waves that gave the same damage ratio, within the error of 10%, varied in the range of 1.0 to 2.0, depending on the conditions. In other words, there was a tendency for the random wave action to be more destructive than the action of regular waves. It is thus better to employ random waves in experiments.

(6) Stability Number N_S and K_D Value

In 1959, Hudson published the so-called Hudson's formula, [120)] replacing the previous Iribarren-Hudson's formula. Hudson developed **equation (6.6.1)** by himself using K_D cot α instead of stability number N_S.

$$N_S{}^3 = K_D \cot\alpha \qquad \textbf{(6.6.3)}$$

where

α : angle of the slope from the horizontal line (°)

K_D : constant determined primarily by the shape of the armor units and the damage ratio

The Hudson's formula was based on the results of a wide range of model experiments and has proved itself well in usage in-site. This formula using the K_D value has thus been used in the calculation of the required mass of armor units on a slope.

However, the Hudson's formula that uses the stability number in **equation (6.5.1)** has been used for quite a while for calculating the required mass of armor units on the foundation mound of a composite breakwater as discussed in **Part II, Chapter 2, 6.5.2 Required Mass of Armor Stones and Blocks in Composite Breakwater Foundation Mound against Waves**, and is also used for the armor units of other structures such as submerged breakwaters. It is thus now more commonly used than the old formula with the K_D value.

The stability number N_S can be derived from the K_D value and the angle α of the slope from the horizontal line by using **equation (6.5.3)**. There is no problem with this process if the K_D value is an established one and the slope angle is within a range of normal design. However, most of the K_D values obtained up to the present time have not sufficiently incorporated various coefficients like the characteristics of the structure and the waves. Thus, this method of determining the stability number N_S from the K_D value cannot be guaranteed to obtain economical design always. In order to calculate more reasonable values for the required mass, it is thus preferable to use the results of experiments matched to the conditions in question, or else to use calculation formulas, calculation diagrams, that include the various relevant coefficients as described below.

(7) Van der Meer's Formula for Armor Stones

In 1987, van der Meer carried out systematic experiments concerning the armor stones on the slope of a sloping breakwater with a high crown. He proposed the following calculation formula for the stability number, which can consider not only the slope gradient, but also the wave steepness, the number of waves, and the damage level. [122)] Note however that the following equations have been slightly altered in comparison with van der Meer's original one in order to make calculations easier. For example, the wave height $H_{2\%}$ for which the probability of exceedance is 2% has been replaced by $H_{1/20}$.

$$N_S = \max\left(N_{sp\ell}, N_{ssr}\right) \tag{6.6.4}$$

$$N_{sp\ell} = 6.2 C_H P^{0.18}\left(S^{0.2}/N^{0.1}\right) I_r^{-0.5} \tag{6.6.5}$$

$$N_{ssr} = C_H P^{-0.13}\left(S^{0.2}/N^{0.1}\right)\left(\cot\alpha\right)^{0.5} I_r^{P} \tag{6.6.6}$$

where

N_{spl} : stability number for plunging breakers

N_{ssr} : stability number for surging breaker

I_r : iribarren number ($\tan\alpha/S_{om}^{0.5}$), also called the surf similarity parameter

S_{om} : wave steepness ($H_{1/3}/L_0$)

L_0 : deepwater wavelength ($L_0=gT_{1/3}^2/2\pi$, g=9.81 m/s^2)

$T_{1/3}$: significant wave period

C_H : breaking effect coefficient {$=1.4/(H_{1/20}/H_{1/3})$}, (=1.0 in non-breaking zone)

$H_{1/3}$: significant wave height

$H_{1/20}$: highest one-twentieth wave height, see **Fig. 6.6.1**

α : angle of slope from the horizontal surface (°)

D_{n50} : nominal diameter of armor stone ($=(M_{50}/\rho_r)^{1/3}$)

M_{50} : 50% value of the mass distribution curve of an armor stone namely required mass of an armor stone

P : permeability index of the inner layer, see **Fig. 6.6.2**

S : deformation level ($S = A/D_{n50}^2$), see **Table 6.6.1**

A : erosion area of cross section, see **Fig. 6.6.3**

N : number of acting waves

The wave height $H_{1/20}$ in **Fig. 6.6.1** is for a point at a distance $5H_{1/3}$ from the breakwater, and H_0' is the equivalent deepwater wave height. The deformation level S is an index that represents the amount of deformation of the armor stones, and it is a kind of damage ratio. It is defined as the result of the area A eroded by waves, see **Fig. 6.6.3**, being divided by the square of the nominal diameter D_{n50} of the armor stones. As shown in **Table 6.6.1**, three stages are defined with regard to the deformation level of the armor stones: initial damage, intermediate damage, and failure. With the standard performance verification, it is common to use the deformation level for initial damage for N = 1000 waves. However, in case where a certain amount of deformation is permitted, usage of the value for intermediate damage may also be envisaged.

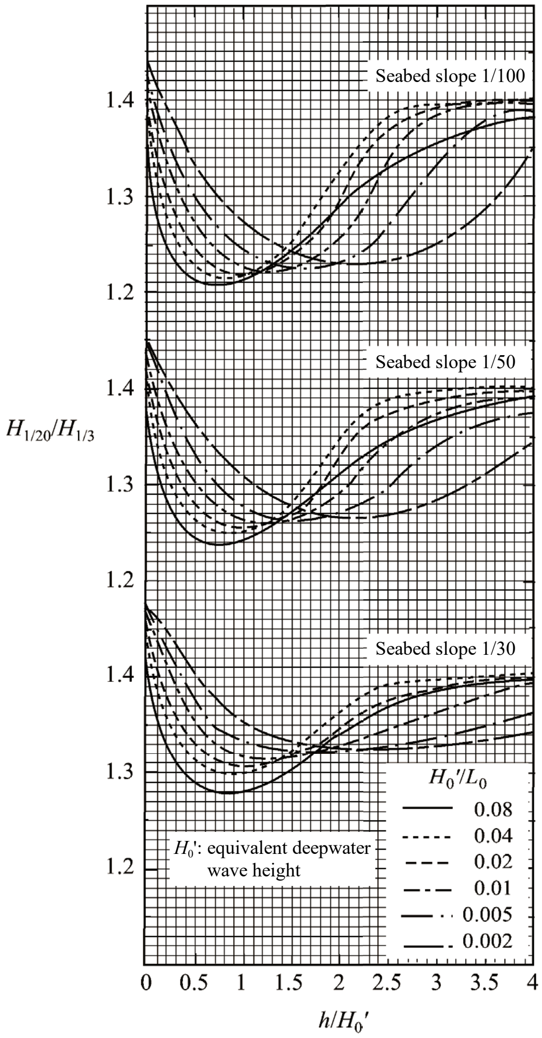

Fig. 6.6.1 Ratio of $H_{1/20}$ to $H_{1/3}$ ($H_{1/20}$ Values are at a Distance $5H_{1/3}$ from the Breakwater)

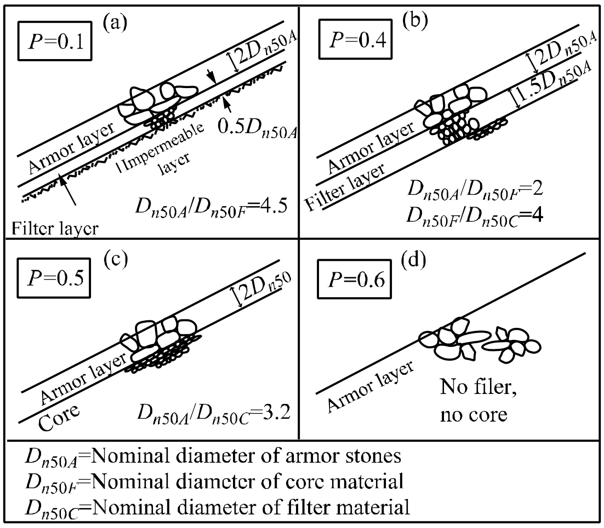

Fig. 6.6.2 Permeability Index P

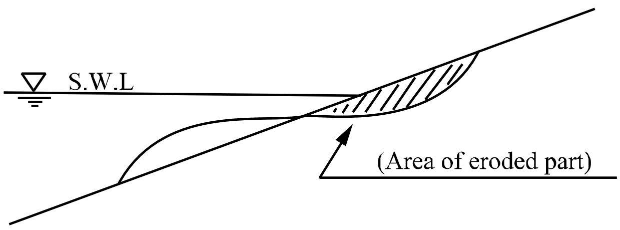

Fig. 6.6.3 Erosion Area A

Table 6.6.1 Deformation Level S for Each Failure Stage for a Two-layered Armor

Slope	Initial damage	Intermediate damage	Failure
1∶1.5	2	3–5	8
1∶2	2	4–6	8
1∶3	2	6–9	12
1∶4	3	8–12	17
1∶6	3	8–12	17

(8) Formulation for Calculating Stability Number for Armor Blocks including Wave Characteristics

Van der Meer has carried out hydraulic model experiments on several kinds of precast concrete blocks, and proposed the formulas for calculating the stability number N_S. [123] In addition, other people have also conducted research into establishing calculation formulas for precast concrete blocks. For example, Burcharth and Liu [124] have proposed a calculation formula. However, it should be noted that these are based on the results of experiments for a sloping breakwater with a high crown.

Takahashi et al. [129] showed a performance verification method of the stability against wave action for armor stones of a sloping breakwater using Van der Meer's formula as the verification formula, and proposed the performance matrix used for performance verification.

(9) Formulas for Calculating Stability Number for Concrete Blocks of Breakwater Covered with Wave-dissipating Blocks

The wave-dissipating concrete block parts of a breakwater covered with wave-dissipating blocks may have various cross sections. In particular, when almost all the front face of an upright wall is covered by wave-dissipating concrete blocks, the stability is higher than that of armor concrete blocks of an ordinary sloping breakwater because the permeability is high. In Japan, much research has been carried out on the stability of breakwaters covered with wave-dissipating concrete blocks. For example, Tanimoto et al. [126], Kajima et al. [127], and Hanzawa et al. [128] have carried out systematic research on the stability of wave-dissipating concrete blocks. In addition, Takahashi et al. [129] have proposed the following equation for wave-dissipating concrete blocks that are randomly placed in all the front face of an upright wall.

$$N_S = C_H\left\{a\left(N_0/N^{0.5}\right)^{0.2} + b\right\} \quad \textbf{(6.6.7)}$$

where

N_0 : degree of damage, a kind of damage rate that represents the extent of damage: it is defined as the number of concrete blocks that have moved within a width D_n in the direction of the breakwater alignment

D_n : nominal diameter of the concrete blocks: $D_n = (M/\rho_r)^{1/3}$, where M is the mass of a concrete block

C_H : breaking effect coefficient; $C_H = 1.4/(H_{1/20}/H_{1/3})$, in non-breaking zone $C_H = 1.0$

a, b : coefficients that depend on the shape of the concrete blocks and the slope angle. With deformed shape blocks having a K_D value of 8.3, it may be assumed that $a = 2.32$ and $b = 1.33$, if $\cot\alpha = 4/3$, and $a = 2.32$ and $b = 1.42$, if $\cot\alpha = 1.5$

Takahashi et al. [125] have further presented a method for calculating the cumulative degree of damage, the expected degree of damage, over the service lifetime. In the future, reliability design methods that consider the expected degree of damage is important as the more advanced design method. In the region where wave breaking does not occur, if the number of waves N is 1000 and the degree of damage N_0 is 0.3, the design mass as calculated using the method of Takahashi et al. is more-or-less the same as that calculated using the existing K_D value. The value of N_0 = 0.3 corresponds to the conventionally used damage rate of 1%.

(10) Increase of Mass in Breakwater Head

Waves attack the head of a breakwater from various directions, and there is a greater risk of the armor units on the top of the slope falling to the rear rather than the front. Therefore, rubble stones or concrete blocks which are to be used at the head of a breakwater should have a mass greater than the value given by **equation (6.6.1)**.

Hudson proposed increasing mass by about 10% in the case of rubble stones and about 30% in the case of concrete blocks. However, because this is thought to be insufficient, it is preferable to use rubble stones or concrete blocks with a mass at least 1.5 times the value given by **equation (6.6.1)**. Kimura et al. [130] have shown that, in a case where perpendicular incident waves act on the breakwater head, the stable mass can be obtained by increasing the required mass of the breakwater trunk by 1.5 times. In case of oblique incidence at 45°, in the breakwater head on the upper side relative to the direction of incidence of the waves, the necessary minimum mass is the same as for 0° incidence, whereas, on the lower side of the breakwater head, stability is secured with the same mass as the in the breakwater trunk.

As there is a risk of an impulsive breaking wave force at the end of wave-absorbing works, it is preferable to round the breakwater head, circumvoluting inside the port. The range is commonly set to on the order of one caisson.

(11) Mass of Submerged Armor Units

Since the action of waves on a sloping breakwater below the water surface is weaker than above the water surface, the mass of stones or concrete blocks may be reduced at depths greater than $1.5H_{1/3}$ below the still water level.

(12) Correction for Wave Direction

In cases where waves act obliquely to the breakwater alignment, the extent to which the incident wave angle affects the stability of the armor stones has not been investigated sufficiently. However, according to the results of experiments carried out by Van de Kreeke, [131] for the wave angles of 0°, i.e., direction of incidence is perpendicular to the breakwater alignment, 30°, 45°, 60° and 90°, i.e., direction of incidence is parallel to the normal line were adopted, the damage rate for a wave direction of 45° or smaller is more-or-less the same as that for a wave direction of 0°, and when the wave direction exceeds 60°, the damage rate decreases. Considering these results, when the incident wave angle is 45° or less, the required mass should not be corrected for wave direction. Moreover, Christensen et al. [132] have shown that stability increases when the directional spreading of waves is large.

(13) Strength of Concrete Blocks

In case of deformed shape concrete block, it is necessary not only to ensure that the block has a mass sufficient to be stable for the variable situation in respect of waves, but also to confirm that the block itself has sufficient structural strength.

(14) Stability of Wave-dissipating Blocks in Reef Area

In general, a reef rises up at a steep slope from the relatively deep sea, and forms a relatively flat and shallow sea bottom. Consequently, when a large wave enters at such a reef, it breaks around the slope, and then the regenerated waves afterward propagate over the reef in the form of surge. The characteristics of waves over a reef are strongly dependent on not only the incident wave conditions but also the water depth over the reef and the distance from the shoulder of the reef. The stability of wave-dissipating concrete blocks situated on a reef also varies greatly due to the same reasons. Therefore, the characteristics over a reef are more complicated than those in general cases. The stability of wave-dissipating concrete blocks situated on a reef must thus be examined based either on hydraulic model experiments matching the conditions in question or on field experiences for sites having similar conditions.

(15) Stability of Wave-dissipating Blocks on Low Crest Sloping Breakwater

For a low crown sloping breakwater covered by wave-dissipating blocks without a supporting wall, it is necessary to note that the wave-dissipating blocks around its crown in particular at the rear are easily damaged by waves. [133] For example, for detached breakwater composed of wave-dissipating blocks, unlike a caisson breakwater covered with wave-dissipating blocks, there is no supporting wall at the back and the crown is not high. This means that the concrete blocks near the crown in particular at the rear are easily damaged, and indeed such cases of block damage have been reported. In the case of a detached breakwater, it is pointed out that some kind of concrete blocks at the rear of the crown should have a larger size compared to those at the front of the crown.

(16) Stability of Blocks on Steep Slope Seabed

In cases where the bottom slope is steep and waves break in a plunging wave form, a large wave force may act on the blocks, depending on their shapes. Therefore, appropriate examination should be carried out, considering this fact. [134], [135], [136]

(17) High-density Blocks

The required mass of blocks that are made of high-density aggregate may also be determined using the Hudson's formula with the stability number shown in **equation (6.5.1)**. As shown in the equation, high-density blocks have a high stability, so a stable armor layer can be made using relatively small blocks. [137]

(18) Effect of Structural Conditions

The stability of wave-dissipating blocks varies depending on structural conditions and on the method of placement, such as regular or random placement etc. According to the results of experiments under conditions of random placement over the entire cross section and regular two-layer placement on a stone core, the regular placement with good interlocking had remarkably higher stability in almost all cases. [126] Provided, however, that if the layer of blocks is thinner and the permeability of fill material is lower, the stability of blocks actually decreases in some cases. [138]

The stability of wave-dissipating blocks is also affected by the crown width and crown height of the blocks. For example, according to the results of a number of experiments, there is a tendency of having greater stability when the crown width and the crown height are greater.

(19) Standard Method of Hydraulic Model Tests

The stability of concrete blocks is influenced by a very large number of coefficients, and so it has still not been sufficiently elucidated. This means that when actually verifying the performance, it is necessary to carry out studies using hydraulic model experiments, and it is needed to progressively accumulate the results of such tests. The following points should be noted when carrying out model hydraulic experiments.

① It is standard to carry out experiments using random waves.

② For each particular set of conditions, the experiment should be repeated at least three times i.e., with three different wave trains. However, when tests are carried out by systematically varying the mass and other coefficients and a large amount of data can be acquired, one run for each test condition will be sufficient.

③ It is standard to study the action of 1000 waves in a run for each wave height level. Even for the systematic experiments, it is desirable to apply more than 500 waves or so in a run.

④ For the description of the extent of damage, in addition to the damage ratio which has been commonly used in the past, the deformation level or the relative damage level may also be used. The deformation level is suitable when it is difficult to count the number of armor stones or concrete blocks that have moved, while the degree of damage is suitable when one wishes to represent the damage to wave-dissipating blocks. The damage rate is the ratio of the number of damaged armor units in an inspection area to the total number of armor units in the same inspection area. The inspection area is taken to whichever is shallower, the depth of $1.5H$ below the still water level or to the bottom elevation of the armor layer, where the wave height H is inversely calculated from the Hudson's formula by inputting the mass of armor units. However, for the deformation level and the degree of damage, there is no need to define the inspection area. For evaluating the damage rate, an armor block is judged to be damaged if it has moved over a distance of more than about 1/2 to 1.0 times its height.

(20) K_D Value Proposed by C.E.R.C.

Table 6.5.2 shows the K_D value of armor stones proposed by the Coastal Engineering Research Center, C.E.R.C., of the United States Army Corp of Engineers. This value is proposed for the breakwater trunk, parts other than the breakwater head, in the 1984 Edition of the C.E.R.C.'s **Shore Protection Manual**.[139)] In the table, the values not in parenthesis are based on experiment results by regular waves, and it is considered that those corresponds to 5% or less of the damage rate due to action of random waves. The values in parentheses are estimated values. For example, the value (1.2) for rounded rubble stones which are randomly placed in two-layer under the breaking wave conditions is estimated as the value which is half of 2.4, because the K_D value of two-layer angular rubble stones under the breaking waves condition is 1/2 of the value under the non-breaking wave conditions.

However, in cases where the wave height of regular waves corresponds to the significant wave height, the wave which is close to the maximum wave height of random waves acts continuously under the breaking wave condition in the regular wave experiments. Therefore, the regular wave experiment under the breaking wave condition falls into an extremely severe state in comparison with that under the non-breaking wave conditions. In random waves experiments, as described previously, it is considered that so long as the significant wave height is a standard, K_D has a tendency to increase, conversely, as the breaking wave conditions gets severe. Thus, at least it is not necessary to reduce the value of K_D under the breaking wave conditions.

Table 6.5.2 K_D Value of Rubble Stones Proposed by C.E.R.C. (Breakwater Trunk)

Type of armor	Number of layers	Placement method	K_D Breaking waves	K_D Non-breaking waves	$\cot\alpha$
Rubble stones (rounded)	2	Random placement	(1.2)	2.4	1.5–5.0
	3 or more	〃	(1.6)	(3.2)	〃
Rubble stones (angular)	2	〃	2.0	4.0	〃
	3 or more	〃	(2.2)	(4.5)	〃

( ) shows estimated values.

6.6.2 Required Mass of Armor Stones and Blocks in Composite Breakwater Foundation Mound against Waves

(1) Geneal

The required mass of armor stones and blocks covering the foundation mound of a composite breakwater varies depending on the wave characteristics, the water depth where the facility is placed, the shape of the foundation mound such as thickness, front berm width and slope angle etc., and the type of armor unit, the placement method, and the position (breakwater head or breakwater trunk), etc. In particular, the effects of the wave characteristics and the foundation mound shape are more pronounced than those of the armor stones and blocks on a sloping breakwater. Adequate consideration should also be given to the effects of wave irregularity. Accordingly, the required mass of armor stones and blocks on the foundation mound of composite breakwater shall be determined by performing hydraulic model experiments or proper calculations using an appropriate equation in reference with the results of past research and actual experiences in the field. However, the stability of the armor units covering the foundation mound of a composite breakwater is not necessarily determined purely by their mass. Depending on the structure and the arrangement of the armor units it may be possible to achieve stability even when the armor units are relatively small in mass.

(2) Basic Equation for Calculation of Required Mass

As the equation for calculation of the required mass of armor stones and blocks in the foundation mound of a composite breakwater, Hudson's formula with the stability number N_S, as shown in the following equation, can be used in the same manner as with armor stones and blocks on sloping breakwater. This partial safety coefficient is the value in cases where the limit value of the damage rate is 1% or the limit value of the degree of damage is 0.3.

$$M = \frac{\rho_r H^3}{{N_S}^3 (S_r - 1)^3} \qquad \textbf{(6.6.1) reshown}$$

This equation was widely used as the basic equation for calculating the required mass of the foundation mounds of upright walls by Brebner and Donnelly. [140)] In Japan, it is also called Brebner-Donnelly's formula. Because it has a certain degree of validity, even from a theoretical standpoint, it can also be used as the basic equation for calculating the required mass of armor unit on the foundation mound of a composite breakwater. [141)] However, the stability number N_S varies not only with the water depth, the wave characteristics, the shape of the foundation mound, and the characteristics of the armor units, but also with the position of placement, breakwater trunk, breakwater head etc. Therefore, it is necessary to assign the stability number N_S appropriately based on hydraulic model experiments corresponding to the conditions. Moreover, the wave height used in the performance verification is normally the significant wave height, and the waves used in the hydraulic model experiments should be random waves.

(3) Stability Number for Armor Stones

The stability number N_s may be obtained using the method proposed by Inagaki and Katayama, [142)] which is based on the work of Brebner and Donnelly and past damage case of armor stones. However, the following formulas proposed by Tanimoto et al. [141)] are based on the current velocity in the vicinity of the foundation mound and allow the incorporation of a variety of conditions. These formulas have been extended by Takahashi et al. [143)] so as to include the effects of wave direction.

(a) Extended Tanimoto's formulas

$$N_s = \max\left\{1.8,\ 1.3\frac{1-\kappa}{\kappa^{1/3}}\frac{h'}{H_{1/3}} + 1.8\exp\left[-1.5\frac{(1-\kappa)^2}{\kappa^{1/3}}\frac{h'}{H_{1/3}}\right]\right\} \ :\ B_M / L' < 0.25 \qquad \textbf{(6.6.8)}$$

$$\kappa = \kappa_1 (\kappa_2)_B \qquad \textbf{(6.6.9)}$$

$$\kappa_1 = \frac{4\pi h' / L'}{\sinh(4\pi h' / L')} \qquad \textbf{(6.6.10)}$$

$$(\kappa_2)_B = \max\left\{ \alpha_S \sin^2\beta \cos^2(2\pi l \cos\beta / L'),\ \cos^2\beta \sin^2(2\pi l \cos\beta / L')\right\} \qquad \textbf{(6.6.11)}$$

where

h' : water depth at the crown of rubble mound foundation excluding the armor layer (m) (see **Fig. 6.6.4**)

λ : in the case of normal wave incidence, the front berm width of foundation mound B_M (m) in the case of oblique wave incidence, either B_M or B'_M, whichever gives the larger value of $(\kappa_2)_B$ (see **Fig. 6.6.4**)

L' : wavelength corresponding to the design significant wave period at the water depth h' (m)

α_s : correction coefficient for when the armor layer is horizontal (=0.45)

β : incident wave angle, angle between the line perpendicular to the breakwater face line and the wave direction, no angle correction of 15° is applied (see **Fig. 6.6.5**)

$H_{1/3}$: design significant wave height (m)

The validity of the above formulas has been verified for the breakwater trunk for oblique wave incidence with an angle of incidence of up to 60°.

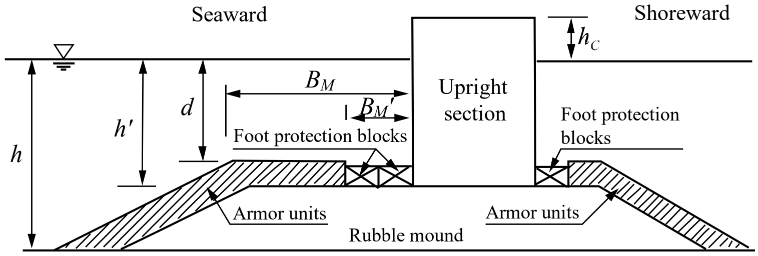

Fig. 6.6.4 Standard Cross Section of a Composite Breakwater and Notations

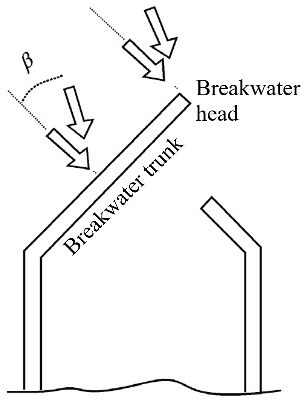

Fig. 6.6.5 Effects of Shape of Breakwater Alignment and Effects of Wave Direction

(b) Stability Number When a Certain Amount of Damage is Permitted

Sudo et al. [144] have carried out stability experiments for the special case such that the mound is low and no wave breaking occurs. They proposed the following equation that gives the stability number N_S^* for any given number of waves N and any given damage rate D_N (%).

$$N_S^* = N_S\left[D_N / \exp\{0.3(1-500/N)\}\right]^{0.25} \tag{6.6.12}$$

where N_S is the stability number given by the conventional Tanimoto's formula when N = 500 and the damage rate is 1%. In the performance verification, it is necessary to take N = 1000 considering the progress of damage, while the damage rate 3% to 5% can be allowed for a 2-layer armoring. If N = 1000 and D_N = 5%, then N_S^* = 1.44 N_S. This means that the required mass decreases to about 1/3 of that required for N = 500 and D_N = 1%, which leads to $N_S^* = N_S$.

(4) Stability Number for Concrete Units

The stability number N_S for concrete blocks varies according to the shape of the block and the method of placement. It is thus desirable to evaluate the stability number by means of hydraulic model experiments. [145] [146]

Based on the calculation method proposed by Tanimoto et al., [141] Fujiike et al. [147] newly introduced reference stability number, which is a specific value for blocks, and separating the terms which is determined by the structural conditions of the composite breakwater etc., and then, presented the following equation regarding the stability number for armor blocks in cases where wave incidence is perpendicular.

$$N_S = N_{S0} \max\left\{ 1.0,\ A\frac{1-\kappa}{\kappa^{1/2}}\frac{h'}{H_{1/3}} + \exp\left[-0.9\frac{(1-\kappa)^2}{\kappa^{1/2}}\frac{h'}{H_{1/3}}\right] \right\} \tag{6.6.13}$$

$$\kappa = \kappa_1(\kappa_2)_B \qquad \text{refer to (6.6.9)}$$

$$\kappa_1 = \frac{4\pi h'/L'}{\sinh(4\pi h'/L')}$$ **refer to (6.6.10)**

$$(\kappa_2)_B = \begin{cases} \sin^2 \dfrac{2\pi B_M}{L'} & \left(\dfrac{B_M}{L'} \le 0.15\right) \\ 1.309 - \sin^2 \dfrac{2\pi B_M}{L'} & \left(0.15 < \dfrac{B_M}{L'} \le 0.25\right) \\ 0.309 & \left(0.25 < \dfrac{B_M}{L'}\right) \end{cases}$$ **(6.6.14)**

where

N_{S0} : reference stability number

A : constant determined based on wave force experiments (= 0.525)

(5) Conditions for Application of Stability Number to Foundation Mound Armor Units

In cases where the water depth above the armor units on the mound is shallow, wave breaking often causes the armor units to become unstable. Therefore, the stability number for foundation mound armor units shall be applied only when $h'/H_{1/3}>1$, and it is appropriate to use the stability number for armor units on a slope of a slope structure when $h'/H_{1/3}\le 1$. The stability number for armor stones in the Tanimoto's formulas have not been verified experimentally in cases where $h'/H_{1/3}$ is small. Accordingly, when $h'/H_{1/3}$ is approximately 1, it is preferable to confirm the stability of the armor units by hydraulic model experiments.

On the other hand, Matsuda et al. [148] carried out model experiments in connection with armor blocks, including the case in which $h'/H_{1/3}$ is small and impulsive waves act on the blocks, and proposed a method that provides a lower limit of the value of κ corresponding to the value of the impulsive breaking wave force coefficient α_I of **equation (6.2.13)** in the case where α_I is large.

(6) Armor Units Thickness

Two-layers are generally used for armor stones. It may be acceptable to use only one layer provided that consideration is given to examples of armor units construction and experiences of damaged armor units. It also may be possible to use one layer by setting the severe damage rate of 1% for N=1000 acting waves in **equation (6.5.12)**. One layer is generally used for armor blocks. However, two layers may also be used according to the shape of the blocks or sea conditions.

(7) Armor Units for Breakwater Head

At the head of a breakwater, strong currents occur locally near the corners at the edge of the upright section, meaning that the armor units become liable to move. It is thus necessary to verify the extent to which the mass of armor units should be increased at the breakwater head by carrying out hydraulic model experiments. If hydraulic model experiments are not carried out, the mass should be increased to at least 1.5 times that at the breakwater trunk. As the extent of the breakwater head in the case of caisson type breakwater, the length of one caisson may be usually adopted. The mass of the armor stones at the breakwater head may also be calculated using the extended Tanimoto's formula. Specifically, the dimensionless velocity parameter κ in **equation (6.6.9)** should be rewritten as follows:

$$\kappa = \kappa_1 (\kappa_2)_T$$ **(6.6.15)**

$$(\kappa_2)_T = 0.22$$ **(6.6.16)**

Note however that if the calculated mass turns out to be less than 1.5 times that for the breakwater trunk, it is preferable to set the mass to 1.5 times that for the breakwater trunk.

(8) Armor Units at Harbor Side

It is preferable to decide the necessity and required mass of armor units at the harbor side, not only referring to past examples, but also performing hydraulic model experiments if necessary, under the consideration of the waves at the harbor side, the wave conditions during construction work and wave overtopping etc.

(9) Reduction of Mass of Armor

The equations for calculation of the required mass of armor units are normally applicable to the horizontal parts and the top of slope. In cases where the mound thickness is minimal, armor units of the entire slope have the same mass in many cases. However, in cases where the mound is thick, the mass of armor units placed on the slope in deep water may be reduced.

(10) Foundation Mound Armor Units in Breakwaters Covered with Wave-dissipating Blocks

In the case of breakwaters covered with wave-dissipating blocks, the uplift pressure acting on the armor and the current velocities in the vicinity of the mound are smaller than those of conventional composite breakwaters. Fujiike et al. [147)] carried out hydraulic model experiments in connection with the stabilities of both the armor units of the conventional composite breakwaters and the breakwaters covered with wave-dissipating blocks, and proposed a method of multiplying **equation (6.6.9)** by the compensation rate for breakwater shape influence. Namely,

$$\kappa = C_R \kappa_1 (\kappa_2)_B \tag{6.6.17}$$

where

C_R : breakwater shape influence coefficient, 1.0 may be used for conventional composite breakwaters and approximately 0.4 for breakwaters covered with wave-dissipating blocks.

(11) Flexible Armor Units

Using bag-type foot protection units, consisting of synthetic fiber net filled with stones, as the flexible armor units on the rubble mound has various advantages: large stones are not required, and mound leveling is almost unneeded because they have high flexibility and can adhere to the irregular sea bed. Shimosako et al. [149)] proposed a method for calculating the required mass of such armor units on the rubble mound, and also examined their durability. Moreover, a durable stone net filled with fillings in steel wires, covered with resin, may be used as armor units on the rubble mound [150)]. It is preferable to use these considering the strength of synthetic fibers or steel wires against wave actions.

6.6.3 Required Mass of Armor Stones and Blocks against Currents

(1) General

The required mass of rubble stones and other armor materials for foundation mounds to be stable against water currents may generally be determined by appropriate hydraulic model experiments or calculated using the following equation.

$$M = \frac{\pi \rho_r U^6}{48 g^3 (y)^6 (S_r - 1)^3 (\cos\theta - \sin\theta)^3} \tag{6.6.18}$$

where

M : stable mass of rubble stones or other armor material (t)

ρ_r : density of rubble stones or other armor material (t/m^3)

U : current velocity of water above rubble stones or other armor material (m/s)

g : gravitational acceleration (m/s^2)

y : Isbash's constant, for embedded stones, 1.20; for exposed stones, 0.86

S_r : specific gravity of rubble stones or other armor material relative to water

θ : slope angle in axial direction of water channel bed (°)

This equation was proposed by the C.E.R.C. for calculation of the mass of rubble stones required to prevent scouring by tidal currents and is called Isbash's formula. [139] As also shown in the equation, attention should be given to the fact that the required mass of armor units against currents increases rapidly as the current velocity increases. The required mass also varies depending on the shape and density of the armor units, etc.

(2) Isbash's Constant

Euation (6.6.18) was derived considering the balance of the drag force of the flow acting on a spherical object on a slope and the friction resistance force. The constant y is Isbash's constant. The values of 1.20 and 0.86 for embedded stones and exposed stones, respectively, are given by Isbash, and are also cited by Kudo [151]. It should be noted that, because **equation (6.6.18)** was obtained considering the balance of forces in a steady flow, it is necessary to use rubble stones with a larger mass in the place where strong vortices will be generated.

(3) Armor Units on Foundation Mound at Openings of Tsunami Protection Breakwaters

Iwasaki et al. [152] conducted experiments on 2-dimensional steady flows for the case in which deformed concrete blocks are used as the armor units on a foundation mound in the opening of the submerged breakwaters of tsunami protection breakwaters, and obtained a value of 1.08 for Isbash's constant in **equation (6.6.18)**. Tanimoto et al.[153] carried out a 3-dimensional plane experiment for the opening of breakwaters, clarifying the 3-dimensional flow structure near the opening, and also revealed the relationship between Isbash's constant and the damage rate for the cases where stone materials and deformed concrete blocks are used as the armor units.

6.7 Tsunami Wave Force

6.7.1 Tsunami Wave Force Acting on Composite Type Breakwater

(1) General

Tsunami wave force acting on composite type breakwater can be calculated according to the calculation procedure shown in **Fig. 6.7.1**, considering whether tsunami bores or overflowing exist [154].

Tsunamis can, firstly, be classified into bore condition or not. Tsunami bores, which become bore shaped by breaking of the front end of tsunamis with long wave lengths, into several short-period waves (soliton fission) may have quite large impulsive bore wave forces. Therefore, Tanimoto's formula is used in the case of no tsunmai bores. As the tsunami bores strengthen the tsunami wave force, modified Tanimoto's formula is used, corresponding to this case.

Tsunami bores occur when the seabed slope is quite gentle, while a small ratio of tsunami wave height to water depth (tsunami height / water depth) or relatively steep seabed slope does not generate bores. The soliton fission is considered generated when the incident tsunami height is 30% or more of the water depth (the height of tsunami standing waves generated by simulation or others is 60% or more of the water depth) and in a shoal with the seabed slope around 1/100 or less.

If no tsunami bores occur, but overflowing does, calculation equations, corrected by the coefficients of the hydrostatic pressures acting on the front side and rear side of a caisson, are applied. The overflowing case indicates the state that the tsunami height, calculated with the numerical simulation, exceeds the crown height of the breakwater. When a calculation equation correcting the hydrostatic pressure is applied to a slightly overflowing condition, compare the equation and Tanimoto's formula and adopt the result of larger tsunami force. Applying Tanimoto's formula to the condition just before overflowing, which is shallower in water level, may show a larger wave force.

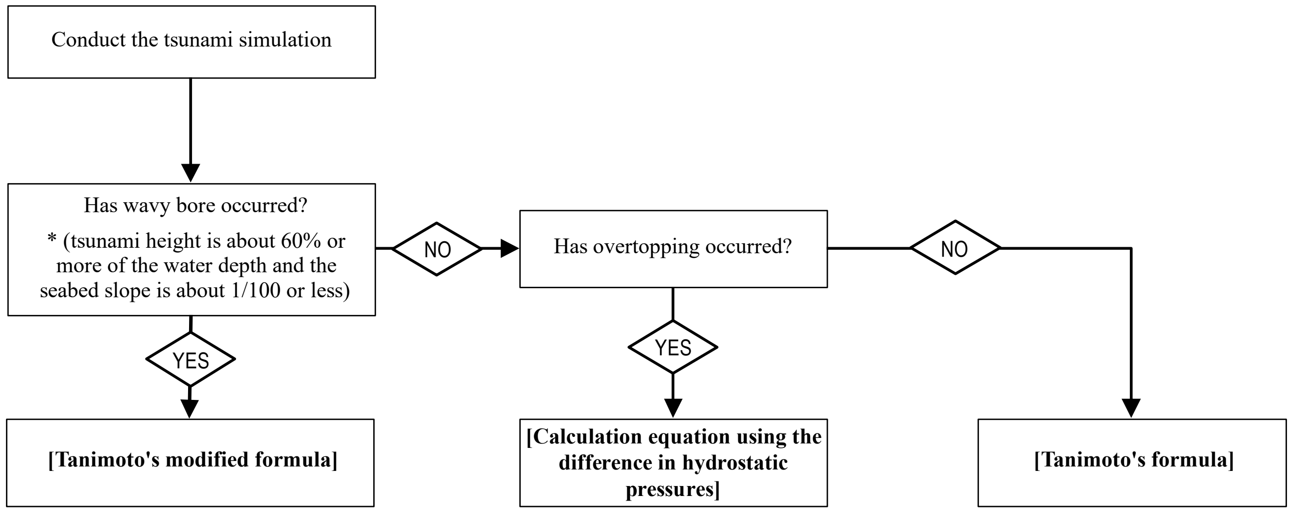

Fig. 6.7.1 Calculation Procedure of Tsunami Wave Force

The tsunami height for calculating the tsunami wave force acting on the breakwater is basically calculated using the numerical simulation result under the condition where the breakwater has been installed. The height of an incident tsunami above the still water a_I for Tanimoto's formula and modified Tanimoto's formula is used to calculate the wave force by defining the incident tsunami height as 1/2 of the tsunami height (above the still water level) numerically simulated. Here, the still water level is the standard water level for the calculation of the tsunami height on the surface on which the tsunami acts. The tsunami height is generally the water level (including the effect of reflected waves) to consider the effect of inundation, etc. Therefore, half of the tsunami height is also defined, in principle, as the incident tsunami height a_I. Since the tsunami height is generally, and often expressed in, the water level above T.P., it must be halved after converting to the height above the design tide level (normally H.W.L.).

(2) Tanimoto Method and Modified Tanimoto Method

Tsunami wave force on an upright wall may be determined as in **Fig. 6.7.2 (a)**, in which the wave pressure distribution can be assumed as a linear distribution with a value of p=0 at a height of η^* = 3.0 a_I above the still water level and a value of $p=2.2\rho_0 g a_I$ (Tanimoto method) or $p=3.0\rho_0 g a_I$ (modified Tanimoto method) at the still water level, and a constant value in the depth direction for the wave pressure below the still water level.

When the water level behind the breakwater becomes lower than the still water level, negative wave force is generated behind the breakwater, as shown in **Fig. 6.7.2 (b)**, and the distribution of the uplift pressure is a distribution obtained by linearly connecting the pressures on the front side and the rear side. The breakwater buoyancy is calculated as the volume (hatched line part), assuming that the foreside still water level extends to the rear side.

Maruyama et al. [155)] indicated that the impact force by the wave breaking of soliton fission is mitigated when the upright walls are covered with the wave-dissipating blocks.

$$\eta^* = 3.0 a_I \quad \textbf{(6.7.1)}$$

$$p_1 = \begin{cases} 2.2\rho_0 g a_I & : \text{Tanimoto's formula} \\ 3.0\rho_0 g a_I & : \text{Tanimoto's modified formul} \end{cases} \quad \textbf{(6.7.2)}$$

$$p_2 = \rho_0 g \eta_B \quad \textbf{(6.7.3)}$$

$$p_u = p_1 \quad \textbf{(6.7.4)}$$

$$p_L = p_2 \quad \textbf{(6.7.5)}$$

where

η^* : wave pressure acting height above the still water level (m)

η_B : water level behind the caisson (m)

a_I : incident tsunami height (amplitude) (m)

$\rho_0 g$: unit weight of the seawater (kN/m^3)

p_1 : wave pressure at the still water level (kN/m^2)

p_u : uplift pressure at the lower edge of the front wall of the caisson (kN/m^2)

p_2 : negative pressure on the rear side of the caisson (kN/m^2)

p_L : uplift pressure at the lower edge of the rear surface of upright walls (kN/m^2)

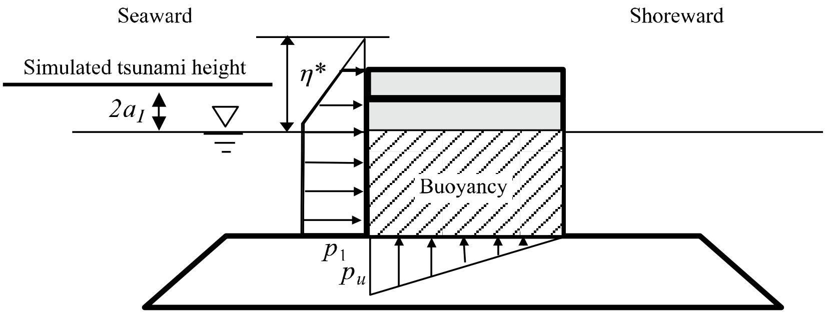

Fig. 6.7.2 (a) Tanimoto's Formula and Tanimoto's Modified Formula
(When the rear water level is not lower than the still water level)

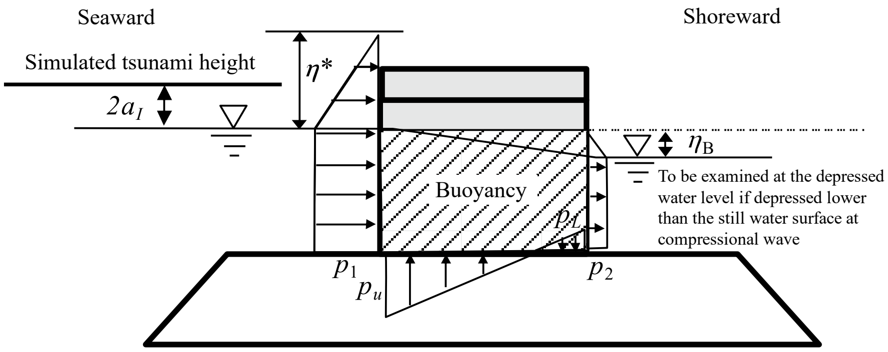

Fig. 6.7.2 (b) Tanimoto's Formula and Tanimoto's Modified Formula
(When the rear water level is lower than the still water level)

(3) Calculation Equation Using the Difference in Hydrostatic Pressure (When tsunami overflows breakwater)

When tsunamis overflow the breakwater, calculate the difference in the highest water levels between the front wall and the rear one, and confirm the breakwater's stability using the difference in hydrostatic pressure between the breakwater's front and rear water level, as shown in **Fig. 6.7.3**.

The hydrostatic pressure on the front wall shall be multiplied by α_f (= 1.05) and on the rear wall by α_r (= 0.9). The rear wall hydrostatic pressure correction coefficient α_r significantly decreases as the difference between the front water level and the rear one at upright walls increases [156]. Tsuruta et al. [157] proposed a calculation equation for the hydrostatic pressure correction coefficient, which may be referenced.

$$p_1 = \alpha_f \rho_0 g(\eta_f + h') \quad \textbf{(6.7.6)}$$

$$p_2 = \frac{\eta_f - h_c}{\eta_f + h'} p_1 \quad \textbf{(6.7.7)}$$

$$p_3 = \alpha_r \rho_0 g(\eta_r + h') \quad \textbf{(6.7.8)}$$

where

p_1 : wave pressure at the front bottom of caissons (kN/m^2)

p_2 : wave pressure at the front crown of caissons (kN/m^2)

p_3 : wave pressure at the rear bottom of caissons (kN/m^2)

$\rho_0 g$: unit volume weight of the seawater (kN/m^3)

h' : water depth at the bottom of caissons (m)

h_c : height between the still water level and the crown height of upright walls (m)

η_f : tsunami height from the still water level at the front side of upright walls (m)

η_r : tsunami height from the still water level at the rear side of upright walls (m)

α_f : hydrostatic pressure correction coefficient at the front side of upright walls

α_r : hydrostatic pressure correction coefficient at the rear side of upright walls

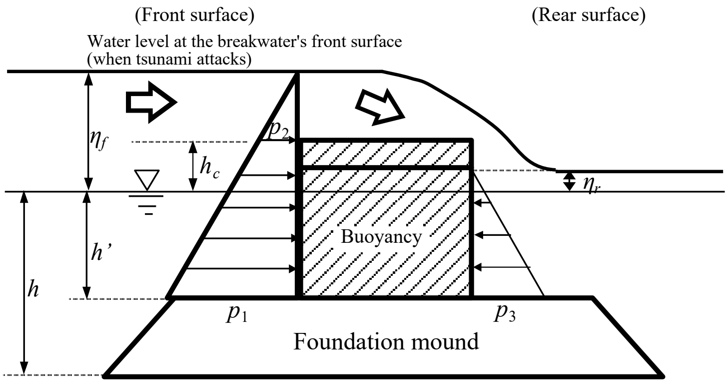

Fig. 6.7.3 Hydrostatic Pressure Difference Equation (Wave Force Equation When Tsunami Overflows Breakwater)

(a) The buoyancy shall be calculated as the submerged whole wall body (hatched line part), excluding the uplift. However, when the parapet is large, the uplift becomes large. When the overflowing velocity is large, the centrifugal force applied to the water mass at the front crown part of the upright wall decreases the pressure. In these cases, the vertical upward force may become larger than the buoyancy [158].

(b) When applying a calculation equation of the hydrostatic pressure difference to the slightly overflowing condition, compare to the case where Tanimoto's formula is applied to the condition just before overflowing and adopt a more disadvantageous case to the caisson's stability.

6.7.2 Tsunami Wave Force Acting on Onshore Upright Walls

(1) General

The tsunami wave force acting on onshore upright walls, such as the parapet, shall be calculated according to the procedure shown in **Fig. 6.7.4**, referring to the wave force calculation equation, considering the existence of tsunami overflowing in **Concept of Parapet Design Considering Tsunami (Preliminary Version)** [159].

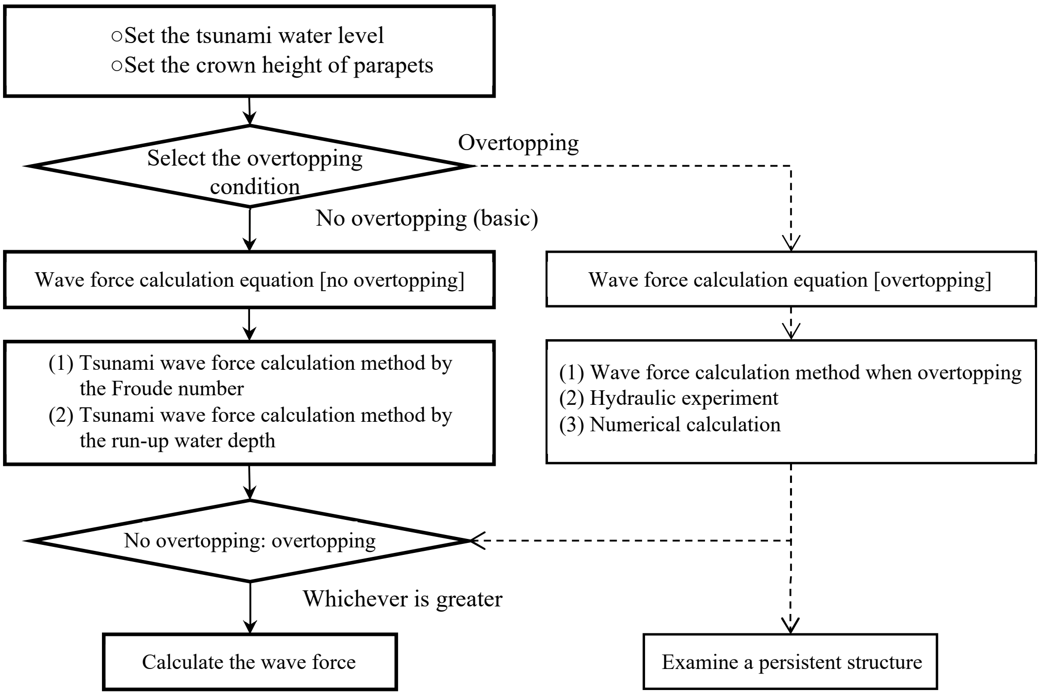

Fig. 6.7.4 Procedure for Calculating Tsunami Wave Force Acting on Parapets

(2) Tsunami wave force without overflowing

The tsunami wave force without overflowing can be calculated by using the run-up water depth or the Froude number.

① **Tsunami wave force estimating from inundation depth of tsunami standing wave**

The inundation depth η of running-up tsunami in front of upright walls shall be calculated by the tsunami run-up simulation. Then, the wave force shall be calculated from this inundation depth η, as shown in **Fig. 6.7.5**. The wave pressure acting height shall be the inudation depth η, and the acting water pressure is expressed by **equation (6.7.9)**.

$$p_1 = \alpha \rho_0 g \eta \tag{6.7.9}$$

where

p_1 : wave pressure at the lower edge of upright walls (kN/m^2)

η : inundation depth of tsunami standing wave in front of upright walls (m)

$\rho_0 g$: unit volume weight of the seawater (kN/m^3)

α : wave pressure coefficient of hydrostatic pressure (= 1.1)

However, the maximum wave pressure, significantly exceeding the hydrostatic pressure, may be generated at the bottom of the upright wall. Moreover, note that the wave pressure may exceed 1.1 times of the hydrostatic pressure when breaking tsunami acts on the upright wall.

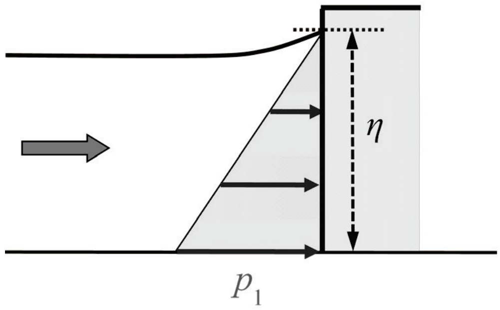

Fig. 6.7.5 Wave Pressure Distribution of Wave Force Calculation Equation without Overtopping (Tsunami Wave Force Calculation by Wall Erection Calculation)

② **Wave force estimation as progressive tsunami with Froude number**

The inundation depth of progressive tsunami shall be calculated by the tsunami inundation simulation without upright walls.

When the Froude number F_r of progressive tsunami is less than 1.5, the wave pressure is expressed by **equation (6.7.10)**. The wave pressure acting height shall be α' times the inundation depth of progressive tsunami.

$$\frac{p_{\max}}{\rho_0 g \eta_{\max}} = \alpha\left(1 - \frac{z}{\alpha' \eta_{\max}}\right) \qquad \textbf{(6.7.10)}$$

$$\alpha' = \max\{3, \alpha\} \quad \text{Coefficient of the dimensionless wave pressure acting height} \qquad \textbf{(6.7.11)}$$

where

$p_{\max}$: maximum tsunami wave pressure (kN/m^2)

$\eta_{\max}$: maximum inundation height of progressive waves (m)

$\rho_0 g$: unit volume weight of the seawater (kN/m^3)

z : height of the wave pressure acting location from the ground (m)

The dimensionless wave pressure coefficient α is given as the following equation.

$$\boldsymbol{\alpha = 1.0 + 1.35Fr^2} \quad \text{Coefficient of the dimensionless wave pressure acting height} \qquad \textbf{(6.7.12)}$$

When the Froude number F_r exceeds 1.5, examine the dimensionless wave pressure coefficient α (wave pressure acting height coefficient α' shall be 3) using the exisiting research results, hydraulic experiments, numerical calculations, etc.

If the Froude number F_r is unknown, employ the maximum water depth $\eta_{0\max}$ at the shore line as the water depth $\eta_{\max}$, and apply Tanimoto's formula (α' = 3.0, α' = 2.2) in **Part II, Chapter 2, 6.7.1 (1).**

The dimensionless wave pressure coefficient α can be calculated with the method of Ishida et al, [160] which uses the inundation depth and flow rate at the highest specific energy. As $\eta_{\max}$ and the Froude number vary according to the topography behind the parapet or existence of structures, it is preferable to consider the effects of them. [161].

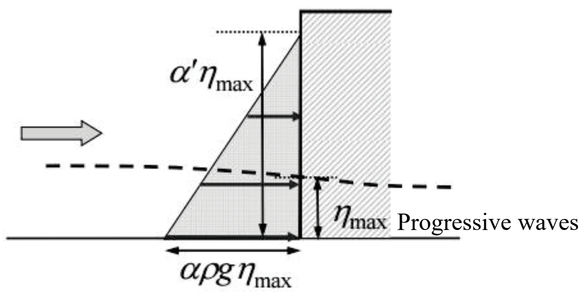

Fig. 6.7.6 Wave Force Distribution without Overtopping (Method Using the Froude Number)

③ **Uplift applied to the upright wall**

The upright wall is subjected to the uplift when there is rubble mound beneath it.

(3) Tsunami wave force during overflowing

The tsunami wave force during overflowing shall be calculated as shown in **Fig. 6.7.7** by using the water levels at the front and rear sides of the upright wall. The water levels are calculated by tsunami inundation simulation.

① **Wave pressure on front side**

$$p_1 = \alpha_1 \rho_0 g \eta \quad \textbf{(6.7.13)}$$

$$p_2 = p_1(\eta - h_C)/\eta \quad \textbf{(6.7.14)}$$

The value of α_1 shall be calculated by the following equation when using the water depth η at the foot of a front slope of the wall.

$$\alpha_1 = -0.17 h_C/\eta + 1.27 \qquad 0.4 \le h_C/\eta < 1.0 \quad \textbf{(6.7.15)}$$

The value of α_1 shall be given by the following equation when using the offshore water level η_0 (where the water level varies little).

$$\alpha_1 = 1.1 \quad \textbf{(6.7.16)}$$

② **Wave pressure on rear side**

$$p_3 = \alpha_{1B} \rho_0 g \eta^* \quad \textbf{(6.7.17)}$$

$$p_4 = p_3(\eta^* - h_{CB}{}^*)/\eta^* \quad \textbf{(6.7.18)}$$

$$h_{CB}{}^* = \min\{\eta^*, h_C\} \quad \textbf{(6.7.19)}$$

Here, the water level at the rear η_B shall be used as water depth η^*. Note that the wave pressure at the rear differs by the effect of topography behind, etc.

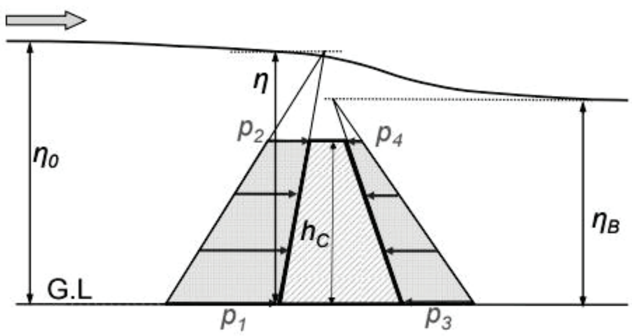

Fig. 6.7.7 Wave Pressure Distribution during Tsunami Overflowing

③ **Vertical force**

Although the water pressure is applied to the upper part of the upright wall during tsunami overflowing, it is reduced by the effect of centrifugal force when the overflowing velocity is fast. Also, the uplift force acts on the bottom face of the upright wall when there is rubble mound under the upright walls.

④ **Wave force applied to the ground behind**

Naito et al. [162] may be referred to for the tsunami overflowing force applied to the ground behind the wall.

6.7.3 Required mass for an armor unit against the tsunami overflowing

(1) General

Rubble mound and armor works behind the upright wall may be scoured by tsunami overflowing. As the overflowing phenomenon changes intricately in accordance with the shape of the upright wall, the required mass of armor units shall basically be obtained by the hydraulic model experiments. However, if the upright wall shape is relatively simple, the following method may be used to verify the required mass.

(2) Calculation using the Isbash formula

The required mass can be verified by obtaining the overflow velocity acting on the armor works through hydraulic model experiments or numerical simulations and by using the Isbash formula explained in **Part II, Chapter 2, 6.5.3, Required Mass of Armor Stones and Blocks against Currents** [163] [164].

(3) Stability number against overflowing

The required mass may also be verified using the stability number N_s against the overflowing shown below [165]. In this case, the required mass of the armor works against overflowing shall be calculated with the following equations.

$$M = \rho_r D_n^3 \qquad \textbf{(6.7.20)}$$

$$D_n = \frac{h_1}{(\rho_r / \rho_w - 1) N_S} \qquad \textbf{(6.7.21)}$$

Here, ρ_w and ρ_r are the density of seawater and concrete, respectively. D_n is the nominal diameter of armor works and is the cube root of the armor unit volume. h_1 is the overflowing depth shown in **Fig. 6.7.8**.

The stability number N_s is the function of ratio B/L, where B is the mound crown width, L is the driving position of overtopping shown in **Fig. 6.7.8**, and the ratio d_2/d_1 where d_2 is the height between the mound crown height and the still water level, d_1 is the height between the caisson crown height and the still water level, and is calculated using the calculation diagram obtained from experiments per various armor units. The manual for required mass calculation of armor works on the additional rubble mound behind the breakwater against tsunami overflowing describes calculation diagrams for various armor units[166].

The driving position of overflowing L can be calculated by the following equations.

$$u_2 = q/h_2 = 0.35 \frac{h_1}{h_2} \sqrt{2gh_1} \qquad \textbf{(6.7.22)}$$

$$h_2 = rh_1 \qquad \textbf{(6.7.23)}$$

$$x_3 = u_2 \sqrt{2(d_1 + h_2/2)/g} \qquad \textbf{(6.7.24)}$$

$$u_{3x} = u_2 \qquad \textbf{(6.7.25)}$$

$$u_{3z} = \sqrt{2g\left(d_1 + h_2/2\right)} \qquad \textbf{(6.7.26)}$$

$$L = x_3 + (u_{3x}/u_{3z})d_2 \tag{6.7.27}$$

Here, q is the overflowing rate, r is the ration of overflowing depth expressed as $r = h_2/h_1$. The above equations can be applied when $h_1/B < 0.5$. $r = 0.42$ to 0.45, or the following calculation equation can be used for the ratio of overflowing depth r [156].

$$r = 0.43 + 0.324 \times (h_1 / B) - 0.5 \tag{6.7.28}$$

However, as the ratio of overflowing depth r needs caution against versatility and applicability to various structures, the driving position of overtopping L shall be estimated preferably with the aid of numerical simulation, such as CADMAS-SURF [1].

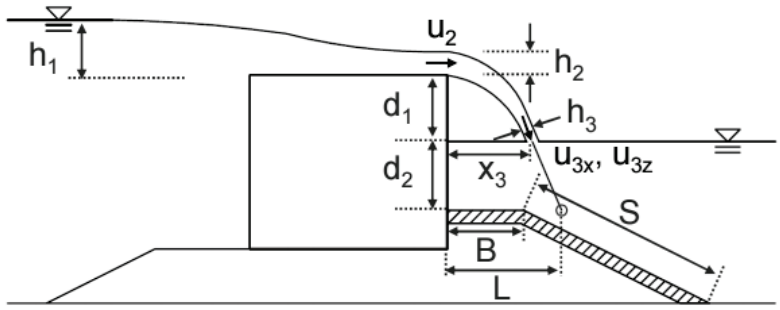

Fig. 6.7.8 Definition of Variables for Calculation Equation of the Mass Required for Armor Blocks

(4) Stability of armor works where overflowing concentrates

The concentrated overflowing may increase the flow rate acting on the armor works at the corner of breakwater or where the breakwater width becomes discontinuous [167]. When verifying the blocks' stability, it is preferable to estimate the flow velocity with the numerical simulation and verify the stability using the Isbash formula, or estimate the stability with the hydraulic model experiments.

6.8 Wave Force during Storm Surge

6.8.1 When the Tide Level during Storm Surge is Lower than the Crown Height of Structures

(1) Simultaneous action of storm surges and high waves

During storm surges, the storm surges and high waves generally act on structures at the same time. Therefore, the water pressures increased by the storm surge, and the wave one due to high waves, simultaneously act on the protective facilities for the harbor, such as breakwaters, seawalls, dikes, and parapets. When verifying this stability, calculate the increased hydrostatic pressure due to storm surges, and the wave pressure due to high waves, as shown in **Fig. 6.8.1**.

However, because of the effect of seabed topography or the rubble mound in front of structures, the wave force most disadvantageous to structures does not necessarily occur when the tidal level is highest, but the broken wave may generate stronger impulsive wave force at the lower tidal level (**Part II, Chapter 2, 6.2.4, Impulsive Breaking Wave Force**). Therefore, it is necessary to calculate the wave force by varying the tidal levels from low tide to the highest water level during storm surge.

Moreover, when the wave-dissipating blocks do not shield the front surface wall up to its crown height, the increased tide level makes the wall surface an incompletely shielded cross section and generates the impulsive wave force (**Part II, Chapter 2, 6.2.5 Wave Force Acting on Upright Wall Covered with Wave-dissipating Concrete Blocks**) and may break the parapet. The front surfaces of shore seawalls or revetments, in particular, are often shielded incompletely and may apply strong impulsive wave forces to the parapet. Therefore, it is preferable to verify the stability of the whole parapet or the strength of internal arrangement of reinforcement bars [168].

The seawalls, dikes, and parapets have intricated cross sections due to topography at the front surface of structures, hinterland utilization, or others, which often make it difficult to calculate the wave force. Therefore, it is preferable, in principle, to conduct a hydraulic model experiment to calculate the wave force.

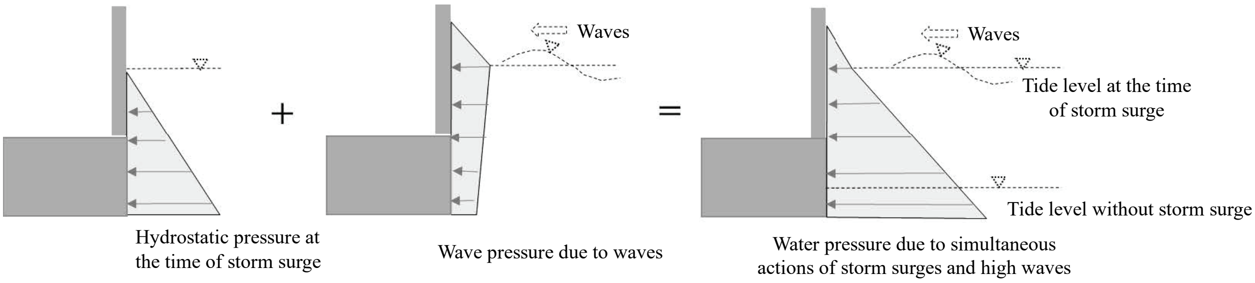

Fig. 6.8.1 Wave Pressure Distribution during Stomr Surge

(2) Uplift and mound transmitted waves applied to gravity-type structures at storm surges

The increased hydrostatic pressure (or buoyancy), due to storm surges, and the uplift, due to high waves, simultaneously act on the bottom part of wall body of the caisson type or block type breakwater. Therefore, these vertical upward pressures shall be considered when verifying breakwater stability. On the other hand, the increased hydrostatic pressure, due to storm surges, and the mound transmitted wave pressure, due to high waves (**Part II, Chapter 2, 6.5 Mound Transmitted Wave Pressure and Wave Pressure within Joints Acting on behind the Revetments**), occur simultaneously inside the rubble mound or backfill stones behind the caisson type or block type seawall. Therefore, the hinterland ground stability shall be verified as the reclamation ground in the upper part of the backfill stones may be uplifted by this pressure and broken [169]. The seawater may invade the hinterland through the mound when the ground height behind the seawall is lower than the tide level during storm surges.

(3) Wave overtopping

If the storm surge raises the tidal level higher than the design high water level, the amount of wave overtopping increases and may break pavement behind the structures. To prevent these phenomena, the crown height of seawall shall be verified so the permissible amount of wave overtopping is not exceeded.

6.8.2 When the Tide Level during Storm Surge is Higher than the Crown Height of Structures

If the tidal level during storm surge is higher than the crown height of structures, the overflowing and wave overtopping occur at the same time, and the massive seawater flows in behind the coastal defenses to cause huge flood damage [169]. Furthermore, increased hydrostatic pressure due to storm surge, and the wave force due to high waves, simultaneously act on the lower part of and behind the structures, and the seawater may permeate the mound and inundate the hinterland. As these phenomena intricately vary according to the shape of structures and usage condition of hinterland, it is preferable to conduct a hydraulic model experiment for calculating the wave force or the amount of overtopping. Moreover, as the storm surge continues for a long time, it is preferable to verify to avoid scouring, or leakage of reclaimed soil, from the sandy ground behind the seawall.

It is necessary to append toughness to structures to cope with such storm surges exceeding the design tide level. One simple and indirect rule of thumb for "toughness" can be the degree of margin for the simultaneous action of the hydrostatic pressure at the time of storm surge, and the force of high waves in the verification equation of sliding and overturning of wall body, the strength of reinforcing bars inside the parapet and others, i.e., the level of safety coefficient exceeding 1.0.

Moreover, a construction method to avoid failures of coastal defenses in the elongation direction by installing an intervening wall in the elongation direction of revetments or seawalls as a tough structure [170] may be an option.

[References]

1) Study Group on application of numerical wave tank to structural design against waves: Study and development of numerical wave channel, Coastal Development Technology Library, CDIT, pp. 156-163, 2001

2) Koji Kawasaki, Sho Matsuura and Taiki Sakatani: Validation of Free Surface Analysis Method in Three-Dimensional Computational Fluid Dynamics Tool “OpenFOAM”, J.JSCE, Ser.B3, Ocean Engineering, I_748-I_753

3) Hitoshi Gotoh・Kojiro Suzuki・Hiroyuki Ikari・Taro Arikawa・Abbas Khayyer・Naoki Tsuruta: Development ofParticle-Based Numerical Wave Flume for Multiphase Flow Simulation, J.JSCE, Ser.B2, Coastal Engineering, I_25-I_30.

4) Mitsuyasu, H. : Theory of wave pressure, Summer Training on Hydraulic Engineering B Coast and Harbour 1965, Hydraulic Committee, JSCE pp. B-16-1-B-16-25, 1965

5) ITO, Y. M. FUJISHIMA and T. KITATANI: ON THE STABILITY OF BREAKWATERS, Rept. Of PHRI Vol. 5 No. 4, p. 134, 1966

6) Goda, Y.: Wave forces on port facilities, Lecture Note of Summer Training on Hydraulic Engineering B Coast and Harbour 1967, Hydraulic Committee, JSCE pp. B-10-1-B-10-34, 1967

7) Tanimoto, K: Wave forces on composite breakwaters, Proceeding of Lecture Meeting of PHRI 1976, pp. 1-26, 1976

8) Goda, Y.: Motion of Composite Breakwater on Elastic Foundation under the Action of Impulsive Breaking Wave Pressure, Rept. Of PHRI Vol. 12 No. 3, pp. 31-69, 1973

9) Tanimoto, K, K. Moto, S. Ishizuka and Y. Goda: Discussions on formula of design wave forces on breakwaters, Proceedings of 23rd Coastal Eng. JSCE pp. 11-16, 1976

10) Takahashi, S., K. Tanimoto, K. Shimosako and T. Hosoyamada: Proposal of Pressure coefficient of impact-breaking waves on composite type breakwater considering foundation mound profile, Proceedings of Coastal Eng. JSCE Vol. 39, pp. 676-680, 1992

11) G. Sainflou: Essai sur les diques maritimes verticales, Annales des Ponts et Chaussees, Vol. 98, No. 1, pp.5–48, 1928

12) I. Hiroi: On a method of estimating the force of waves, Journal of School of Engineering, Tokyo Imperial University, Vol. X, No. 1, p. 19, 1919

13) Kuroda, S. and T. Ishiwata: Disaster Prevention Engineering, Sankaido Publishing Co., 1960, 276p

14) Nagai, K, T. Ozawa, Y. Hishira and T. Nishimura: Characteristics of field waves having a bi-modal wave spectrum generated by typhoon, Proceeding s of 33rd Coastal Eng. JSCE, pp. 144-148, 1986

15) Tanimoto, K, K. KIMURA, A. P. dos Santos Pinto: Random Wave Forces and Design Wave Periods of Composite Breakwaters under the Action of Double Peaked Spectral Waves, Rept of PHRI Vol. 25 No. 2, pp. 3-25, 1986

16) Nakata, K. K. Terauchi, H. Nishida and I. Umeki: Characteristics of low crest breakwaters, Proceedings of 31st Coastal Eng. JSCE, pp. 532-536, 1984

17) Mizuno, Y. Y. Sugimoto, K. Kimura, K. Yamanaka and S. Kikuchi: Study of Characteristics of wave force on high crest breakwaters, Proceedings of Coastal Eng. JSCE Vol. 40, pp. 721–725, 1993

18) TANIMOTO, K., K. KIMURA: A Hydraulic Experimental Study on Trapezoidal Caisson Breakwaters, Technical Note of PHRI No. 528, p. 28, 1985

19) Keiji Esaki・Tomotsuka Takayama・Tae-Min Kim・Masaki Arai: Experimental Investigation of Uplift and Compressive Pressures on a Footing of a Hybrid Caisson, Proceedings of Civil Engineering in the Ocean,Vo.20, p.73-78, 2004.

20) Keiji Esaki・Tomotsuka Takayama・Tomohiro Yasuda : Verification of Wave Pressure Acting on a Breakwater with Footing, Proceedings of Civil Engineering in the Ocean,Vo.22, p.319-324, 2006.

21) Nagai, S, T. Kubo and K. Tokikawa: Study on Steel pile breakwater (First Report)Proceeding of Coastal Eng, JSCE, pp. 209-218, 1965

22) Hayashi, T, T. Kano, M. Shirai and S. Hattori: Hydraulic characteristics of cylindrical permeable breakwaters, Proceeding of 12th Coastal Eng. JSCE, pp. 193-197, 1965

23) Goda, Y. and S. Kakizaki: STUDY ON FINITE AMPLITUDE STANDING WAVES AND THEIR PRESSURES UPON A VERTICAL WALL, Repot of PHRI Vol. 5 No. 10, pp. 1-57, 1966

24) TANIMOTO, K., S. TAKAHASHI and T. KITATANI: Experimental Study of Impact Breaking Wave Forces on a Vertical wall Caisson of Composite Breakwater, Rept of PHRI Vol. 20 No. 2, pp. 3-39, 1981

25) H. Mitsuyasu: Experimental study on wave force against a wall, Report of Trans. Tech. Res. Inst. No. 47, pp.1-39, 1962

26) Honma, M., K. Horikawa and N. Hase: Wave forces on sea dikes, Proceeding of 9th Coastal Eng. JSCE, pp. 133-137, 1962

27) MORIHIRA, M. S. KAKIZAKI and T. KIKUYA: EXPERIMENTAL STUDY ON WAVE FORCE DAMPING EFFECTS DUE TO DEFORMED ARTIFICIAL BLOCKS, Rept. PHRI Vol. 6 No. 4, pp. 3-31, 1967

28) GODA, Y. and S. HARANAKA: Title AN EXPERIMENT ON THE SHOCK PRESSURE OF BREAKING WAVES, Technical Note of PHRI No. 32, pp. 1-18, 1967

29) Horikawa, K. and Y. Noguchi: Relationship between breaker pressure and wave profile acting on a vertical wall, Proceeding of 17th Coastal Eng. JSCE, pp. 177-184, 1970

30) Fujisaki, H, A. Sasada and Y. Takahashi: Discussion on the construction techniques of breakwaters on steep slope sea bed, Proceeding of Chubu Branch of JSCE, pp. 181-183, 1996

31) TAKAHASHI, S., K. TANIMOTO and S. SUZUMURA: Generation Mechanism of Impulsive Pressure by Breaking Wave on a Vertical Wall, Rept of PHRI, Vol. 22 No. 4, pp. 3-31, 1983

32) Shimosako, K and N. Osaki: Study on the Application of the Calculation Methods of Wave Forces acting on the Various Type of Composite Breakwaters, Technical Note of PHRI, No. 1107, pp. 1-14, 2005

33) Goda, Y: Motion of Composite Breakwater on Elastic Foundation under the Action of Impulsive Breaking Wave Pressure, Rept. Of PHRI, Vol. 12 No. 3, pp. 3-29, 1973

34) Takahashi, S., K. Shimosako, T. Uwabe and K. Tanimoto: Dynamic response of composite type breakwaters to impact breaking waves, Proceedings of Coastal Engineering JSCE, Vol. 40, pp. 766-770, 1993

35) Tanimoto, K, M. Osato, S. Takaoka, T. Uchida and T. Ikada: An experiment on stability of breakwaters with wave-absorbing blocks against random waves, Proceedings of the 26th Coastal Eng., JSCE, pp. 343-347, 1979

36) TANIMOTO, K. S. TAKAHASHI and, K. MIYOSE: Title Experimental Study of Random Wave Forces on Upright Sections of Breakwaters, Repot of PHRI Vol. 23 No. 3, pp. 47-100, 1984

37) TAKAHASHI, S. K. TANIMOTO and K. SHIMOSAKO: Title Wave and Block Forces on a Caisson Covered with Wave Dissipating Blocks, Rept. Of PHRI Vol. 29 No. 1, pp. 54-75, 1990

38) Sekino, T., T. Kadono and T. Imoto: Study on design methods for wave-absorbing block armored breakwaters having unarmored parapet, Journal of Public Works Research Institute, Hokkaido Regional Development Bureau No. 397, pp. 14-20, 1986

39) Tanaka, H., N. Abe and M. Kato: Evaluation of horizontal wave force on wave-absorbing block armored caisson breakwater. Proceedings of the 32nd Conference on Coastal Eng. JSCE, pp. 490-494, 1985

40) TANIMOTO, K. and R. OJIMA: Title Experimental Study of Wave Forces Acting on a Superstructure of Sloping Breakwaters and on Block Type Composite Breakwaters, Technical Note of PHRI No. 450, p. 32, 1983

41) Hiromoto, F., H. Nishijima, S. Konno and I. Kimura: Load of blocks of wave-observing block armored breakwaters under wave actions, Proceedings of the 40th Conference on Coastal Eng. JSCE, pp. 347-351, 1983

42) Yuichiro Kawabata・Ema Kato・Mitsuyasu Iwanami : A Study on the Design Method of RC Caissons for Breakwaters against Impact Loads Considering Maintenance Strategy, Technical Note of PARI, No.1279, 56p., 2013.

43) Kougamu, Y. and K. Tokikawa: Experimental study on the wave-pressure decreasing effect of wave absorbing blocks during the construction, Report of the Public Works Research Institute (PWRI), Hokkaido Regional Development Bureau (HRDB) No. 53, pp. 81-95, 1970

44) Shiomi, M., H. Yamamoto, A. Tsugawa, T. Kurosawa and K. Matsumoto: Damages and countermeasures of breakwaters due to the wave force increase at discontinuous points of wave-absorbing blocks, Proceedings of the 41st conference on Coastal Eng. JSCE, pp. 791-795, 1994

45) Shigeo Takahashi・Yasunori Ohki・Ken-ichiro Shimosako・Sadao Isayama・Kunirou Ishinuki : Seawall Failures by Typhoon 9918 and Their Reproduction in Wave Flume Experiments, Technical Note of PARI, No.973, 50p., 2000.

46) T. Hosoyamada, S. Takahashi and K. Tanimoto: Application of sloping top caisson breakwater at isolated islands, proceedings of Conference on Coastal Eng. JSCE, Vol. 41, pp. 325-329, 1994

47) Morihira, M. and O. Kunita: A model experiments on hydraulic characteristics of sloping breakwater, Proceedings of the 26th Conference on Coastal Eng. JSCE, pp. 295-298, 1979

48) Sato, T. N. Yamagata, M. Furukawa, S. Takahashi and T. Hosoyamada: Hydraulic characteristics of sloping-top breakwaters armored with wave-absorbing blocks- Development of a new structural type of breakwaters in deep water area in Naha Port, Proceedings of Coastal Eng. JSCE Vol. 39, pp. 556-560, 1992

49) Katayama, H., T. Sekimoto, Y. Kawamata and K. Ueki: On wave force characteristics acting on submerged sloping-top caisson breakwaters, Proceedings of Coastal Eng. JSCE Vol. 45, pp. 776-780, 1998

50) TAKAHASHI, S., K. SHIMOSAKO and H. SASAKI: Title Experimental Study on Wave Forces Acting on Perforated Wall Caisson Breakwaters Rept of PHRI Vol. 30 No. 4, pp.3-34, 1991

51) TANIMOTO, K., S. HARANAKA, E. TOMIDA, Y. IZUMIDA and S. SUZUMURA : Title A Hydraulic Experimental Study on Curved Slit Caisson Rept of PHRI Vol. 19 No. 4, pp. 3-53, 1980

52) TANIMOTO, K., S. TAKAHASHI and T. MURANAGA : Title Uplift Forces on a Ceiling Slab of Wave Dissipating Caisson with a Permeable Front Wall- Analytical Model for Compression of an Enclosed Air Layer-, Rept of PHRI Vol. 19 No. 1, pp. 3-31, 1980

53) TAKAHASHI, S. and K. TANIMOTO: Title Uplift Forces on a Ceiling Slab of Wave Dissipating Caisson with a Permeable Front Wall (2nd Report)-Field Data Analysis- Rept of PHRI Vol. 23 No. 2, pp. 3-25, 1984

54) ITO, FY. And K. TANIMOTO: Title Meandering Damages of Composite Type Breakwaters. Technical Note of PHRI No. 112, pp. 13, 1971

55) Kougami, Y., N. Fujiki and Y. Uehara: An experiment on wave height and pressure at a corner of breakwater, Journal of Public Works Research Institute (PWRI), Hokkaido Regional Development Bureau (HRDB) No. 218, pp. 1-11, 1971

56) Y. Kougami, N. Fujiki and T. Tsutsumi: An experiment on wave height and pressure at a corner of breakwater (Second Rep.), Journal of Public Works Research Institute (PWRI), Hokkaido Regional Development Bureau (HRDB) No. 230, pp. 1-13, 1972

57) Goda, Y, T. YOSHIMURA and M. ITO: Reflection and Diffraction of Water Waves by an Insular Breakwater, Rept of PHRI Vol. 10 No. 2, pp.3-52, 1971

58) ITO, Y., K. TANIMOTO, K. KOBUNE, T. KITATANI and M. TODOROKI: Title An Experimental Investigation of Upright Breakwaters on Reefs, Technical Note of OHRI No. 189, p. 18, 1974

59) Tominaga, M. and I. Kuzumi: braking wave pressure on coastal dikes, Proceedings of the 18th Conference on Coastal Eng. JSCE, pp. 215-221, 1971

60) Coastal Engineering Research Center, Shore Protection Manual Vol. II, Department of Army Corps of Engineers, 1984

61) JSCE Edition: Guideline and commentary for design of Offshore Structures (Draft), JSCE, pp. 28-53, 1973

62) J. R. Morison, M. P. O. Brien, J. W. Johnson, S. A. Schaaf: The force exerted by surface waves on piles, Petroleum Trans., 189, TP 2846, pp. 149–154, 1950

63) T. E. Stelson and F. T. Mavis: Virtual mass and acceleration in fluids, Proc, ASCE., Vol. 81, Separate No. 670, pp. 670-1–670-9, 1955

64) Hamada, H., Mitsuyasu, H. and N. Hasegawa: Wave forces on structures, Proceedings of the 3rd Conference on Coastal Eng. JSCE, pp. 67-83, 1956

65) Keulegan, G. H. and L. H. Carpenter: Forces on cylinders and plates in an oscillating fluid, Journal of the National Bureau of Standards, Vol. 60, No. 5, pp. 423–440, 1958.

66) Sarpkaya, T.: Forces on cylinders and spheres in a sinusoidally oscillating fluid, Journal of Applied Mechanics, Trans. of ASME, Vol. 42, No. 1, pp. 32-37, 1975

67) Sarpkaya, T.: In-line and transverse forces on cylinders in oscillatory flow at high Reynolds number, Proc. of the Offshore Technology Conference, Vol. II, pp. 95-108, 1976

68) Sarpkaya, T., N, J. Collins and S.R. Evans: Wave forces on rough-walled cylinders at high Reynolds numbers, Proc. Of OTC, Vol. III, #2901, pp. 167-184, 1977

69) Y. Goda: Wave-forces on a vertical circular cylinder; Experiments and proposed method of waveforce computation, Report of P.H.T.R.I., No. 8, p. 74, 1964

70) Yamaguchi, M.: Fundamental study on wave forces on sphere and standing waves, Kyoto Univ. Dissertation, p. 147, 1974

71) Nakamura, M.: Study on wave forces on coastal structures and their dynamic response, Osaka Univ. Dissertation, p. 297, 1977

72) Chakrabarti, S.K., A.L. Wollbert, and A.T. William: Wave forces on vertical circular cylinder, Journal of Waterways, Harbors and Coastal Engineering Division, ASCE, Vol. 102, No.WW2, pp. 203-221, 1976

73) Chakrabarti, S.K.: Inline forces on fixed vertical cylinder in waves, Journal of the Waterway, Port, Cow and Ocean Division, ASCE, Vol. 106, WW2, pp. 145–155, 1980

74) Koterayama, W. and M. Tashiro: Wave forces on semi-submerged horizontal cylinder in diagonal incident wave and vertical cylinder in deep water waves, Report of Research Institute for Applied Mechanics Kyushu Univ. Vol. 50, pp. 35-61, 1979

75) Oda, K.: Wave forces on structures- Cylindrical structures-, Lecture note of Summer training for Hydraulic Engineering 1982, (18th) Course B, Hierodulic Committee of JSCE, pp. B-4-1-B-5-27, 1982

76) Mizuno, Y. T. Kadono, Y. Nagai, O. Momose and T. Sekino: Field experiment on offshore structure in a rough sea zone, Rept. of the Public Works Research Institute (PWRI), Hokkaido Regional Development Bureau (HRDB) No. 87, p. 77, 1988

77) Kim, Y. Y. and H. C. Hibbard: Analysis of simultaneous wave force and water particle velocity Measurements, Proc. of OTC, Vol. 1, No. 2192, pp. 461-469, 1975

78) Ogusu, A.: Wave forces on multiple row cylinders, Proceedings of the Society of Naval Architects of Japan No. 131, 1972

79) Nakamura, H. and N. Abe: Hydraulics of intake tower of power plant, Proceedings of the 19th Conference on Coastal Eng. JSCE, pp. 391-394, 1972

80) GODA, Y. S. HARANAKA and M. KITAHATA: Title STUDY OF IMPULSIVE BREAKING WAVE FORCES ON PILES, Rept of PHRI Vol. 5 No. 6, pp. 1-30, 1966

81) TANIMOTO, K. S. TAKAHASHI, T. KANEKO, K. SHIOTA and K. OGURA: Title Experimental Study on Impulsive Forces by Breaking Waves on Circular Cylinder Rept of PHRI Vol. 2 No.2, pp. 33–87, 1986

82) Goda, Y.: Design of marine structures- wave forces-, Jour. of JSCE Vo55 No. 9, pp. 2-7, 1970

83) Nagasaki, S. and K. Ogata: Wave forces on underwater pipelines (First Rept.), Proceedings of the 18th Conference on Coastal Eng. JSCE, pp. 223-227, 1971

84) T. Sarpkaya, M. Isaacson: Mechanics of Wave Forces on Offshore Structure, Van Nostrand Reinhold Company, p. 651, 1981

85) T. Yamamoto, J.H. Nath: Forces on many cylinders near a plane boundary, ASCE, National Water Resources and Ocean Engineering Convention, Preprint No. 2633, 1976

86) T. Sarpkaya: In-line and transverse forces on cylinders near a wall in oscillatory .ow at high Reynolds numbers, OTC paper No. 2898, pp. 161–166, 1977

87) T. Sarpkaya, F. Rajabi.: Hydrodynamic drag on bottom-mounted smooth and rough cylinders in periodic flow, OTC Paper No. 3761, pp. 219–226, 1980

88) Borgman, L. E.: Spectral analysis of ocean wave forces on pilling, Proc. ASCE, Vol. 93, No. WW2, pp. 129–156, 1967

89) Hino, M.: Spectral theory of wave forges on piles, Proceedings of the 15th Conference on Coastal Eng. JSCE, pp. 103-108, 1968

90) Borgman, L. E.: Ocean wave simulation for engineering design, Proc. ASCE, Vol. 95, No. WW4, pp. 557–583, 1969

91) ITO, Y. K. TANIMOTO and K. KOBUNE: Title Dynamic Response of an Offshore Platform to Random Waves Rept of PHRI Vol. 11 No. 3, pp. 59-86, 1972

92) Hudspeth, R.T.: Wave force prediction from non-linear random sea simulation, 7th OTC, # 2193, pp. 471-486, 1975

93) Sharma, J. and Dean, R.G.: Second-order directional seas and associated wave forces, 11th OTC, #3645, pp. 2505-2514, 1979

94) Tickell, R.G. and Elwany, M.H.S.: A probabilistic description of forces on a member in a short-crested random sea, Mechanics of Wave-Induced Forces on Cylinders, Pitman Pub. Ltd., London, pp. 561-576, 1979

95) Kimura, A. A., Seyama and A. Ueno: Stochastic characteristics of random wave forces acting on cylinder, Proceedings of 27th Conference on Coastal Eng. JSCE ,pp. 373-377, 1980

96) GODA, Y. T. IKEDA, T. SASADA and Y. KISHIDA: Title Study on Design Wave Forces on Circular Cylinders Erected upon Reefs Rept of PHRI Vol. 11 No. 4, pp. 45-81, 1972.12

97) Hiraishi, T. Y. Tomita and Y. Suzuki: Effect of wave directionality on wave forces on Cylinder, Proceedings of 27th Conference on Coastal Eng. JSCE Vol. 41, pp. 836-840, 1994

98) MacCamy, R.C. and R.A. Fuchs: Wave Forces on Piles, a Diffraction Theory, U.S. Army, Corps of Engineers, Beach Erosion Board, Tech. Memo. No. 69, p. 17, 1954

99) GODA, Y. and T. YOSHIMURA: Title Wave Force Computation for Structures of Large Diameter, Isolated in the Offshore, Rept of PHRI Vol. 10 No. 4, pp. 3-52, 1971

100) Yamaguchi, M: Wave forces on pile structures, Lecture note of Summer training for Hydraulic Engineering 1975, (11th) Course B, Hierodulic Committee of JSCE, pp. B-6-1-B-6-26, 1975

101) TANIMOTO, K., S. TAKAHASHI and Y. IZUMIDA: A Calculation Method of Uplift Forces on a Horizontal Platform, Rept. of PHRI Vol. 17 No. 2, pp. 3-47, 1978

102) ITO, Y. and H. TAKEDA: Uplift on Pier Deck due to Wave Motion, Rept. of PHRI Vol. 6 No. 4, pp. 37-68, 1967

103) Murota, A. and M. Furudoi: Experimental study on uplift force on deck of pier, Proceedings of the 13th Conference on Coastal Eng. JSCE, pp. 120-125,1966

104) Nagai, S. T. Kobo and K. Tokikawa: Study on uplift on piers (First Rep.), Proceedings of the 13th Conference on Coastal Eng. JSCE, pp. 112-119, 1966

105) Horikawa, K., T. Nakao and A. Yajima: Experimental study on uplift on piers, Proceedings of the 14th Conference on Coastal Eng. JSCE, pp. 148-153, 1967

106) Sawaragi, T. and M. Nochino: Discussion on Similarity law for hydraulic model tests on uplift acting on decks of piers, Proceedings of Coastal Eng. JSCE Vol. 35, pp. 677-681, 1988

107) TANIMOTO, K., Shigeo TAKAHASHI, Masahiko TODOROKI and Yoshikazu IZUMIDA: Horizontal Wave Forces on a Rigid Platform, Rept. of PHRI Vol. 16 No. 3, pp. 39-68, 1977

108) Tirindelli, M., Cuomo, G., Allsop, W., and McConnell, K.: Exposed jetties: Inconsistencies and gaps in design methods for wave-induced forces, Proc. Of the 28th International Conference on Coastal Engineering, Cardiff, pp. 1684-1696, 2002

109) Tirindelli, M., Cuomo, G., Allsop, W., and McConnell, K.: Physical model studies of wave-induced loading on exposed jetties: Towards new prediction formulae, Proc. Of the International Conference Coastal Structures 2003, Portland, pp. 382-393, 2003

110) Cuomo, G., Allsop, W., and McConnell, K.: Dynamic Wave Loads on Coastal Structures: Analysis of impulsive and pulsating wave loads, Proc. Of the International Conference Coastal Structures 2003, Portland, pp. 356-368, 2003

111) Bentiba, R., Cuomo, G., Allsop, W., and Bunn, N.: Probability of occurrence of wave loading on fatty deck elements, Proc. Of the 29th International Conference on Coastal Engineering, Lisbon, pp. 4113-4125, 2004

112) Kubou, M. M. Takezawa and T. Ueki: Experimental study on wave pressure at the vicinity of wave crest, Proceedings of the 20th Conference on Coastal Eng. JSCE, pp. 279-284, 1973

113) Michio Morihira, Shusaku Kakizaki and Yoshimi Goda :EXPERIMENTAL INVESTIGATION OF A CURTAIN-WALL BREAKWATER ,REPORT OF PORT AND HARBOUR TECHNICAL RESEARCH INSTITUTE MINISTRY OF TRANSPORTATION Vol. 3, No. 1, p. 16, 1964

114) Sekimoto, T., H. Kondo, T. Oshita, S. Imai and M. Nakamura: Design wave force of curtain-wall type breakwater considering incident wave angle, Proceedings of Coastal Eng. JSCE Vol. 35, pp. 657-661, 1988

115) Shigeo Takahashi, Kojiro Suzuki, Katsumasa Tokubuchi, Ken-ichiro Shimosako:Experimental Analysis of the Settlement Failure Mechanism Shown by Casson-Type Seawalls, 25th, I.C.C.E., pp. 1902 -1915, 1996

116) Waterfront Vitalization and Environment Research Center: Design・Construction・Management Manual of Controlled Type Waste Disposal Revetment (Revised Edition), 134p., 2008.

117) Yuichiro Takebe, Kojiro Suzuki, Yoshio Nishino, Yasushi Nishimoto : The Verification of Deformation Model and Design Method of Joint Plate, J.JSCE, Ser.B2, Coastal Engineering, Vol.71, No.2, I_1177-I_1182, 2015.

118) JSCE Edition: Handbook of design of coastal protection facilities (Revised Edition), pp. 174-176, 1969

119) Literature survey Committee: Deformed wave absorbing blocks, Journal of JSCE, Vol. 49, No. 4, pp. 77-83, 1964

120) R.Y. Hudson: Laboratory investigation of rubble-mound breakwater, Proc. ASCE., Vol. 85, W.W.3., pp. 93–121, 1959

121) Kashima, R., T. Sakakiyama, T. Shimizu, T. Sekimoto, H. Kunisu and O. Kyoutani: Evaluation equation of deformation of wave absorbing works due to random waves, Proceedings of Coastal Eng. JSCE Vol. 40, pp. 795-799, 1995

122) J.W. van der Meer: Rock slopes and gravel beaches under wave attack, Doctoral thesis, Delft Univ.of Tech., p. 152, 1988 or J.W. Van Der Meer: Stability of breakwater armor layer -Design formulae, Coastal Engineering, 11, pp. 219–239, 1987

123) J. W. van der Meer: Stability of cubes, Tetrapods and Accropode, Proc.of Breakwater. 88, Eastbourne, UK, pp. 71–80, 1988

124) H. F. Burcharth and Z. Liu: Design of Dolos armour units, Proc.of the 23rd International Conference on Coastal Engineering, Venice, pp. 1053–1066, 1992

125) Takahashi S., M. Hanzawa and K. Shimosako: Performance verification of stability of armour stones of rubble-mound breakwaters against waves, Proceedings of Coastal Eng. JSCE Vol. 50, pp. 761-765, 2003

126) Tanimoto, K., Y. Haranaka K. Yamazaki: Experimental Study on the Stability of Wave Dissipating Concrete Blocks against Irregular Waves, Rept. of PHRI Vol. 24, No. 2, pp. 85-121, 1985

127) Kashima, r., T. Sakakiyama, T. Shimizu, T. Sekimoto, H. Kunisu and O. Kyoutani: Evaluation equation of deformation of wave absorbing works due to random waves, Proceedings of Coastal Eng. JSCE Vol. 42, pp. 795-799, 1995

128) Hanzawa, M., H. Sato, T. Takayama, S. Takahashi and K. Tanimoto: Study on evaluation equation for the stability of wave absorbing blocks, Proceedings of Coastal Eng. JSCE Vol. 42, pp. 886-890, 1995

129) Takahashi, S., M. Hanzawa, H. Sato, M. Gomyou, K. Shimosako, K. Terauchi, T. Takayama and K. Tanimoto: Lifetime Damage Estimation with a New Stability Formula for Concrete Blocks, Report of PHRI, Vol.37, No.1, pp.3-28, 1998.

130) Kimura, K., K. Kamikubo, Y. Sakamoto, Y. Mizuno, H. Takeda and M. Hayashi: Stability of blocks at the end of breakwaters armored with wave absorbing blocks, Proceedings of Coastal Eng. JSCE Vol. 44, pp. 956-960, 1997

131) Van de Kreeke, J.: Damage function of rubble mound breakwaters, ASCE., Journal of the Waterway and Harbors Division, Vol. 95, WW3, pp. 345–354, 1969

132) F. T. Christensen, P. C. Broberg, S. E. Sand, and P. Tryde: Behavior of rubble-mound breakwater in directional and uni-directional waves, Coastal Eng., Vol. 8, pp. 265–278, 1984

133) Sokabe, T. and T. Yajima: Outstanding technical issues in designing of detached breakwaters, Lecture note of Summer training for Hydraulic Engineering 1982, (18th) Course B, Uralic Committee of JSCE, pp. B-5-1-B-5-24, 1982

134) Takeda, H., Y. Yamamoto, K. Kimura and T. Sasazima: Impact wave forces and stability of wave absorbing blocks on breakwaters placed on steep slope, Proceedings Offshore Development Vol. 11, pp. 287-290

135) Kamikubo Katsumi, Yasuji Yamamoto, Katsutoshi Kimura, Toshiaki Shimizu, Masafumi Yoshino : Armor Stability of Block Mound Seawall for Steep Foreshore Conditions, Proceedings of Civil Engineering in the Ocean,Vo.26, p.489-494, 2010.

136) Kenji Motoyama, Katsumi Kamikubo and Yasuji Yamamoto : Stability of Wave-Dissipating Blocks of Caisson Breakwater for Steep and Shallow Foreshore Conditions, J.JSCE, Ser.B3, Ocean Engineering, Vol.70, I_265-I_270,2014.

137) Coastal Development Institute of Technology (CDIT): Technical Manual for wave absorbing blocks of large specific gravity, p. 45, 1995

138) Kubota, S., S. Kobayashi, A. Matumoto, M. Hanzawa and M. Matuoka: On the effect of the layer thickness and filling materials of wave absolving blocks on their stability against waves, Proceedings of Coastal Eng. JSCE Vol. 49, pp. 756-760, 2002

139) Coastal Engineering Research Center: Shore Protection Manual, Vol. II, Department of Army Corps of Engineering, 1977

140) A. Brebner, D. Donnelly: Laboratory study of rubble foundations for vertical breakwaters, Proc. 8th Conf. of Coastal Engg., New Mexico City, pp. 408–429, 1962

141) Tanimoto, K., T. Yanagisawa, T. Muranaga, K. Shibata and Y. Goda: Stability of Armor Units for Foundation Mounds of Composite Breakwaters Determined by Irregular Wave Tests, Rept. of PHRI Vol. 21, No. 3, pp. 3-42, 1982

142) Inagaki, K. and T. Katayama: Analysis of damage to armor stones of mounds in composite breakwaters, Technical Note of PHRI No. 127, pp. 1-22, 1971

143) Takahashi S., K. Kimura and K. Tanimoto: Stability of Armour Units of Composite Breakwater Mound against Oblique Waves, Rept. of PHRI Vol. 29 No. 2, pp.3-36, 1990

144) Sudo, K., K. Kimura, T. Sasajima, Y. Mizuno and H. Takeda: Estimation equation of requited weight of armour units of rubble-mound of composite breakwaters considering the allowable deformation, Proceedings of Coastal Eng. JSCE Vol. 42, pp. 896-900, 1995

145) Kougami, Y. and T. Narita: On the stability of armour layer, made with wave-absorbing blocks, of rubble foundation of composite breakwaters, Journal of Public Works Research Institute (PWRI), Hokkaido Regional Development Bureau (HRDB) No. 232, pp.1-13, 1972

146) Kashima, R., S. Saitou and H. Hasegawa: Required weight of armour concrete cube for rubble mound foundation of composite breakwaters, Report of the Second Technical Research Institute of the Central Research Institute of Electric Power Industry 70022, p. 18, 1971

147) Fujiike, T., K. Kimura, T. Hayashi and y. Doi: Stability against waves of armor units placed at front face of rubble-mound of wave-absorbing-block-armored breakwaters, Proceedings of Coastal Eng. JSCE Vol. 46, pp. 881-885, 1999

148) Matuda, S., W. Nishikiori, A. Matumoto and M. Saitou: Estimation method of stable weight of armour blocks of rubblemound of composite breakwaters considering impact wave force actions, Proceedings of Coastal Eng. JSCE Vol. 47, pp. 896-900, 2000

149) Shimosako, K., S. Kubota, A. Matumoto, M. Hanzawa, Y. Shinomura, N. Oike, T. Ikeya and S. Akiyama: Stability and Durability of Filter Unit Covering Rubble Mound of Composite Breakwater, Report of PARI, Vol.43, No.1, pp.49-83, 2004.

150) Association of Nationwide Disaster Prevention: Kujukuri and Minamikujukuri No.1 Coasts Disaster Restoration projects- Composite Measure of Large Gabion Seawall and Foot Protection, Examples of Disaster Restoration Projects in 2013, pp.82-85, 2013 (in Japanese)

151) Kudou, T.: Temporary river closing dikes and its overflow, Journal of JSCE, Vol. 58 No. 11, pp. 63-69, 1973

152) Iwasaki, T., A. Mano, T. Nakamura and N. Horikoshi : Experimental study on fluid dynamic force in steady flow acting on mound materials of submerged breakwaters and prepacked breakwaters, Proceedings of the 31st Conference on Coastal Eng. JSCE, pp. 527-531, 1984

153) Tanimoto, K., K. Kimura and K. Miyazaki: Study on Stability of Submerged Dike at the Opening Section of Tsunami Protection Breakwaters, Rept. of PHRI Vol. 27 No. 4, pp. 93-121, 1988

154) Ministry of Land, Infrastructure, Transport and Tourism Port and Harbours Bureau: Guideline for Tsunami-Resistant Design of Breakwaters, p.37, 2015 (in Japanese)

155) Sohei Maruyama, Tomotsuka Takayama, Kenichiro Shimosako, Akiihikoo Yahiro, Kojiro Suzuki, Toru Aota, Masashi Tanaka, Akira Matsumoto and Minoru Hanzawa : Estimation of Tsunami Force Acting on the Block Armored Breakwater in the State of Soliton Fission, J.JSCE, Ser.B2, Coastal Engineering, Vol.71, No.2, pp.I_265-I_270, 2015.

156) Masafumi Miyata, Yasuo Kotake, Masahiro Takenobu, Tomoaki Nakamura, Norimi Mizutani and Shigeki Asai : Experimental Study on Hydraulic Characteristics of Tsunami Overtopping Flow over a Caisson-Type Breakwater, J.JSCE, Ser.B3, Ocean Engineering, VOL.70, NO.2, PP.I_504-I_509, 2014.

157) Naoki Tsuruta, Kojiro Suzuki, Tsukasa Kita, Masafumi Miyata, Masahiro Takenobu, Enhancement of accuracy of prediction of tsunami force in overflow for design of tenacious breakwater, Report of PARI, Vol.56, No.1, pp.26-51., 2016.

158) Kojiro Suzuki and Tsukasa Kita: Uplift and overburden pressure acting on breakwater caisson under tsunami overflow, Asian and Pacific Coasts, pp. 817-824, 2017

159) Fisheries Agency Fishing Port Fisheries Development Department Disaster Prevention Fishing Village Division・Ministry of Land, Infrastructure, Transport and Tourism Port and Harbours Bureau Coastal and Disaster Management Office: Guideline for design of tidal embankment against tsunami, pp.22., 2015.

160) Nobuhiro Ishida, Hiroshi Moritani, Kisaburo Azuma, Takuya Toriyama and Hidetaka Nakamura : Water Depth Coefficients for Evaluating Tsunami Pressure on Seawall, NRA Technical Report, NTEC-2016 -4001, 113p., 2016.

161) Kei Ando, Kojiro Suzuki and Naoki Tsuruta : A Study on Inundation Depth in Evaluating Tsunami Wave Pressure Acting on Land Vertical Walls, J.JSCE, Ser.B2, Coastal Engineering, Vol.73, No.2, I_895-I_900, 2017.

162) Ryoji Naito, Kentaro Kumagai, Tadashi Asai, Takeshi Suzuki : Measurement of Height, Velocity and Pressure of the Water Overflow over a Seawall, Technical Note of NILIM, No.917, 24p., 2016.

163) Jun Mitsui, Akira Matsumoto and Minoru Hanzawa : Derivation Process of the Isbash Formula and Its Applicability to Tsunami Overtopping Breakwater, J.JSCE, Ser.B2, Coastal Engineering, Vol.71, No.2, I_1063-I_1068, 2015.

164) Jun Mitsui, Shin-ichi Kubota, Akira Matsumoto and Minoru Hanzawa : Influence of Superstructures on Stability of Armor Units Covering Breakwater Rubble Mounds against Tsunami, J.JSCE, Ser.B2, Coastal Engineering, Vol. 72, No. 2, p. I_1111-I_1116, 2016.

165) Jun Mitsui, Akira Matsumoto, Minoru Hanzawa and Kazuo Nadaoka : Stability Verification Method for Armor Units Covering Breakwater Rubble Mounds against Tsunami Overflow, J.JSCE, Ser.B2, Coastal Engineering, Vol.72, No.2, I_1111-I_1116, 2016.

166) Association for Innovative Technology on Fishing Ports and Grounds: Manual for calculating required mass of mound covering block with breakwater belly against tsunami overflow, pp.45, 2014 .

167) Sogo Jikuhara, Kojiro Suzuki, Kazunori Tatewaki and Yoshihiro Hosokawa : Effect of the Oblique Incident Tsunami on the Mound Cover Layer behind the Vertical Type Breakwater Having Abrupt Change of the Breakwater Width, J.JSCE, Ser.B2, Coastal Engineering, Vol.72, No.2, pp.I_991-I_996, 2016.

168) Yoshimi Goda : Coastal Engineering – Its Birth and Development, Gihodo, pp.38, 2012.

169) Tsukasa Kita and Kojiro Suzuki: Study on the Stability of Pavement behind Seawall against Overflow with High Waves, J.JSCE, Ser.B2, Coastal Engineering, Vol.73, No.2, I_991-I_996, 2017.

170) Senri Tsuruta and Yoshimi Goda: Failure of Coastal Structures by Typhoon Vera and the Characteristics, Proceedings of Coastal Engineering Conference in Japan, Vol.7., pp.195-199., 1960.

7 Water Currents

7.1 The Flow of Sea Water in Coastal Zones

[Public Notice] (Flow of Sea Water)

Article 10

Flow of sea water shall be appropriately defined in terms of current velocity and current direction on the basis of measured values or estimated values.

[Interpretation]

7. Setting of Natural Conditions

(4) Items related to the flow of water (Article 6 of the Ministerial Ordinance and the interpretation related to Article 10 to 12 of the Public Notice)

① **Setting Methods for the Flow of Sea Water**

In the performance verification of facilities subject to the technical standards, when combining the flow of sea water with other actions, out of all the possible flows of sea water that have a high probability of occurring simultaneously with other actions, specify the current velocities and current directions that would be appropriate from the viewpoint of the stability of the target facilities, consideration to the environment, etc.

7.1.1 General

The movements of sea water are the superpositions of currents that have various periods and are caused by different natural actions, and their current velocities and directions are greatly affected by topography and structures and change in complicated ways both in space and time. The movements of sea water cause sediment on the sea bottom to move, thus leading to problems such as siltation in navigation channels and basins and the scouring of the area around facilities. Furthermore, changes in the flow of sea water due to coastal development can cause wide-scale changes in the natural environment, such as water quality, sedimentation changes, and biological and ecosystem[1] changes. With regard to their origins and their scales over time and space, the flows of sea water are classified as ocean currents, tide currents, tidal residual flow, wind-driven currents, density currents, and nearshore currents.

7.1.2 Ocean Current

Ocean current flows in the spatial scale of the ocean with an almost balanced Coriolis force and pressure gradient (geostrophic balance). The effect of the ocean current on the facilities under the technical standards appears as the inflow of oceanic water into the coast, the change in mean water level, etc.

7.1.3 Tidal Current

Tidal current is the horizontal flow of sea water accompanying the wave motion on the sea surface (tidal wave) caused by the tide-producing force generated by the movement of heavenly bodies (mainly the moon and the sun). Considering that the tidal wave is affected by the seabed topography during the propagation process in the ocean, the tide condition differs by location. The tidal current periodically changes according to the four principal tidal constituents **(Part II, Chapter 2, 3.1 Astronomical Tide**). The harmonic constant (i.e., the flow rate amplitude and the lag of each northern and eastern component) obtained by the harmonic analysis of the tidal current observation data differs by sea area and location. The forced oscillation of the bay water caused by the tide in the ocean is significant in Japan's inner bays, where the tidal current amplitude increases from the entrance to the inner part of the bay almost simultaneously, thus repeating the tide. The tidal current becomes faster when the difference in tidal level is larger or when the width of a waterway is narrower such as in a channel. Given that the tidal current is strongly affected by the topography, shape of structures, and other factors, the nearby flow condition varies by the change in topography, shape of structures, and other factors.

7.1.4 Tidal Residual Flow

Tidal residual flow is the flow generated by the nonlinearity of tidal current and the effect of topography when a mean of one tide period is taken. It is important to understand the long-term movement of seawater, such as the mixture and exchange of water in the bay. The tidal residual flow is one of the origins of the permanent current component obtained by the harmonic analysis of flow condition observation data. Other permanent current components include the wind-drive current and the density current.

7.1.5 Wind-Drive Current

Wind-drive current is the flow generated by wind and is an important flow component on the coast and in the inner bay. The wind exerts shear force by friction on the sea surface, and the seawater is dragged to the wind direction. If the sea area is narrow and surrounded by shores, structures, etc., the sea surface in the leeward side rises, and the sea surface in the windward side decreases and causes a slope on the sea surface. This slope on the sea surface acts to press the seawater to the lower sea surface side, thus leading to the generation of vertical return flow to the wind direction on the surface layer and to the opposite direction of the wind in the bottom layer.

If the sea area is broad and the wind-drive time is long, the effect of earth rotation (the Coriolis force) against the generated flow becomes hard to ignore. The force to deflect the flow to its right direction acts in the northern hemisphere and the seawater flows deflecting to the right direction of wind (Ekman wind-drive current). When wind blows constantly for a long time on the borderless ocean of uniform density, the flow is displaced to the right as the depth from the sea surface increases, the velocity is rapidly reduced, and the Ekman spiral flow is generated.

7.1.6 Density Current

Density current is the flow generated by the pressure gradient owing to the uneven distribution of seawater density. The density of seawater is determined by the salt content and the water temperature. On the coast, the uneven distribution of salt content due to the inflow of fresh water from rivers and other factors, the inflow of oceanic water from beyond the bay, and the pressure gradient due to the uneven distribution of water temperature in the shallow sea area by insolation, heat dissipation, etc., drive the density current.

In the inner bay, the low-density river water flows in from the land side, and the high-density seawater flows in from the ocean. This type of inflow causes an unbalanced pressure field, and a flow to coordinate the density field is generated to cancel the imbalance. Light water flows out of the bay on the surface layer, and heavy water flows toward the bay in the bottom layer. This is called estuarine circulation.

7.1.7 Nearshore Current

Nearshore current is the flow generated by the coastal topography and the wave transformation. The water particles of the progressive waves move almost elliptically, but their orbit does not close in one wave period but shifts little by little to the direction of movement of the waves. The movement of water mass from the sea surface to the seabed during this one wave period is called the mass transport by waves and increases with wave shoaling. The seawater pushed to the shore direction by the mass transport of the waves progressing toward the shore increases the mean water level near the shore line (wave setup). The spatial uneven distribution of the increase in mean water level forms the nearshore current system, such as longshore currents, along the shore line and the rip current of converged longshore currents flowing out offshore.

7.2 Fluid Force Due to Currents

(1) General

The fluid force due to currents acting on members and facilities in the water or near the water surface, such as a pile-supported structure (e.g., a piled pier, a pipeline, or armor material of a mound), is proportional to the square of the flow velocity. It may be divided into the drag force acting in the direction of the current and the lift force acting in the direction perpendicular to the current. Also note that a thin, tube-like object in the water may be subject to vibrations excited by induced vortices.

① **Drag force**

Drag force is generally calculated using the following equation:

$$F_D = \frac{1}{2} C_D \rho_0 A U^2 \qquad \textbf{(7.2.1)}$$

where

F_D : drag force acting on the object in the direction of the current (N)

C_D : drag coefficient

ρ_0 : density of water (kg/m^3)

A : projected area of the object in the direction of the current (m^2)

U : flow velocity (m/s)

② **Lift force**

Lift force is generally calculated using the following equation:

$$F_L = \frac{1}{2} C_L \rho_0 A_L U^2 \qquad \textbf{(7.2.2)}$$

where

F_L : lift force acting on the object in the direction perpendicular to the current (N)

C_L : lift coefficient

A_L : projected area of the object in the direction perpendicular to the current (m^2)

(2) Drag Coefficient

The drag force due to currents is expressed as the sum of the surface resistance due to viscosity, and the shape resistance due to pressure is expressed generally in **equation (7.2.1)**. The drag coefficient varies according to the shape and roughness of the object, the direction, and the Reynolds number of the current. Therefore, the value that is appropriate to the conditions in question must be used.

When the Reynolds number is greater than 10^3, the values listed in **Table 7.2.1** may be used as standard values for the drag coefficient. Note that for a circular cylinder or sphere with a smooth surface, the value of the drag coefficient decreases suddenly when the Reynolds number is approximately 10^5. However, for a circular cylinder with a rough surface, this decrease in drag coefficient is not particularly large, and the drag coefficient settles down to a constant value that corresponds to the relative roughness. The data for the cube have been obtained from wave force experiments performed by Hamada, Mitsuyasu, and Hase[2)]. The values for rectangular cylinders and L-shaped members placed diagonally to the current can be found in Ref. [3)].

(3) Lift Coefficient

Similar to the drag coefficient, the lift coefficient varies with the shape of the object, the direction of the current, and the Reynolds number, but these values are not well known.

(4) Current Force Acting on the Coping of Submerged Dike at the Opening of Tsunami Protection Breakwater

For the current force acting on the coping of the submerged dike at the opening of tsunami protection breakwater, Iwasaki et al.[4)] measured the pressure and obtained a value of 0.84 for the drag coefficient and a value of 0.48 for the lift force coefficient. Tanimoto et al.[5)] performed similar measurements and obtained values of 1.0 to 1.5 for the drag coefficient and 0.5 to 0.8 for the lift coefficient. They have also indicated that when the flow velocity in the breakwater opening is large, the effect of the water surface gradient causes the coefficient values to increase. Sakunaka and Arikawa[6)] conducted a plane experiment of the opening of breakwater and a reproduction calculation by using the numerical wave flume Cadmas-Surf/3D and indicated that Cadmas-Surf/3D can enable the calculation of the experimental values of horizontal pressure and uplift with a 10% to 30% error range. Furthermore, the Isbash formula can be used to determine the initial movement of armor blocks.

(5) Vibration Due to Vortex

Care should be taken because vibration perpendicular to the flow may be generated by the vortex behind a thin member and others by the action of flow. This is because the lift force by vortex varies periodically and because a resonant state is induced when the period come close to the natural period of the member. The period of vortex generation can be calculated from the diameter of the member, the flow rate, and the Strouhal number. A long natural vibration period necessitates a vibration-proof countermeasure.

Table 7.2.1 Drag Coefficients

Object shape		Standard area	Drag coefficient
Circular cylinder (rough surface)	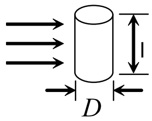	Dl	1.0 ($l > D$)
Rectangular cylinder	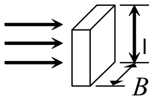	Bl	2.0 ($l > B$)
Circular disk	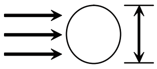	$\frac{\pi}{4}D^2$	1.2
Rectangular plate	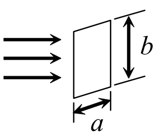	ab	*When* a/b=1 1.12 ″ ″ 2 1.15 ″ ″ 4 1.19 ″ ″ 10 1.29 ″ ″ 18 1.40 ″ ″ ∞ 2.01
Sphere	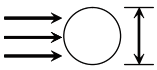	$\frac{\pi}{4}D^2$	0.5–0.2
Cube	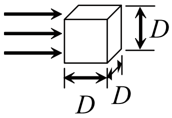	D^2	1.3–1.6

7.3 Estuarine Hydraulics

[Public Notice] (Estuarine Hydraulics)

Article 11

The influence of estuarine hydraulics shall be assessed with appropriate methods by taking into account the river flow on the basis of measured values or estimated values.

[Interpretation]

7. Setting of Natural Conditions

(4) Items related to the flow of water (Article 6 of the Ministerial Ordinance and the interpretation related to Article 10 to 12 of the Public Notice)

② **Effect of Estuarine Hydraulics**

The effects of estuarine hydraulics include tides in rivers, river runoff, density currents at the river mouth, waves entering into the river mouth, and siltation. Their evaluation shall be performed appropriately by considering the action from the seaside on estuaries and also the freshwater and sediment discharge variations from rivers due to flood and drought.

7.3.1 General

The range of estuarine hydraulics to be defined is not necessarily clear. If it is broadly taken as the area over which fresh water and sea water are mixed, this area is a large area that extends from the limit of tidal influence in the upstream river to the mouth of the bay. However, from the viewpoint of actions and effects related to port facilities, the estuarine area is generally defined as extending from the upstream point where salt water reaches by mean tidal motion to the front portion of the estuarine terrace that is composed mainly of sand deposited during floods (hereafter, this will simply be called the estuarine areas). In the estuarine area, in addition to actions such as tidal currents, tide motion, waves, and wave induced nearshore currents, river current fluctuations, such as the outflow of river flood or drought, also occur. There are complex hydraulic and sediment transport phenomena such as density currents represented by vertical circulations and such as chemical flocculation and settlement. In an estuarine area, organisms live in an environment that is affected by physical and chemical actions, and the natural environment and biological environment in the estuarine area can easily be influenced by human activities. Therefore, the development of facilities requires sufficient analysis of the impacts and the continuous monitoring of such influences on the area.

7.3.2 Flow in an Estuary

(1) Tidal Motion, Waves, and Water Currents in an Estuary

In an estuary, complex hydraulic phenomena exist because of the mixture of actions from the sea area, such as tidal level fluctuation and tide currents due to tide motion, water level rise due to waves, fluctuation of nearshore currents, and action from the river. There are still many issues to be resolved to take all of these factors into account in calculating the current field. However, with regard to the intrusion of tidal currents into river channels due to factors such as river bed slope and fresh water discharge, the duration of flood tide is shorter and that of ebb tide is longer, generally; therefore, the maximum and minimum values of the current velocity and discharge occur later than the times of the highest and the lowest water. These various phenomena vary in time and space in accordance with the location of the river mouth, its shape, and the hydraulic parameters of the river and outer sea. In general, the current at the river mouth can be characterized as follows:

① The downward current is dominant under higher fresh water discharge through the river and the current is assumed as a uniform flow when it behaves as the gradient current.

② When the fresh water discharge is normal condition, the water flow becomes complicated because tidal currents and density currents are superposed onto the gradient current.

③ During times of drought, the tidal current characteristics becomes dominant. However, in estuaries where the tidal range is small (e.g., the coast of the Sea of Japan), the tidal current is not strong even during periods of drought and the density current characteristic is intensified.

④ In estuaries where the tidal range is large (e.g. the coast of the Pacific Ocean), the tidal current is dominant.

(2) Density Currents at the River Mouth

In an estuary, where river water meets sea water, the sea water penetrates the lower layer of the river water owing to the difference in their densities, and they flow and mix to achieve dynamic equilibrium. These flows are called "density currents at the river mouth" or estuarine circulation. They are divided into three main types, namely, weakly mixing, moderate mixing, and fully mixing, depending on how the density layers form in the river water and sea water. However, even in the same river estuary, the flow field changes according to the change in seasonal or temporal hydraulic conditions, such as river flow rate and tidal phase, and topographical conditions.

① **Weakly mixing type**

This is a type wherein river water flows down in the upper layer and the wedge-shaped sea water invades the upstream in the lower layer, the river water and the sea water hardly mix, and there is a clear boundary plane where the abrupt density change exists. This type of estuary is generally observed in the river mouth on the coast of the Sea of Japan where the tidal range is small compared to the river flow rate.

② **Moderate mixing type**

This type appears when the tidal flow slightly increases compared with the river flow. The river water and sea water mix relatively well in this type, and the density gradient appears in the directions of flow down and water depth. This type is generally seen in inner bays on the coast of the Pacific Ocean.

③ **Fully mixing type**

This type occurs when the tidal flow is quite strong compared with the river flow, and they are mixed by the strong turbulence caused by tide movement. The density will be uniform in the vertical direction, and the distribution of salinity concentration becomes a function of location from the river mouth only. This type is seen in the Chikugo River in the Ariake Sea, at the mouth of the Rokkaku River, and so on.

(3) Waves Entering into a River Mouth

When waves enter an estuary, the waves are transformed by the effects of the topography and the river currents. The wave height increases owing to the refraction and concentration caused by the topography of the estuarine terrace and owing to wave shoaling. Wave propagation is disturbed by river currents that flow in the opposite direction to wave propagation increasing wave height. Given that incident waves with heights that have been increased run up in the river channel, they are attenuated by the effects of wave breakings, bottom friction, and turbulent flow. Furthermore, when the river current is extremely fast, the waves are unable to run up against the current.

7.3.3 Siltation

The sediment within the estuary of a bay is mostly mixture of sand and mud that contains small particles of clay and silt. The sediment moves under the action of wave and current and forms characteristic tidal flats, sand spits, river mouth terraces, and bars in the estuary. When the bottom sediment mainly consists of sand particles, the movement phenomenon of the bottom sediment based on wave and current actions is called littoral drift. Furthermore, fine particles such as clay and silt are widely dispersed because they are suspended by the currents and accumulate in calm areas, such as waterways and basins, or in places with slower currents in the harbor. This causes problems for facility maintenance and environmental management in waterways and basins.

The movement and accumulation phenomenon of mud, which include resuspension of fine particles from the seabed and the supply of high density mud from rivers and their transport by waves and currents, are specifically called "siltation". The main difference between "siltation" and "littoral drift" is that mud flocculates by mixing with sea water in the estuary, thus its settling characteristics are significantly variable. Moreover, it should also be noted that when considering the deposition due to siltation, a transport form called fluid mud, which moves as a gravitational flow along the inclined sea bottom, may occur under a condition with densely concentrated mud before being consolidated. Therefore, it is necessary to examine a numerical simulation[7)] for siltation predictions by using a model that considers the characteristics of such siltation transport form for the siltation phenomenon of navigation channels and basins where a bottom sediment mainly consists of clay and silt.

Furthermore, the mud that is deposited at the bottom of the sea is capable of changing into harder sediment via consolidation over a long period. Their ability to be resuspended by the action of waves and currents is affected by factors such as mud characteristics, salinity of the sea water, particle size, water content, and organic material content, all of which change with time after deposition (degree of consolidation). These characteristics of mud make it difficult to solve the problems caused by siltation. Moreover, if the strength of mud increases in the vertical direction from a high water content condition near the surface to consolidated mud in deeper layer owing to the characteristics of the time history of deposited mud, it is necessary to note that there is a difference between the result of sounding with an echo sounding equipment and the result with a lead sounding [8)].

7.4 Littoral Drift[9) 10) 11) 12) 13) 14) 15)]

[Public Notice] (Littoral Drift)

Article 12

The influence of littoral drift shall be assessed by appropriate methods based on measured values or estimated values.

[Interpretation]

7. Setting of Natural Conditions

(4) Items related to the flow of water (Article 6of the Ministerial Ordinance and the interpretation related to Article 10 to 12 of the Public Notice)

③ **Effect of Littoral Drift**

The evaluation of the effect of littoral drift appropriately takes into account seasonal and annual changes in topography due to such factors as sediment grain size, threshold depth of sediment movement, longshore sediment transport rate, predominant direction of longshore sediment transport and cross-shore littoral drift.

7.4.1 General

Littoral drift refers to either the phenomenon wherein the sediment composed mainly of sand on a sea coast and a lakeshore is moved by the actions of some forces such as waves and currents, or the material itself is moved by the above processes. Although the movement of sand by wind and the sand itself that is thus moved is referred to as windblown sand, in the broad definition littoral drift is also considered to include windblown sand at beaches. When port facilities are affected by the littoral drift phenomena, the characteristic values of littoral drift shall be established appropriately for sediment grain size, threshold depth of sediment movement, longshore sediment transport rate, and predominant direction of longshore sediment transport.

Sediment that forms a beach is supplied from nearby rivers, coastal cliffs, and adjacent coastline. The sediment is exposed to the actions of waves and currents during the supply process or after it has accreted on the beach, hence the sediment property reflects the characteristics of external forces such as waves and currents (Refer to **Part II, Chapter 2, 7.4.3 Characteristics and Distribution of Bottom Sediment**). This is referred to as the sediment sorting action by external forces.

When waves approach a coast from offshore, the movement of water particles near the sea floor does not have the force to move the sediment in places with sufficient water depth. However, at a certain water depth, the sediment begins to move. The water depth at the boundary where the sediment begins to move is called the threshold depth of sediment movement (see **Part II, Chapter 2, 7.4.4 Form of Littoral Drift Movement**). Sato[16)] studied the movement of sediment by placing radioactive glass sand on the sea floor and by investigating the distribution of their movement. He defined two conditions: the surface layer sediment movement threshold and the total sediment movement threshold. He applied the former term to the situation in which sand in the surface layer on the sea floor is moved collectively in the direction of wave movement. He applied the latter term to the situation wherein sand shows striking movement with a distinctly visible change in water depth.

Given that a natural beach is repeatedly subjected to the process of erosion when storm waves attack and the process of accretion during periods when waves are moderate, a natural beach achieves a relatively balanced topography over a long period. This balance may be lost after a reduction in the supply of sand due to river improvements, changes in sand supply conditions following the construction of coastal structures, and changes in external forces such as waves and currents. Beach deformation will then occur as the beach moves toward new equilibrium conditions. When building structures such as breakwaters, groins, detached breakwaters, and training jetties, careful attention should be paid to the changes that will be caused by construction works in the balance of the beach. Topographical changes that might be induced by a construction project should be sufficiently investigated in advance. Furthermore, careful attention should be paid to the deformation conditions of the beach both during construction and after the completion of any structure, and appropriate coastal protection countermeasures are recommended to be taken when there are concerns about the possibility of a disaster triggered by coastal erosion.

Littoral drift parallel to the coastal line is called longshore sediment transport. Longshore sediment moves in either the right or left direction along a coast, corresponding to the direction of incoming waves. The direction with the larger volume of movement during a year is called the predominant direction. In the long term, the topographical changes due to longshore sediment transport are often irreversible. For example, considering topographical changes near a groin, if waves come in from the right side (looking out toward the sea from the coast), there will be accumulation and erosion on the right and left sides of the groin, respectively. If the waves originate from the left side, the opposite topographical change occurs. By taking the direction perpendicular to the coastline as a standard, the energy of the waves originating from the right for most coasts is not equal to the energy of the waves coming in from the left, but one of them usually predominates. For example, if the average energy of the waves originating from the right is larger than that of the waves originating from the left, even though the right side of the groin sees repeated accumulation and erosion the amount of accumulation will grow eventually, and erosion will increase on the left side of the groin. Therefore, topographical changes due to longshore sediment transport are considered irreversible. It is desirable to first understand the predominant direction of the longshore sediment transport for that coast, as well as the longshore sediment transport rate, to estimate the degree of coastal deformation in that area if facilities are built.

7.4.2 Coastal Topography

① **Terminology for various sections of a beach profile**

The typical sections of a sandy beach are defined with the terminology shown in **Fig. 7.4.1**. The "offshore" is the area on the most offshore side where normal waves do not break, and the bottom slope is comparatively gentle in many cases. The "inshore" refers to the area between the landward boundary of the offshore and the ebb tide shoreline, where waves break and cross shore topography as longshore bars or steps are formed. The "foreshore" is the zone from the ebb tide shoreline to the location where waves will reach normally, and the "backshore" is the zone from the landward boundary of the foreshore to the coastline, where waves will reach during stormy weather with the rise in water level.

The names shown along the top row of **Fig. 7.4.1** classify regions based on the types of wave and sediment movement. In the surf zone, the sediment is suspended due to the action of large eddies generated by breaking waves and is carried in high concentration suspended sand. For the littoral drift in the swash zone, when the wave is uprush, the sand is lifted up and carried by the agitation at the front edge of the running-up waves. However, when the wave is in downwash, the agitation on the sea bottom predominates and the sediment is carried as bedload.

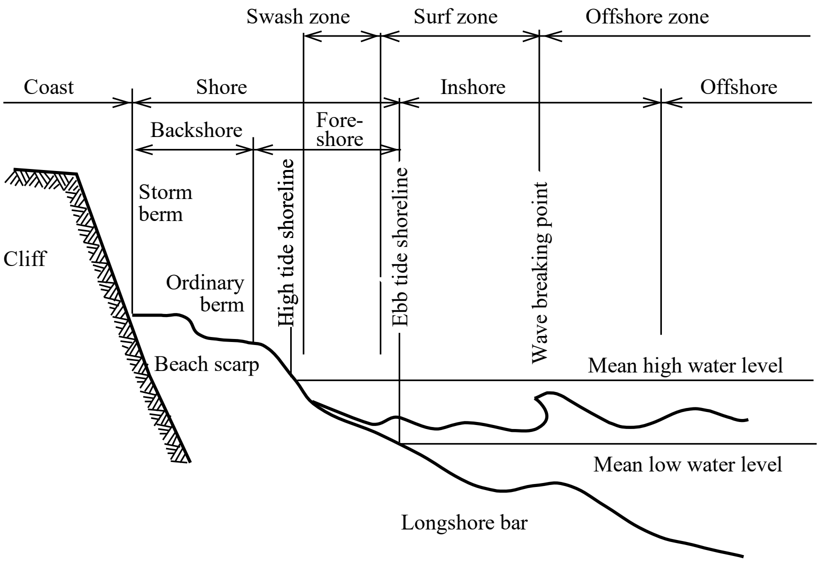

Fig. 7.4.1 Terminology of the Beach Profile[15)]

② **Horizontal Forms of Sandy Beaches**

A longshore bar is one of the most distinctive topographical features of a sandy beach. When viewing the shape of a longshore bar horizontally, it is roughly classified into either ①long and linear (roughly parallel to the shoreline, as in **Fig. 7.4.2 (a)**) or ②a repeating arch (**Fig. 7.4.2 (b)**). In particular, the latter type of longshore bar is called a crescentic bar. Furthermore, the longshore bar often forms multiple stages in a sequence leading out to sea; in this case, it exists on a large scale as an offshore longshore bar. According to **Fig. 7.4.3**, which shows the relation between the water depths at the crest and the trough of longshore bars, their ratio is 1.3 to 1.5.

When an arc-shaped longshore bar is formed, the shoreline often shows periodic longshore undulation in the same phase as that of the longshore bar (**Fig. 7.4.2 (b)**). This undulation of the shoreline does not have any official name but is referred to as cusp or shoreline rhythm[11) 17)]. The mean distance perpendicular to the shoreline between the most onshore side and most offshore side on one arc of the rhythmic topography is 15 m and the maximum distance is at most around 50 m.

In addition to the periodic longshore undulation described above, there is rhythmic topography with a wave length of several meters to several tens of meters called cusp near the shoreline. **Fig. 7.4.4** shows that the cusp is the topography formed by the repeated wave actions of swash and backwash on the shore. This cusp is the wavelike topography formed along the edge of the rhythmic topography of the shoreline corresponding to the abovementioned longshore bar and is often observed near shorelines.

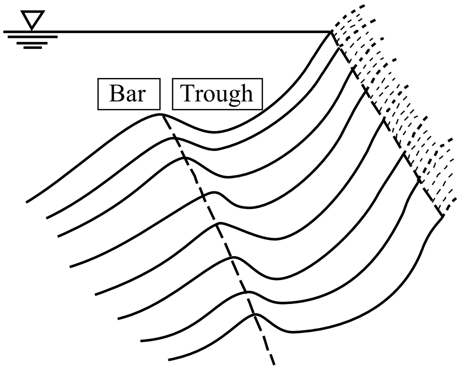

Fig. 7.4.2 (a) Longshore Bar Parallel to the Shoreline

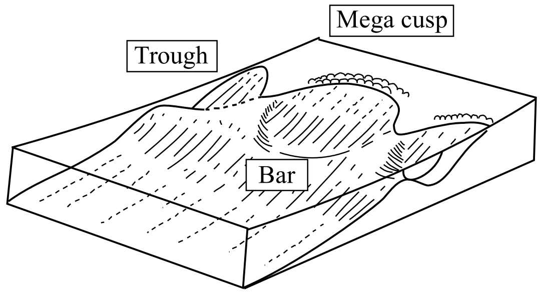

Fig. 7.4.2 (b) Crescentic Bar[11)]

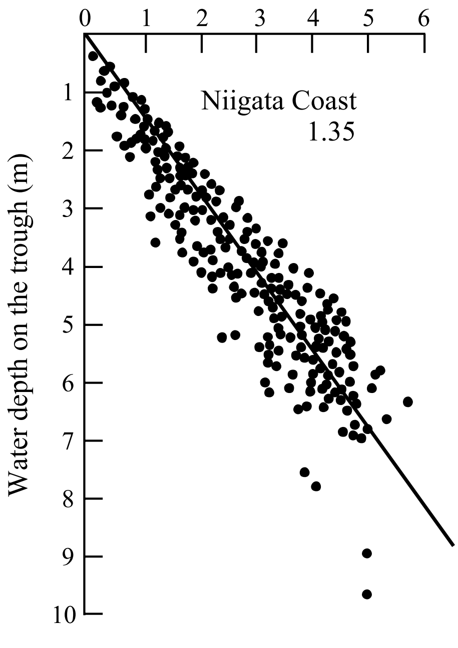

Fig. 7.4.3 Relation between the Water Depth at the Tip of Longshore Bars and the Water Depth on the Trough[11)]

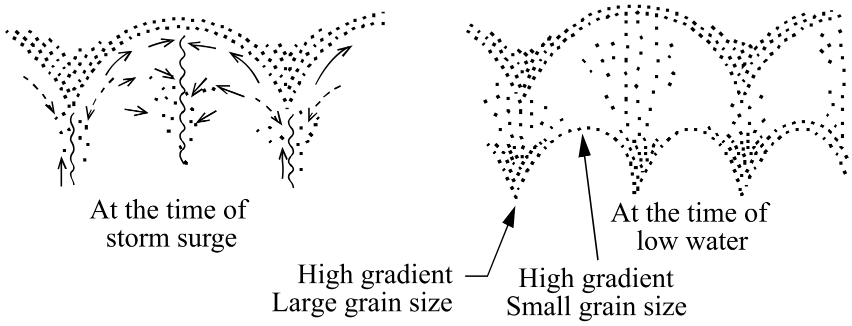

Fig. 7.4.4 Shape of the Cusp[11)]

③ **Foreshore topography**

As shown in **Fig. 7.4.5**, when there is continued calmness, a nearly horizontal area or sometimes slanting one toward the land forms in the foreshore, somewhat higher than the high tide level. This topography is called a berm. When conditions are rough, the berm is eroded, thus forming a sandbar called an inner bar near the position of the last breakers. Inner bars dissipate the wave energy when waves break upon them and are thought to prevent the further erosion of the foreshore. The sediments of the inner bars that form during rough conditions gradually return to the foreshore when it is calm, and the foreshore eventually returns to its condition prior to the rough period. The change in the shoreline at this time is described in **Part II, Chapter 2, 7.4.8 Topographical or Shoreline Deformation in the Swash Zone**.

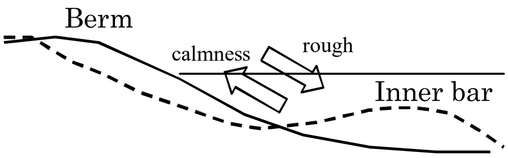

Fig. 7.4.5 Foreshore Topography

④ **Other special topography on natural beaches**

(a) Tombolo

A relatively calm water area is formed behind offshore islands, ledges, detached breakwaters, etc. A current from an exposed area to a sheltered one is generated, and the sand carried by the current deposits in the sheltered area to form a tongue-shaped topography moving shoreline offshore (**Fig. 7.4.6**). This tongue-shaped topography connected to an island or others is called Tombolo.

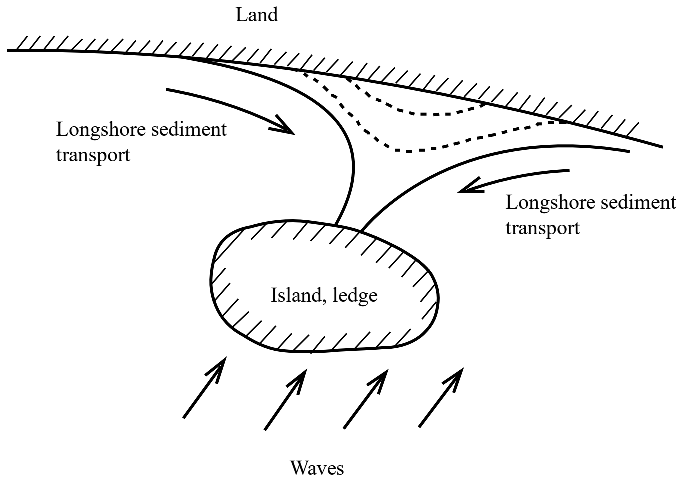

Fig. 7.4.6 Formation of a Tombolo

(b) Sand spit

The sand spit is a sandbar that is grown perpendicular to the shore formulated by the accumulation of sand drifted with longshore currents. A sand spit tends to grow at such a location as near a cape where the shore direction changes significantly (**Fig. 7.4.7**). Its tip slightly curves toward the inner bay in general, and its foreshore slope is larger on the ocean side. Typical examples in Japan include Miho-no-Matsubara, the Notsuke Peninsula in Hokkaido and Ama-no-Hashidate.

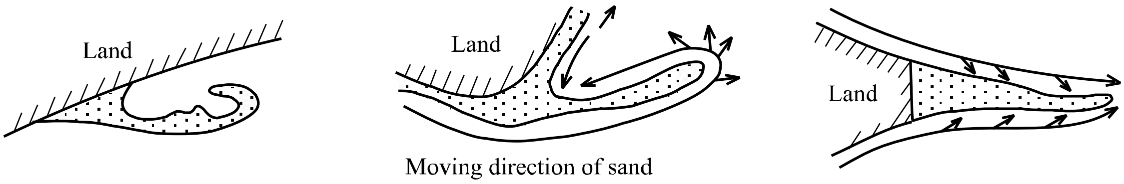

Fig. 7.4.7 Formation of Sand Spit

(c) River mouth bar

The river mouth bar is a bar formed (**Fig. 7.4.8**) by accumulation of sediment near the river mouth discharged through the river or by littoral drift pushed into the river mouth by waves. The intrusion of seawater and the flood of river water make the hydraulic condition at the river mouth complicated and the topography unstable.

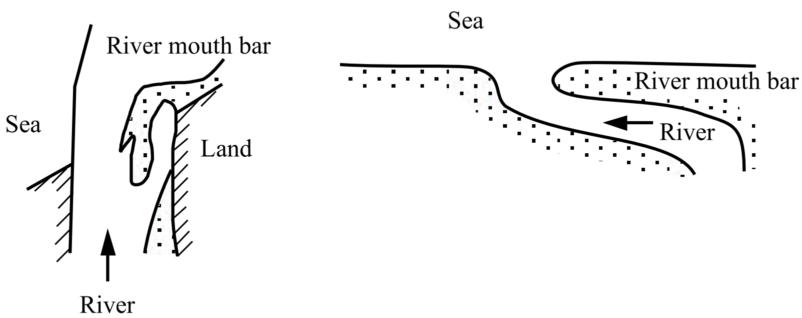

Fig. 7.4.8 Development of a River Mouth Bar

(d) Sand wave

Sand wave is the generic name of the wavelike topography that develops on the surface of sand bed in a broad sense and includes sand ripples of approximately several centimeters to several tens of centimeters in wave length and several centimeters in wave height. In a narrow sense, it indicates that a large-scale wavelike topography of approximately several meters to several hundred meters in wave length and 1 m to 30 m in wave height formed on the seabed or at the river mouth. **Fig. 7.4.9** shows an echo sounding record of a sand wave existing on the seabed of the Bisanseto in the Seto Inland Sea[18].

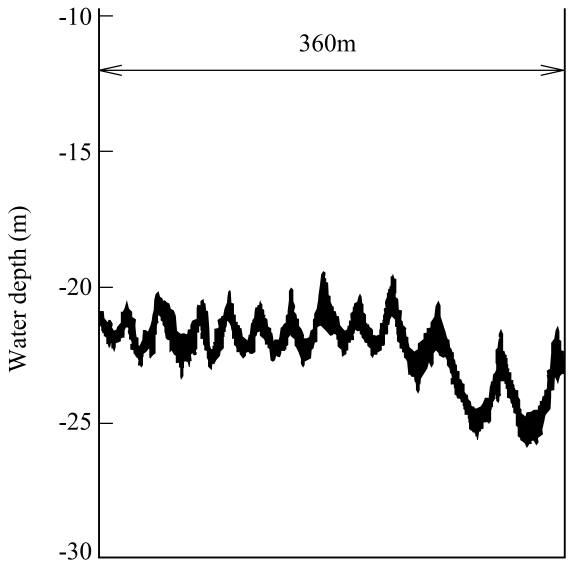

Fig. 7.4.9 Echo Sounding Record of a Sand Wave[18] (Bisan Seto)

(e) Sea cliff[19) 20)]

A cliff coast made of soft rocks is easily eroded by waves and the accompanying movement of pebbles. This type of erodible cliff is called a coastal cliff, and the collapsed sediment supplies littoral drift. Typical examples in Japan include Byobugaura in Chiba Prefecture[21], Enshu-Atsumi Coast in Aichi Prefecture, Joban Coast in Fukushima Prefecture, and Tokachi and Nozuka Coasts in Hokkaido.

7.4.3 Characteristics and Distribution of Bottom Sediment

① The grain size characteristics of the bottom sediment are generally shown with the following indices:

(a) Median diameter (d_{50}): the grain size corresponding to 50 % of the cumulative mass (p = 50%) of the cumulative grain size distribution curve

(b) Mean grain size (d_m):
$$d_m = \frac{\sum_{p=0}^{100} d_p \Delta p}{\sum_{p=0}^{100} \Delta p} \tag{7.4.1}$$

(c) Sorting coefficient (S_0):
$$S_0 = d_{75} / d_{25} \tag{7.4.2}$$

(d) Deflection distortion (S_k):
$$S_k = d_{75} \times d_{25} / (d_{50})^2 \tag{7.4.3}$$

where

p : cumulative percentage (%)

Δp : increment of the cumulative percentage

d_{25} : grain size corresponding to the cumulative percentage (25%)

d_{75} : grain size corresponding to the cumulative percentage (75%)

② Grain Size Distribution of the Bottom Sediment in the Cross Section Perpendicular to the Shoreline

Fig. 7.4.10 shows the survey result of the grain size distribution in the bottom sediment of the cross section perpendicular to the shoreline of the US Pacific coast[22] and shows the sorting situation of the bottom sediment in the cross section. This figure shows the distribution of grain sizes by setting the mean grain size as 100% at a selected foreshore point as standard point, which is easily subjected to wave actions at a mean tide level. In general, this distribution has two peaks: the offshore side and the onshore side across the standard point. One peak is located at the shallowest wave breaking point, and the other peak is located at around the center of the ordinary berm, which is between the foreshore and backshore (**Fig. 7.4.1**).

The grain size of the bottom sediment near the shoreline greatly affects the foreshore gradient. A coarser bottom sediment corresponds to a steeper gradient of the foreshore.

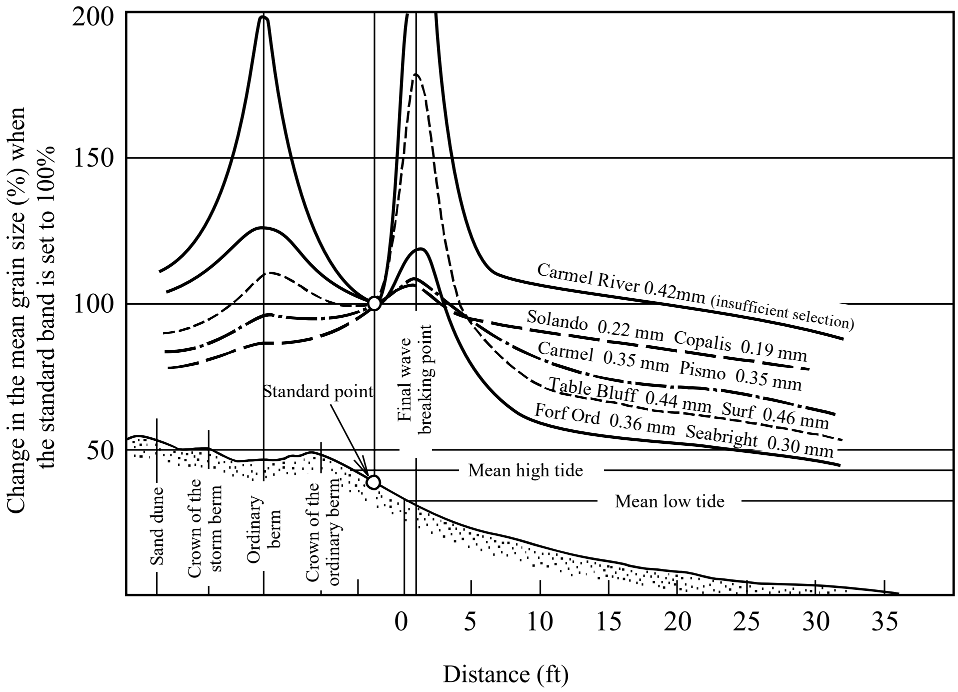

Fig. 7.4.10 Change in the Mean Grain Size on the Cross Section Perpendicular to the Shoreline[22]

③ Grain Size Distribution of the Bottom Sediment in the Longshore Direction

The grain size characteristics of the bottom sediment also change in the longshore direction. Among the sediment components supplied from rivers or coastal cliffs, the coarser gravel remains near the point of sediment source and the finer fractions are carried farther. **Fig. 7.4.11** shows the spatial distribution of the median diameter on the seabed in front of the mouth of the Yoshino River with the contour of sediment diameter[23]. The largest grain size appears near the left bank at the mouth (a sounding-map comparison indicates that this portion is the deepest part of the channel). From the area, the median diameter decreases toward every direction of the sea area. The isoline (d_{50} = 0.15 mm) surrounding the river mouth shows onshore retreat most at the slightly right bank at the river mouth and extends to the right and left shores. These features almost correspond to the direction of movement of the littoral drift that was comprehensively estimated from the seabed topography, predominant wave direction, change in river mouth bar, movable bed model experiment, and others.

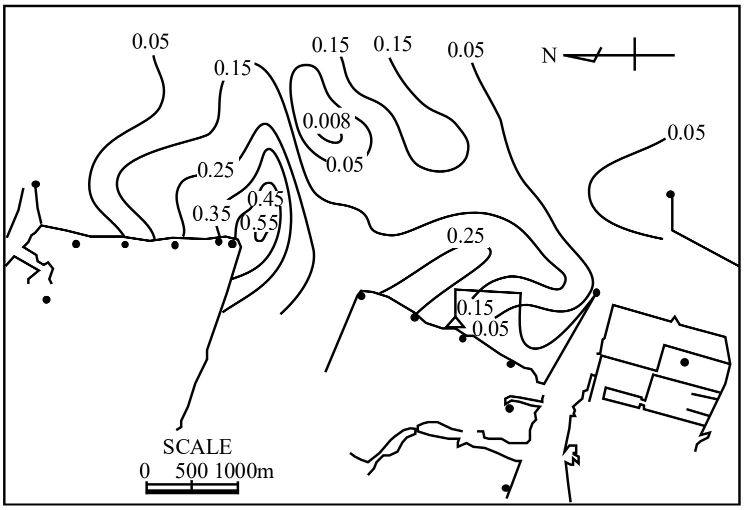

Fig. 7.4.11 Planar Distribution of the Grain Size of the Bottom Sediment in Front of the Mouth of the Yoshino River (Unit in the Figure: mm)[23)]

④ **Mineral composition and heavy mineral analysis of the bottom sediment**

The sand on the beach mainly comprises feldspar (specific gravity: 2.5 to 2.9) and quartz (specific gravity: 2.65 to 2.69) but contains some other heavy minerals with a specific gravity of three or more. There are several types of these heavy minerals, and the most commonly seen are five kinds of iron ore, hypersthene, augite, brown amphibole, and green amphibole. When several rivers flow into a shore, if the kinds of heavy minerals in the bottom sediment discharged from the rivers are different, the analysis of heavy minerals of the bottom sediment around the beach and river can provide the direction of the littoral drift.

7.4.4 Form of Littoral Drift Movement

Littoral drift is classified into three categories, namely, bedload, suspended load, and sheet flow, according to the modes of sediment movement.

① Bedload: littoral drift that moves by tumbling, sliding, or bouncing along the surface of the sea floor via the direct action of waves and currents

② Suspended load: littoral drift that is suspended in seawater by turbulence of breakers and others

③ Sheet flow: littoral drift that moves as a layer of high-density flow near the bed surface

Shallow water zones can be classified into three regions (**Fig. 7.4.12**) depending on the physical properties of waves that provide the external forces for the littoral drift phenomenon. The dominant mode of littoral drift movement in each region is as follows:

[Offshore zone] In order for sand to be moved by the action of fluid motion and oscillatory movement, the current velocity of the fluid must exceed a certain value. This condition is generally called the "threshold of movement." For littoral drift, the threshold of movement is defined with the water depth called the threshold depth of sediment movement. When the water depth is shallower than the threshold depth of sediment movement, regular and small undulating topographic contours called sand ripples will form on the sea bottom surface. When sand ripples form, vortices are generated by the fluid motion in the vicinity of the sand ripples, and the movement of suspended sediment trapped in the vortices occurs. As the water depth becomes shallower, sand ripples are extinguished, and a sheet flow condition occur in which sediment moves in stratified layers extending several layers below the sea bed surface.

[Surf zone] Inside the surf zone, the high-density suspension of sediment is formed by the severe agitation and action of large-scale vortices generated by breakers. The volume of sand that moves near the seabed surface in a bedload state also increases. For convenience, the sand movement inside the surf zone is divided into two components; one is called the longshore sediment transport, which moves parallel to the shoreline, and the other is called the cross-shore sediment transport, which is perpendicular to the shoreline. Although the time frame for the beach deformation caused by longshore sediment transport is long, the time frame for cross-shore sediment transport is relatively short (i.e., from a few days to approximately one week), similar that for periods of storms passing.

[Swash zone] The sand movement in a swash zone differs for the times of wave runup and downflow. During the time of wave runup, sand is placed in suspension by the agitation at the front of a wave and is transported by running-up water. During the downflow, sand is carried in bedload mode.

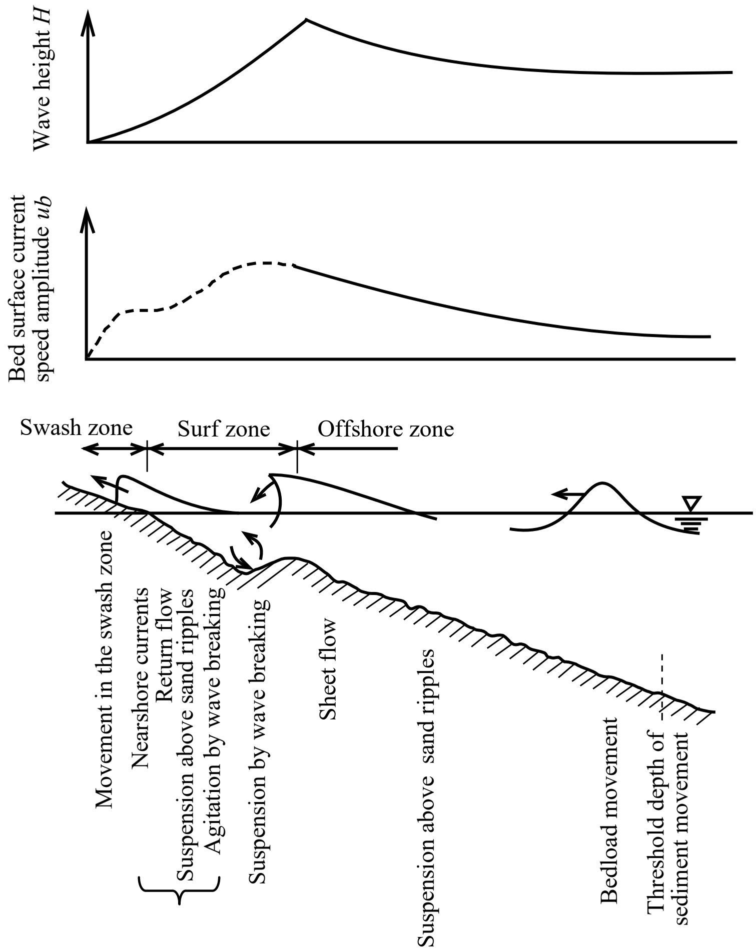

Fig. 7.4.12 Changes in Sediment Movement Modes in Cross-Shore Direction[15)]

7.4.5 Physical Meaning and Estimation Formulas for the Threshold Depth of Sediment Movement

With respect to the threshold depth of sediment movement, which is required to determine the extension of breakwater or the water depth at the head and offshore boundary of beach deformation, Sato and Tanaka[16) 24)] conducted a number of field surveys by using radioactive glass sand as a tracer. On the basis of their observed results, they defined the littoral drift movement conditions as follows.

Surface layer sediment movement: As shown in **Fig. 7.4.13 (a)**, the elongation of the isometric lines that show the distribution of radioactive glass sand after waves acted upon it on the sea floor demonstrates that all sand has moved in the direction of the waves. However, the location of the highest count remained at the injection point of glass sand, thus indicating no movement. This corresponds to a situation in which the surface layer sand is moved collectively by traction parallel to the wave direction.

Total sediment movement: As shown in **Fig. 7.4.13 (b)**, this refers to a situation in which both the isometric lines and the portion of the highest count move in the wave direction. This corresponds to a situation of distinct sand movement with the result of apparent change in water depth. The threshold depth of total sediment movement is often used as the threshold depth of sediment movement for engineering purposes.

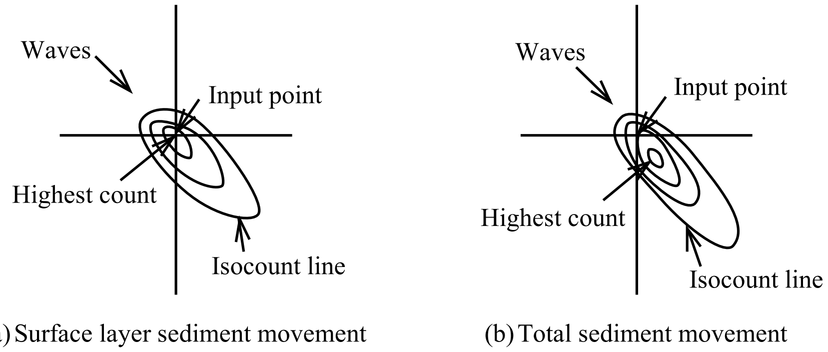

Fig. 7.4.13 Spread of Radioactive Glass Sand in Surface Layer Sediment Movement and Total Sediment Movement

On the basis of the field data, two equations were proposed by Sato and Tanaka for estimating the threshold depth of surface layer sediment movement and the threshold depth of total sediment movement.

① **Threshold depth of surface layer sediment movement**

$$\frac{H_0}{L_0} = 1.35\left(\frac{d}{L_0}\right)^{1/3} \sinh\frac{2\pi h_i}{L}\frac{H_0}{H} \tag{7.4.4}$$

② **Threshold depth of total sediment movement**

$$\frac{H_0}{L_0} = 2.40\left(\frac{d}{L_0}\right)^{1/3} \sinh\frac{2\pi h_i}{L}\frac{H_0}{H} \tag{7.4.5}$$

where

L_0 : deepwater wavelength (m)

H_0 : equivalent deepwater wave height (m)

L : wavelength at water depth h_i (m)

H : wave height at water depth h_i (m)

d : sediment grain size, average grain size or median diameter (m)

h_i : threshold depth of sediment movement (m)

Repeated calculations are required to estimate the threshold water depths by using **equations (7.4.4)** and **(7.4.5)**. Therefore, calculation diagrams such as those in **Fig. 7.4.14 (a)** and **(b)** have been prepared so that the depths can be easily estimated. By specifying d/L_0 and H_0/L_0, it is possible to determine h_i/L_0. Specific calculation examples are shown in Ref. 9).

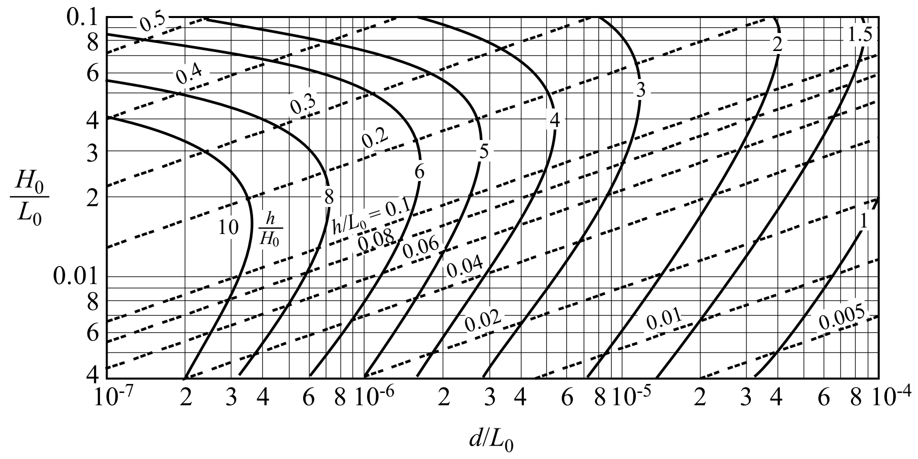

Fig. 7.4.14 (a) Calculation Diagram for Threshold Depth of Surface Layer Sediment Movement[9)]

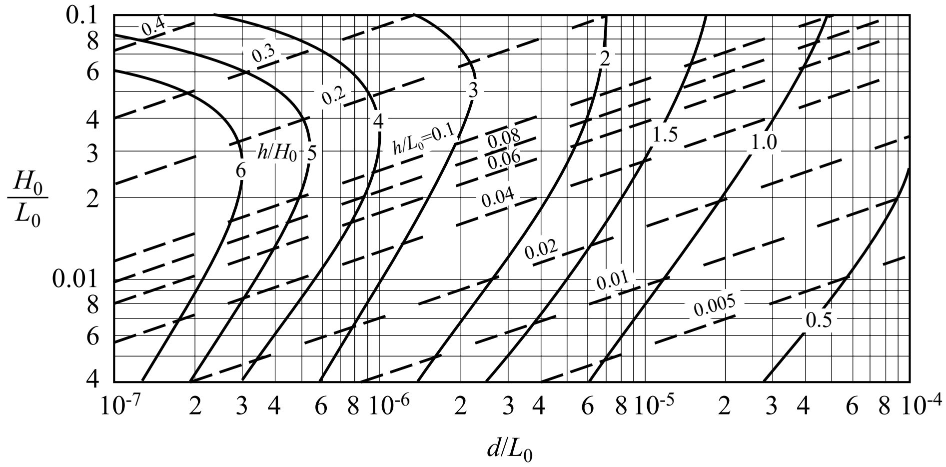

Fig. 7.4.14 (b) Calculation Diagram for Threshold Depth of Total Sediment Movement[9)]

7.4.6 Longshore Sediment Transport

① The predominant direction of longshore sediment transport is determined using the following information:

(a) Topographies of the natural coast and around coastal structures (see **Fig. 7.4.15**)

(b) Alongshore distribution of the sediment characteristics such as median diameter and mineral composition

(c) Direction of movement of fluorescent sand tracers

(d) Direction of incident wave energy flux

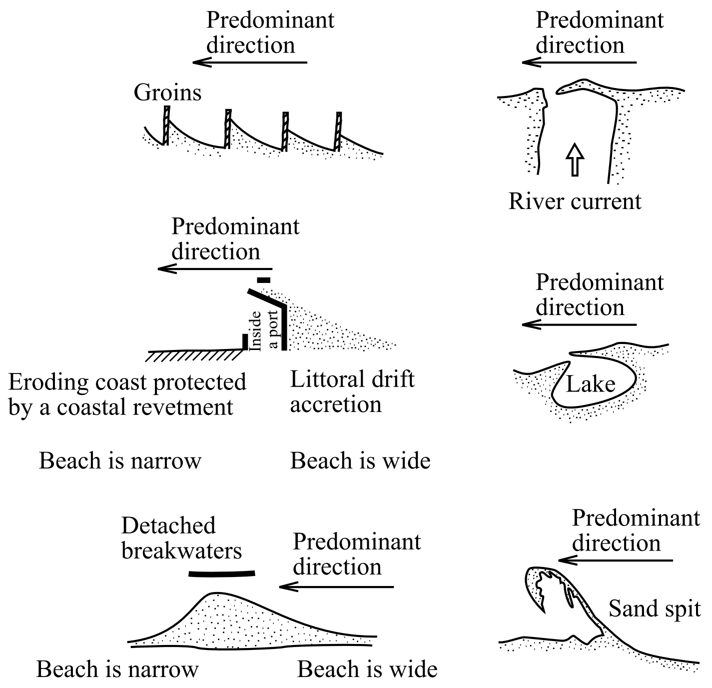

Fig. 7.4.15 Typical Coastal Topography Showing the Predominant Direction of Longshore Sediment Transport

② To estimate the longshore sediment transport rate, the following data must be prepared and sufficiently investigated:

(a) Continuous observation data of the change in sediment volume around a coastal structure

(b) Data on the alongshore component of wave energy flux

(c) Data concerning the littoral drift rate at the surrounding coast

(d) Data on past dredging volume

(e) Continuous observation data on deposition volume at the experimental dredging site

(f) Data on the volume of movement of tracers, such as fluorescent sand, placed within the surf zone

③ Various formulas can be used to estimate an approximate value of longshore sediment transport rate[9) 25) 26) 27)]. The formulas are normally given in the expression shown in **equation (7.4.6)**, and the coefficient for various formulas is given in **Table 7.4.1**.

$$Q_x = aE_x$$
$$E_x = \Sigma K_r^2 \left(\frac{n_A w_0 H_A^2 L_A}{8T} \right) \sin\alpha_b \cos\alpha_b \qquad \textbf{(7.4.6)}$$

where

Q_x : longshore sediment transport rate (m^3/s)

E_x : alongshore component of wave energy flux (kN·m/m/s)

K_r : refraction coefficient between the wave observation point and the wave breaking point

n_A : ratio of group velocity to wave celerity at the wave observation point

w_0 : unit weight of sea water (kN/m^3)

H_A : wave height at the wave observation point (m)

L_A : wavelength at the wave observation point (m)

T : wave period (s)

α_b : angle of wave incidence at the wave breaking point (°)

Table 7.4.1 Coefficient *a* for Longshore Sediment Transport Rate Formula

Savage[26)]	Sato and Tanaka[25)]	U.S. Army Corps of Engineers[27)]
0.022	0.03	0.04

7.4.7 Littoral Drift Phenomena in the Surf Zone

Inside the surf zone, large quantities of sand move by the turbulence caused by breakers, by the increase of the wave orbital velocity near the bottom due to shallower water depth, and by the existence of nearshore currents.

On the basis of the longshore sediment transport rates obtained from studies of fluorescent sand, Komar[28)] reported that bedload dominates in the surf zone. Sternberg et al.[29)] reported that most of the longshore sediment transport rate can be explained by suspended load. As a counterpoint to these two conflicting results, Kato et al.[30)] used fluorescent sand to measure the local sediment transport rates within the surf zone and found that bedload dominates when the velocity of water particle due to waves is small, whereas suspended load dominates when the velocity becomes larger.

The sediment movement when suspended sediment is predominant can be examined by dividing the movement into two processes.

① Sediment suspension process caused by organized vortices formed by wave breaking

② Settling process during which sediment is buffeted by random external forces following the breakup of organized vortices

Fig. 7.4.16 shows the temporal variations of suspended sediment concentration and horizontal current velocity measured by Katoh et al.[31)] inside the surf zone in the field. The white arrows in the figure indicate the waves that broke on the seaward side of the observation point, and the black arrows indicate the waves that passed the observation point and broke on the shoreward side. The suspended sediment concentration increased rapidly when waves broke on the seaward side. This result indicates that sediment suspension is related to the organized vortices, particularly obliquely descending vortices[32)] that occur after waves break.

The suspended sediment concentration by wave breaking is also related to the type of wave breaking. Kana[33)] measured the suspended sediment concentration at the on-site beach and reported that the suspended sediment concentration by plunging wave breaking is approximately 10 times of the suspended sediment concentration by spilling wave breaking.

The bottom sediment suspended by wave breaking is carried to the same direction as the flow by the subsequent flow, i.e., it is carried to the onshore direction by the flow toward the shore just after wave breaking and then to the offshore direction by the flow toward the sea when the next wave trough passes. Therefore, it is carried to the onshore direction if suspended for a short period of time but is carried to the offshore direction if suspended for a long period. Given this situation, Dean[34)] indicated that the direction of movement of littoral drift at the wave breaking point can be sorted by the ratio of the settling velocity of sand particles to the wave period.

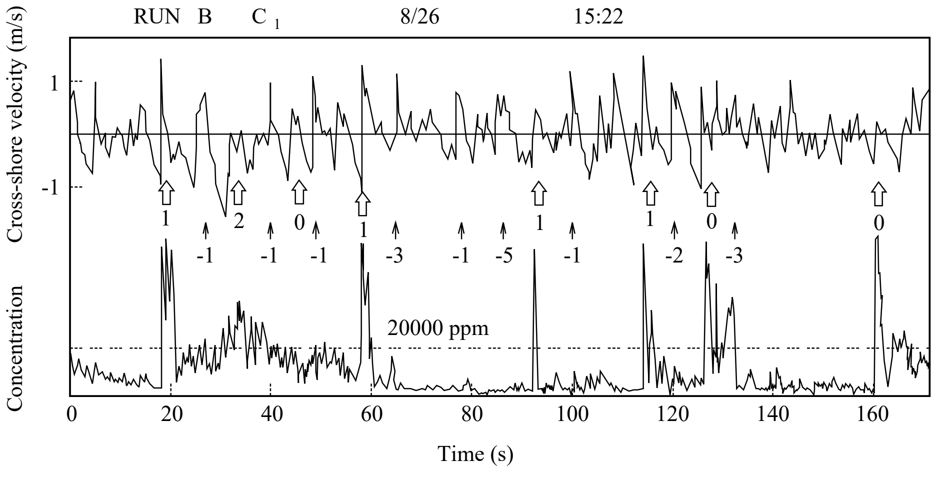

Fig. 7.4.16 Example of Field Observation of Concentration of Suspended Sediment[31)]

7.4.8 Topographical or Shoreline Deformation in the Swash Zone

Horikawa et al.[35] investigated the criteria for shoreline advance and retreat due to sand movement in the swash zone on the basis of laboratory experiments and proposed **equation (7.4.7)**, which is also applicable for the field condition.

$$\frac{H_0}{L_0} = C_s \left(\tan\beta\right)^{-0.27} \left(\frac{d}{L_0}\right)^{0.67} \qquad \textbf{(7.4.7)}$$

where

H_0 : deepwater wave height (m)

L_0 : deepwater wavelength (m)

$\tan\beta$: average bottom slope from the shoreline to a water depth of 20 m

d : sediment grain size (m)

C_s : coefficient

According to **equation (7.4.7)**, a shoreline will retreat when $C_s \geq 18$ (see **Fig. 7.4.17**).

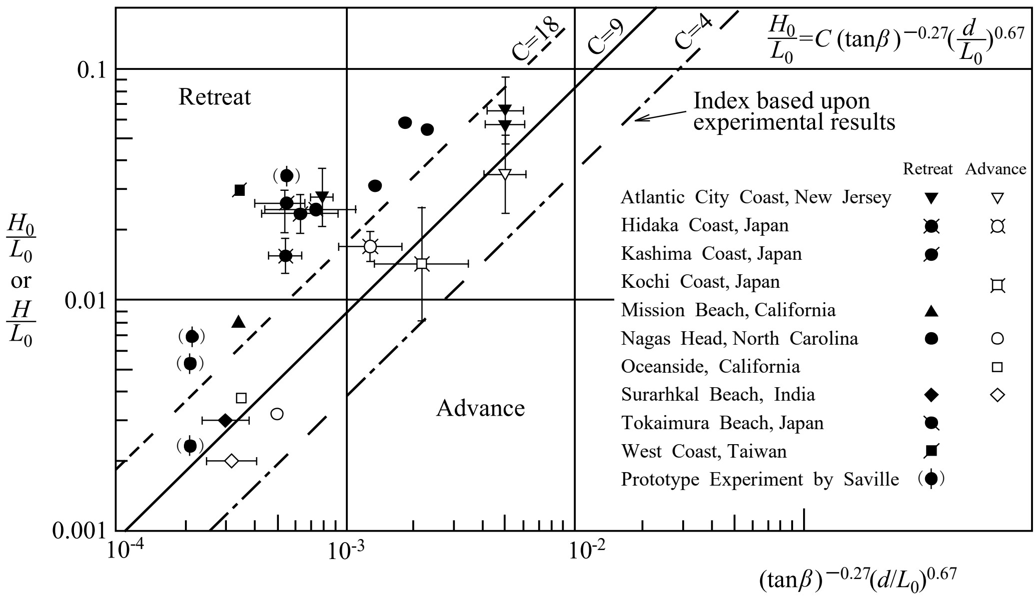

Fig. 7.4.17 Advance and Retreat of Shorelines in the Field[35]

Katoh et al.[36] revised **equation (7.4.7)** by using deepwater wave energy flux and presented a model to predict the daily shoreline change. **Fig. 7.4.18** is a comparison of the predicted and measured results of shoreline location.

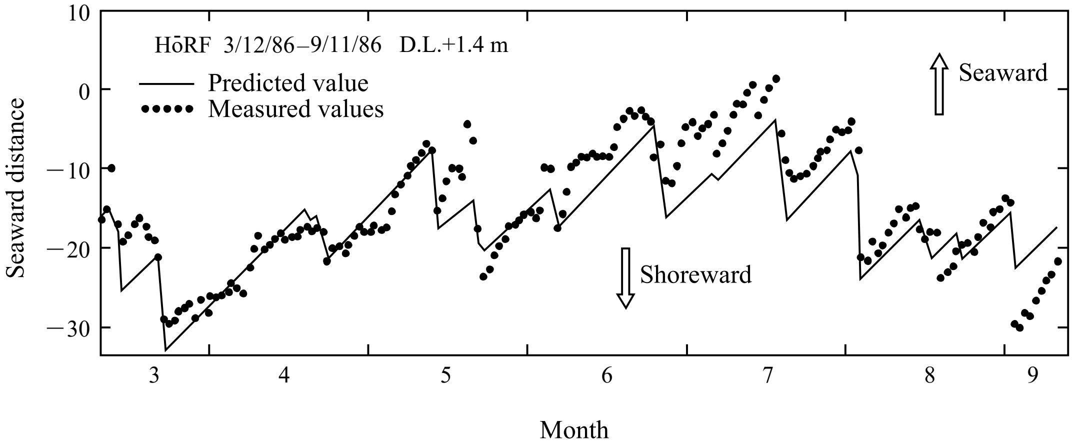

Fig. 7.4.18 Comparison of Prediction and Measurement of Shoreline Location[36)]

7.4.9 Relationship between Foreshore Topographical Changes and Groundwater Level

The topographical changes that accompany the tidal level changes in the foreshore can be explained as follows by using **Fig. 7.4.19**[37)]. When the tidal level changes, the beach groundwater level also changes as a response. However, because the response of the groundwater level is behind the change of the tidal level, the groundwater level at the flood tide differs from that at the ebb tide even though the tide level is the same. This means that **(a)** during **the flood tide**, the groundwater level is low, and it is easy for the seawater running up on the beach to permeate underground. Therefore, the sediment carried by the seawater when it runs up on the beach will accrete in this location. **(b)** On the contrary, during **the ebb tide** the groundwater level is high, and it is difficult for seawater to run up on the beach and to permeate underground. At certain conditions, the groundwater may flow out of the beach surface during the ebb tide. As shown in **Fig. 7.4.19**, the result is that the sediment that accreted during the flood tide will be eroded and will return to its original location.

When waves run up to a high level on a beach during storms, a high groundwater level condition continues throughout the stormy weather period because the runup seawater permeates into the beach, and the condition becomes that as shown in **Fig. 7.4.19 (b)**. The occurrence of rapid foreshore erosion during such a condition has been confirmed by field data[38)].

Some shore protection methods make use of this relationship between the foreshore groundwater level and sand movement, i.e., lowering the groundwater level by forced means or gravity to prevent erosion. In the method making use of gravity, a highly water-permeable layer is installed in the foreshore sand to cause the groundwater flow down offshore of the foreshore and to lower the groundwater level. With this method it is possible to preserve beach conditions that are very close to those of a natural beach in appearance because no structures are laid above the beach floor[39)].

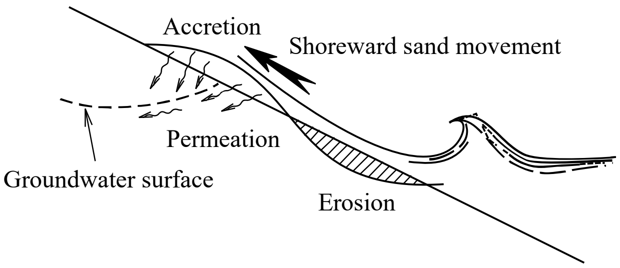

(a)Flood Tide

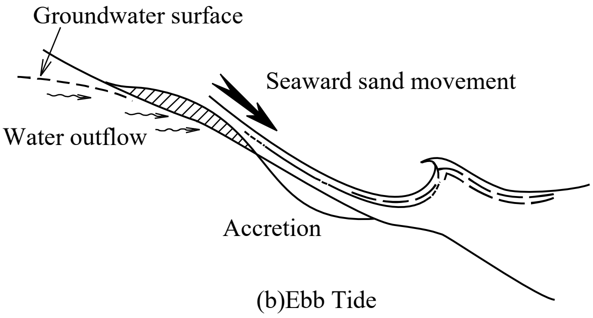

(b)Ebb Tide

Fig. 7.4.19 Relationship between Foreshore Topographical Changes and Groundwater Level[37)]

7.4.10 Movement of Longshore Bars

Longshore bars form periodically and move offshore[40)]. Although longshore bars move offshore, cross-shore sediment transport may occur offshore or onshore in various places; therefore, offshore sediment transport occurs near the bar crests, whereas onshore sediment transport occurs in trough areas[40)]. The period of cyclic offshore bar movement depends on the sea coast and can range from 1 year to 20 years.

7.4.11 Windblown Sand[15)]

The windblown sand causes harbor shoaling or river mouth closure, deteriorates human living environment, and causes problems when utilizing a beach for agriculture or cars passing roads near the beach. The most dominant factor related to the windblown sand is wind, but other factors such as grain seize, specific gravity, wet–dry state of ground sand, ground armoring conditions, armor units, topography, and effect of facilities related to the phenomenon. It is said that windblown sand moves in three types of transport states: ① bedload state, ② suspended state, and ③ saltation state. Among them, very few moves in the suspended state. Most sands move in the saltation state while the wind velocity is small. As the wind velocity increases, 20% of the whole windblown sand moves in the bedload state, and the remaining 80% moves in the saltation state[41)]. Although the vegetation on the shore is just approximately 10 cm in height, but it is shown that it is useful in reducing the amount of windblown sand on the basis of on-site data[42) 43)].

7.4.12 Relationship between Climate Change and Topographic Change

It is predicted that the future rise in sea level and the change in wave characteristics probably due to climate change[44) 45)] cause a long time change in the topography of coastal zones[46)].

The sea level rise causes the erosion of the foreshore and the retreat of shorelines. A change in water depth due to the sea level rise also changes the magnitude of the wave energy acting on the field; therefore, the sandy beach is transformed to the corresponding new equilibrium state. Considering that the coastal topography changes to balance the total amount of erosion and accretion, the shallow sea area, including the foreshore, is eroded (**Fig. 7.4.20**), and the sediment accumulates farther offshore. If the change is small, the amount of change in the shoreline is approximated by **equation (7.4.8)**[47)]. **Equation (7.4.8)** is usually called Bruun's law.

$$s = la / h \tag{7.4.8}$$

where

s : amount of retreat of the shoreline (m)

l : onshore–offshore distance between the threshold depth of the sediment movement of littoral drift and the crown of the berm (m)

a : amount of sea level rise (m)

h : vertical height between the threshold depth of the sediment movement of littoral drift and the crown of the berm (m)

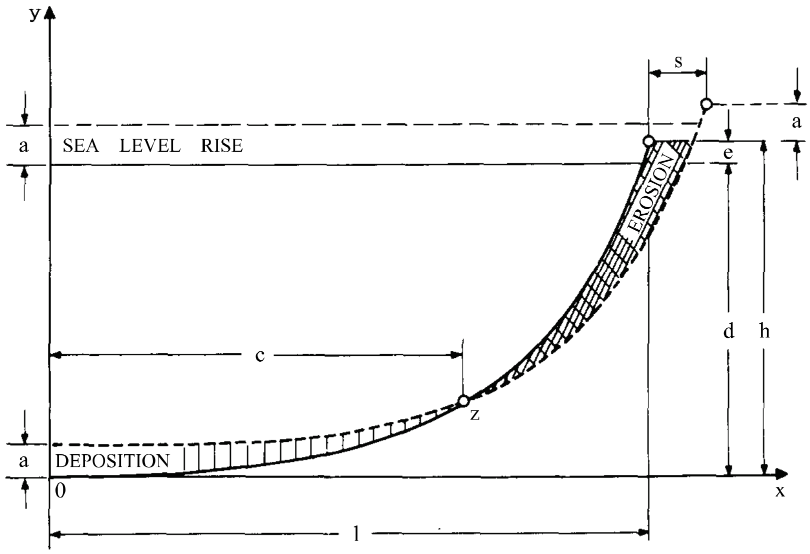

Fig. 7.4.20 Retreat of the Shoreline Caused by the Change in Equilibrium Topographic Cross Section Due to Sea Level Rise[48)]

On the contrary, the change in wave characteristics in the future also affects the topographical change. Among the wave statistic, the mean wave affects the beach profile in normal times, and the peak wave is also related to the amount of the maximum erosion or occurrence of coastal disasters due to wave runups. Given that the change in coastal topography due to waves occurs in addition to the erosion of foreshore due to the abovementioned rise in sea level, massive erosion may occur because of the constant erosion due to the sea level rise and the temporary erosion due to the increase of peak waves. Furthermore, if the wave direction changes in the future, the predominant direction of the longshore sediment transport or the longshore sediment transport rate changes, and a littoral drift problem may occur even where no particular problems have occurred thus far[49)].

7.5 Scouring and Sucking

7.5.1 General

If there is a risk of impairing the stability of facilities brought about by scouring of the foundation of the facilities concerned, the ground, and others and by leakage of reclaimed soil in hinterland ground of the structures, it is necessary to take proper countermeasures to prevent scouring and leakage of reclaimed soil, considering the structural types of the facilities concerned.

7.5.2 Scouring

(1) Scouring shall be taken into consideration, as necessary, if scouring around facilities, such as breakwaters, groins, and training jetties, is proven to affect the safety of the facilities.

(2) Wave characteristics that act on natural beaches can be considered as nearly constant over a long period of time. Topographies that form in response to these characteristics are nearly stable as well. Scouring will occur when facilities are constructed and the equilibrium between the external forces and topography will be disturbed locally or over a broad area. The mechanism and amount of scouring will change according to the location of a structure because the wave action on the structure changes, and hence, when choosing methods for scouring prevention, the ranges, strength, and the like of such works must be considered carefully.

(3) Scouring in front of coastal revetment

It is well known that scouring in front of coastal revetment is closely correlated with wave reflection coefficient. For example, **Fig. 7.5.1** has been proposed for determining scouring or accretion by means of the reflection coefficient K and the parameter $(H_0/L_0)(l/d_{50})\sin\alpha$ which is defined with the wave steepness H_0/L_0, mean diameter of sediment d_{50}, slope gradient of coastal revetment α (for a vertical breakwater, α = 90º), and the distance l from the wave run-up point on an equilibrium profile to the location of the coastal revetment[50]. The diagram indicates that all other conditions being equal, it is advantageous against scouring in front of coastal revetment to make the front surface of revetment inclined.

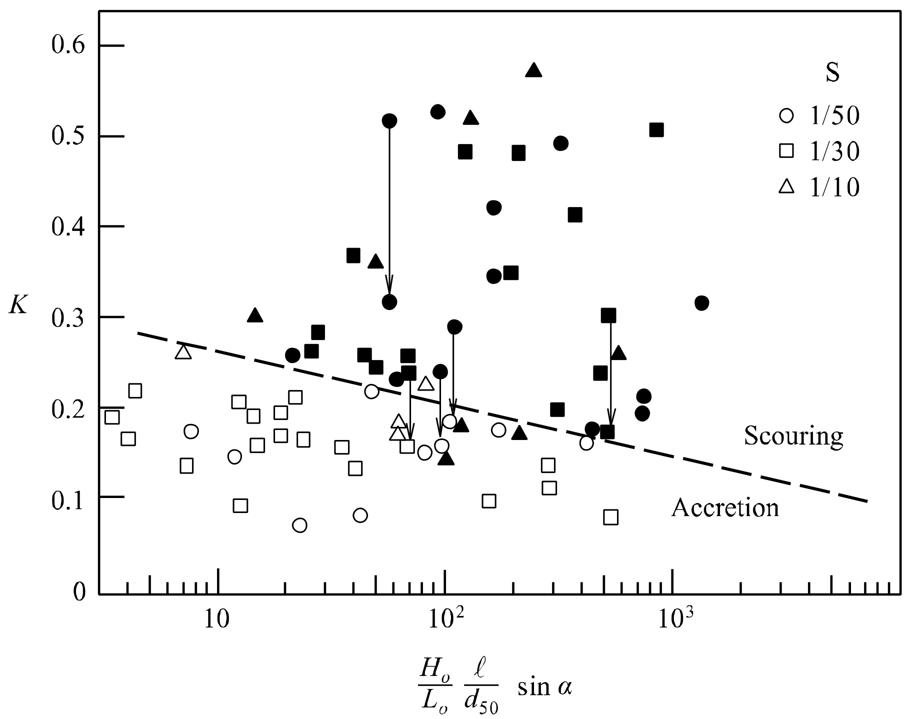

Fig. 7.5.1 Threshold Conditions Between Scouring and Accretion in Front of Coastal Revetment [50)]

(4) Local scouring around breakwaters

① **Scouring mainly in the surf zone**

(a) Local scouring at the breakwater head

Figure 7.5.2 shows the local scouring conditions around a breakwater head, as analyzed by Tanaka.[51)] The maximum scouring depth is found to be nearly equal to the maximum significant wave height $(H_{1/3})_{max}$ during the period up to 15 days prior to the time of scouring measurements. In addition, **Fig. 7.5.3** shows the relationship between the water depth around a breakwater head and scouring depth. The scouring depth is at its maximum value when the water depth at the breakwater head is about 3 to 5 m (namely, in the surf zone).

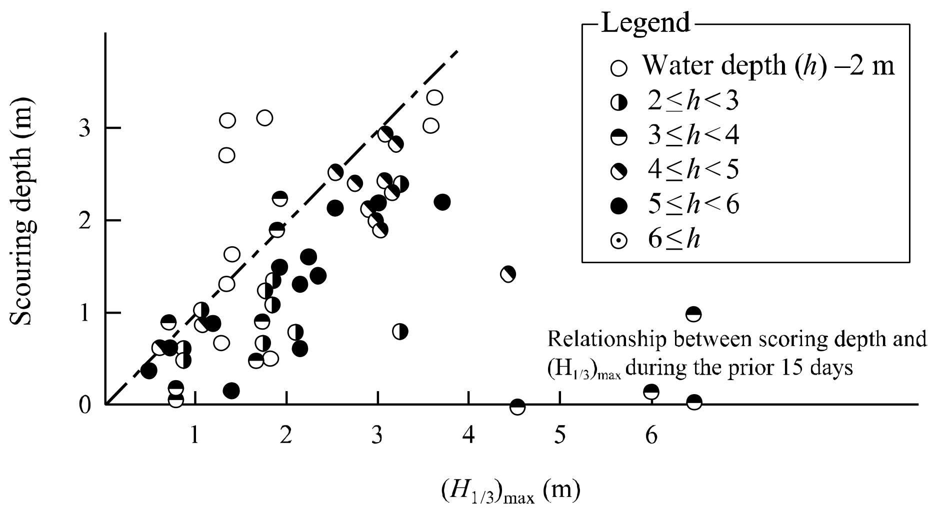

Fig. 7.5.2 Relationship Between Scouring Depth at the Breakwater Head and Maximum Significant Wave Height During the Prior 15 Days [51)]

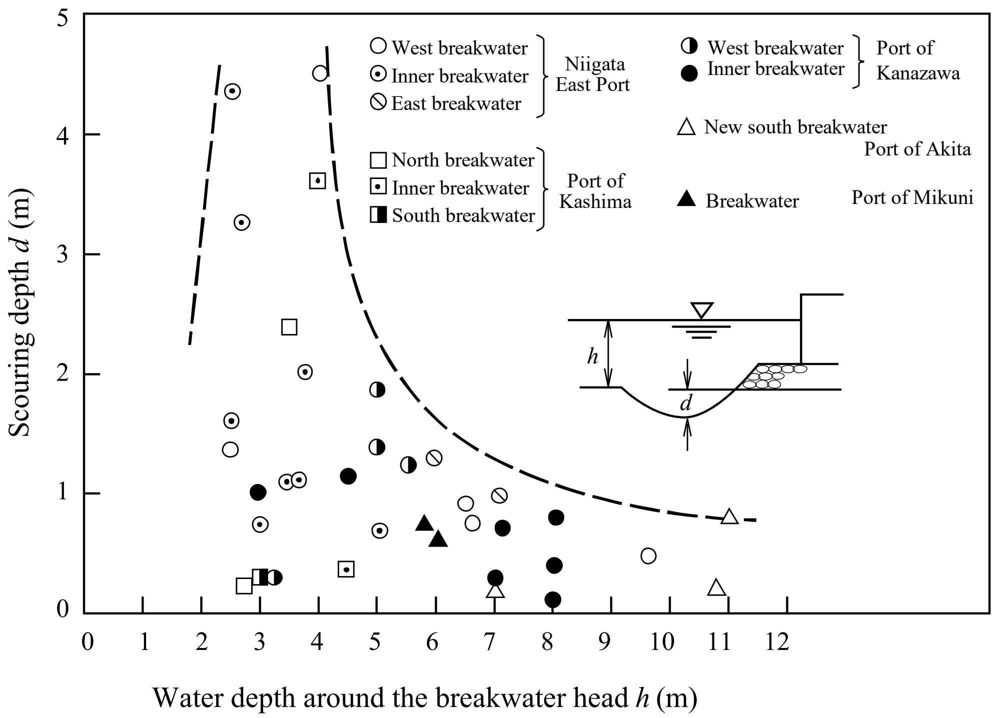

Fig. 7.5.3 Relationship Between Scouring Depth and Water Depth Around the Breakwater Head [51)]

(b) Scouring in front of breakwaters

Figure 7.5.4 shows the relationship between the scouring depth in front of a breakwater and water depth. [51] The black circles in the figure indicate the condition of scouring around the oblique part of the breakwater. The scouring depth is at its maximum value at the bend of the breakwater, where the water depth is about 7 m, and gradually decreases seaward. On the other hand, the scouring depth in front of the straight part of the breakwater, which is indicated by the white circles, has its maximum value at around a water depth of 2 m. The location of the maximum scouring depth corresponds to the location of a longshore bar.

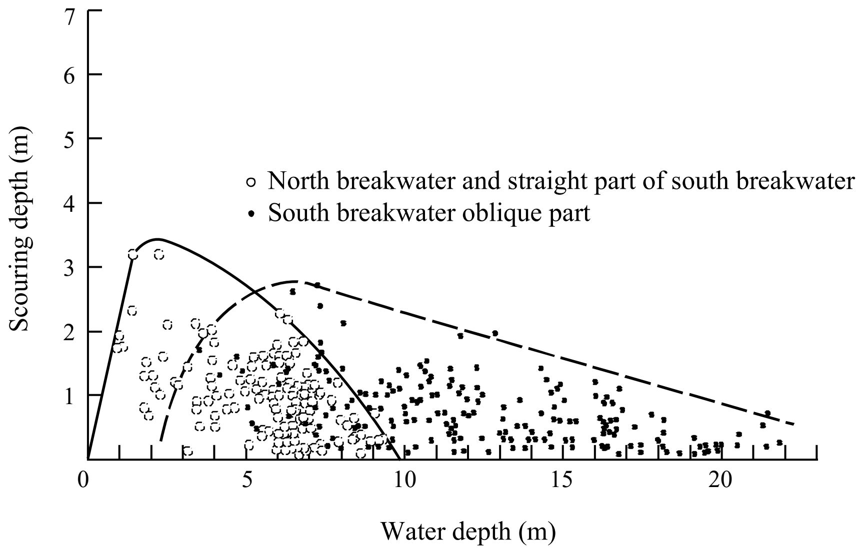

Fig. 7.5.4 Relationship Between Scouring Depth in Front of a Breakwater and Water Depth [51]

(c) Local scouring outside breakwaters

Figure 7.5.5 shows examples of places where typical local scouring occurs as a result of breakwater extension:

(i) Breakwater head (especially pronounced when the breakwater head is in the surf zone).

(ii) Around the straight portion of the breakwater (especially pronounced near the point where the breakwater crosses the longshore bar).

(iii) Around a front mound or a submerged breakwater (especially pronounced inside the harbor).

(iv) Places where the breakwater bends.

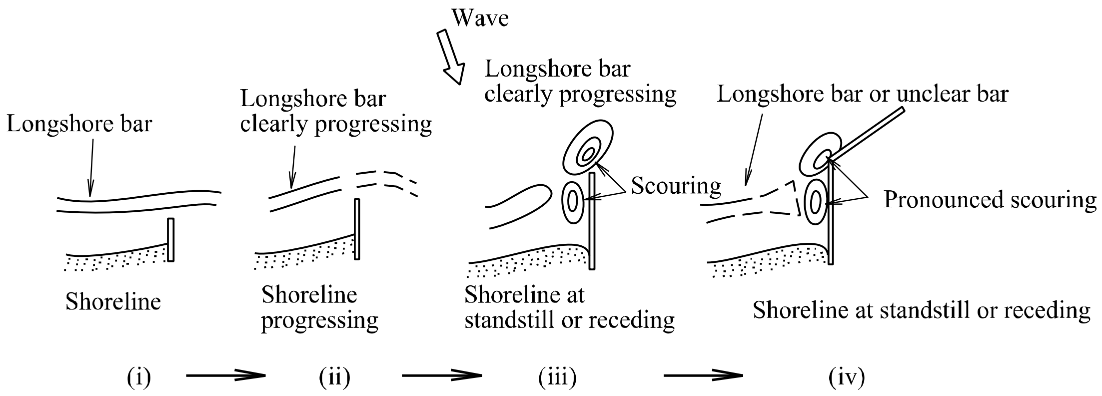

Fig. 7.5.5 Local Scouring Outside the Breakwater [52]

② **Scouring in standing wave domain**

Scouring depth in front of a vertical wall tends to decrease as the initial water depth in front of the wall increases, and the wave condition is shifted into the standing wave domain. In the case of composite-type breakwaters, where the toe of the rubble mound is somewhat away from the wave reflection face of the upright section, scouring at the toe of the rubble mound by standing waves sometimes becomes a problem. Irie et al. [53] conducted experiments concerning this type of scouring and highlighted the following issues:

(a) The basic parameter is U_b/ω, the ratio of the maximum horizontal velocity of water particles at the bottom by incident waves U_b to the settling velocity of sediment ω. When $U_b/\omega > 10$, sediment will move from the location of the node of standing waves to the location of the antinode, with scouring occurring at the node and accretion taking place at the antinode. It is called L-type scouring. When $U_b/\omega < 10$, the opposite phenomenon will occur. It is called N-type scouring (refer to **Fig. 7.5.6**). The L-type scouring refers to the phenomenon where accretion occurs at the antinode of standing waves and scouring occurs at the node, whereas the N-type scouring refers to the opposite phenomenon where scouring occurs at the antinode and accretion occurs at the node.

(b) As the flow velocity at the sea bottom in the field is higher than that in the experiment, the value of U_b/ω tends to be larger than 10 in the field, and generally, scouring at the node of standing waves is predominant. Normally, because a toe of the rubble mound is located at the distance of about 1/4 wavelength or so from the upright wall, scouring and subsidence of the rubble mound of breakwater will occur at its toe as the sediment there moves toward the location of the antinode at one-half wavelength from the upright wall.

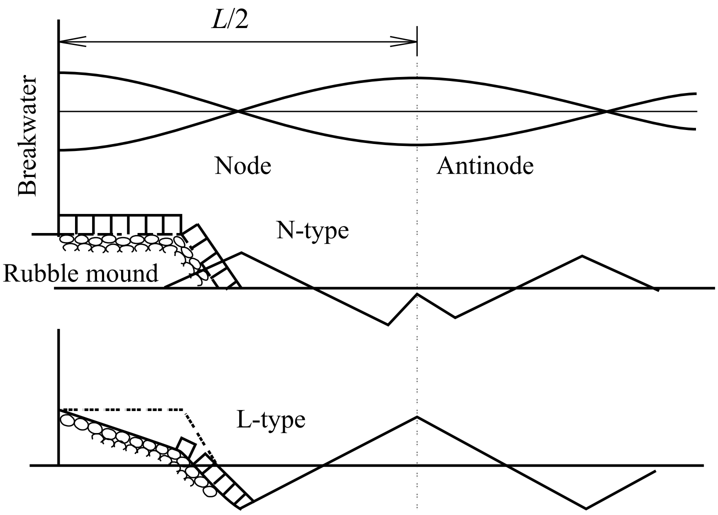

Fig. 7.5.6 Sketch of Scouring by Standing Waves [53]

③ Scour of sandy seabed under wave-dissipating blocks

One of the causes of settlement failure of wave dissipating blocks is scour of sandy seabed under the blocks. Even if the mass of wave-dissipating blocks satisfies the required mass estimated by Hudson's or other formulas, the scour of sandy seabed gradually settles the blocks. This settlement decreases the interlocking of the blocks resulting in scatter and breakage of the blocks.

Oscillatory flows by waves occur inside the rubble mounds or wave-dissipating blocks, and the flows scour the sandy seabed below the rubble mound or the wave-dissipating blocks. Thus, the wave-dissipating blocks settle down [54]. The sand below the wave-dissipating blocks is often scoured by the wave breaking on the slope of wave-dissipating blocks (**Fig. 7.5.7**). The scoured sand suspends on the sea surface near the wave-dissipating blocks and deposits behind the caisson by wave overtopping.

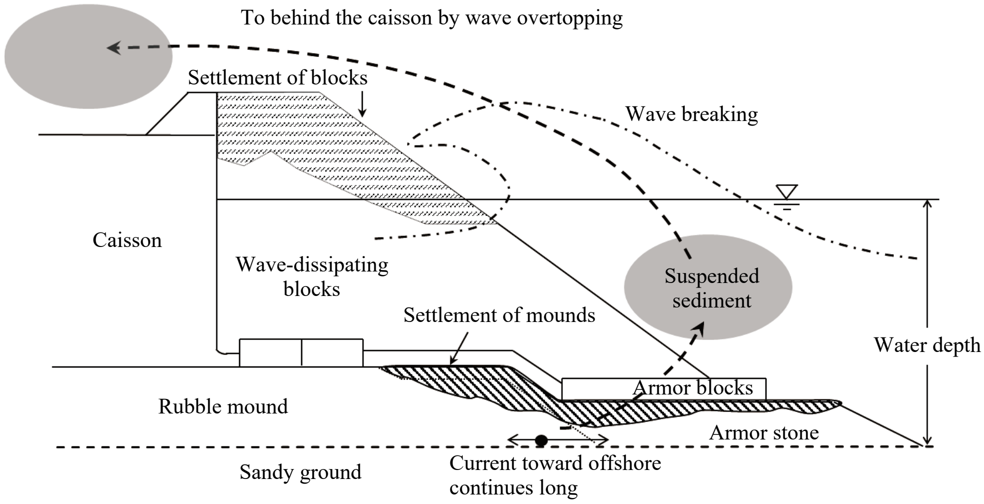

Fig. 7.5.7 Settlement of Mounds and Wave-Dissipating Blocks

The amount of scoured sandy seabed below the wave-dissipating blocks can be estimated by the following equation [55]. The definition of the amount of scour is shown in **Fig. 7.5.8**.

$$\frac{A_e}{A_T} = F_C\left(\frac{D_m}{B_{mb}} - \frac{800d_{50}}{h^{0.2}}\right) \tag{7.5.1}$$

$$D_m = \frac{H}{\sinh(2\pi h / L)} \tag{7.5.2}$$

where

A_e : amount of scour (m^2) (no scour occurs when negative)

A_T : cross-sectional area of a wave-dissipating block (m^2)

D_m : orbital diameter of a water particle below the wave-dissipating blocks (or in the mound if there is a mound below the wave-dissipating blocks) (m)

H : significant wave height (m)

L : wave length (m)

B_{mb} : length from the caisson wall to the slope of a wave-dissipating block (m)

d_{50} : median grain size of sand in the surface layer of sandy seabed (m)

h : water depth where the breakwater is installed (m)

F_C : coefficient related to the cross-sectional shape below the wave-dissipating blocks (0.84 if $h_F = 0$ and the wave-dissipating blocks are put directly on sandy seabed, 0.64 if the thickness of rubble mound is thin ($h_F < 4d_R$), and 0.32 if the thickness of rubble mound is thick ($h_F \geq 4d_R$). Armor block is not included in this rubble mound.)

h_F : thickness of rubble mound installed at the foot of wave dissipating blocks (m)

$d_R = (M_R/\rho_R)^{1/3}$: nominal diameter of the rubble mound stone(m)

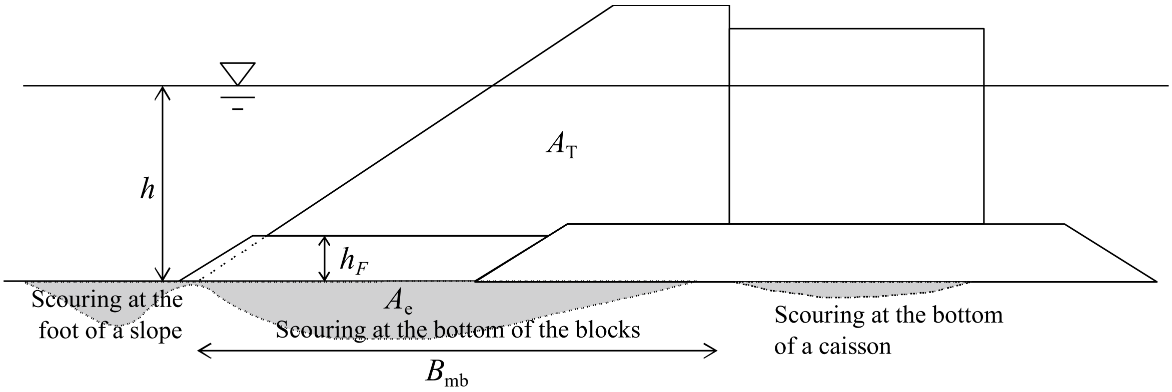

Fig. 7.5.8 Definition of the Amount of Scour (Equation (7.5.1) only Covers Scour below the Wave-Dissipating Blocks)

Scour tends to stabilize at its maximum value with actions by several thousands of waves. The amount of scouring estimated by **equation (7.5.1)** indicates its maximum value. Moreover, scouring is significant in long-period swelling waves, and it may be noticeable in long-period waves even if the wave height is small.

When scour under wave-dissipating blocks is predicted, it is necessary to examine the preliminary countermeasure work considering the type and scale of the target facilities, degree of difficulty, construction period, construction cost, and past scour prevention works and to select proper measures including corrective measures after the settlement of wave dissipating blocks.

The scour prevention work is basically laid under the rubble mound from the front edge to the rear one as shown in **Fig. 7.5.9**. Moreover, stronger scour prevention work such as mats is needed to be installed at the foot of a slope.

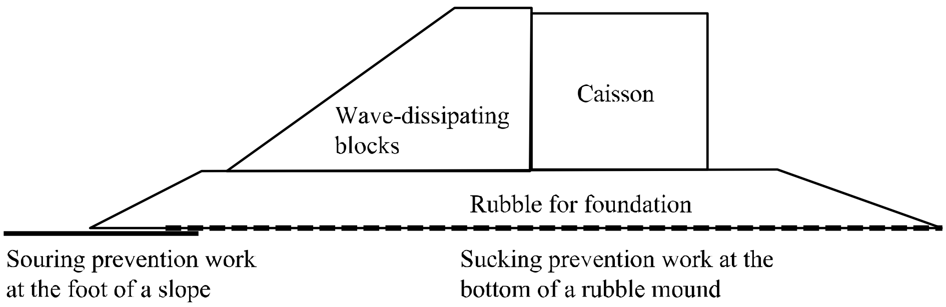

Fig. 7.5.9 Scouring Prevention Work

7.5.3 Leakage of reclaimed soil behind seawalls

(1) If facilities are predicted to become unstable due to leakage of reclaimed soil behind seawalls, it is necessary to take proper prevention countermeasures considering the structural type of the facilities. The leakage of reclaimed soil is caused by mound-transmitted waves, waves acting through the joint between caissons, or wave overtopping. As the reclaimed soil leaks gradually, a hollow space may be created inside the reclamation soil. Attention should be paid to these hollow spaces as they may result in a significant depression of land. Moreover, if the mound-transmitted waves are large, their uplift may cause extensive damage by boiling of the reclamation sand [56) 57)].

(2) Leakage prevention works

Backfills (stones) may be installed behind the caisson to reduce the earth pressure. Geotextile sheets or mats which prevent sand leakage are laid on the slope of the backfills, and the reclamation sand is installed on it. However, if there is a problem in durability of the sand leakage prevention sheets or mats, there may occur a hollow space inside the reclamation sand due to their damages by the mound transmitted waves or tides and subsequent natural dropping or leakage of the reclamation sand into the backfills. Therefore, sufficient attention should be paid to the installation of the sheets or mats that enable the prevention of sand leakage.

The grain size of the stones to be installed may gradually be reduced from the backfilling stone to the reclamation sand according to the filter rule (**Part III, Chapter 4, 3.3 Gravity-type Breakwater (Sloping Breakwaters)**). Moreover, stones of small grain size and sheets or mats may be combined.

A joint plate to prevent sand leakage is installed in the joint between caissons. However, since the wave pressure acting on the joint plate is almost as same as that in the front wall of a caisson, the joint plate that is not durable can easily be broken. Moreover, direct installation of the reclamation sand behind the caisson is not preferable because sand leaks more easily from the joint.

7.6 Prediction of Beach Deformation

All the related factors shall be thoroughly investigated when predicting beach deformation, taking into consideration the predicted results by an appropriate method and the data of past beach deformation at the site in question. Various methods for predicting beach deformation exist, including (1) empirical prediction techniques; (2) estimation based on hydraulic model experiments, especially with movable bed model experiments; and (3) numerical simulations. Because beach deformation is strongly governed by the characteristics of the region in question, it is inappropriate to rely on any single method. It is necessary to predict beach deformation by investigating the local data and information as comprehensively as possible. Moreover, combining two or more prediction methods is desirable.

7.6.1 Empirical Prediction Techniques

The empirical method is a procedure in which, on the basis of analysis of the past examples of beach deformation on the coasts other than the coast in question, the layout and characteristics of the structures to be built on the coast in question are compared with the past examples of similar environment. Based on the similarities, beach deformation caused by the construction of new structures is predicted. Tanaka[58)] has conducted research on modeling of the complicated topographical changes that occur after the construction of structures. He classified characteristics of typical topographical changes in numerous examples of beach deformation. As a result of this research, it is possible to understand the topographical changes in the vicinity of Japanese ports in several representative patterns (see **Fig. 7.6.1**). Exceptions to these patterns are relatively rare. By judging which pattern in **Fig. 7.6.1** is applicable to the coast under investigation, a qualitative prediction of beach deformation becomes possible.

As the empirical prediction method is based on the site-scaled actual performance, it is a powerful method for predicting an outline. However, no quantitative discussion is possible because it has an aspect to pattern the beach deformation.

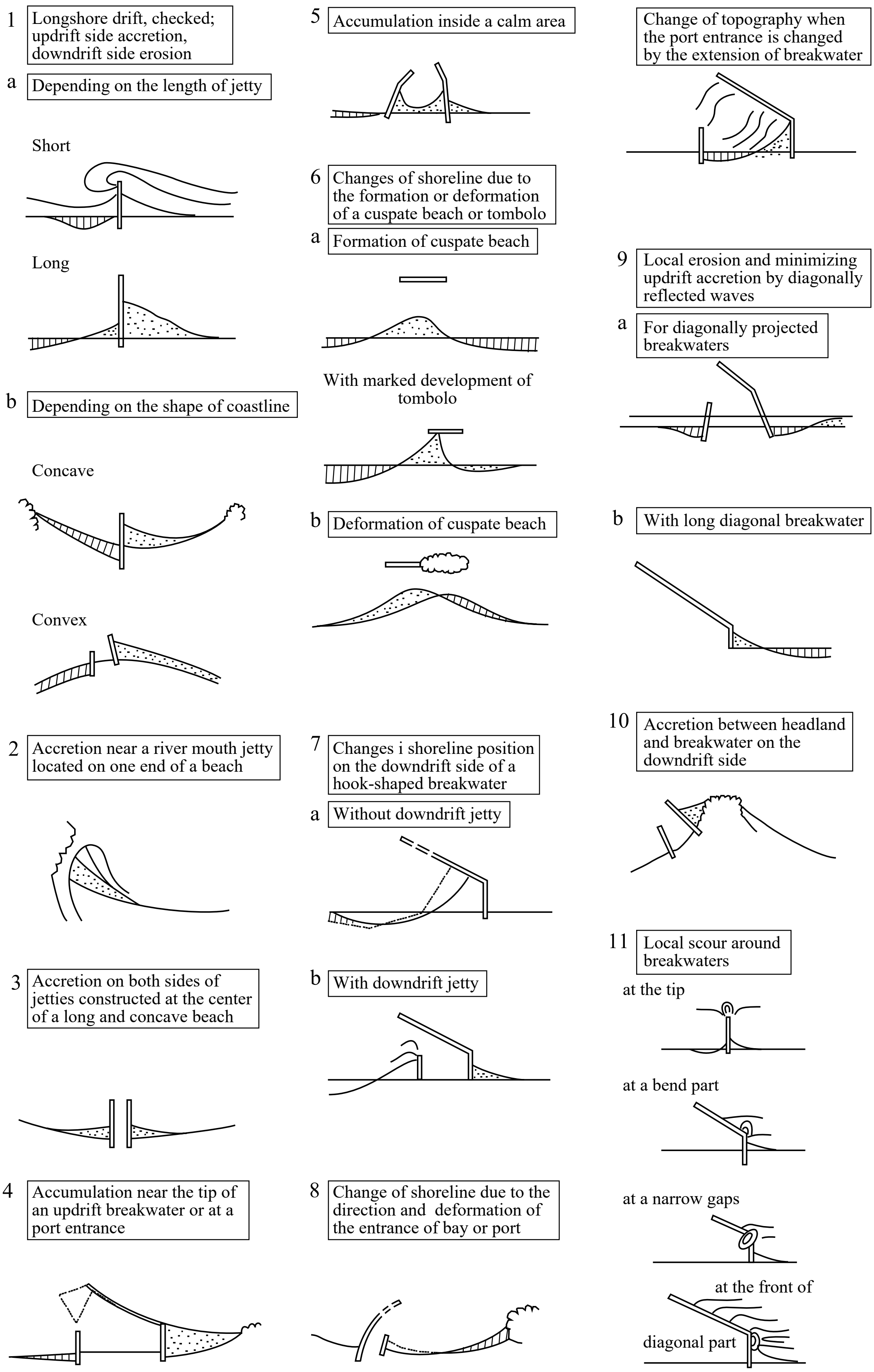

Fig. 7.6.1 Classification of Patterns of Topographical Changes After Construction of Structures

7.6.2 Hydraulic Model Experiments, Particularly Movable Bed Model Experiments

The accuracy of predicting beach deformation based on hydraulic model experiments, particularly movable bed model experiments, is limited because the problem of similarity remains unsolved. But the advantage of model experiments is such that specific topographical changes can be reproduced in a laboratory basin and the phenomenon to be forecasted can be understood visually.

In the experiment, fabricate a model by considering the result of preliminary calculation using an empirical equation concerning the past similarity and setting the model scale and the region to be reproduced. Before predicting future beach deformation, it is necessary to verify the model for reproducibility of the topographical changes that occurred in the past in the study area and to confirm the model's kinematic similarity. The degree of kinematic similarity will be judged by the reproductive accuracy of the experiment, which, therefore, cannot exceed the accuracy of the data collected on beach deformations in the past.

One can assume that adequately effective engineering predictions are possible if sufficient care is taken in the preliminary experiments to study the reproducibility of actual beach deformations, and in particular, the following problems can be addressed:

① The area of qualitative topographical changes caused by the construction of coastal facilities.

② Comparisons among alternative plans for measures to prevent coastal erosion, such as jetty or detached breakwaters.

③ Qualitative evaluation of shoreline changes due to large-scale offshore facilities.

However, predictions of beach deformation are difficult in the following types of cases:

(a) Stable cross-sectional shapes of large-scale artificial beaches that face rough seas.

(b) Deformation problems caused by large-scale offshore facilities on beaches that face rough seas.

(c) Prediction of deposition rates in navigation channels and harbors and effects of their countermeasures.

(d) Countermeasures against deposition in small-scale ports, such as marinas.

(e) Experiments concerning effects of permeable detached breakwaters and submerged breakwaters on beach stability.

For details concerning movable bed model experiments, see Reference 58).

7.6.3 Predictions by Numerical Simulations

In the case of numerical simulation, it is preferable to model phenomena that are not yet fully figured out, such as the nearshore current by wave breaking, subsequent shore erosion, and siltation inside the harbor, by focusing on dominating phenomena and introducing various presumptions. Therefore, as in the hydraulic experiments, the validity of the numerical model should be verified by the numerical reproducibility of the past changes in topography of the target shore before the prediction of the future.

At the present time, numerical simulations are divided into two models: those that predict changes in the shoreline location and those that predict three-dimensional changes in water depth, i.e., beach topographical changes. However, many unresolved portions still exist as of today, and such calculations are performed under various assumptions. Therefore, it should be noted that the numerical result may be incorrectly used unless the various assumptions in the simulations are understood until the result can be obtained. Many types of models have been proposed until now to predict various changes in topography (changes in cross sections, changes in shorelines, and three-dimensional changes). The result of estimation and comparison of typical models [59)] shows that it is necessary to use models properly according to the mechanism of changes in the beach of interest and their time and space scales when applying each model to sites.

On the other hand, prediction of changes in beach topography for a long period of some 10 years or longer is required for the topographic changes in coast caused by the sea level rise and changes in the wave field due to future climate changes. The numerical models to predict changes in the shoreline due to these climate changes are currently being developed.

(1) Shoreline Change Model (One-Line Theory) [15) 60) 61)]

This model predicts the long-time change in the shoreline considering only the longshore sediment transport rate by ignoring the cross shore littoral drift. They are called a shoreline change model, a coastline change model, or a one-line theory as they predict the change in one shoreline, but they are all essentially the same model. In this model, the shoreline moves by the balance of the longshore sediment transport rate driven by the longshore directional component of the energy flux of the incident wave and finally stabilizes after the shoreline direction changes so that the waves enter perpendicularly to the shoreline. This model is relatively frequently applied, and the results of the predictions are fully put to practical use. However, in order to improve the precision of the prediction, accumulation of enough data concerning a long-time shoreline change should be required and the reproducibility should be verified based on it.

Beach sediment is transported by waves and currents both in the perpendicular direction to the shoreline and in the alongshore direction. Because littoral drift is caused mainly by the direct action of waves, the littoral drift during storm periods will be predominantly towards the offshore, and the coast will be eroded with a retreat of shoreline. When the sea becomes calm, however, the sediment will be carried towards the shore, and the shoreline will advance. Along with these movements, changes of the beach profile will occur. This topographical change in the shoreline location and beach profiles caused by the onshore–offshore transport is normally seasonal. When viewed on the average profile over a long period of time, the changes caused by onshore–offshore transport are less significant compared with those caused by longshore transport. Thus, when focusing on beach erosion or accretion over a period of several years, one can assume that there is no change in the shape of the beach profile and that beach erosion and accretion will correspond to the retreat and advance of the shoreline. Then, the changes in the shoreline location can be predicted primarily from the longshore transport as the basis on the balance of the deposition and removal of the longshore sediment volume.

Figure 7.6.2 illustrates the calculation principles of a shoreline change prediction model. As shown in the figure, the shoreline should be divided into sections of the width Δy along the alongshore direction of the shoreline, and the inflow and outflow of sediment volume between those widths are considered. That is, when the inflow $Q\Delta t$ and outflow $\left(Q+\frac{\partial Q}{\partial y}\Delta y\right)\Delta t$ of sediment volume during the time period Δt are compared, accretion will occur if the former is larger, and erosion will take place if the latter is larger.

By introducing the assumption that the beach profile remains unchanged over time and any imbalance between the inflow and outflow sediment volumes simply shifts the beach profile parallel to offshore or onshore directions, it is possible to express the advance and retreat of the shoreline as a result of the imbalance. When this is expressed in the continuity of sediment flux, the result is presented by **equation. (7.6.1)**.

$$\frac{\partial x_s}{\partial t}+\frac{1}{D_s}\left(\frac{\partial Q}{\partial y}-q\right)=0 \qquad \textbf{(7.6.1)}$$

where

x_s : shoreline location (m)

t : time (s)

y : coordinate in alongshore direction (m)

D_s : vertical distance of the littoral drift movement zone (m)

Q : longshore sediment transport rate (m^3/s)

q : cross-shore inflow ($q > 0$) or outflow ($q < 0$) of the sediment transport rate across the onshore–offshore boundary per unit width in the alongshore direction ($m^3/m/s$)

Therefore, if D_s, Q, and q are given, the time change of the shoreline location can be calculated using **equation (7.6.1)**.

As the evaluation of the cross shore littoral drift rate q is quite difficult, the onshore–offshore boundary should normally be set where the cross shore littoral drift rate can be ignored. In other words, the onshore boundary shall be set to the maximum run-up location of incident waves on the beach, and the movement of the bottom sediment due to wave action is neglected. On the other hand, the offshore boundary should be set to the location of little sand movement, outside of the surf zone at which the littoral drift phenomenon is active. However, when the sediment supplied by rivers is not negligible, when there is sand mining or dumping from the onshore side, or when sand flows out to the offshore direction and never comes back to the beach, their impacts can be incorporated into the model by considering the quantities in the variable of q.

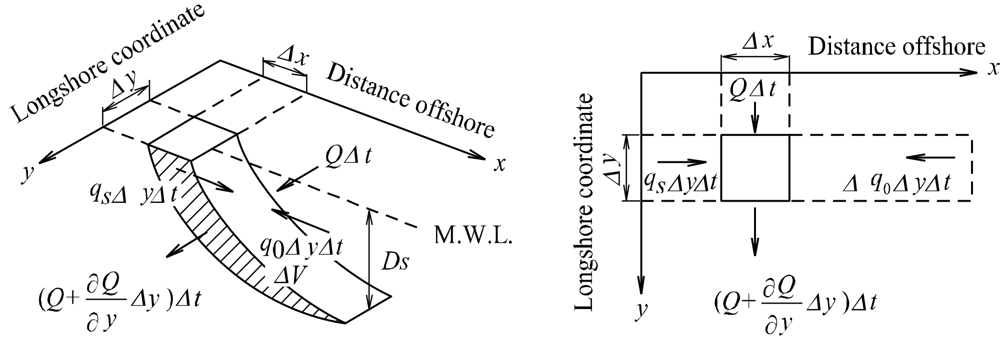

(a) Model view (b) Plan view

Fig. 7.6.2 Relationship Between Shoreline Change and Sand Movement

The longshore sediment transport rate Q is often estimated using an equation, including the alongshore component of the incident wave energy flux at the wave breaking point. In such equations, the longshore sediment transport rate is determined only from the wave height and direction at the wave breaking point as wave conditions. In the coastal zone where beach deformation is predicted, however, there will normally exist some structures that create an area sheltered from incident waves. Because of this sheltered area, the wave height varies alongshore; thus, currents are induced. Hence, the following equation in which Ozasa and Brampton [62)] incorporated the abovementioned effect is often used.

$$Q=\frac{H_B{}^2 C_{gB}}{16s(1-\lambda)}\left(K_1 \sin 2\theta_B-\frac{2K_2}{\tan\beta}\cos\theta_B\frac{\partial H_B}{\partial y}\right) \qquad \textbf{(7.6.2)}$$

where

H_B : breaking wave height (m)

C_{gB} : group velocity at the wave breaking point (m/s)

θ_B : angle formed by the wave crest line and the shoreline at the breaker point (°)

$\tan\beta$: equilibrium beach slope

s : $s=(\rho_s-\rho_0)/\rho_0$

ρ_s : density of sediment (g/cm^3)

ρ_0 : density of seawater (g/cm^3)

λ : void ratio of sediment

K_1, K_2 : coefficients

The width of sediment movement zone D_s is the distance perpendicular to the shoreline from the wave run-up point on the beach to the offshore boundary where longshore sediment transport activity becomes significant. The distance D_s is determined basically by investigating the volume of beach profile area change from the bathymetric data of the coast in question. When the available data are inadequate, an energy-averaged representative wave is estimated, and its dimensions are substituted into the equations for the wave run-up height and the threshold depth of sediment movement as a method to conveniently find the distance D_s.

Because **equation (7.6.2)** cannot be solved analytically, except in extremely simple cases, a computer is required to perform the numerical computation. In the numerical computation, Q must be evaluated at each measuring line. For this purpose, the breaking wave height and angle, the incidence wave angle to the shore line, and the water depth at the wave breaking point at each measuring line must be calculated separately by using the wave transformation calculation (for details concerning numerical computation, see Reference 15).

(2) Three-Dimensional Deformation Models or Prediction Model for Bathymetric Change

While the shoreline change model treats the surf zone phenomena as a black box, the water depth model (three-dimensional model) needs to integrate the phenomena in the surf zone, especially the following phenomena, by properly formulating them.

① As wave transformation in shallow sea, refraction, diffraction, wave breaking and wave transformation after wave breaking.

② Wave energy attenuation due to wave breaking and roughness coefficient of the sea bottom

③ Planar and vertical distributions of the nearshore current

④ Mechanisms of bedload, suspended sediment, etc.

Prediction models for bathymetric change predict the change in the water depth at each grid point in a calculation domain, and consider not only longshore sediment transport but also cross-shore sediment transport. Several models have been presented as the prediction model for bathymetric change, but in every model, the method is to first calculate the fields of waves and nearshore currents and then determine the bathymetric changes. As the nearshore currents, depth averaged currents or vertically distributed ones may be employed in the numerical model. (They are called the water depth model, three-dimensional model, coastal topography change prediction model, and so on, but they are all the same.)

Prediction models for bathymetric change are divided into two main types depending on the method of predicting the bathymetric changes. One type of model is based on local sediment transport rates calculated from hydraulic factors and sediment particle diameters at the location in question, and the other type of model considers sediment advection and diffusion. The models based on local sediment transport rates determine bathymetric changes based on the difference between the incoming and outgoing amounts of the local sediment transport, and one of these models is that of Watanabe et al. [63)], which uses the sediment transport rate formulas of Watanabe et al. Other local sediment transport rate formulas are those of Bijker[64)] and Bailard [65)], which separately calculate the bedload and the suspended load. The model of Watanabe et al. [63)] has been improved several times and has developed into a model that considers the grain size distribution. [66)]

Models that consider the advection and diffusion of sediment, either in three dimensions or just in horizontal two dimensions, have been proposed, for example, by Sawaragi et al. [67)] (hereafter, the Sawaragi model) and by Lesser et al. [68)] (hereafter, the Delft 3D-flow model). In these models, the bathymetric changes are dominated by the difference between the amount of uplifting of suspended sand and its settling rate and by the difference between the incoming amount of bedload and its outgoing amount. The concentration of suspended load at reference points near the sea bottom, which is used in the calculation of uplifted amounts of suspended sand, may be found in the formula of Deguchi and Sawaragi [69)] used in the Sawaragi model or in the formula of van Rijn [70)] used in the Delft 3D-flow model. An example of a formula for bedload is that of van Rijn [71)] (used in the Delft 3D-flow model).

The prediction model for bathymetric change have been mainly applied to the areas where offshore topographical changes are significant, such as the problem of siltation in ship channels and basins and bathymetric changes due to large-scale submerged breakwaters.

(3) Prediction Simulation of the Shoreline Change due to Climate Change

In the numerical model where the physical processes are realistically resolved like prediction models for bathymetric change, a vast amount of time is required to calculate the prediction of the shoreline change for a long time of several-year to several-10-year scale. Furthermore, the calculation accuracy is not necessarily improved more than the calculation result using simpler models called process based or empirical model [72)]. Therefore, the latter model is currently often applied for the prediction of long-period phenomenon for several-10-year-scale, such as topographical change due to climate change. They are classified into the following three types:

① **Prediction by a shoreline change model**

The shoreline change model (one-line theory) explained in **7.6.3 (1)** evaluates the topographical change based on the change in future wave height or wave direction. This model is capable of reproducing the shoreline change in a relatively long period.

② **Prediction using Bruun's law**

Bruun's law calculates the shoreline change caused by the movement of sediment in the onshore–offshore direction (see **Part II, Chapter 2, 7.4.12 Relations Between the Climate Change and the Topographical**

Change), considering the change in the equilibrium cross section of beach corresponding to the change in sea level. Although this model calculates only the change in equilibrium condition and does not reproduce the change in beach topography according to the temporal variation of wave condition, it has an advantage of allowing relatively easy estimation of future amount of shoreline retreat.

③ **Prediction using the equilibrium shoreline change model**

This model assumes that the shoreline advances or retreats asymptotically to the equilibrium shoreline location corresponding to the time dependent change in wave condition. This is capable of reproducing not only the short-term shoreline changes caused by waves but also long-term shoreline changes. Although the equilibrium shoreline location or the external force term may be treated differently, it is basically expressed by **equaton (7.6.3)**. One-half power of the wave energy is often used as the external force term, and the equilibrium shoreline location is usually dominated by the wave energy [73) 74)].

$$\frac{dy}{dt} = CE^{\frac{1}{2}}\left(y - y_{eq}\right) \tag{7.6.3}$$

where

dy/dt : shoreline change rate per unit time (m/day)

C : coefficient ($1/N^{0.5}day^{0.5}$)

E : wave energy (N/day)

y : present shoreline location (m)

y_{eq} : equilibrium shoreline location corresponding to the current waves (m)

Since the above three process-based models basically treat mutually independent events, prediction of the shoreline change, for example, the change due to the changes in sea level and the wave condition, becomes possible by combining each model. Specifically, the Banno–Kuriyama model incorporates the concept of Bruun's law into the equilibrium shoreline change model [74)] or the CoSMoS-COATS model [75)], adding together the results of the three process-based models.

[References]

1) Ports and Harbour Bureau of MLIT and Nature Conservation Bureau of MOE: For the Regeneration of Tidal Network, Report of the workshop for the regeneration of ecosystems including tidal flats in Tokyo Bay, National Printing Bureau, p.118, 2004 (in Japanese)

2) Hamada, T., H. Mitsuyasu and N. Hase: Wave force on structures, Proceedings of the 3rd Conference on Coastal Eng. JSCE Vol. pp. 67-83, 1956

3) Japan Society of Mechanical Engineers: Handbook of Mechanical Engineering, pp. A5-97-106, 1989

4) Iwasaki T., A. Mano T. Nakamura and N. Horikoshi: Experimental study on stationary fluid dynamic force acting on mound material of submerged breakwater and pre-packed breakwaters, Proceedings of 31st Conference on Coastal Eng. JSCE, pp. 527-531, 1984

5) TANIMOTO, K., K. KIMURA and K. MIYAZAKI: Study on Stability of Submerged Dike at the Opening Section of Tsunami Protection Breakwaters, Rept. of PHRI Vol. 27 No. 4, pp. 93-102, 1988

6) Sakunaka, J. and T. Arikawa: Research on Stability of Opening Section at Baymouth Breakwater, Technical Note of the Port and Airport Research Institute, No.1274, p.26, 2013 (in Japanese)

7) Tsuruya, H., K. Murakami and I. Irie: Mathematical Modeling Mud Transport in Ports with a Multi-layered Model, Report of the Port and Harbour Research Institute, Vol.29 No.1, pp.3-51, 1990 (in Japanese)

8) Nakagawa, Y., K. Watanabe, H. Tanigawa and Y. Kuroda: Measurement of Vertical Profile of Mud Density near the Bottom Boundary, Annual Journal of Coastal Engineering, JSCE, Vol.51, pp.986-990, 2004 (in Japanese)

9) Goda, Y.: Ports and Harbours (Second Edition), Easy-to-understand Civil Engineering Lecture, Shokokusha Publishing, p. 321, 1998

10) Horikawa, K.: New Edition, Coastal Engineering- Introduction to Offshore Engineering, Tokyo Univ. Press, 1991

11) Mogi, A.: Basic Lectures of Marine Science 7, Geology in Shallow Water, Shore line and serf zone, Tokyo Univ. Press, pp. 109-252, 1971

12) Toyoshima, O.: Coastal Engineering at construction site, Morikita Publishing, 1972

13) Sawaragi, T.: Littoral drift and coastal erosion, Disaster Prevention Series 3, Morikita Publishing, 1992

14) Noda, H. and H. Hashimoto: Littoral drift and shore protection facilities, New Series Civil Engineering 79, Giho-do Publishing, 1981

15) Honma, M. and K. Horikawa: Coast-environmental engineering, Tokyo Univ. Press, 1985

16) Sato, S.: Study related to port construction, Technical Note of PHRI, No. 5, 1962

17) Sonu, C. J.: Three-dimensional beach changes, Journal of Geology, Vol. 81, pp. 42–64, 1973

18) OZASA, H.: Field Investigation of Submarine Sand Banks and Large Sand Waves, Rept of PHRI Vol. 14 No. 2, pp. 3-46, 1975

19) Horikawa, K. T. Sunamura: Study of retreat of coastal cliff by aerial photographs, Proceedings of 14th Conference on Coastal Eng. JSCE, pp. 315-324, 1967

20) Horikawa, K. and M. Sunamura: Experimental study on erosion of sea cliff, Proceedings of 15th Conference on coastal Eng. JSCE, pp. 315-324, 1968

21) Horikawa, K. and T. Sunamura: Coastal erosion at Byobuga-ura, Chiba Prefecture (1), (2), & (3), Proceedings of on Coastal Eng. JSCE, Vol. 16 pp. 137–146, Vol. 17 pp. 289–296, Vol. 19 pp. 13–17, 1969, 1970, 1972

22) Bascom, W. N.: The relationship between sand size and beach – face slope, Transactions of AGU, Vol. 32 No. 6, pp. 866–874, 1951

23) KATO, K, N. TANAKA, H. KIMURA and M. AKAISHI: Movable-bed Model Experiments of a Large River-mouth and its Surroundings- On Deformation of Topography at the Yoshino River- Rept of PHRI Vol. 22 No. 2, pp. 3-87, 1983

24) Sato S. and N. Tanaka: Sand movement on horizontal bed, Proceedings of 9th Conference on Coastal Eng. JSCE, pp. 95-100, 1962

25) Sato, S. and N. Tanaka: Field investigation on sand drift at Port Kashima facing the Pacific Ocean, Proc. 10th Conf. on Coastal Eng., pp. 595-614, 1966

26) Savage, R. P.: Laboratory determination of littoral-transport rate, Proc. of ASCE., Vol. 88, WW2, 1962

27) U.S. Army Coastal Engineering Research Center: Shore Protection Manual, Vol. 1, Department of the Army Corps of Engineers, 1977

28) Komar, P. D.: Relative quantities of suspension versus bed-load transport on beaches, Journal of Sediment Petrology, Vol. 48, pp. 921–932, 1978

29) Sternberg, R. W., N. C. Shi and J. P. Dowing: Field observations of suspended transport in the nearshore zone, Proc. 19th Int. Conf. on Coastal Eng., pp. 1782–1798, 1984

30) Katoh, K., N. Tanaka, T. Kondoh, M. Akaishi and K. Terasaki: Field observation of local sand movement in the surf zone using fluorescent sand tracer (Second Report), Report of PHRI Vol. 24 No. 4, pp. 3–63, 1985

31) Katoh, K., N. Tanaka and I. Irie: Field observaion on suspended-load in the surf zone, Proc. of 19th Int. Conf. on Coastal Eng., pp. 1846–1862, 1984

32) Hino, M. K. Nadaoka and A. Omata: Organizational structure of turbulence and water particle motion in the surf zone, Proceedings of 31st Conference on Coastal Eng. JSCE, pp. 1-5, 1984

33) Kana, T.W.: Surf zone measurement of suspended sediment, Proc. of 16th Int. Conf. on Coastal Eng., pp. 1725–1741, 1978

34) Dean, R.G.: Heurestic models of sand transport in the surf zone, Proc. Conf. on Eng. Dynamics in the surf zone, pp. 208–214, 1973

35) Horikawa, K., T. Sunamura, H. Kondo and S. Okada: Discussion on 2-dimensional shore line change due to waves, Proceedings of 22nd Conference on Coastal Eng. JSCE, pp. 329-334, 1975

36) Kato, K. S. Yanagishima, H. Murakami and K. Suetsugu: Trial for modeling of short-term shore line change, Proceedings of 34th Conference on Coastal Eng. JSCE, pp. 297-301, 1987

37) Komar, P.D.: Beach process and sedimentation, Prentice-Hall, Inc., 1976

38) Kato, K., S. Yanagishima: Berm erosion due to infra-gravity waves, Jour. Of JSCE, No. 452/II-20, pp. 41-50, 1992

39) Kato K.: Shore protection by underground permeable layer, Journal of JSCE, February, pp. 18-21, 1996

40) Kuriyama, Y.: Long-term cross-shore movement of longshore bar and associated sediment transport, Jour. Of JSCE, No. 677, pp. 115-128, 2001

41) Tsuchiya, Y. and Y. Kawada: Wind brown sand transport rate law based on sand particle siltation. Proceedings of 19th Conference on Hydraulics, pp. 7-12, 1975

42) KURIYAMA, Y., T. NAKASHIMA, K. KAMIDOZONO and N. MOCHIZUKI: Field Measurements of the Effect of Vegetation on Beach Profile Change in the Region from a Backshore to the Foot of the Fore-dune and Modeling of Aeolian Sand Transport with Consideration of Vegetation, Rept of PHRI Vol. 40 No. 1, pp. 47-80, 2001

43) YANAGISHIMA, S.: Field Measurement of the Effect of Vegetation on Beach Profile Change In the Backshore, Technical Note of PHRI No. 1091, p. 35, 2004

44) IPCC fifth assessment report, http://www.ipcc.ch/, 2015

45) Mark A. Hemer, Yalin Fan, Nobuhito Mori, Alvaro Semedo and Xiaolan L. Wang (2013): Projected changes in wave climate from a multi-model ensemble, Nature Climate Change, Vol. 3

46) Banno, M. and Y. Kuriyama: Development of Shoreline Change Model Considering Time Heterogeneity and Tidal Impact and Prediction of Future Shoreline Position under Global Climate Change, Journals of JSCE Series B2 (Coastal Engineering), Vol.69 No.2, pp.I_541-I_545, 2013 (in Japanese)

47) Bruun,P.,1962. Sea level rise as a cause of shore erosion. Proc. Am. Soc. Civ. Eng., J. Waterways Harbors Div., 88:117-130

48) Bruun, P., 1983. Review of conditions for uses of the Bruun rule of erosion. Coastal Engineering, 7, pp. 77 -89

49) Shibutani, Y., M. Kuroiwa, K. Hayashi, K. Ikeda, N. Mori, Y. Matsubara and H. Mase: Long-term Beach Prediction and Impact Assessment of Climate Change on Contour Line Change, Journals of JSCE Series B2 (Coastal Engineering), Vol.70 No.2, pp.I_684-I_689, 2014 (in Japanese)

50) Saeki, H., T. Sato, T. Ono and K. Hamanaka: Experimental Study on scoring of foundation of sea walls, Proceedings of 32nd Conference on Coastal Eng. JSCE, pp. 440-444, 1985

51) Tanaka, N.: Transformation of sea bed and beach near port constructive in sandy beach, Proceedings of Lecture meeting of PHRI 1974, pp. 1-46,1974

52) Sato, S. and I. Irie: Variation of topography of sea-bed caused by the construction of breakwaters, Coastal Engineering in Japan, Vol. 13, pp. 141–152, 1970

53) IRIE, I., K. NADAOKA, T. KONDO and K. TERASAKI : Two Dimensional Seabed Scour in Front of Breakwaters by Standing Waves-A Study from the Standpoint of Bed load Movement- Report of PHRI Vol. 23 No. 1, pp. 3-52, 1984

54) Suzuki, K., S. Takahashi, T. Takano and K. Shimosako: Settlement Failure of Wave Dissipation Blocks in front of Caisson Type Breakwater due to Scouring under the Rubble Mound, Report of the Port and Airport Research Institute, Vol.41 No.1, pp.1-39, 2002 (in Japanese)

55) Suzuki, K. and S. Takahashi: Estimation of Scouring at the Bottom of Wave Dissipating Block Breakwater, Journals of Coastal Development Institute of Technology, No.12, pp.1-3, 2012 (in Japanese)

56) Takahashi, S., K. Suzuki, K. Tokubuchi, T. Okamura, K. Shimosako, K. Zen and H. Yamazaki: Hydraulic Model Experiments on the Settlement Failures of Caisson-type Seawalls, Report of the Port and Harbour Research Institute, Vol.35 No.2, pp.3-64, 1995 (in Japanese)

57) Takahashi, S., K. Suzuki and W.S. Park: Numerical Calculations on Wave Pressure Propagation into Backfill Rubbles of Caisson Type Seawall, Journals of JSCE Division B3 (Ocean Engineering), 2002 (in Japanese)

58) Kato, K.: Movable bed experiment and field observation, Monthly Magazine Marine Science, No. 169, pp. 417-423, 1984

59) Shimizu, T. and T. Takagi, K. Sato and M. Yamada: Mutual comparison of beach deformation models, Proceedings of Coastal Eng. JSCE Vol. 44, pp. 506-510, 1997

60) TANAKA, N. and K. NADAOKA: Development and Application of a Numerical Model for the Prediction of Shoreline Changes, Technical Note of PHRI No. 436, 1982

61) Watanabe, A.: Numerical simulation of beach change, Monthly Magazine Marine Science, Littoral Drift, Vol. 16 No. 7, pp. 409-416, 1984

62) OZASA, H. and A. H. BRAMPTON: Models for Predicting the Shoreline Evolution of Beaches Backed by Seawalls, Rept of PHRI Vol. 18 No. 4, pp. 77-103, 1979

63) Watanabe, A., Y. Maruyama, Y. Shimizu and T. Sakakiyama: Numerical model for the prediction of s-dimensional beach transformation due to the construction of structures, Proceedings of the 31st Conference on Coastal Eng. JSCE Vol. pp. 406-410, 1984

64) Bijker, E.W.: Longshore transport computations, J. Waterways, Harbors and Coastal Engineering Division, Vol. 97, No. 4, pp. 687–703, 1971

65) Bailard, J.A.: An energetics total load sediment transport model for a plane sloping beach, J. Geophys. Res., Vol. 82, No. C11, pp. 10938–10954, 1981

66) Kobayashi, H., T. Honda, S. Sato, A. Watanabe, M. Isobe and T. Ishii: A numerical model of three-dimensional beach deformation due to graded sediment transport under atilt waves, Jour. Of JSCE No. 740/II-64, pp. 157-169, 2003

67) Sawaragi, T. S. Ri, and I. Deguchi: Study on nearshore current around river mouth and model for topographic transformation, Proceedings of 31st Conference on Coastal Eng. JSCE Vol. pp. 411-415, 1984

68) Lesser, G.R., Roelvink, J.A., van Kester, J.A.T.M. and Stelling, G.S.: Development and validation of a three-dimensional morphological model, Coastal Eng., Vol. 51, pp. 883–915, 2004

69) Deguchi, I. and Sawaragi, T.: Calculation of the rate of net on-offshore sediment transport on the basis of flux concept, Proc. 19th Int. Conf. on Coastal Eng., ASCE, pp. 1325–1341, 1984

70) van Rijn, L.C.: Sediment transport: Part II, Suspended load transport, J. Hydraulic Eng., Vol. 11, pp. 1613–1641, 1984

71) van Rijn, L.C.: Principles of Sediment Transport in Rivers, Estuaries and Coastal Seas, Aqua Publications, Amsterdam, 1993

72) Murray, A. B. (2007): Reducing model complexity for explanation and prediction, Geomorphology, 90 (3), pp. 178-191

73) Yates, M. L., Guza, R. T. and O. Reilly W. C. (2009): Equilibrium shoreline response: Observation and modeling, Journal of Geophysical Research: Oceans, 114 (C9)

74) Banno, M., Y. Kuriyama and N. Hashimoto: Uncertainty Estimation of Equilibrium Beach Profile by Non-linear Mixed Effect Model with Long-term Measured Data, Journals of JSCE Series B2 (Coastal Engineering), Vol.70 No.2, pp.I_546-I_550, 2014 (in Japanese)

75) Vitousek, S., P. L. Barnard, P. Limber, L. Erikson, and B. Cole (2017), A model integrating longshore and cross-shore processes for predicting long-term shoreline response to climate change, J. Geophys. Res. Earth Surf., 122, 782–806, doi:10.1002/ 2016JF 004065.

8 Other Meteorology and Oceanology Items

8.1 Other Meteorology Items to be Considered

(1) General

The following meteorology items and effects on port facilities should be considered with regard to the performance verification of port facilities:

① Rain is a factor in determining the capacity of drainage facilities within the port and can interfere with cargo handling and other port operations.

② Fog interferes with ships' navigation and entry to and departure from the port. It can also decrease the usability of port facilities.

③ Snowfall may need to be considered with regard to its surcharge on port facilities.

④ Atmospheric temperature may affect the stress distribution on port facilities, creating temperature stress.

(2) Rain

Rain can generally be classified into a thunderstorm in which precipitation concentrates in a short time and a long-duration rain which is an indication of typhoon. When conducting a performance verification of drainage facilities, rainfall intensity shall generally be set for both cases where the outflow instantaneously increases and the efflux time is long. In the performance verification of sewage lines and others where the rainfall density concerns as in thunderstorms and others, Sherman's formula or Talbot's formula may be used:

Sherman's formula

$$R = \frac{a}{t^n} \tag{8.1.1}$$

Talbot's formula

$$R = \frac{a}{t+b} \tag{8.1.2}$$

where

R : rainfall intensity (mm/h)

t : rainfall duration (min)

a, b, n : constants

It is known that the relation between the maximum rainfall P and the rainfall duration can generally be expressed by $P = aT$n [1]. Also, an experimental equation has been proposed which takes into consideration the type of rain and topography [2]. The rainfall intensity in a scale of 1 hour or less is generally determined from an observed hourly precipitation by **equation (8.1.3)**.

$$R = 7.7 R_0 T^{0.5} \tag{8.1.3}$$

where

R : rainfall intensity in a target time scale (mm/h)

R_0 : rainfall intensity observed in an hour (mm/h); use a N-year probability rainfall for 60-min if available

T : target time scale less than 1 hour (min)

The maximum rainfall can be calculated using **equation (8.1.4)** when the total precipitation is massive as in typhoon or rain outflow from mountainous drainage basin is of concern.

$$P = 83 D^{0.33} \tag{8.1.4}$$

where

P : maximum rainfall (mm)

D : rainfall duration (h)

(3) Fog

Fog interferes with ships' navigation and entry to and departure from the port. It also degrades the availability of port facilities. Although a few systematic investigations have been conducted on troubles caused by fog, a hearing survey example in the Seto Inland Sea and others has been reported [3)].

(4) Snowfall

In districts where snowfall is expected, snowfall on the apron becomes live load as it is or hardened with rolling compaction by vehicles and others. **Part II, Chapter 10, 3.1 Live Load** may be referred to for more details.

(5) Atmospheric temperature

In the performance verification of statically indeterminate structure, consider the impact of temperature stress due to temperature change as an environmental action when needed.

8.2 Assessment of the Operating Rate of Construction Work Considering Meteorology and Oceanology

(English translation of this section from Japanese version is currently being prepared.)

[References]

1) Kawabata Y.: Hydro-meteorology, Chijinn Shokan Publishing, p. 33, 1961

2) Yamada, T., T. Hibino, T. Araki and M. Nakatsugawa: Statistical characteristics of rainfall in mountainous basins, Jour. JSCE No. 527, pp. 1-13, 1995

3) Sasa, K., Mizui, S. and Hibino, T.: A Basic Study on Difficulties of Ship Operation Under Restricted Visibility Due to Heavy Fog, Journal of Japan Institute of Navigation, Vol. 112, 2005